
# XVIII Congreso de Física Estadística

## 25 años

# Libro de resúmenes

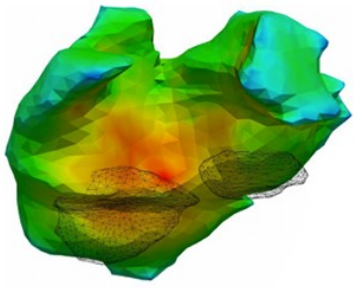

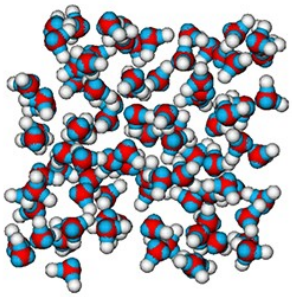
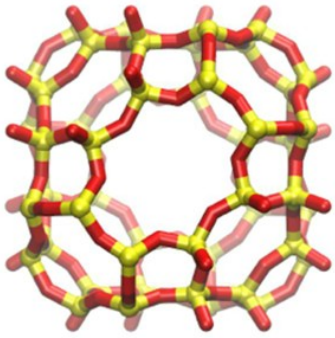
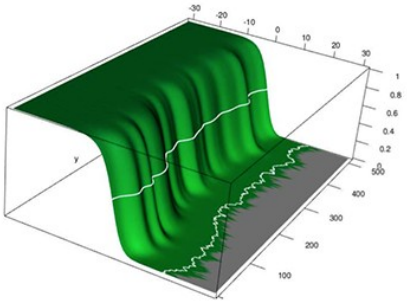
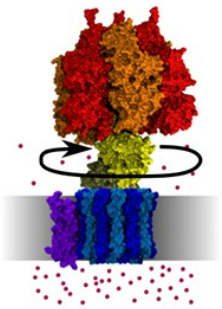

Palma, 18-20 de octubre de 2012

IFISC (UIB – CSIC)


Cubierta: composición con seis figuras seleccionadas de entre las contribuciones al congreso. En sentido horario, y empezando por el panel superior izquierdo, O. Pont *et al.* (O-13); D. Walgraef *et al.* (P-53); P. Nicolini *et* al. (P-94); R. Pérez-Carrasco *et al.* (O-12); S. Nesic *et al.* (P-91); S. Rodríguez-Gómez *et al.* (P-105).

Banner: panorámica del campus de la Universitat de les Illes Balears (UIB) con el edificio Rectorado en el centro y el edificio donde se celebrará el congreso a la izquierda. La foto fue tomada desde la última planta del Instituto de Física Interdisciplinar y Sistemas Complejos (IFISC).

Maquetación y compilación: comité organizador de FisEs '12 y equipo técnico del IFISC (David de la Montaña, Antònia Tugores y Rubén Tolosa).


# Horarios

Leyenda:

- Conferencias invitadas (50 min.)
- Conferencias invitadas (30 min.)
- Conferencias contribuídas (15 min.)
- Pausas
- Paneles
- Otros

| Hora | Jueves, 18 de octubre |
|---|---|
| **08:00-09:00** | Inscripción |
| **09:00-09:30** | Inauguración |
| **09:30-10:20** | Evans, R.: *Binary hard-sphere mixtures re-visited: depletion and the elusive fluid-fluid phase transition* |
| **10:20-10:35** | García-Almarza, N.: *Equilibrios líquido-vapor atípicos en coloides decorados* |
| **10:35-10:50** | Sanz, E.: *Crystallization versus vitrification in hard spheres* |
| **10:50-11:15** | Café |
| **11:15-11:45** | Fernández-Barbero, A.: *Hybrid Systems for Tunable NanoPhotonics* |
| **11:45-12:00** | Rascón, C.: *Phase Transition of a Meniscus in a Capillary under the Influence of Gravity* |
| **12:00-12:15** | Roldán, E.: *Mimicking high-temperature reservoirs for colloidal particles using noisy electric fields* |
| **12:15-12:30** | Romero, J. M.: *Generalización del modelo de Berreman para la energía libre superficial de un cristal líquido nemático en presencia de un sustrato de dientes de sierra* |
| **12:30-12:45** | Santos, M. J.: *Estudio de ángulos de contacto y fuerzas de retención de gotas líquidas sobre superficies inclinadas* |
| **12:45-15:00** | Comida |
| **15:00-17:00** | Paneles 1-70 |
| **16:30-17:00** | Café |
| **17:00-17:50** | Hernando, A.: *Permanent magnetism, in Gold nanoparticles and nanorods* |
| **17:50-18:20** | Sanchez, L. R.: *The complex dynamics of turbulent plasmas of interest for fusion energy* |
| **18:20-18:50** | FISES 25 años |

| Hora | Viernes, 19 de octubre |
|---|---|
| **09:00-09:50** | Maritan, A: *Physics approach to ecosystem dynamics* |
| **09:50-10:05** | von Kameke: *Passive and Active Transport in Turbulent Fluid Flow caused by Faraday Waves* |
| **10:05-10:20** | Casanellas, L.: *Large amplitude oscillatory shear of wormlike micellar solutions: shear-banding and vortex like instabilities* |
| **10:20-10:50** | Serrano, M. A.: *Networks meet Geometry: The S1 model and beyond* |
| **10:50-11:15** | Café |
| **11:15-11:45** | Pazó, D.: *Predictibilidad, Caos Espacio-Temporal, y Mecánica Estadística de No Equilibrio* |
| **11:45-12:00** | Pont, O.: *Microcanonical multifractal analysis of electric potential maps on the heart surface* |
| **12:00-12:15** | Orlandi, J. G.: *The emergence of coherent activity in living neuronal networks* |
| **12:15-12:30** | Lyra, L.: *Towards a statistical mechanics of neurons: The excitable-wave mean-field approximation* |
| **12:30-12:45** | Durán-Olivencia, M. A.: *Un nuevo marco estocástico para la nucleación* |
| **12:45-15:00** | Comida |
| **15:00-17:00** | Paneles 71-138 |
| **16:30-17:00** | Café |
| **17:00-17:50** | Eguíluz, V.: *Opinion dynamics: is the voter model a model for voters?* |
| **17:50-18:05** | Erola, P.: *Modeling international crisis synchronization in the World Trade Web* |
| **18:05-18:20** | Martínez-Vaquero, L. A.: *Prevalencia de la generosidad en reciprocidad directa* |
| **18:20-18:35** | Presentación de la candidatura de Barcelona para Statphys 2016 |

| Hora | Sábado, 20 de octubre |
|---|---|
| **09:30-10:20** | Sagués, F: *Compensation of distinct chiral forces: A proof of concept in soft matter-based self-assembly* |
| **10:20-10:35** | Nicola, E.: *Connecting the nonlinear building-blocks inside the ear with their environment* |
| **10:35-10:50** | Buceta, J.: *Dynamics of the Quorum Sensing Switch: Stochastic and Non-equilibrium Effects* |
| **10:50-11:15** | Café |
| **11:15-11:45** | Pigolotti, S.: *Thermodynamics of biological copying systems* |
| **11:45-12:00** | Formosa, P: *Biological pattern formation: an eye on neurogenic wavefronts* |
| **12:00-12:15** | Sánchez, D.: *Spintronic Fluctuation Relations* |
| **12:15-12:30** | Alemany, A.: *Recent progress in free energy recovery from irreversible pulling experiments* |
| **12:30-12:45** | Perez-Carrasco, R.: *Rotatory Molecular Machines: Dynamics, Power and Efficiency* |
| **12:45-13:00** | Closing |

# Comité científico

- Claudio Cerdeiriña, Universidad de Vigo.
- Rodolfo Cuerno, Universidad Carlos III de Madrid.
- Jordi Garcia Ojalvo, Universitat Politècnica de Catalunya.
- Juan Manuel López, IFCA (CSIC - Universidad de Cantabria).
- Diego Maza, Universidad de Navarra.
- Miguel Ángel Muñoz, Universidad de Granada.
- Ignacio Pagonabarraga, Universitat de Barcelona.
- María José Ruiz, Universidad de Sevilla.
- Andrés Santos, Universidad de Extremadura.
- Raul Toral, IFISC (CSIC - Universitat de les Illes Balears).
- Enrique Velasco, Universidad Autónoma de Madrid.
- Juan Antonio White, Universidad de Salamanca.

# Comité organizador local

- Pere Colet.
- Emilio Hernández-García.
- Manuel Matías.
- Raúl Toral.

# Índice general


**I Conferencias invitadas** **23**

**1.** **Opinion dynamics: is the voter model a model for voters?** **25**
V.M. Eguiluz

**2.** **Binary hard-sphere mixtures re-visited: depletion and the elusive fluid-fluid phase transition** **26**
Robert Evans

**3.** **Hybrid Systems for Tunable NanoPhotonics** **27**
Antonio Fernández-Barbero

**4.** **Permanent magnetism, in Gold nanoparticles and nanorods** **28**
Antonio Hernando

**5.** **Physics approach to ecosystem dynamics** **29**
Amos Maritan

**6.** **Predictibilidad, Caos Espacio-Temporal, y Mecánica Estadística de No Equilibrio** **30**
Diego Pazó

**7.** **Thermodynamics of biological copying systems** **31**
Simone Pigolotti

**8.** **Compensation of distinct chiral forces: A proof of concept in soft matter-based self-assembly** **32**
Francesc Sagués

**9.** **The complex dynamics of turbulent plasmas of interest for fusion energy** **33**
Raul Sanchez

**10.** **Networks meet Geometry: The S1 model and beyond** **34**
M. Ángeles Serrano

**II** **Orales** **35**

**1.** **Recent progress in free energy recovery from irreversible pulling experiments** **37**
Anna Alemany, Felix Ritort

**2.** **Dynamics of the Quorum Sensing Switch: Stochastic and Non-equilibrium Effects** **38**
Javier Buceta, Marc Weber

**3.** **Large amplitude oscillatory shear of wormlike micellar solutions: shear-banding and vortex like instabilities** **39**
Laura Casanellas, C.J.Dimitriou, T.J.Ober, G.H.McKinley, J.Ortín

**4.** **Un nuevo marco estocástico para la nucleación** **40**
Miguel A. Durán-Olivencia, Fermín Otálora

**5.** **Modeling international crisis synchronization in the World Trade Web** **41**
Pau Erola, Albert Díaz-Guilera, Sergio Gómez, Alex Arenas

**6.** **Biological pattern formation: an eye on neurogenic wavefronts** **42**
Pau Formosa-Jordan, Marta Ibañes Miguez, Saúl Ares and José María Frade

**7.** **Equilibrios líquido-vapor atípicos en coloides decorados** **43**
Noé García Almarza

**8.** **Towards a statistical mechanics of neurons: The excitable-wave mean-field approximation** **44**
Leonardo L. Gollo, Osame Kinouchi, Mauro Copelli

**9.** **Prevalencia de la generosidad en reciprocidad directa** **45**
Luis Alberto Martínez Vaquero, José Cuesta, Ángel Sánchez

**10.** **Connecting the nonlinear building-blocks inside the ear with their environment** **46**
Ernesto M. Nicola, D. Ó Maoiléidigh, A.J. Hudspeth

**11.** **The emergence of coherent activity in living neuronal networks** **47**
Javier G. Orlandi, Enric Álvarez-Lacalle, Sara Teller, Jordi Soriano, Jaume Casademunt

**12.** **Rotatory Molecular Machines: Dynamics, Power and Efficiency** **48**
Rubén Pérez-Carrasco, Jose María Sancho

**13.** **Microcanonical multifractal analysis of electric potential maps on the heart surface** **49**
Oriol Pont, Hussein Yahia, Remi Dubois

**14.** **Phase Transition of a Meniscus in a Capillary under the Influence of Gravity** **50**
C. Rascón, A.O. Parry, E.A.G. Jamie, S. Ivell, A. Thorneywork, D.G.A.L. Aarts

**15.** **Mimicking high-temperature reservoirs for colloidal particles using noisy electric fields** **51**
Édgar Roldán, Ignacio A. Martinez, Dmitri Petrov, Juan M. R. Parrondo

**16.** **Generalización del modelo de Berreman para la energía libre superficial de un cristal líquido nemático en presencia de un sustrato de dientes de sierra.** **52**
J. M. Romero-Enrique, O. A. Rojas-Gómez

**17.** **Spintronic Fluctuation Relations** **53**
David Sánchez, Jong Soo Lim, Rosa López

**18.** **Estudio de ángulos de contacto y fuerzas de retención de gotas líquidas sobre superficies inclinadas** **54**
M.J. Santos, J.A. White

**19.** **Crystallization versus vitrification in hard spheres** **55**
Eduardo Sanz, C Valeriani, E Zaccarelli, P N Pusey, W C K Poon, M E Cates

**20.** **Passive and Active Transport in Turbulent Fluid Flow caused by Faraday Waves** **56**
Alexandra von Kameke, F. Huhn, V. Pérez-Muñuzuri, A.P. Muñuzuri

**III Paneles 57**

**1.** **Modeling dynamical T-cell cross-regulation in a mouse model of multiple sclerosis** **59**
Elena Abad, Sara M. Pasamar, Nieves de Mendizábal, Pablo Villoslada y Jordi García-Ojalvo

**2.** **Flocking and coherence emergence on active particle suspensions.** **60**
Francisco Alarcón Oseguera, Ignacio Pagonabarraga Mora

**3.** **A phase-field approach to actin-based motility of lamellar fragments** **61**
Sérgio A. Lira, Carles Blanch-Mercader, Jaume Casademunt

**4.** **Experimental free energy measurements of kinetic molecular states using fluctuation theorems** **62**
Anna Alemany, Alessandro Mossa, Ivan Junier, Felix Ritort

**5.** **Transition State Susceptibility in Single Molecule Force Spectroscopy** **63**
Anna Alemany, Felix Ritort

**6.** **El efecto ratchet en la partícula relativista** **64**
Renato Alvarez-Nodarse, Jose A. Cuesta, N. R. Quintero

**7.** **Modelo con retardo temporal para la infección por Hantavirus** **65**
José María Aparicio Reinoso, Javier de la Rubia

**8.** **Ordinal time-series analysis of low-frequency fluctuations in semiconductor lasers with optical feedback** **66**
Andrés Aragoneses Aguado, Nicolás Rubido, Taciano sorrentino, Maria Carme Torrent, Cristina Masoller

**9.** **Collective modes of coupled phase oscillators with delayed coupling** **67**
Saúl Ares, Luis G. Morelli, David J. Jörg, Andrew C. Oates, Frank Jülicher

**10.** **Optimal oscillator mobility for synchronization arising from the gradual recovery of oscillator coupling** **68**
Saúl Ares, Koichiro Uriu, Andrew C. Oates, Luis G. Morelli

**11.** **Estados hidrodinámicos no estacionarios en el flujo longitudinal uniforme de un gas granular. Cumulantes y función de distribución** **69**
Antonio Astillero, Andrés Santos

**12.** **Avalanches in the 3D-Gaussian Random Field Ising Model** **70**
Jordi Baró, Eduard Vives

**13.** **Structure and fluctuations of adsorbed liquid films closed to a first order wetting transition** **71**
Jorge Benet, Luis G. MacDowell, Eva M. Fernández, Enrique Chacón, Pedro Tarazona

**14.** **Collective migration of cells in spreading epithelia** **72**
Carles Blanch-Mercader, Jaume Casademunt

**15.** **Free energy calculations of molecular inclusions in short capped nanotubes: Targeted molecular Dynamics and Grand Canonical Monte Carlo Calculations** **73**
C. Bores, E. Lomba, H. Dodzyuk, T. Korona

**16.** **Theoretical study of the H-NMR relaxation times in aqueous ionic solutions** **74**
Carles Calero, Elvira Guàrdia, Jordi Martí

**17.** **Force Fields Parametrization of Ion-Water Interactions via the Force Matching Algorithm** **75**
Ausias-March Calvo, Marco Masia, Elvira Guàrdia

**18.** **Affinity measurements of ligands binding nucleic acids using fluctuation theorems** **76**
J. Camunas-Soler, A. Alemany, I. Tinoco Jr., F. Ritort

**19.** **Unraveling the kinetics of aggregation of single peptide-DNA complexes using force spectroscopy** **77**
J. Camunas-Soler, S. Frutos, C.V. Bizarro, S. de Lorenzo,M.E. Fuentes-Perez, R. Ramsch, S. Vilchez, C. Solans, F. Moreno-Herrero, F. Albericio, R. Eritja, E. Giralt, S.B. Dev, F. Ritort

**20.** **Estocasticidad y exclusión competitiva en comunidades ecológicas** **78**
José A. Capitán, Sara Cuenda, José A. Cuesta, David Alonso

**21.** **The role of noise and initial conditions in the asymptotic solution of a continuous opinion dynamics model** **79**
Adrián Carro, Raúl Toral, Maxi San Miguel

**22.** **Stochastic resonance and diversity in an agent-based herding model** **80**
Adrián Carro, Raúl Toral, Maxi San Miguel

**23.** Shape and motility of actin fragments **81**
Jaume Casademunt, Carles Blanch-Mercader

**24.** Phase diagram of a single magnetic filament in bulk, an approach via numerical simulations and theory. **82**
Joan J. Cerdà, Pedro A. Sànchez, Tomas Sintes

**25.** Compressible cell gas models and Yang-Yang critical anomalies **83**
Claudio A. Cerdeiriña, Gerassimos Orkoulas, Michael E. Fisher

**26.** Statisical features of the global velocity of imbibition fronts in disordered media **84**
Xavier Clotet, Stéphane Santucci, Jordi Ortín

**27.** Adler synchronization of spatial laser solitons pinned by defects **85**
Pere Colet, P.V. Paulau, C. McIntyre, Y. Noblet, N. Radwell, W.J. Firth, T. Ackemann, G.-L. Oppo

**28.** Phase Noise Performance of Double-Loop Optoelectronic Microwave Oscillators **86**
Pere Colet, Romain Modeste Nguimdo, Yanne K. Chembo, Laurent Larger

**29.** Clustering of random scale-free networks **87**
Pol Colomer de Simón, Marián Boguñá

**30.** Delay identification in semiconductor lasers with optical feedback **88**
Miguel C. Soriano, Romain Modeste Nguimdo, Pere Colet

**31.** Brownian dynamics and dynamic Monte Carlo simulations of isotropic and liquid crystal phases of anisotropic colloidal particles: a comparative study **89**
Alejandro Cuetos, Alessandro Patti

**32.** Spatiotemporal Bounded Noises in the Ginzburg-Landau model **90**
Sebastiano de Franciscis, Alberto d'Onofrio

**33.** Métodos de discretización para ecuaciones fluctuantes **91**
J. A. de la Torre, P. Español, D. Duque

**34.** Unified model for thermal transport in bulk, thin films and nanowires **92**
C. de Tomas, A. Cantarero, A. Lopeandia, F.X. Alvarez

**35.** Detecting long-range teleconnections in the climate network via ordinal pattern time-series analysis **93**
Juan Ignacio Deza, Marcelo Barreiro, Cristina Masoller

**36.** Cosecha de energía de espectro amplio con osciladores alineales monoestables: mejora con potenciales de paredes finitas y ruidos tipo Lévy **94**
Roberto R. Deza, J. Ignacio Deza, Horacio S. Wio

**37.** Los parámetros mecánicos de la Membrana controlan la Fisión mediada por Dinamina **95**
Luis Dinis, S.Morlot, V.Galli, M.Klein, J.Manzi, F.Humbert,M.Lenz, G.Capello, A.Roux

**38.** Colapso gravitatorio y descomposición espinodal: ¿es lo mismo? **96**
Alvaro Domínguez

**39.** The meaning of niche: Cause or consequence of food-web structure? **97**
Virginia Domínguez-García, Sam Johnson, Miguel A. Muñoz

**40.** Nonlinear methods in modified gravities and the corresponding cosmologies **98**
Emilio Elizalde

**41.** Modeling the interaction of DNA with Terahertz fields **99**
Fernando Falo, Jesús Bergues, Ana Elisa Bergues-Pupo

**42.** Trees as representation of human-like adaptive systems **100**
Miguel Angel Fernandez, Hector Corte, Elka Korutcheva

**43.** Interdependent choices, individual preferences and social influence **101**
Ana Fernández del Río, Elka Korutcheva, Javier de la Rubia

**44.** Characterization of delay propagation in the airport network **102**
P Fleurquin, J.J Ramasco, V M. Eguiluz, M. San Miguel

**45.** Mercados Internacionales de Comercio: una analogía con las redes mutualistas **103**
Maximiliano Fernández, Javier Galeano, Cesar Hidalgo

**46.** Medida de la robustez de redes de polinizacion a partir del k-shell **104**
Javier Galeano, Juan Manuel Pastor

**47.** Evolución temporal de la dinámica de poblaciones en redes mutualistas **105**
Javier García-Algarra, Javier Galeano, Juan Manuel Pastor, José J. Ramasco, José María Iriondo

**48.** **Granular fluids driven by stochastic bath with friction** **106**
M.G. Chamorro, F. Vega Reyes, V. Garzó

**49.** **Ecuaciones fluctuantes de Navier-Stokes para esferas y discos duros inelásticos** **107**
M.I. Garcia de Soria, J.J. Brey, P. Maynar

**50.** **Structure and Thermodynamics of Curved Interfaces** **108**
Jose M. G. Palanco, Victor H. Elvira, Luis G. MacDowell

**51.** **Unzipping DNA at controlled force** **109**
Adan Garriga, Josep Maria Huguet; Fèlix Ritort

**52.** **Logical Operations with Localized Structures** **110**
Damia Gomila, Adrian Jacobo, Manuel A. Matias, Pere Colet

**53.** **Patterns and Domain Walls in Generalized Swift-Hohenberg Dynamics** **111**
Damià Gomila, Daniel Walgraef, Pere Colet, Thorten Ackemann

**54.** **Técnicas numéricas para el estudio del mecanismo de nucleación de burbujas de vapor bajo presiones negativas.** **112**
Miguel Angel Gonzalez , Juan L. Aragones, Chantal Valeriani, Jose Luis F. Abascal

**55.** **A two-component mixture of Janus-like anisotropic sticky hard spheres** **113**
Miguel Ángel G. Maestre, Andrés Santos

**56.** **Simulación del diagrama de fases y autoensamblado de partículas coloidales anisótropasde p** **114**
Eva G Noya, Gunther Doppelbauer, Emanuela Bianchi, Gerhard Kahl

**57.** **2D liquid crystal confined in a square cavity** **115**
Miguel González Pinto, Yuri Martínez-Ratón, Enrique Velasco

**58.** **Hierarchical screening of topological scales in complex networks** **116**
Clara Granell, Sergio Gómez, Alex Arenas

**59.** **Universal reciprocal behavior in iterated prisoner's dilemmas: Three is a crowd** **117**
Jelena Grujic, Burçu Eke, Antonio Cabrales, José A. Cuesta, Angel Sánchez

**60.** **On the Morphology of Turing Instability under Microscopic Transport** **118**
Jacobo Guiu-Souto, Jorge Carballido-Landeira, Alberto P. Muñuzuri

**61.** Statistical Analysis of Investors' Behaviour: Different Temporal Scales **119**
Mario Gutiérrez-Roig, Josep Perelló

**62.** Predicting effects of structural stress in a genome-reduced model bacterial metabolism **120**
Oriol Güell, Francesc Sagués, M. Ángeles Serrano

**63.** Neutron diffraction and computer simulation studies on the plastic phase of C2Cl6 **121**
Andrés Henao, Muriel Rovira-Esteva, Szilvia Pothoczki, Gabriel Cuello, Elvira Guardia, Luis Carlos Pardo

**64.** Biological production and plankton dynamics in a turbulent ocean upwelling system **122**
E. Hernandez-Garcia, I. Hernandez-Carrasco, V. Rossi, V. Garcon, C. Lopez

**65.** Stochastic Amplification of Fluctuations in Neural Networks **123**
Jorge Hidalgo, Luís F. Seoane, Jesús M. Cortés, Miguel Á. Muñoz

**66.** Mixing and transport in chaotic flows analyzed with Lagrangian coherent structures **124**
Florian Huhn, Alexandra von Kameke, Vicente Pérez-Muñuzuri

**67.** Robust Short-Term Memory without Synaptic Learning **125**
Sam Johnson, J. Marro, Joaquín J. Torres

**68.** Threshold phenomenon in the Countdown game **126**
Lucas Lacasa, Bartolo Luque

**69.** Collective effects of heterogeneity and stochasticity in interacting particle systems **127**
Luis F. Lafuerza, Raul Toral

**70.** Large Fluctuations of the Dissipated Energy in a Simple Model System **128**
Antonio Lasanta Becerra, Antonio Prados, Pablo I. Hurtado

**71.** Magnetoasymmetric transport in a quantum dot Aharonov-Bohm interferometer **129**
Jong Soo Lim, David Sanchez, Rosa Lopez

**72.** Lagrangian Coherent Structures in three-dimensional flows **130**
Cristóbal López, Joao B. Bettencourt, Emilio Hernández-García

**73.** **La Estabilidad de los Arcos en un Medio Granular** **131**
Celia Lozano, Iker Zuriguel, Angel Garcimartín, Geoffroy Lumay

**74.** **Spatial correlation of concentration fluctuations in reaction diffusion problems by the Gillespie algorithm** **132**
Jorge Luis Hita, José María Ortiz de Zárate

**75.** **Power Laws and Scaling in the Waiting Time Distribution of Speech** **133**
Jordi Luque, Lucas Lacasa, Bartolo Luque

**76.** **Signal integration shapes the dynamics of neuronal networks** **134**
Leonardo L. Gollo, Claudio Mirasso, Víctor M. Eguíluz

**77.** **A non local spatial model for savannas** **135**
Ricardo Martinez Garcia, Cristobal Lopez

**78.** **A long range interaction model for foragers.** **136**
Ricardo Martinez Garcia, Cristobal Lopez, Justin M. Calabrese

**79.** **A Complex Network Model for Mild Cognitive Impairment Subject Characterization** **137**
Johann Heinz Martínez Huartos, Javier M Buldú, Massimiliano Zanin, Juan Manuel Pastor

**80.** **Synchronization in delayed mutually coupled optoelectronic oscillators** **138**
Jade Martínez-Llinàs, Pere Colet

**81.** **Calculation of surface tension in a confined hard cut spheres liquid crystal using Monte Carlo simulation** **139**
Manuel M Piñeiro, Martín Pérez-Rodríguez

**82.** **Efecto de la polidispersidad y asimetría de partículas oblatas en los diagramas de fases de emulsiones coloidales** **140**
Yuri Martínez Ratón, Enrique Velasco

**83.** **Universal reference state in a driven homogeneous granular gas** **141**
Pablo Maynar, María Isabel García de Soria, Emmanuel Trizac

**84.** **Sobre el oscilador logarítmico como termostato** **142**
Marc Meléndez Schofield

**85.** **El intercambio de energía entre sistemas hamiltonianos desde la teoría del coarse-graining** **143**
Marc Meléndez Schofield, Pep Español Garrigós

**86.** **The evolution of communication ties** **144**
Giovanna Miritello, Rubén Lara, Esteban Moro

**87.** **Stability of Boolean Multiplex Networks** **145**
Yamir Moreno, Emanuele Cozzo, Alex Arenas

**88.** **Simulación multiescala de la formacion de patrones por irradiación** **146**
Ana Moreno Barrado, Mario Castro Ponce

**89.** **Rare region effects in hierarchical networks** **147**
Paolo Moretti, Miguel Angel Munoz

**90.** **Pattern formation of nitrogen fixing cells in filamentous cyanobacteria** **148**
Javier Muñoz-García, Saúl Ares

**91.** **Microscopic tip fluctuations drive the morphology of macroscopic Fisher fronts** **149**
Svetozar Nesic, Rodolfo Cuerno, Esteban Moro

**92.** **A reaction-diffusion system to model symmetry-breaking in the C. elegans worm** **150**
Ernesto M. Nicola, N.W. Goehring, P. Khuc Trong, J.S. Bois, D. Chowdhury, A.A. Hyman, S.W. Grill

**93.** **Image Analysis of the Cavitation Process in Pressure Sensitive Adhesives** **151**
Matteo Nicoli, François Tanguy, Costantino Creton

**94.** **Classical force fields for water from density functional theory based molecular dynamics simulations and force matching algorithm** **152**
Paolo Nicolini, Jonàs Sala, Marco Masia, Elvira Guàrdia

**95.** **Quasiperiodic graphs: structural design, scaling and entropic properties** **153**
Bartolome Luque, Ángel M. Núñez, José Patricio Gómez

**96.** **The role of hydrolysis kinetics on the collective performance of single-headed kinesins** **154**
David Oriola , Jaume Casademunt

**97.** **Spatio-temporal dynamics of cellular decision making** **155**
David Palau-Ortin, Pau Formosa-Jordan, José María Sancho, Marta Ibañes

**98.** **Effects of a defect and drift on dissipative solitons** **156**
Pedro Parra Rivas, Damià Gomila, M.A.Matias, Pere Colet

**99.** Modelling the Self-Assembly of a Model Cationic Surfactant by Lattice Monte Carlo Simulations **157**
Alessandro Patti, Conxita Solans, Javier Burgos

**100.** Self-pulsations, excitability and polarized rogue waves induced by orthogonal optical injection in Vertical-Cavity Surface-Emitting Lasers **158**
Pablo Pérez, Luis Pesquera, Ángel Valle

**101.** Dopant segregation in semiconductor crystal growth due to stochastic g-jitter in microgravity **159**
L. Ramírez-Piscina, X. Ruiz, P. Bitlloch, J. Casademunt

**102.** Resolución de problemas de coherencia mediante redes de consenso **160**
Miguel Rebollo

**103.** Single molecule derivation of base pair free energies in DNA and RNA **161**
M. Ribezzi-Crivellari, C.V. Bizarro, J.M Huguet, F.Ritort

**104.** Fluctuation Relations and Entropy production in a Dual Trap Optical Tweezers Setup **162**
Marco Ribezzi-Crivellari, Felix Ritort

**105.** Estudio del efecto de la temperatura, presión y tipo de catión sobre la estructura flexible de la zeolita RHO mediante técnicas de simulación molecular **163**
Salvador Rodríguez Gómez, Juan José Gutiérrez Sevillano, Sofía Calero Díaz

**106.** Effects of topology on the one-dimensional Kardar-Parisi-Zhang universality class **164**
Javier Rodríguez-Laguna, Silvia N. Santalla, Rodolfo Cuerno

**107.** Viscoelastic properties of vesicles **165**
Guillermo R. Lázaro, Aurora Hernández-Machado, Ignacio Pagonabarraga

**108.** Entropía negativa entre esferas metáticas debida al efecto Casimir **166**
Pablo Rodriguez-Lopez

**109.** Amplitude death in globally coupled chaotic systems with delay **167**
V. M. Rodriguez, M. G. Cosenza

**110.** La corriente promedio en los "rocking ratchets" **168**
Niurka Rodríguez Quintero, Jose A. Cuesta, Renato Alvarez-Nodarse

**111.** Estudio de simulación por ordenador de líquidos iónicos en las cercanías de la transición vítrea **169**
Álvaro Rodríguez Rivas, José Manuel Romero Enrique, Luis F. Rull

**112.** Modeling dynamics of pluripotency in ES cells **170**
Pau Rué, Silvia Muñoz-Descalzo, Fernando Faunes, Alfonso Martinez-Arias, Jordi Garcia-Ojalvo

**113.** Accelerometric nonlinearities in the International Space Station, ISS **171**
Xavier Ruiz, Nuria Saez, Josefina Gavaldà

**114.** Synchronization of moving integrate and fire oscillators with a minimal interaction rule **172**
Oleguer Sagarra, Luce Prignano, Albert Diaz-Guilera

**115.** A new Percus-Yevick equation of state for hard spheres, as derived from the chemical-potential route **173**
Andrés Santos

**116.** Impact of roughness on the entropy of a granular gas in the homogeneous cooling state **174**
Andrés Santos, Gilberto M. Kremer

**117.** Self-organized beat of cilia through the non-equilibrium dynamics of ratchets **175**
Pablo Sartori, V. Geyer, J. Howard, F. Juelicher

**118.** Inhibitory Synaptic Conductances Mediate Transition From Delayed Synchronization to Anticipated Synchronization Between Neuronal Populations **176**
Fernanda S. Matias, Leonardo L. Gollo, Pedro V. Carelli, Mauro Copelli, Claudio R. Mirasso

**119.** Modeling of the mechanical response of solid semicrystalline polymers **177**
Maria Serral Serra, Josep Bonet Avalos

**120.** Defibrillation mechanisms on a one-dimensional ring **178**
A. Simic, J. Bragard, E. M. Cherry, F. H. Fenton, N. Otani

**121.** Random walks on temporal networks **179**
Michele Starnini, Alain Barrat, Andrea Baronchelli, Romualdo Pastor

**122.** Transporte y difusión anómalos de partículas Brownianas en superfícies desordenadas **180**
Marc Suñé Simon, José María Sancho Herrero, Ana Lacasta

**123.** **Experiments on Clustered Neuronal Networks** **181**
Sara Teller, Jordi Soriano

**124.** **Assessing Neuronal Connectivity in Cortical Cultures from Calcium Imaging Signals** **182**
Elisenda Tibau, Jordi Soriano

**125.** **Role of delay in the stochastic birth and death process.** **183**
Raul Toral, Luis F. Lafuerza

**126.** **Study of Fluid Interfaces in Microfluidics** **184**
Claudia Trejo Soto, Ivón Rodríguez Villareal, Aurora Hernández Machado

**127.** **Grid computing for statistical and non-linear physics** **185**
Antònia Tugores, Pere Colet

**128.** **Modeling information diffusion from empirical data** **186**
Paula Tuzón , José J. Ramasco, Víctor M. Eguíluz, Maxi San Miguel

**129.** **Thermodynamic properties and cavitation mechanism of water at negative pressure** **187**
Chantal Valeriani, M.A.Gonzales, J.L.Aragones, J.L.F.Abascal

**130.** **Computer simulation of a 2D liquid crystal confined in a circular cavity** **188**
E. Velasco, D. de las Heras

**131.** **Uso de líquidos iónicos a temperatura ambiente en estructuras metalorgánicas cristalinas para almacenamiento y separación de dióxido de carbono** **189**
José Manuel Vicent Luna, Juan José Gutiérrez Sevillano, Juan Antonio Anta Montalvo, Sofía Calero Díaz

**132.** **Influence of topology in neural networks dynamics** **190**
Paula Villa Martín, Miguel A. Muñoz

**133.** **On the irrationality of consensus in heterogeneous networks** **191**
Daniele Vilone, J. Ramasco, A. Sánchez, M. San Miguel

**134.** **Strong anisotropy in surface kinetic roughening: theory and experiments** **192**
Edoardo Vivo, Matteo Nicoli, Rodolfo Cuerno

**135.** **Noise Induced Phase Transitions and Coupled Brownian Motors: Non Standard Hysteretic Cycles** **193**
Horacio S. Wio

**136.** **Robustness of self-sustained oscillations in complex networks** **194**
Antonio Yáñez Santamaría, Alexandra von Kameke, Alberto Pérez Muñuzuri

**137.** **Synchronization and quantum correlations in networks** **195**
R. Zambrini, G. Manzano, G. Giorfi, F. Galve, P.Colet, E. Hernández-García

**138.** **Synchronization transitions in a growing complex network of Stuart-Landau oscillators** **196**
Jordi Zamora-Munt, Manuel A. Matias, Pere Colet

**IV** **Índice de autores** **198**

**V** **Asistentes al congreso** **206**

# Parte I
# Conferencias invitadas

# Opinion dynamics: is the voter model a model for voters?

Víctor M. Eguíluz*
*IFISC, Instituto de Física Interdisciplinar y Sistemas Complejos (CSIC-UIB)†, 07122 Palma de Mallorca (Spain)*

Mostly due to the similarity with statistical physics models, the study of opinion models has attracted the attention of the community[2,1]. The main questions addressed in this context are whether the opinion models reach consensus, an ordered configuration, or coexistence, that is, disordered configurations, the scaling of the consensus time, and the characterization of the ordering process. With the development of the complex network theory and the description of human activity patterns, opinion models have incorporated more realistic features.

Opinion models aim at capturing plausible mechanisms of social interaction. For example the voter model implements proportional imitation from the neighbors while threshold models requires some degree of consensus in the neighborhood to switch opinion. However, rarely these models have been confronted with empirical observations or experiments mainly due to the lack of results in this direction. So to what extent the rich set of results accumulated are relevant to explain social interactions remains to be explored.

In this talk, we will review the progress made on our understanding of opinion models from a statistical physics perspective, and we will explore the possibilities of the voter model as a model for voters.

---

* victor@ifisc.uib-csic.es
† http://www.ifisc.uib-csic.es/victor

[1] M. San Miguel, V.M. Eguíluz, R. Toral, and K. Klemm, Comput. Sci. & Eng. **7**, 67-73 (2005).
[2] C. Castellano, S. Fortunato, and V. Loreto, Rev. Mod. Phys. **81**, 591-646 (2009).

# Binary hard-sphere mixtures re-visited: depletion and the elusive fluid-fluid phase transition

R. Evans
*H. H. Wills Physics Laboratory, University of Bristol, BS8 1TL, U.K.*

In tackling the statistical mechanics of highly size-asymmetric mixtures it is usually efficacious to integrate out the degrees of freedom of the smaller species to obtain an effective Hamiltonian for the larger species. We describe the results of a set of detailed (classical) density functional theory (DFT) calculations, based on fundamental measure theory, and Monte Carlo simulations, using i) staged particle insertion and ii) the geometrical cluster algorithm, of the effective (depletion) potential between a pair of big hard spheres immersed in a reservoir of much smaller hard spheres. The size disparity is measured by the ratio of diameters $q = \sigma_s/\sigma_b$. We focus on the regime $q < 0.1$ where previous work suggested (metastable) fluid-fluid phase separation might occur. Agreement between DFT and simulation is generally very good for packing fractions of the reservoir up to about 0.35. By calculating the second virial coefficient associated with the effective potential we make new estimates[1] for the onset of this elusive fluid-fluid phase transition. Knowledge of the latter is important for interpreting dynamical observations on colloidal mixtures, such as where in the phase diagram gelation or glassiness might set in.

We also describe recent experimental work[2] on a colloid-polymer mixture studied above the theta temperature of the non-adsorbing polymer (polystyrene).Increasing temperature increases the radius of gyration of the polymer thereby increasing the polymer-colloid size ratio. We find i) onset of gelation occurs very close to the (metastable) fluid-fluid critical point estimated from the Asakura-Oosawa depletion potential and ii) enhancement of the crystallization rate occurs in the neighbourhood of this critical point.

---

[1] 1. D.J.Ashton, N.B.Wilding , R.Roth and R.Evans , Phys.Rev.E. 84, 061136 (2011).

[2] 2. S.Taylor, R.Evans and C.P. Royall , J.Phys.Condens. Matt. (to appear).

# Hybrid Systems for Tunable NanoPhotonics

Antonio Fernández-Barbero
*Group of Complex Fluids Physics and NanoLab, University of Almería, 04120 Almería, Spain.*

Metal nanoparticles exhibit optical properties which differ remarkably from those from bulk materials, one of them being the localized surface plasmon resonance. This phenomenon becomes apparent when an external electromagnetic field incident on a metal nanoparticle induces electron cloud delocalization. Net charge difference on the nanoparticle surface acts as restoring force, producing in the simplest case dipolar oscillation. Optical response is originated from the strong absorption of the metal nanoparticles when the frequency of the electromagnetic field becomes resonant with the coherent electron motion. One of the most challenging problems concerning the photonics of nanoparticles is the possibility of modulating those optical properties through external inputs. In this context, merging of metal-nanoparticle and smart-soft-polymer technologies to make hybrid systems leads to very successful results. In this talk, a set of hybrid nanoparticle systems are first presented, pointing out their main single-particle properties and applications to enhance Raman Spectroscopy. Short-range couplings of metal nanoparticles display intense optical fields concentrated at the interparticle gap, and broad spectral tenability is achieved by simply varying this gap at nanoscale precision. 2D particle arrays have been successfully built through the control of electrostatic and interfacial forces. However, they are dramatically sensitive to the deposition conditions and to the presence of contamination. A simple alternative to those methods bases on the use of tunable mechanical spacers located in between the particles. In this context, smart polymers are excellent candidates to fix those distances, being the particle gap set by the swelling state. We show hybrid Au@PNiPAM core-shell nanoparticles ensembles, thus taking advantage of the intrinsic PNiPAM-polymer temperature-controlled swelling. The thermo-responsive nature of the PNiPAM shells allows high precision and continuous interparticle-gap tuning. Imaging analysis allows accessing the spatial and angular 2D structures. Simple plasma etching removes the polymer, thus releasing the Au cores from the spacer. It results non-invasive to the Au cores and preserves the stability of the 2D Au arrays. Finally, the fabrication of tunable nanovoid photonic surfaces using hybrid particles as template is tacked.

ACKNOWLEDGMENTS This work has been funded by the Spanish Ministerio de Economía y Competitividad/FEDER (project MAT2011-28385), Andalusian Government/FEDER (Project P010-FQM 06104) and EU-COST-Action CM1101.

---

* afernand@ual.es

[1] R.Contreras-Cćeres et al. Adv. Mater.20, 1666 (2008).
[2] R.Contreras-Cćeres et al. Adv.FunctMater.19, 3070 ( 2009).
[3] J. Clara-Rahola et al. J. Chem. Phys. 136, 214903 (2012).
[4] J. Clara-Rahola et al. Nanoscale (print).

# Permanent magnetism, in Gold nanoparticles and nanorods

Antonio Hernando, Patricia Crespo, Francisco J. Recio
*Instituto de Magnetismo Aplicado*
*A6 km.22'5 - Apdo. Correos 155*
*28230 Las Rozas - Madrid*

Gold nanostructures have attracted widespread attention due to their novel optical, electronic and biocompatible properties. They also exhibit a number of remarkable magnetic properties, in sharp contrast with the diamagnetic behaviour characteristic of the bulk material. In particular, thiol capped nanoparticles, 1.5 nm size, have been shown to exhibit ferromagnetic like behaviour. XMCD studies indicate that Au atoms are the magnetic moment carriers.

Using first principle calculations, we consider the bond between thiolate and small Au clusters. Surprisingly, gold thiolate exhibits a dramatic and non-intuitive distribution of charge and spin moment. Our results show that the S-Au bond is such that sulfur does not get charge and an electron is transferred to the sp states of the Au cluster. These sp electrons are almost free in the second gold layer and could orbit and it is these that are responsible for the magnetism.

It is shown that at 0K the sp surface free electrons of Au nanoparticles are distributed within an energy spectrum that may hold a giant orbital magnetic moment. The quantum number that defines the eigenstate is the orbital momentum. When the eigenstate corresponding to the Fermi level is not completely filled the residual orbital moment is of the order of the number of electrons in the band.

# Physics approach to ecosystem dynamics

Amos Maritan
*Dipartimento di Fisica 'G. Galilei', Università di Padova-Italy*

Ecological communities exhibit pervasive patterns and interrelationships between size, abundance, and the availability of resources. Non-equilibrium statistical mechanics is the natural candidate to develop a unified framework for understanding the distribution of organism sizes, their energy use, and spatial distribution. We demonstrate that optimal use of resources, both at the individual and community level, leads to a consistent scaling theory of tropical forest whose prediction agrees with observational data and match perfectly with the scaling behavior of an exactly solvable self-similar model of a forest. The range, over which pure power law behavior is observed, depends on the available amount of resources. The scaling framework can be used for assessing the effects of natural and anthropogenic disturbances on ecosystem structure and functionality.

---

* amos.maritan@pd.infn.it

[1] F. Simini, T. Anfodillo, M. Carrer, J. R. Banavar, and A. M., *Self-similarity and scaling in forest communities*, PNAS, **107**, 7658 (2010).

[2] J. R. Banavar, J. Damuth, A. M., and A. Rinaldo, *Scaling in Ecosystems and the Linkage of Macroecological Laws*, Phys. Rev. Lett. **98**, 068104 (2007).

[3] I. Volkov, J. R. Banavar, , S. Hubbell, A.M, *Patterns of relative species abundance in rainforests and coral reefs*, Nature **450**, 45 (2007).

[4] S. Azaele, S. Pigolotti, J.R. Banavar A. M. *Dynamical evolution of ecosystems*, Nature **444**, 926 (2006).

[5] I. Volkov, J. R. Banavar, , S. Hubbell, A.M, *Neutral theory and relative species abundance in ecology* Nature **424**, 1035 (2003).

[6] Banavar JR, Maritan A, Rinaldo A, *Size and form in efficient transportation networks*, Nature **399** 130 (1999).

# Predictibilidad, Caos Espacio-Temporal, y Mecánica Estadística de No Equilibrio

Diego Pazó*
*IFCA, Instituto de Física de Cantabria*
*CSIC-Universidad de Cantabria, 39005-Santander*

Por todo el mundo los servicios meteorológicos usan, en sus previsiones operativas, la técnica de predicción por conjuntos. Todos los métodos que se engloban dentro de esta denominación emplean la integración numérica de un conjunto de copias del mismo modelo atmosférico (y oceánico) con diferentes condiciones iniciales y/o parametrizaciones. Una razón de su popularidad es que la media del conjunto supera a la predicción determinista basada en una sola condición inicial, y además de ser una técnica eficiente permite asignar probabilidades a distintos eventos futuros.

Los métodos (p. ej. vectores bred o vectores singulares) por los que se selecciona un conjunto de perturbaciones en la condición inicial dependen del centro meteorológico en particular. No existe un método aceptado como óptimo y la construcción del conjunto tiene un tanto de arte. Una razón básica para esta falta de consenso es que a día de hoy aún estamos desarrollando una teoría unificada del crecimiento de perturbaciones en sistemas caóticos extendidos en el espacio, más allá de la amplificación exponencial de perturbaciones infinitesimales inherente al caos.

En esta charla se mostrará como, tomando prestadas las técnicas de la mecánica estadística, se puede construir una teoría general de la dinámica de distintos tipos de perturbaciones en sistemas caóticos extendidos en el espacio. Primeramente se establecerá un marco para los vectores de Lyapunov (perturbaciones infinitesimales). A continuación se demostrará que la teoría puede ampliarse para que incluya los vectores singulares (perturbaciones infinitesimales con máximo crecimiento en un tiempo finito), y los vectores bred (perturbaciones finitas). Veremos que se pueden obtener leyes de escala para los correspondientes exponentes de Lyapunov de tiempo finito y exponentes de Lyapunov de tamaño finito.

Los resultados teóricos obtenidos se fundamentan en los conceptos de universalidad y escalamiento dinámico habituales en el campo del crecimiento de superficies rugosas (como en la ecuación de Kardar-Parisi-Zhang). Es interesante señalar que los resultados de la charla pueden tener implicaciones en otros problemas, aparentemente desconectados, como las matrices aleatorias, el problema del polímero dirigido en un medio desordenado, o la teoría de la probabilidad.

* pazo@ifca.unican.es

# Thermodynamics of biological copying systems

Simone Pigolotti*,[1] and Paolo Sartori
*Universitat Politecnica de Catalunya*
*Edif. GAIA, Rambla Sant Nebridi s/n, 08222 Terrassa (Barcelona)*

Copying information is a fundamental task of biological systems. Examples range from DNA duplication and transcription to translation into a protein. All these operations are performed on the molecular scale and at a finite temperature, so that a finite rate of errors is unavoidable because of thermal fluctuations. Tipical error rates $\eta$ range from $\eta \sim 10^{-4}$ in protein transcription and translation, to $\eta \sim 10^{-10}$ in DNA duplication. What is the lower bound dictated by thermal fluctuations on the error rate? A naive estimate would suggest $\eta \sim \exp(-\Delta F/kT)$ where $\Delta E$ is the binding energy difference between a correct monomer and a wrong one. However, the general picture is slightly more complex.

We consider a case in which the copying bio-machine can be modeled as a three-state system: a blank state $\emptyset$ where no monomer is bound, and two states $r/w$ where the right or wrong monomers are attached. The free-energy landscape is sketched in Fig. 1a. We can see that discrimination can occur in two different ways: via a different energy of the two bound state ($\gamma$ in the figure) or via different kinetic barriers $\delta$ to reach these states.

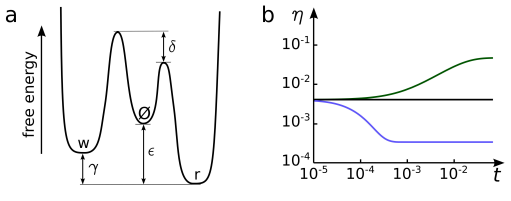


FIG. 1. a) Energy landscape of the three-state model b) error as a function of time in three different cases (green: $\gamma > \delta$, blue: $\gamma < \delta$, black: $\gamma = \delta$.

We study the dynamics of the error $\eta = p_w/(p_r + p_w)$. The short-time error is determined by the barrier $\delta$, while the error at large times is determined by the enrgy difference $\gamma$. This means that if the barrier $\delta$ is large, a small error can be achieved by terminating the reaction before it reaches thermal equilibrium. As shown in Fig. 1b, the error is always a monotonic function, so that it reaches its minimum either at very short or very large times.

What happens if instead of a single base, a long chain has to be copied? We consider a copolymerization model in which a polymerase adds and removes monomers from the copied strand, trying to match a given template. The parameters are the same as in Fig. 1a, only that $\emptyset$ now represent a generic state of the chain, and $r/w$ represent an addition of a right/wrong monomer at the tip.

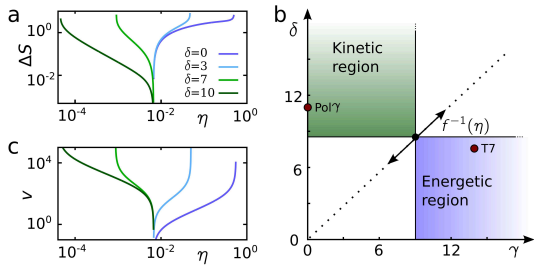


FIG. 2. a) Entropy production per copied base in the copolymerization model as a function of the error $\eta$. In all curves $\gamma = 5$. b) Regions in the $\gamma - \delta$ plane compatible with a given error rate $\eta$ c) Copying velocity.

We calculated the entropy production per copied base (fig. 2a) and copying velocity (fig 2c) of the model as a function of the error rate $\eta$, for different parameter values. For a given choice of the two energies $\delta$ and $\gamma$, the possible values of the error rate are bound from

$$\min\left(\frac{e^{-\delta}}{1+e^{-\delta}}, \frac{e^{-\gamma}}{1+e^{-\gamma}}\right) < \eta < \max\left(\frac{e^{-\delta}}{1+e^{-\delta}}, \frac{e^{-\gamma}}{1+e^{-\gamma}}\right)$$

where energies are in units of $kT$. The above equation naturally defines two disconnected regions (fig. 2b): one where the error is determined by the energy difference $\gamma$ (*energetic discrimination region*) and one where it is defined by the barrier $\delta$ (*kinetic discrimination region*). These two regions correspond to very different biological tradeoffs: in the kinetic region, the minimum error is achieved in a highly dissipative regime where entropy production and velocity both diverge. In the energetic region this limit is adiabatic, and both dissipation and velocity tend to zero.

Comparing this theory with experimentally measured rates of DNA duplication polymerases, we find that a human polymerase, polγ, adopts a kinetic strategy, while a phage, T7, adopts an energetic one. Their estimated values of $\gamma$ and $\delta$ are shown in Fig. 3b. This proves that both strategies can be actually used by biological copying systems. Finally, we discuss how these strategies can be combined in multi-step reactions involving error-correcting steps such as kinetic proofreading.

* simone.pigolotti@upc.edu
[1] `http://www.nbi.dk/ pigo/`
[2] P. Sartori and S. Pigolotti, arxiv/1209.4566.

# Compensation of distinct chiral forces: A proof of concept in soft matter-based self-assembly

F. Sagués
*Departament de Química Física, Universitat de Barcelona*

Chirality, the absence of mirror symmetry, can be equally invoked in relation to physical forces and chemical induction processes, yet a competition between these two types of influences is rarely reported. I will focus on Langmuir monolayers of azobenzene surfactants as a prototypical self-assembled two-dimensional system in which chiral selection is controlled by the combined independent action of a chiral dopant and vortical stirring. The two effects can be arbitrarily coupled, either constructively or destructively, leading to a situation of perfect compensation. The induced enantiomorphic excess is measured in terms of the statistical imbalance of an ensemble of sub-millimeter monolayer domains, where achiral molecules self-assemble with a well-defined orientational chirality, which is unambiguously resolved using Brewster angle microscopy. The observed phenomenon is interpreted in terms of the intervening effect of vortical motion in the dynamics of topological defect recombination and is further modelled in terms of a simple kinetic model.

---

* f.sagues@ub.edu

[1] N. Petit et al., Phys. Rev. Lett. 103, 237802 (2009)
[2] N. Petit et al., Nat. Commun. 3:1001 doi:10.1038/ncomms1987(2012)

# The complex dynamics of turbulent plasmas of interest for fusion energy

Raúl Sánchez*
*Departamento de Física*
*Universidad Carlos III de Madrid 28911-Leganés (Madrid)*

In nature there are many systems that exhibit some form of self-organization from which a priori unexpected structures and dynamical behaviors emerge. These behaviours are unexpected specially when examined in the light of the physical mechanisms that govern each of the individual elements that form the system. Several common ingredients seem to be needed for complex dynamics to emerge: strong nonlinear interactions between many independent elements or degrees of freedom, the presence of instability thresholds, fluctuations and external drives for the system. Examples of complex behaviours can be found in systems like sandpiles[1], solar flares[2], earthquakes, magnetic substorms[3] and even aspects of economics and society itself.

Magnetically confined toroidal plasmas of interest for the production of fusion energy and its conversion into electricity may also exhibit self-organized behavior. Although the underlying equations governing these plasmas are apparently simple, their behavior can be extraordinarily varied and subtle as a result of their extreme susceptibility to the presence of electric and magnetic fields. Complexity in these toroidal plasmas is manifested via the spontaneous formation of interesting spatial structures and complex dynamical behaviors that span a wide range of length and time scales.

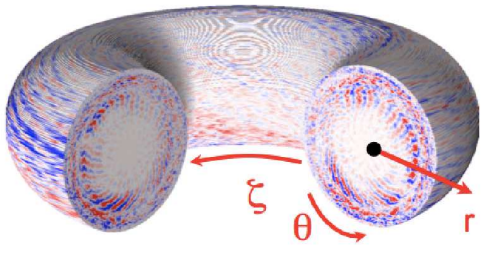


FIG. 1. Gyrokinetic simulation from the UCAN code showing the formation of a strong poloidal zonal flow via the Reynolds stresses in a toroidal plasma and its concomittant action on the radial turbulent structures.

The excitation of poloidal zonal flows by the plasma turbulence via the Reynolds stresses, and the way in which these poloidal zonal flows may control and reduce the leakage of energy and particles out of the toroidal magnetic traps that contain them is one such example (see Fig. 1). In fact, it can be shown that transport across these flows is not only reduced, but its nature suffers a dramatic change in which non-Gaussian, subdiffusive features become important[4]. This has particularly important practical consequences, specially in the era of the next-step $20-billion ITER tokamak experiment actually in construction in the south of France, due to the reliance on strong edge poloidal zonal flows in the standard regime of functioning of this device.

Another regime in which the dynamics of energy confinement in these plasmas is strongly complex is in near-marginal turbulent conditions. By near-marginal, we mean that the local values of temperature and pressure radial gradients wander around their threshold value for the excitation of instabilities. Near-marginality then allows for the formation of strong temporal and spatial correlations imprinted on the plasma profiles that result in strong super-diffusive transport with fat-tailed statistics for the energy distribution of transport events[5,6]. This near-marginal regimes may be of great practical importance in ITER, since turbulence-induced heat fluxes scale with a cubic power of the plasma temperature, what will facilitate the relaxation of unstable profiles below their marginal values quiet rapidly. Thus, understanding the impact of intermittent, superdiffusive transport that will dump its energy on the first wall and divertor parts of tokamaks is quite essential.

In this contribution, the dynamics of these regimes are reviewed and illustrated with the help of experimental results, numerical simulations and theoretical calculations. Some light will be shed on identifying the physical mechanisms that set them in motion. The way in which tools and ideas imported from the so-called 'science of complexity' have helped (and will continue helping) to understand the underlying physics and to thrust the further development of these prototype fusion reactors will also be described in detail. Finally, we will discuss the current efforts towards finding effective mean transport models and equations capable of incorporating these complex dynamics, which require the use of fractional differential operators.

* raul.sanchez@uc3m.es

[1] P. Bak et al, Phys. Rev. Lett. 59, 381 (1987).
[2] E. Lu, R. Hamilton, Astrophys. Journal 380, L89 (1991).
[3] A.J. Klimas et al, J. Geophys. Res. 105, A8 (2000).
[4] R. Sanchez, et al., Phys. Rev. Lett. 101, 205002 (2008).
[5] B.A. Carreras et al, Phys. Plasmas 3, 2903 (1996).
[6] J.A. Mier, et al., Phys. Rev. lett. 101, 165001 (2008).

# Networks meet Geometry: The S1 model and beyond

M. Ángeles Serrano*
*Departament de Física Fonamental*
*Universitat de Barcelona Martí i Franquès 1, 08028 Barcelona*

Hidden geometries underlying real networks appear to provide a simple and natural explanation for their structure[1]. Beyond the ability of these models to simulate the observed topologies, they enable a true cartography of real networks by mapping them to congruent metric spaces using an inverse method. In particular, the euclidean one-dimensional S1 model turns out to be an outstanding paradigm that is able to reproduce the topological properties (including scale-free degree distributions, high levels of clustering, and self-similarity[1]) observed in many real networks. Applications to real networks range from the metabolism of Escherichia coli[2], a bacteria typically found in the human gastrointestinal tract, to the Internet at the autonomous systems level. Besides coupling the topology of networks to geometry by placing the nodes in an underlying geometric space, the model assumes a newtonian-like connection probability such that nodes closer in space –that is, more similar– are more likely to interact and nodes with more connection –that is, more popular– can reach further neighbors. The S1 model has a pure geometric counterpart in terms of hyperbolic space, where the optimization of a certain trade-off between the two dimensions of popularity and similarity has been proved to capture the large-scale growth dynamics of different real networks[3].

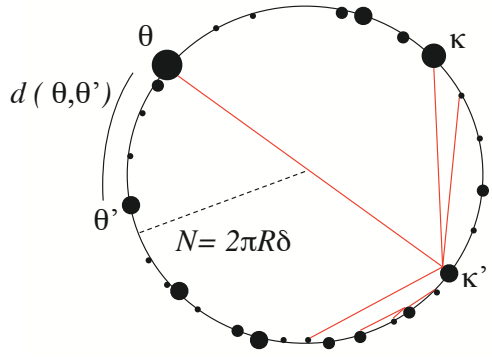


FIG. 1. A sketch of the S1 model. Nodes are randomly distributed in the circle and given expected degrees $\kappa$, symbolically represented by the sizes of the nodes. The distance between two nodes is computed as the length $d(\theta, \theta')$ of the arc separating the nodes. Due to the peculiar rescaling of distances by degrees in the model, a node can connect (red links) not only to nearby nodes but also to far apart nodes with large degrees.

* marian.serrano@ub.edu

[1] M. Á. Serrano, D. Krioukov, and M. Boguñá, Phys. Rev. Lett. 100, 078701 (2008).
[2] M. Á. Serrano, F. Sagués, and M. Boguñá, Mol. BioSyst. 8, 843–850 (2012).
[3] F. Papadopoulos, M. Kitsak, M. Á. Serrano, M. Boguñá, D. Krioukov, Nature, DOI: 10.1038/nature11459.

# Parte II
# Orales

# Recent progress in free energy recovery from irreversible pulling experiments

Anna Alemany[1], Felix Ritort[1,2,*]
*1) Small Biosystems Lab, Departament Física Fonamental, Facultat de Física*
*Universitat de Barcelona, Diagonal 647, 08028 Barcelona (Spain)*
*2) CIBER-BBN, Centre of Bioengineering, Biomaterials and Nanomedicine, ISCIII, Madrid (Spain)*

Fluctuation theorems establish relations governing energy exchange processes in systems in contact with thermal sources, providing new methodologies to obtain equilibrium information from non-equilibrium experiments[1,2]. In this talk I will show new applications to free energy recovery of DNA structures in single molecule experiments using an extended version of Crooks fluctuation relation[3]. New applications extend to free energy recovery of kinetic molecular structures such as intermediate states or misfolded states[4] and protein/peptide nucleic acid binding.

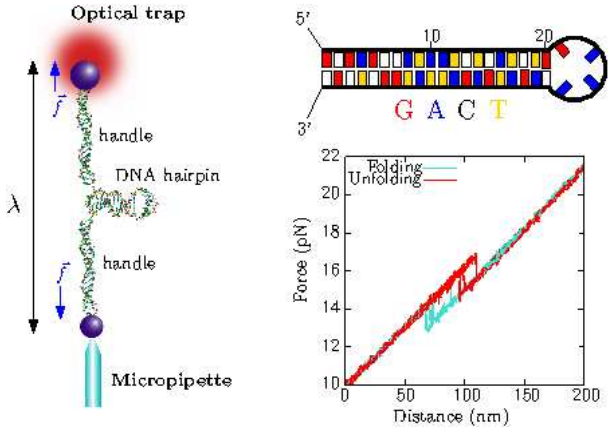


FIG. 1. A 20-bp DNA hairpin is pulled from its 5' and 3' ends using optical tweezers. From the measured irreversible force-distance curves and using the Crooks fluctuation relation it is possible to extract the free energy of formation of the native folded structure. Recently we have extended Crooks relation to extract free energies of more complex molecular structures exhibiting kinetic states[3,4].

* fritort@gmail.com

[1] F. Ritort, *Nonequilibrium fluctuations in small systems: from physics to biology*, Advances in Chemical Physics, **137**, 31-123 (2008). Ed. Stuart. A. Rice, Wiley publications

[2] A. Alemany, M. Ribezzi, F. Ritort, *Recent progress in fluctuation theorems and free energy recovery*, R.Klages, W.Just, C.Jarzynski (Eds.), Nonequilibrium Statistical Physics of Small Systems: Fluctuation Relations and Beyond (Wiley-VCH, Weinheim, 2012; ISBN 978-3-527-41094-1)

[3] I. Junier, A. Mossa, M. Manosas and F. Ritort, *Recovery of free energy branches in single molecule experiments*, Physical Review Letters, **102** (2009) 070602

[4] A. Alemany, A. Mossa, I. Junier and F. Ritort, *Experimental free energy measurements of kinetic molecular states using fluctuation theorems*, accepted in Nature Physics

## Dynamics of the Quorum Sensing Switch: Stochastic and Non-equilibrium Effects

Marc Weber and Javier Buceta *
*Computer Simulation and Modelling (Co.S.Mo.) Lab, Parc Científic de Barcelona, 08028 Barcelona, Spain*

Cells must face the ubiquitous presence of noise at the level of signaling molecules. The latter constitutes a major challenge for the regulation of cellular functions including communication processes. In the context of prokaryotic communication, the so-called quorum sensing (QS) mechanism relies on small diffusive molecules that are produced and detected by cells. This poses the intriguing question of how bacteria cope with the fluctuations for setting up a reliable information exchange. I will present models of gene expression that accounts for the main biochemical processes that describe the QS mechanism. Within that framework we have studied the role that diffusion plays in the regulation of the dynamics and the fluctuations of signaling molecules. In addition, we have unveiled the contribution of different sources of noise, intrinsic and transcriptional, in the QS mechanism. I will show that the interplay between noisy sources and the communication process produces a repertoire of dynamics that depends on the diffusion rate. Importantly, the total noise shows a non-monotonic behavior as a function of the diffusion rate. QS systems seems to avoid values of the diffusion that maximize the total noise. These results point towards the direction that bacteria have adapted their communication mechanisms in order to improve the signal-to-noise ratio and to promote adaptability.

* javier.buceta@pcb.ub.es

# Large amplitude oscillatory shear of wormlike micellar solutions: shear-banding and vortex like instabilities

L. Casanellas[a,b*], C. J. Dimitriou[b], T. J. Ober[b], G. H. McKinley[b], J. Ortín[a†]
[a] *Departament d'Estructura i Constituents de la Matèria*
*C. Martí Franquès 1, Facultat de Física, Universitat de Barcelona*
*08028 Barcelona*
[b] *Hatsopolous Microfluids Laboratory, Department of Mechanical Engineering, Massachusetts Institute of Technology, Cambridge, MA, USA*

The shear rheology of the wormlike micellar solution CPyCl-NaSal (100/60) mM is well described by a viscoelastic Maxwell model at low shear rates but it exhibits strong shear-thinning above a critical shear rate. We experimentally explore the non-linear rheological behaviour of this solution in two different geometries using time-resolved Particle Image Velocimetry (PIV).

In the cone and plate geometry we use a Rheo-PIV device that incorporates the PIV visualization technique into a cone-plate rheometer, providing simultaneously bulk rheological data, represented in terms of Lissajous figures (stress vs. strain), and local velocity fields in the sample. By performing steady shear as well as large amplitude oscillatory shear (LAOS) experiments, we observe the transition from linear to shear banded velocity profiles as we progressively increase the applied shear rate, further into the non-linear regime. The shear banded profiles show three different bands, with two low sheared bands at the boundaries and a highly sheared band at the center[1]. Analogous measurements done with the more diluted, but yet strongly shear-thinning micellar solution CPyCl-NaSal (66/40) mM show qualitatively different steady flow curves and velocity profiles, elucidating the influence of the micellar concentration on the shear-banding formation.

We also make the (100/60) mM solution to oscillate in a vertical straight cylinder of large aspect ratio. We characterize the fluid flow by measuring the velocity and vorticity fields within a meridional plane of the tube. The laminar flow is known to resonate at well defined driving frequencies[2]. For increasing amplitudes of the applied forcing it becomes unstable against the formation of several toroidal vortices distributed along the tube with a well defined spatial and temporal structure. The transition from the laminar to the unstable flow exhibits hysteresis when the forcing amplitude is ramped up and down, elucidating the subcritical nature of the bifurcation. Although this transition occurs well into the non-linear regime, the role of shear banding on the onset of the instability is not yet clear.

* laurac@ecm.ub.es
† ortin@ecm.ub.es

[1] Dimitriou, C.J., Casanellas, L. , Ober, T.J. & McKinley, G.H. 2012. Rheo-PIV of a shear-banding wormlike micellar solution under large amplitude oscillatory shear. *Rheol. Acta* **51**, 395–411.
[2] Casanellas, L. & Ortín, J. 2012. Experiments on the laminar oscillatory flow of wormlike micellar solutions. *Rheol. Acta* in press, DOI 10.1007/s00397-012-0620-3.

# Un nuevo marco estocástico para la nucleación

Miguel A. Durán-Olivencia*, Fermín Otálora
*LEC, Laboratorio de Estudios Cristalográficos*
*IACT, Instituto Andaluz de Ciencias de la Tierra*
*CSIC-Universidad de Granada 18100-Armilla (Granada)*

La primera etapa de una transición de fase, también conocida como etapa de nucleación, ha sido y sigue siendo uno de los retos teóricos de la física estadística. En los últimos años han surgido multitud de resultados experimentales[1–3] que parecen no ajustarse a las teorías clásicas de nucleación (CNT). El marco clásico establece un balance intuitivo que queda descrito mediante una ecuación maestra que resulta ser demasiado compleja para poder ser resuelta analíticamente. No obstante, bajo la asunción de Szilard[4] esta ecuación se convierte fácilmente en una ecuación de Fokker-Planck (FPE) cuyos coeficientes son funciones de las frecuencias de colisión y desorción de monómeros. Una de las magnitudes más empleadas para comprobar la veracidad de la CNT es el tiempo de inducción, i.e. el tiempo requerido para la aparición de un primer agregado crítico. Dicho tiempo ha sido estimado clásicamente mediante el flujo de nucleación calculado desde la termodinámica y posteriormente a través del tiempo medio de escape, considerando la FPE obtenida para el parámetro de orden "tamaño de agregado":

$$\frac{\partial P(N,t)}{\partial t} = \frac{\partial}{\partial N}\left[f(N,t)\frac{\partial \beta\Omega}{\partial N}(N,t) + f(N,t)\frac{\partial}{\partial N}\right]P(N,t)$$

siendo $\Omega$ el potencial de Landau, $f(N,t)$ la frecuencia de colisiones y $\beta = 1/k_BT$. Dicha ecuación también es conocida como ecuación de Zeldovich-Frenkel[5] generalizada por Kashchiev[6]. Nuestro estudio tiene como objetivo describir la ecuación de evolución temporal de la variable $N$, considerando que dicho parámetro de orden se puede entender como un proceso de escape térmicamente activado. En dicho caso, la ecuación de evolución puede postularse como una ecuación de tipo Langevin en presencia de un campo de fuerza:

$$\frac{dN}{dt} = -\frac{1}{\eta(N,t)}\frac{\partial \beta\Omega(N,t)}{\partial N} + \sqrt{\frac{2k_BT}{\eta(N,t)}}\xi(t) \qquad (1)$$

denotando $\eta(N,t)$ la *viscosidad aparente* del eje $N$ y $\xi(t)$ un proceso estocástico tal que $\langle\xi(t)\rangle = 0$ y $\langle\xi(t)\xi(t')\rangle = \delta(t-t')$. En aras de cerrar la ecuación (1) en términos de magnitudes conocidas utilizamos la definición límite del primer coeficiente de Kramers-Moyal y su expresión en función del cálculo estocástico escogido en términos de los coeficientes de la ecuación (1):

$$D^{(1)}(N,t) = \lim_{\tau\to 0}\frac{\langle N(t+\tau) - N(t)\rangle}{\tau} \approx -\frac{1}{\tau_{\leftarrow}} \qquad (2)$$

$$D^{(1)}(N,t) = -\frac{1}{\eta(N,t)}\frac{\partial}{\partial N}\left(\beta\Omega(N,t) - \frac{\alpha}{\beta}\ln\eta(N,t)\right) \qquad (3)$$

donde $\alpha = 0,\ \frac{1}{2},\ 1$ corresponden al cálculo de Itô, Stratonovich y anti-Itô respectivamente, y $\tau_{\leftarrow}$ el tiempo medio necesario para que el tamaño de un agregado se reduzca en una unidad. Aplicando la definición de $\tau_{\leftarrow}$ en función de las frecuencias de colisión y desorción de monómeros, además de la hipótesis de balance detallado, se llega finalmente a la ecuación:

$$\frac{dN}{dt} = -f(N,t)\frac{\partial\Omega(N,t)}{\partial N} + \sqrt{2f(N,t)}\xi(t) \qquad (4)$$

A partir de la ecuación anterior se deduce de manera casi inmediata la ecuación de evolución de la función densidad de probabilidad (PDF):

$$\frac{\partial P(N,t)}{\partial t} = \frac{\partial}{\partial N}\left[f(N,t)\frac{\partial\Omega(N,t)}{\partial N} + (1-\alpha)\frac{\partial f(N,t)}{\partial N} + f(N,t)\frac{\partial}{\partial N}\right]P(N,t) \qquad (5)$$

que incorpora un término adicional con respecto a la teoría clásica salvo en el caso de considerar la imagen de anti-Itô, que es la que asegura el equilibrio térmico[7]. En este trabajo se discutirán las implicaciones de considerar éste y los demás cálculos estocásticos mediante el estudio de los propagadores generalizados para cualquier valor de $\alpha$, observándose que el cálculo de anti-Itô a pesar de asegurar el equilibrio térmico puede conllevar una sobrestimación del flujo de nucleación. A su vez se observa que la nueva FPE (5) contiene la teoría de nucleación deducida recientemente por J.F. Lutsko[8] desde argumentos puramente hidrodinámicos. Por último, en aras de comprobar la validez del modelo Browniano se puede estimar el tiempo medio de escape, usualmente denotado $\tau_{\text{MFPT}}$. Siguiendo el razonamiento de Kramers hemos obtenido una nueva expresión para el tiempo medio de escape que en caso de $\alpha = 1$ concuerda bastante bien con la teoría clásica, demostrando ésto la validez de (3) como descripción del tamaño de agregado a nivel microscópico.

* maduran@lec.csic.es

[1] J.F. Lutsko, Adv. Chem. Phys. **151**, 137 (2012)
[2] D. Gebauer, A. Völkel, H. Cölfen, Science **322**, 1816 (2008)
[3] A.E.S. Van Driessche, L.G. Benning, J.D. Rodriguez-Blanco, M. Ossorio, P. Bots, J. M. García-Ruiz, Science **336**, 6077 (2012)
[4] L. Farkas, Z. Phys. Chem **125**, 236 (1927)
[5] J.B. Zeldovich, Acta Physicochim. URRS **18**, 1 (1943)
[6] D. Kashchiev, Surf. Sci. **18**, 293 (1969)
[7] A.W.C Lau and T.C. Lubensky, Phys. Rev. E **76**, 011123 (2007)
[8] J.F. Lutsko, J. Chem. Phys. **136**, 034509 (2012)

# Modeling international crisis synchronization in the World Trade Web

Pau Erola [†,*], Albert Díaz-Guilera[‡], Sergio Gómez[†] and Alex Arenas[†]
[†] *Departament d'Enginyeria Informàtica i Matemàtiques, Universitat Rovira i Virgili, 43007 Tarragona (Spain)*
[‡] *Departament de Física Fonamental, Universitat de Barcelona, 08028 Barcelona (Spain)*

The study of financial crises has always attracted a fair amount of interest, specially since the bankruptcy of Lehman Brothers in September 2008, but we still know very little about them. Minsky[1] defined financial crises as a natural consequence of changes in the economic cycle and the fragility of the structure of debt. Recent theories of financial fragility link globalization with economic cycles, i.e. when local crises coincide with bad credit regulation and failures in international monetary arrangements. Here we analyze how the effects of globalization can affect the financial crisis spread. To this end, we use the network of international trade (WTW)[2] where we will represent each country economical cycle with a oscillator and the interaction between them will be performed through the commercial channels. We analyze how this synchronization is driven at the mesoscopic scale, by the existence of modules in the network representing stronger associations of trading between certain groups of nations.

WTW is formed by $N$ nodes, one for each country, and $L$ links that correspond to weighted trade flows. To model the economic cycle of each country we associate a Mirollo and Strogatz Integrate-and-Fire oscillator (IFO)[3] to every node. These oscillators are characterized by a monotonic increasing state variable $x \in [0,1]$ that evolves according to a phase $\phi \in [0,1]$. When the variable $x$ of a node attains the threshold $x = 1$ it is said to *fire*, and it is instantly reset to zero, after which the cycle repeats. This node, in turn, transmits to all its neighbors $j$ an excitation signal of magnitude $\varepsilon_{ij} > 0$, thus leaving their state variables with value $x_j^+ = x_j + \varepsilon_{ij}$, or 0 if node $j$ also fires.

When a nation *fires*, it propagates the problem to other countries by boosting their own evolution to a crisis. WTW presents a large diversity in the economic weights, and it is reasonable to think that a shock in a small country is not spread to a large country with the same intensity than vice versa. To reflect this dependence we set the excitation signal of node $i$ to its neighbors $j$ as

$$\varepsilon_{ij} = \frac{w_{ji}}{s_j^{\text{out}}}\,, \tag{1}$$

which is the fraction of total exports of country $j$ going to the firing node $i$.

To simulate this system we have choosen two snapshots of the WTW network belonging to the pre-globalization period (1970) and to the globalization period (2000). To evaluate the interaction dynamics, we follow the classical analysis of the order parameter $r$ that indicates the degree of synchronization of the system. In our setup, synchronization will reflect the scope of the crisis at the international level. The order parameter, which only depends on the phases $\phi_j$ of the oscillators, is

$$r = \left| \frac{1}{N} \sum_{j=1}^{N} e^{2\pi i \phi_j} \right| . \tag{2}$$

In Fig. 1 we show the comparison of the results of $r$ of the WTW in front of that of each community of the network ($r_\alpha$). The dispersion along the diagonal shows the discrepancies between the mesoscopic view and the global view. In 2000 the signs of globalization are clear, the dynamic effect of the mesoscopic structure is practically collapsed to the global world scale behavior. These observations allow us to conjecture that the effect of topological borders of the communities have almost no effect after globalization emerges.

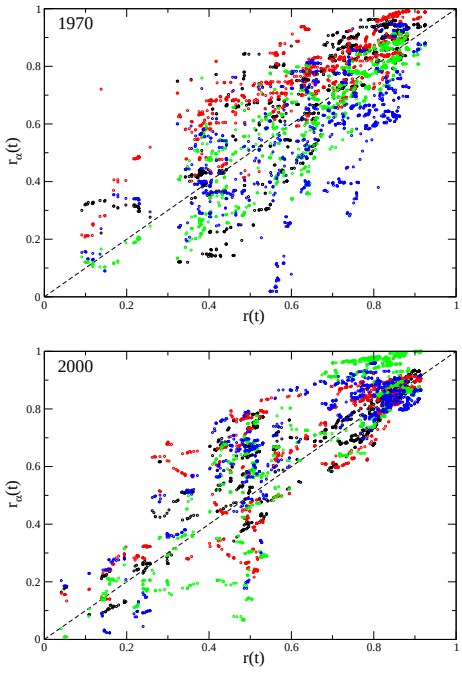


FIG. 1. Deviation of the synchronization of the communities $r_\alpha$ in front of the global $r$. Colors correspond to the communities found by modularity maximization[4].

* pau.erola@urv.cat

[1] Minsky, Jerome Levy Economics Institute, Working Paper **74** (1992).
[2] Gleditsch, J. Conflict Resolut., **46** (2002), 712–724.
[3] Mirollo and Strogatz, SIAM J. Appl. Math., **50** (1990), 1645–1662.
[4] `http://deim.urv.cat/~sgomez/radatools.php`

# Biological pattern formation: an eye on neurogenic wavefronts

Pau Formosa-Jordan* [1,2], Marta Ibañes Miguez[1], Saúl Ares [2,3] and José María Frade[4]
[1] *Departament d'Estructura i Constituents de la Matèria, Facultat de Física, Universitat de Barcelona, Spain*
[2] *Max Planck Institute for the Physics of Complex Systems, Dresden, Germany*
[3] *Logic of Genomic Systems Laboratory, Spanish National Biotechnology Centre CNB-CSIC, Madrid, Spain; and GISC*
[4] *Instituto Cajal, CSIC, Madrid, Spain*

Pattern formation is an essential part of embryonic development. When an organism develops, cells become distinct from each other creating robust patterns. Neurogenesis is an example of such a process in which individual cells single out to become neurons from a group of equivalent progenitor cells.

Pattern formation during neurogenesis has two features that strongly differ from those common in Physics pattern formation processes: it drives a spatially discrete fine-grained pattern (composed of two cell types) and it does not involve any transport of a chemical but just short-range cell-to-cell communication. In addititon, pattern formation during neurogenesis often does not occur through pattern nucleation at different spatial locations or through spontaneous propagation over a less stable state. Instead, the neurogenic pattern grows regularly from a single expanding domain (Fig. 1) and its spreading is both externally and internally regulated. Pattern expansion requires a diffusing molecule (morphogen) that enables the dynamics of patterning to occur and whose production is, in turn, controlled by the pattern itself. Note that this morphogen is not involved itself in the pattern formation. This scenario is what we call a self-regulated wavefront.

How this propagation and the pattern left behind depend on the state of the invaded tissue? We have addressed this question combining both theory and experiments[1]. First, we have provided evidence of the molecular state of the invaded tissue in the vertebrate embryonic retina. Second, we have evaluated computationally the implications of such a state. To this end, we have modelled the neurogenic wavefront in terms of four variables: the morphogen, two variables that set the spatial interaction between cells, and a fourth variable that is a readout of the state of differentiation. Since this process is the result of biochemical interactions, we have extended our description to Langevin dynamics in which a multiplicative noise takes into account the intrinsic randomness of such reactions. Finally, we have also included the irregular shape and arrangement of cells in tissues.

Our results predict that a change in the state of the invaded tissue from the normal wild type conditions strongly alters pattern formation and wavefront propagation, frequently yielding irregular growing patterns. These results are consistent with previous experimental observations[2] and provide a potential explanation. Moreover, we have extended our conclusions to the context of neurogenesis in the fruit fly's eye, by first mimicking computationally experimental data previously reported[3].

Altogether, our work exemplifies the complexity of biological pattern formation and the benefit of using hybrid computational-experimental strategies.

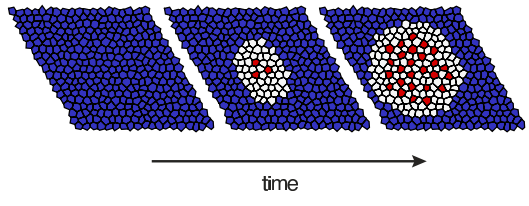


FIG. 1. Snapshots from simulation results, showing a growing pattern of different cell types, mimicking the neurogenic wavefront in the vertebrate eye. Red cells are newly differentiated neural cells, white cells have the potential to commit to the neural fate, and blue cells correspond to non-neural tissue invaded by the neurogenic wavefront.

* pformosa@ecm.ub.es

[1] P. Formosa-Jordan, M. Ibañes, S. Ares and J.M. Frade. *Development*, in press.
[2] S.F. Rocha, S.S. Lopes, A. Gossler, and D. Henrique. *Dev. Biol.* **328**, 54 (2009).
[3] N.L. Brown, C.A. Sattler, S.W. Paddock and S.B. Carroll. *Cell* **80**, 879 (1995).

# Equilibrios líquido-vapor atípicos en coloides decorados

Noé G. Almarza*
*Instituto de Química-Física Rocasolano*
*Consejo Superior de Investigaciones Científicas*
*C/ Serrano 119, E-28006 Madrid*

Los recientes avances en la preparación de partículas coloidales a cuyas superficies se incorporan centros de interacción *enlazantes* están abriendo un interesante campo de estudio de la química-física supramolecular.[1,2] Resulta de gran interés, tanto teórico como práctico, el análisis del efecto del número y de la topología de los citados centros de interacción sobre el diagrama de fases de estos sistemas.[1,2] Por otra parte, el alto grado de direccionalidad de las interacciones presentes en los correspondientes modelos, así como el hecho de que las interacciones energéticas involucradas en la formación de fases condensadas sean mucho mayores que la energía térmica plantean interesantes retos desde el punto de vista de la simulación *molecular*.

Los modelos de partículas coloidales esféricas decoradas con dos tipos de centros de interacción ($A$ y $B$) son particularmente interesantes[3]. Jugando con el número de centros de cada tipo, tamaños, distribución sobre la superficie de la esfera, e interacciones, pueden obtenerse distintos mecanismos de autoensamblado y diagramas de fase peculiares.

Uno de los resultados más sorprendentes es la aparición de los denominados líquidos *vacios* (*empty* liquids)[2,4–6]. En estos sistemas la densidad de una fase líquida, en equilibrio termodinámico con su vapor, puede disminuir con la temperatura, (FIG. 1) alcanzándose a bajas temperaturas densidades del líquido anormalmente bajas (típicas de aerogeles).

En esta contribución se presentarán resultados de simulación mediante métodos de Monte Carlo de modelos primitivos (en el continuo y sobre redes regulares) que ilustran la física subyacente a la aparición de diagramas de fases con distintas topologías.

Los modelos considerados representan partículas coloidales esféricas cuya superficie contiene dos zonas con características físico-químicas bien diferenciadas. Estas zonas se corresponden por una parte con dos centros de interacción (tipo A), y por otra con el resto de la superficie (zona de tipo B). Las interacciones entre pares de partículas son de corto alcance y dependen de las zonas de la superficie de las esferas que son atravesadas por el segmento que une los centros de las partículas.

Dentro de este marco, se mostrará como una adecuada selección de los parámetros de los modelos permite obtener distintos diagramas de fase. En concreto se considerarán los siguientes casos:

(a) Equilibrios líquido-vapor con fases líquidas presentando propiedades de líquidos vacios, mediante modelos en red y en el continuo.

(b) Formación de fases con orden orientacional[7–9], incluyendo fases nemáticas, originadas por la presencia de *moléculas* elongadas formadas por procesos de autoensamblado de partículas coloidales, considerándose modelos en red y en el continuo.

(c) Finalmente, considerando sistemas monocomponente, se discutirá la posibilidad de encontrar diagramas de fase líquido-vapor reentrantes, en los que la coexistencia de fases aparece acotada entre dos temperaturas (temperaturas crítica inferior y superior).

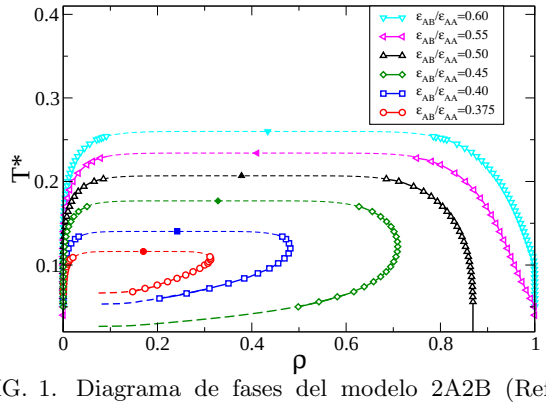


FIG. 1. Diagrama de fases del modelo 2A2B (Ref. 6) definido sobre una red bidimensional cuadrada

* noe@iqfr.csic.es

[1] F. Sciortino, Collect. Czech. Chem. Commun. **75**, 349 (2010).
[2] F. Sciortino and E. Zaccarelli, Current Opinion in Solid State and Materials Science, **15**, 246 (2011).
[3] J.M. Tavares, P.I.C. Teixeira, and M.M. Telo da Gama, Phys. Rev E **80**, 021506 (2009).
[4] J. Russo, J.M. Tavares, P.I.C. Teixeira, M.M. Telo da Gama, and F. Sciortino, J. Chem. Phys. **135**, 034501 (2011).
[5] J. Russo, J.M. Tavares, P.I.C. Teixeira, M.M. Telo da Gama, and F. Sciortino, Phys. Rev. Lett. **106**, 085703 (2011).
[6] N.G. Almarza, J.M. Tavares, M. Simões, and M.M. Telo da Gama, J. Chem. Phys. **135**, 174903 (2011).
[7] N.G. Almarza, J.M. Tavares, and M.M. Telo da Gama, Phys. Rev. E **82**, 061117 (2010);
[8] N.G. Almarza, J.M. Tavares, and M.M. Telo da Gama, J. Chem. Phys. **134**, 071101 (2011).
[9] N.G. Almarza, J.M. Tavares, and M.M. Telo da Gama, Phys. Rev. E **85**, 053102 (2012).

# Towards a statistical mechanics of neurons: The excitable-wave mean-field approximation

Leonardo L. Gollo*, Osame Kinouchi†, Mauro Copelli‡
*IFISC, Instituto de Física Interdisciplinar y Sistemas Complejos*
*CSIC-Universidad de las Islas Baleares 07122-Palma de Mallorca, Spain*

Most neurons present cellular tree-like extensions known as dendrites, which receive input signals from synapses with other cells. Some neurons have impressive dendritic arbors [as illustrated in Fig. 1 (a)], and exhibit dendritic excitability through the expression of a variety of voltage-gated ion channels. Why neurons have such elaborated spiking dendrites?

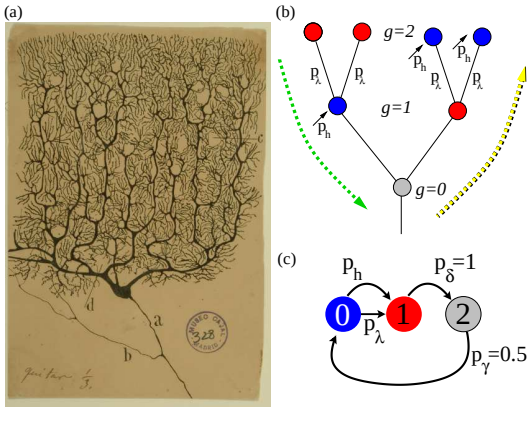


FIG. 1. Model of an active dendritic tree. (a) A famous drawing by Ramon y Cajal of a human Purkinje cell. (b) Excitable elements (circles) connected (bars) in a Cayley tree topology with G = 2 layers and coordination number z = 3 (one mother and two daughter branches). Dendritic branchlets are driven by independent Poisson stimuli (small arrows). (c) Each dendritic branchlet can be in one of three states: quiescent (0), active (1) or refractory (2).

Dendrites have been studied for decades, but the field of *dendritic computation* is still in its infancy. Since the dendritic arbor and its synapses are always suffering spatio-temporal restructuring, one major theoretical goal is to propose reliable computations that do not depend on an exact tree morphology, static synaptic density or fine details of dendritic branchlets. A robust and recently proposed function for active dendritic trees is to enhance the neuronal dynamic range[1], which measures the range of incoming stimulus intensity giving rise to distinguishable neuronal response. However, most of the insights for such proposal were gained based on numerical simulations and a few experimental data. A formal mathematical attempt to tackle the problem was still missing.

We analytically study the input-output properties of a neuron whose active dendritic tree, modeled as a Cayley tree of excitable elements, is subjected to Poisson stimulus, see Fig. 1 (b) and (c). Traditional mean-field approaches, single-site (1S) and two-site (2S) mean-field approximations, incorrectly predict a phase transition which is not allowed in the model. We introduce a new excitable-wave (EW) mean-field approximation, which keeps track of the direction of propagation of the excitable waves, thus reproducing the main results of the model[2]. As shown in Fig. 2, the novel EW mean-field approximation correctly describes the dynamic range ($\Delta$) of the dendritic arbor for any probability of propagation of excitation from branchlet to branchlet ($p_\lambda$).

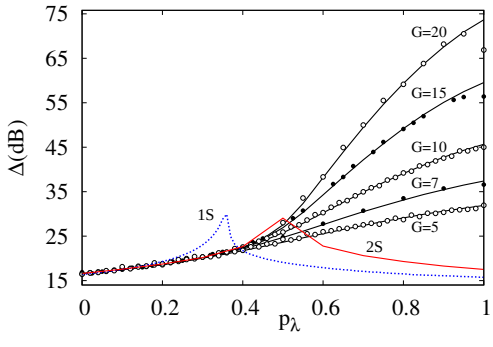


FIG. 2. Dynamic range as a function of the coupling parameter for 1S (G = 10), 2S (infinite tree), EW (black lines) mean-field approximations compared to simulations (open and closed symbols) for different trees sizes G.

Based in properties of the excitable media, the active dendritic trees analogically perform non-linear signal transformations that generate robust and efficient computations. Both simulations and analytical treatments of excitable trees enable the test of several hypothesis and the comparison with experiments in the area of dendritic computation.

* leonardo@ifisc.uib-csic.es
† Faculdade de Filosofia, Ciências e Letras de Ribeirão Preto, Universidade de São Paulo, Ribeirão Preto, SP, Brazil.
‡ Departamento de Física, Universidade Federal de Pernambuco, Recife, PE, Brazil.

[1] L. L. Gollo, O. Kinouchi, and M. Copelli, PLoS Comput. Biol. 5, e1000402 (2009).
[2] L. L. Gollo, O. Kinouchi, and M. Copelli, Phys. Rev. E 85, 011911 (2012).

# Prevalencia de la generosidad en reciprocidad directa

Luis A. Martinez-Vaquero*, José A. Cuesta, Angel Sánchez
*Grupo Interdisciplinar de Sistemas Complejos (GISC)*
*Departamento de Matemáticas, Universidad Carlos III de Madrid*
*Avda. de la Universidad 30, 28911 Leganés, Madrid*

La reciprocidad directa es uno de los mecanismos que más a menudo promueve la cooperación en sistemas sociales y biológicos[1,2]. En Teoría de Juegos la reciprocidad directa se modela a través de juegos repetidos. En ellos, los jugadores interactúan un número indefinido de veces basando sus decisiones en sus actuaciones previas. En este trabajo abordamos un estudio evolutivo de la reciprocidad directa como se manifiesta a través de juegos repetidos.

Como en la mayoría de los trabajos, nuestro estudio[3] considera juegos de dos jugadores, cada uno de los cuales pueden optar entre dos opciones diferentes: colaborar o defraudar (los denominados "juegos simétricos $2 \times 2$"). Los pagos que recibe cada jugador en cada ronda dependerán de si ambos colaboran, ambos defraudan o uno colabora y el otro defrauda, existiendo así cuatro posibles valores. Dos de ellos se pueden fijar sin pérdida de generalidad, por lo que los juegos vendrán parametrizados por los otros dos.

Para tomar su decisión consideraremos únicamente estrategias que vienen caracterizadas por cuatro probabilidades, definidas como las probabilidades de colaborar en función de las cuatro posibles combinaciones de acciones de la ronda anterior. Estudios previos[4] muestran que las más importantes son las estrategias *casi* puras, es decir, aquellas cuyas probabilidades toman los valores $\epsilon$ o $1-\epsilon$, en el límite en el que $\epsilon \to 0^+$. De esta manera tenemos un total de 16 diferentes estrategias. Es posible calcular el pago en el estado estacionario que recibe cada una de estas estrategias al enfrentarse a otra cualquiera de ellas, describiendo el proceso iterado como una cadena de Markov.

Para estudiar la estabilidad de estas estrategias se ha procedido a invadir cada una de ellas con todas las restantes, para lo cual se han reemplazado 10 individuos (mutantes) de los 1000 que formaban la población residente. La dinámica procede eligiendo dos jugadores al azar y enfrentando sus estrategias, de tal forma que la probabilidad de que uno de los jugadores adopte la estrategia del otro es proporcional a la diferencia de pagos que ambos reciben. Este proceso es repetido hasta que la población llega a un equilibrio estable, a saber, la prevalencia de la estrategia residente, de la mutante o a un equilibrio mixto de ambas. Los equilibrios mixtos que nacen de este proceso son también invadidos de la misma forma por las estrategias puras. Ya que estos procesos son estocásticos, para cada invasión se han llevado a cabo 100 realizaciones diferentes.

Los resultados de estas invasiones pueden representarse utilizando grafos dirigidos y pesados, cuyos vértices son los distintos equilibrios obtenidos y cuyos enlaces unen la comunidad invadida con la comunidad resultante tras la invasión, llevando como peso la probabilidad de que tal transición ocurra y como etiqueta la estrategia invasora que causa dicha transición. Analizando los grafos resultantes como cadenas de Markov se pueden identificar conjuntos recurrentes que indican qué estrategias acaban dominando en el proceso.

Los resultados obtenidos muestran que, para un amplio espectro de juegos, las estrategias denominadas *win-stay, lose-shift* son dominantes. Los jugadores que siguen estas estrategias repiten la misma acción que llevaron a cabo en la ronda anterior si el pago que obtuvieron tras dicha ronda es mayor que un determinado nivel de aspiración y cambian de acción si es inferior. Así, existen estrategias *win-stay, lose-shift* modestas, equilibradas y ambiciosas, definidas por el nivel de aspiración. Se ha comprobado que las ambiciosas nunca son evolutivamente estables. Por otro lado, también se ha observado la importancia de incluir los equilibrios mixtos surgidos de los procesos de invasiones. Estos equilibrios dominan algunos de los juegos y tienen influencia en otros muchos.

---

* luisalberto.martinez@uc3m.es

[1] R. Axelroad, *The Evolution of Cooperation* (Basic Books, New York, 1984).
[2] M. Nowak, *Five rules for the evolution of cooperation*, Science **314**, 1560–1563 (2006).
[3] L.A. Martinez-Vaquero, J.A. Cuesta, A. Sanchez, *Generosity Pays in the Presence of Direct Reciprocity: A Comprehensive Study of* $2\times2$ *Repeated Games*, PLoS ONE 7, e35135 (2012)
[4] M. Nowak, *Evolutionary Dynamics* (The Belknap Press of Harvard University Press, Cambridge, 2006).

# Connecting the nonlinear building-blocks inside the ear with their environment

Ernesto M. Nicola[†*], Dáibhid Ó Maoiléidigh[‡] and A.J. Hudspeth[‡]
[†] *IFISC, Instituto de Física Interdisciplinar y Sistemas Complejos CSIC-Universidad de las Islas Baleares 07122-Palma (Mallorca)*
[‡] *Howard Hughes Medical Institute and Laboratory of Sensory Neuroscience, The Rockefeller University, New York, NY 10065-6399, USA*

Receptor cells in each sensory system convert different types of energy into an electrochemical nerve impulse which can be processed by the brain. In the case of hearing this transduction is performed by the *hair cells*. These receptor cells are responsible for the conversion of mechanical movements (air's vibrations) into an electrical signal (see Fig 1). The hair cell's mechano-electrical transduction process is highly non-linear and has been experimentally characterized only during the last few years[1]. Hair cells should amplify the incoming (mechanical) signal in order to distinguish it form background noise. This amplification process results in the exquisite capabilities of the auditory system[1,2]. Consequently, it can be said that the hair cells are the nonlinear building-blocks of the ear.

In the last few years a small number of mathematical models have been proposed that describe the transduction process occurring in the hair-cells[1,2]. Those models are rather complicated and include many parameters with poorly known values. Moreover, the analysis of those models has relayed only on numerical simulations. In this work we characterize the dynamics of these models and show that they are all topologically equivalent (see Fig. 2). We also propose a simpler mathematical model describing the dynamics of the hair-cells. This *minimal model* arises form a simplified description of the main biophysical processes taking place inside the hair-cell bundles. We showed in a recent publication in PNAS[3] that the dynamics of the minimal model can be treated analytically to a large degree and that it is very rich. Furthermore, the dynamics of the minimal model is topologically equivalent[3] to the other, more complex, models (see Fig. 2).

Hair cells in the auditory, vestibular, and lateral-line systems of vertebrates receive inputs through a remarkable variety of accessory structures that impose complex mechanical loads on the mechanoreceptive hair bundles. Although the physiological and morphological properties of the hair bundles in each organ are specialized for detecting the relevant inputs, we suggest that the mechanical load on the bundles also adjusts their responsiveness to external signals.

We augment the minimal model to explore how the mechanical environment can regulate a bundle's innate behavior and response to input[3]. We find that an unloaded hair bundle can behave very differently from one subjected to a mechanical load. Depending on how it is loaded, a hair bundle can function as a switch, active oscillator, quiescent resonator, or low-pass filter. Moreover, a bundle displays a sharply tuned, nonlinear, and sensitive response for some loading conditions and an untuned or weakly tuned, linear, and insensitive response under other circumstances. Our simple characterization of active hair-bundle motility explains qualitatively most of the observed features of bundle motion from different organs and organisms[3].

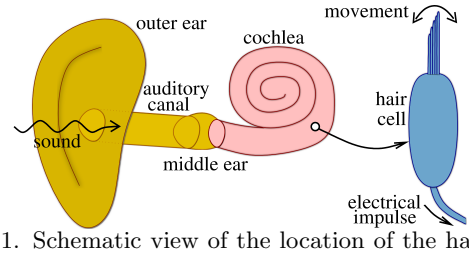


FIG. 1. Schematic view of the location of the hair cells in the inner ear and the mechano-electrical transduction process.

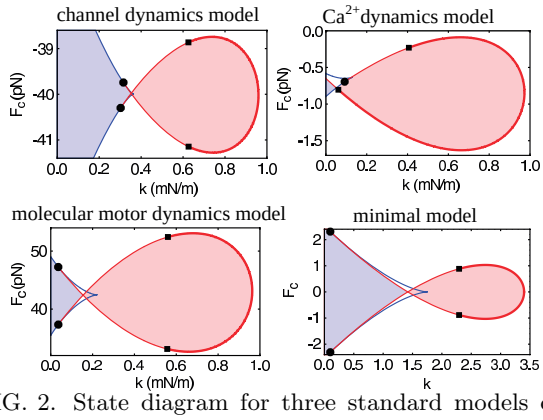


FIG. 2. State diagram for three standard models of the hair cell and our minimal model. Note that all four models are qualitatively equivalent. In the horizontal axis the stiffness is plotted and in the vertical the external force applied in the hair bundle. In the red areas the system oscillates spontaneously and in the blue ones it behaves as a bistable switch.

* ernesto.nicola@ifisc.uib-csic.es

[1] A.J. Hudspeth, *Making an Effort to Listen: Mechanical Amplification in the Ear*, Neuron **59**, 530 (2008)
[2] Martin, in *Active Processes and Otoacustic Emission*, Manley, Fay and Popper Eds., Springer (2007)
[3] D. Ó Maoiléidigh, E.M. Nicola and A.J. Hudspeth, *The diverse effects of mechanical loading on active hair bundles*, **Proc. Natl. Acad. Sci. USA, 109**, 1943-1948 (2012).

# The emergence of coherent activity in living neuronal networks

Javier G. Orlandi[1*], Enric Álvarez-Lacalle[2], Sara Teller[1], Jordi Soriano[1] and Jaume Casademunt[1]
[1] *Departament d'Estructura i Constituents de la Matèria, Universitat de Barcelona, Barcelona, Spain*
[2] *Departament de Física Aplicada, Universitat Politècnica de Catalunya, Barcelona, Spain*

How collective, spontaneous activity emerges in neuronal networks is a fundamental problem both in neuroscience and in statistical physics. It is the ultimate paradigm of complex emergent behavior. Unraveling the mechanisms behind the emergence of spontaneous activity is key to understand more complex phenomena like brain rythms, retinal waves, epileptic seizures and synchronization and communication of distant brain areas[1].

In recent years, the study of well controlled in vitro neuronal cultures as simple model systems of neuronal tissues has emerged as a fruitful complementary approach. The fact that relatively simple neuronal cultures already exhibit rich patterns of activity makes them particularly appealing in the search of general physical organization principles behind collective behavior of neurons.

When neurons are left to grow freely *in vitro*, they create their own network of connections and spontaneouslly reach a coherent state of collective firing in a pattern of nearly periodic giant bursts[2,3] (Fig 1). By combining high-resolution calcium fluoresence imaging with modelling *in silico*, we show that this behavior is controlled by the propagation of waves that nucleate randomly within a set of points that is specific to each culture. Stochastic nucleation is made consistent with highly periodic bursting by the phenomenon of *noise focusing*, a form of implosive avalanche dynamics in integrate-and-fire networks that provides an ultra-fast nucleation mechanism. The resulting scenario challenges previous understanding of spontaenous activity of neuronal cultures while providing a quantitative explanation of the early stages of network self-organization as a noise-driven phenomenon.

Experimentally we studied the initiation and propagation of spontaneous activity in primary cultures of rat cortical neurons. We used high-speed calcium fluorescence imaging to resolve the sequence of neuronal activiation with high spatial ($\mu m$) and temporal ($5ms$) resultion. We were able to resolve the temporal sequence of ignition of each neuron and identify those that initiated the activity. The analysis showed that activity starts in a confined group of neurons and later propagates steadily through all the culture. The analysis also showed that prefered ignition zones exist in the culture. We were also able to resolve the statistics of the probability of nucleation in different sites of the culture.

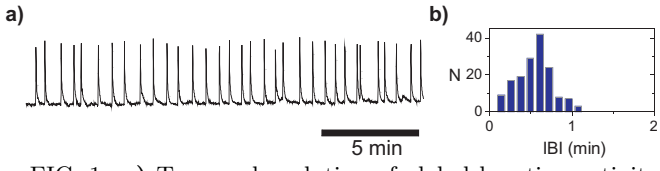


FIG. 1. **a)** Temporal evolution of global bursting activity through calcium imaging (fluorescence intensity in a.u.). **b)** Histogram of the interburst interval (time between two consecutive global bursting events).

Through *in silico* modeling we were able to identify the key factors behind the emergence of spontaneous activity in neuronal cultures. A new mechanism of directed noise amplification which we call *noise focusing* is responsible for the observed behavior. The observed spontaneous activity is a result of a cyclic sequence of: (i) an implosive phase (noise focusing); (ii) an explosive phase (activity propagation); and (iii) a silent phase of network recovery. The bursts appear nearly periodic because steps (i) and (ii) are much faster than (iii). The fast nucleation (i) however, is a nontrivial step that challenges simple statistical analysis, and tracks down novel insights into the interplay between topology and dynamics in directed networks.

---

* orlandi@ecm.ub.es

[1] A. G. Blankenship and M. B. Feller, Nat. Rev. Neurosci. **11**, 18-29 (2010).
[2] J. P. Eckmann , O. Feinerman, L. Gruendlinger, E. Moses, J. Soriano and T. Tlusty, Phys. Rep., **449**, 54 (2007).
[3] J. Soriano, M. Rodríguez Martínez, T. Tlusty and E. Moses, Proc. Natl. Acad. Sci. USA, **105**, 13758 (2009).

# Rotatory Molecular Machines: Dynamics, Power and Efficiency

R. Perez-Carrasco* and J.M. Sancho
*Departament d'Estructura i Constituents de la Matèria*
*Facultat de Física, Universitat de Barcelona 08028-Barcelona*

Cells are the minimum unit of life. They are systems out of equilibrium with a continuous active flux of energy and matter. The macromolecules in charge of such functions are the Molecular Machines, which are continuously transducing between energies of different nature. At first glance, these machines may look as its macroscopic counterpart, however, they live under a very different physical conditions. The scales involved provide very viscous dynamics which overcome the inertial effects. Additionally, the thermal energy is smaller but comparable to the rest of the energies involved in the motor cycle making thermal fluctuations essential in a proper description of such machines. Thus the dynamics of Molecular Machines can be addressed through an overdamped Langevin equation,

$$\gamma\dot{x} = -V'(x,t) + F_E + \xi(t). \qquad (1)$$

Being $x$ the spatial coordinate of the motor with an effective friction coefficient$\gamma$. The forces generating the motion are: the force induced by the motor through the internal motor potential $V(x,t)$, the thermal force $\xi(t)$, which can be described as a white noise and finally an the external force $F_E$. The aim of the theoretical study of Molecular Machines is to find the mechanism of transduction of the motor, i.e. the shape and dynamics of the motor potential. This is done by studying experimental trajectories under different experimental conditions and obtaining the different processes (mechanic and catalytic) composing the work cycle of the motor. The two main tunable experimental parameters are $\gamma$ (attaching a passive load to the motor) and $F_E$ which introduce respectively dissipative and conservative forces to the dynamics of the motor[1].

Molecular Motors are fueled by two different energy sources: The hydrolysis of nucleotides and a gradient of ions across a membrane, an example of a motor with both sources is $F_0F_1$ATPsynthase (Fig. 1). Specifically, the $F_1$ part can hydrolyze ATP to rotate its central shaft. From a study of the dependence of the motor with [ATP], and dissipative and conservative forces the motor potential has been successfully reconstructed and can be expressed as a flashing ratchet mechanism[1,2]. The resulting potential not only is able to reproduce the experimental observations through simulations but also allows an analytical insight of the structural configuration and how is related to optimizes the function of the motor[2,1,3]. The motor potential makes possible also to compute the power and the efficiency of the motor showing the importance of thermal fluctuations to study Molecular Machines[4].

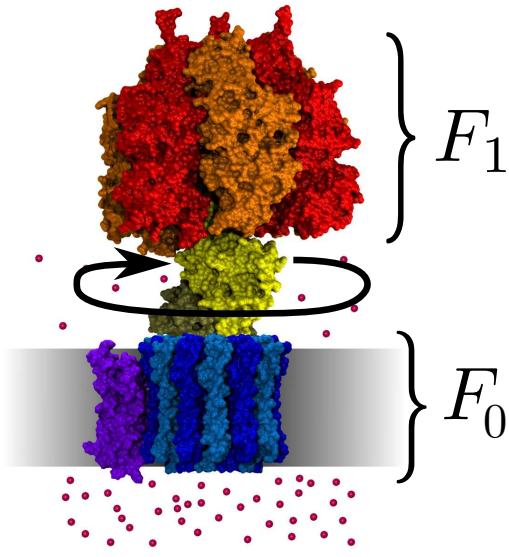


FIG. 1. $F_0F_1$ ATPsynthase is a molecular motor. The $F_0$ portion transduces a membrane flux into a rotation that is used by the $F_1$ subunit to synthesize ATP. It can also work in reverse mode, hydrolyzing ATP to generate membrane potential. Both subunits can be separated and work as individual motors working with a rotatory motion.

Alternatively, the basic mechanism for a molecular machine working with a flux of particles (as the $F_0$) allows the same formalism. Depending on the direction of the flux with respect to the particle gradient, this machine can work in both regimes turbine and pump. Setting out the most simple molecular flux machine of a piston under a Brownian force the dynamics of such a machine can be studied[5]. From the exact solution for the velocity of the motor and the flux, a new regime near the stall force arises where no useful energy can be obtained from the motor. This new regimes modifies completely the deterministic scenario for the power and the efficiency creating new maxima on account of the thermal fluctuations.

* rperez@ecm.ub.es

[1] R. Perez-Carrasco and J.M. Sancho, Phys. Rev. E **84** 041915 (2011)
[2] R. Perez-Carrasco and J.M. Sancho, Biophys. J. **98** 2591 (2010)
[3] R. Perez-Carrasco and J.M. Sancho, EPL **91** 60001 (2010)
[4] J.M. Sancho and R. Perez-Carrasco, Fluct. Noise Lett. **11:1** 1240003 (2012)
[5] R. Perez-Carrasco and J.M. Sancho, (Submitted, 2012)

# Microcanonical multifractal analysis of electric potential maps on the heart surface

Oriol Pont*[a,b], Hussein Yahia[a], Rémi Dubois[b]
[a] *EPI GeoStat, INRIA Bordeaux Sud-Ouest*
*351 Cours de la Libération A29bis, F-33405 Talence, France*
[b] *L'Institut de rythmologie et modélisation cardiaque, IHU LIRYC*
*Université de Bordeaux, F-33000 Bordeaux, France*

Some characterizations of heartbeat dynamics as stochastic processes has been done as effective dynamics, with variability fluctuations following a multifractal distribution[1,2]. Such characterizations have shown applicability as automatic tools to help diagnosis of some arrhythmias, but very specific non-linear signal-analysis methods become necessary to tackle the whole dynamical complexity of the cardiac electrical activity.

In this context, methodological frameworks such as the Microcanonical Multifractal Formalism provide appropriate techniques for such characterization e.g., by means of the singularity exponents of the signals[3–5]. Singularity exponents correspond to the (fractional) leading order of expansion of a given multiscale measure on the signal. They are as such concepts of functional analysis independent of any particular model for the data, and they can be accurately calculated for every point of an empirical discrete signal.

The use of singularity exponents to characterize heartbeat dynamics has been successfully applied to skin electric potential measures from electrocardiograms and also catheter electrode measures on endocardial cavities[6], where it has permitted to identify and characterize arrhythmic regimes like atrial fibrillation.Nevertheless it is possible to go further and characterize not only time series of electric potential but also time sequences of spatial maps of electric potential on the heart, with singularities evaluated both in space and time domain. Additionally, these types of data can be obtained in a non-invasive way (which drastically increases their clinical value) from epicardial projections of the electric potential obtained by solving the inverse problem of potential measures around the chest: a vest containing a grid of ECG electrodes measures the potential maps and from them they are projected on the epicardial surface.

This inversion is an ill-posed problem and several assumptions are needed to regularize the reconstructions. The robust estimation of dynamical transitions as singularity exponents can be used in such regularizations and help improve the information on areas of abnormal activity. We derive an effective cardiodynamical description with a simple and fast orientational dynamics modulated by a slow, more complex field. Gradient orientation on the most singular points is compatible with a stochastic process without memory. Modulation of this singularity orientation defines a complex but slow dynamics called *source field*[7] and defined as the Radon-Nykodim derivative between a measure on the signal and another one on the orientation. The singularity degree at a point in a signal is conceptually linked to how rare or unreconstructible is the value at that point from the rest of the signal, therefore the reconstruction is required to preserve these dynamical transitions. This can potentially be used to help automatic diagnosis and as a guide to catheter ablation procedures.

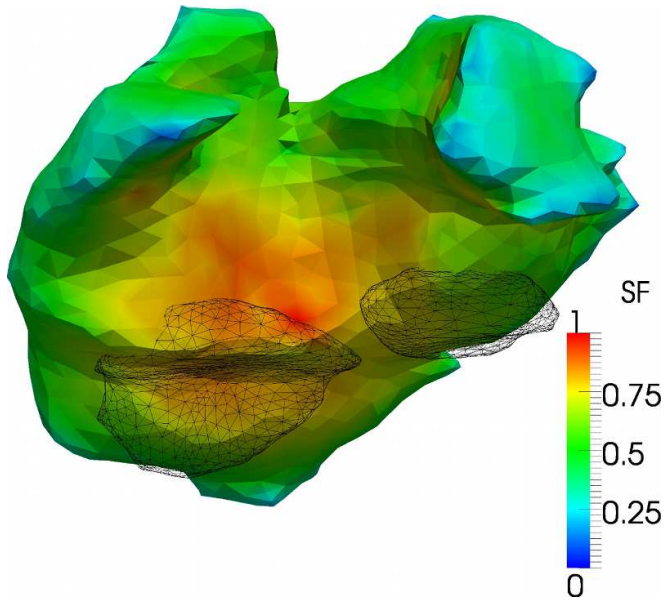


FIG. 1. Average source field on the epicardial surface of the heart atria and position of the mitral and tricuspid valves, for a case of a patient with atrial flutter.

* oriol.pont@inria.fr

[1] P. Ivanov *et al.*, Nature **383**, 323 (1996).
[2] P. Ivanov *et al.*, Nature **399**, 461 (1999).
[3] O. Pont, A. Turiel, and C. J. Pérez-Vicente, Physical Review E **74**, 061110 (2006).
[4] A. Turiel, H. Yahia, and C. Pérez-Vicente, Journal of Physics A **41**, 015501 (2008).
[5] O. Pont, A. Turiel, and C. Perez-Vicente, Int. J. Wavelets Multi., IJWMIP **9**, 35 (2011).
[6] O. Pont, M. Haïssaguerre, H. Yahia, N. Derval, and M. Hocini, Transactions on Mass-Data Analysis of Images and Signals **4** (2012), Accepted.
[7] A. Turiel and C. Pérez-Vicente, Physica A **355**, 475 (2005).

# Phase Transition of a Meniscus in a Capillary under the Influence of Gravity

C. Rascón*, A.O. Parry†, E.A.G. Jamie‡, S. Ivell‡, A. Thorneywork‡, D.G.A.L. Aarts‡

* *GISC, Departamento de Matemáticas. Universidad Carlos III de Madrid*
† *Department of Mathematics, Imperial College London*
‡ *Department of Physical Chemistry, Oxford University*

Phase transitions of inhomogeneous fluids such as wetting and capillary-condensation that occur when a fluid is confined near a substrate or in parallel-plate geometries have received enormous attention over the last few decades. In most theoretical studies of these transitions the influence of a gravitational field is either considered secondary or, more often, completely neglected. However, it is clear that gravity plays a central role in many practical situations and, in combination with the confinement, induces further interfacial behaviour. Consider, for example, a large volume of a non-volatile liquid in a tall vertical capillary-slit or cylindrical pore which is capped at its bottom. What happens to the liquid when the capillary is slowly turned to the horizontal? Common experience tells us that the liquid will escape from the open end if the capillary is wide, as when water drains from a tipped glass, but will remain trapped if it is sufficiently narrow such as a drinking straw. It is somewhat surprising to find that this rather basic aspect of capillarity has not been investigated in depth. We show here some theoretical and experimental results of this phenomenon, and point out that this common phenomena is analogous to an interfacial unbinding phase transition involving the meniscus shape and reveals an unexpected connection between capillary-condensation and the theory of wetting transitions[1].

* carlos.rascon@uc3m.es

[1] A.O. Parry, C. Rascón, E.A.G. Jamie, D.G.A.L. Aarts, Phys. Rev. Lett. (accepted)

# Mimicking high-temperature reservoirs for colloidal particles using noisy electric fields

Édgar Roldán[1,*], Ignacio A. Martínez[2], Dmitri Petrov[2,3] and Juan MR Parrondo[1]
[1] *Departamento de Física Atómica, Molecular y Nuclear and GISC, Universidad Complutense de Madrid, 28040 Madrid, Spain*
[2] *ICFO–Institut de Ciencies Fotoniques, Mediterranean Technology Park, 08860 Castelldefels (Barcelona), Spain*
[3] *ICREA–Institució Catalana de Recerca i Estudis Avançats, 08010 Barcelona, Spain*

In the last decades, several models have been introduced to describe Brownian motion of particles in gases and liquids in conditions where fluctuations are important. An experiment in which the temperature of a colloidal particle is controllable is of interest to study the Brownian motion at different temperatures and to construct microscopic-sized heat engines[1].

We design an experiment to control the effective temperature of a colloidal particle from room temperature to several thousand kelvins. We trap microscopic polystyrene particles in water using optical tweezers. Our particles have inherit electric changes, therefore by applying an electrostatic force that is of the form of a Gaussian white noise we can mimic a second thermal bath in our system. We experimentally observe that the amplitude of the Brownian motion in the direction of the force increases when increasing the intensity of the electrostatic force. The particle moves like if it were in a thermal bath of a higher temperature than the surrounding water. To check that our setup is equivalent to a thermal bath that is at a higher temperature than the water, we study the fluctuations of the position of the bead and the response of the bead to nonequilibrium perturbations.

We first study the fluctuations of the position of the bead in the direction in which the electric field is applied ($x-$axis for simplicity). Let $x$ be the position of the bead and $x_t$ the position of the center of the trap, both in $x-$axis. The trap generates a harmonic optical potential of stiffness $\kappa$ that is centered around $x_t$, i.e. $V(x) = \frac{1}{2}\kappa(x - x_t)^2$. We define the *kinetic temperature* of the bead as $T_{\rm kin} = \kappa\langle(x-x_t)^2\rangle_{\rm ss}/k$, where ss stands for steady state and $k$ is Boltzmann's constant. Kinetic temperature is equal to the temperature of the water when no field is applied, and it increases with the amplitude of the field. The maximum temperature that we experimentally observe is around $3000K$ as we show in Fig. 1. Notice that Brownian motion at high temperatures has only been observed in laser-heating experiments[2], where the temperature achieved is always smaller than the vaporization temperature of water. Another proof that the particle is describing Brownian motion at high temperatures is done by calculating the Fourier transform of the correlation of the position, called Power Spectrum Density (PSD). When applying the external field, the shape of the PSD is equal to the PSD of a bead trapped with the same stiffness $\kappa$ but immersed in a thermal bath that is at a larger temperature than the temperature of the water in our experiment.

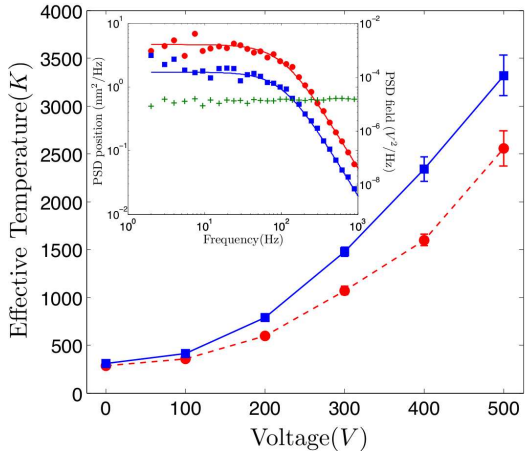


FIG. 1. Experimental value of the effective temperature of the bead as a function of the maximum voltage applied between the electrodes: $T_{\rm kin}$ (blue squares), and $T_c$ (red circles). *Inset*: Power spectrum density of the position of the bead as a function of the frequency: Without external field (blue squares) and with a maximum voltage of $200V$ (red circles). Solid lines are fits to a Lorentzian. We also plot the PSD of the electric noise (green "+").

To analyse the response of the particle in the presence of the random electric field we move the trap center following the nonequilibrium protocol that we now describe: First the trap is moved at constant velocity $v$ and the bead is allowed to relax to the new equilibrium position. Then, the reverse process is implemented, moving the trap with velocity $-v$ and letting the bead to relax to equilibrium again. We experimentally check Crooks fluctuation theorem[3] when no external field is applied. We then define by $T_c$ the temperature at which Crooks theorem is satisfied when the electric field is on. We show in Fig. 1 that $T_c$ is of the same order of magnitude than the kinetic temperature obtained from the analysis position fluctuations.

We therefore prove that our setup is equivalent to a thermal bath where the temperature can be externally controlled. With a simple experiment, we are able to use our setup to heat a particle from $300K$ to $3000K$ in a timescale that is of order $\gamma/\kappa$, being $\gamma$ the friction coefficient of the bead in water.

* edgar.roldan@fis.ucm.es

[1] V. Blickle and C. Bechinger, Nat. Phys. **8**, 143-146 (2012).
[2] M.L. Cordero, E. Verneuil, F. Gallaire, and C.N. Baroud, Phys. Rev. E. **79**, 011201(2009).
[3] G. E. Crooks, Phys. Rev. E **60**, 2721 (1999).

# Generalización del modelo de Berreman para la energía libre superficial de un cristal líquido nemático en presencia de un sustrato de dientes de sierra.

O. A. Rojas-Gómez* y J. M. Romero-Enrique†

*Departamento de Física Atómica, Molecular y Nuclear (Área de Física Teórica), Universidad de Sevilla, Apartado de Correos 1065 41080 Sevilla*

La presencia de sustratos rugosos puede frustrar el orden orientacional de largo alcance que presentan los cristales líquidos nemáticos. Como consecuencia, la densidad de energía libre superficial de exceso del nemático en contacto con el sustrato tiene una contribución asociada a las distorsiones del campo de orden orientacional $f_e$. Si la rugosidad es periódica a lo largo de una dirección y con un vector de ondas $q$, Berreman propuso que, cuando la rugosidad es pequeña, dicha contribución tiene la forma $f_e \sim Kq(qA)^2/4$, siendo $A$ la amplitud de la rugosidad y $K$ una constante elástica[1,2]. Trabajos posteriores extendieron sus argumentos para situaciones donde la rugosidad no era pequeña, encontrándose que, si el sustrato es suave, la contribución tiene la forma $Kq\chi(qA)$, siendo $\chi(x)$ una función que depende de la forma del sustrato pero no de sus dimensiones absolutas[3,4].

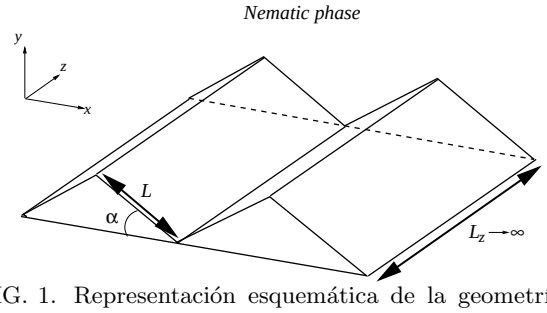


FIG. 1. Representación esquemática de la geometría del problema

El escalamiento de la contribución elástica con $q$ se rompe cuando consideramos sustratos que nuclean defectos topológicos. Un ejemplo es el sustrato en forma de dientes de sierra que favorece el anclaje homeotrópico[5–7] (véase la Fig. 1). En este caso, $f_e$ sigue la siguiente ley[8]:

$$f_e \approx -\frac{\mathcal{K}(\alpha)}{2\pi} q \ln \frac{q\cos\alpha}{\pi} + \frac{q}{2\pi} B(\alpha, w) \qquad (1)$$

donde $\mathcal{K}(\alpha)$, dependiendo de si el nemático se orienta lejos del sustrato a lo largo del eje $x$ (textura $N^{\parallel}$) o a lo largo del eje $y$ (textura $N^{\perp}$), tiene la siguiente expresión:

$$\begin{aligned} \mathcal{K}(\alpha) &= \frac{K\pi\alpha^2}{\left(\frac{\pi}{2}\right)^2 - \alpha^2} \qquad \text{textura } N^{\perp} \\ &= K\pi \frac{\frac{\pi}{2} - \alpha}{\frac{\pi}{2} + \alpha} \qquad \text{textura } N^{\parallel} \end{aligned} \qquad (2)$$

El término $B(\alpha, w)$ tiene dos orígenes: las desviaciones del campo director nemático respecto al campo referencia correspondiente a los defectos nucleados en las singularidades del sustrato, y la contribución de los núcleos de los defectos[8]. Al comparar la predicción de la Ec. (1) con los resultados numéricos en el modelo de Landau-de Gennes, el acuerdo es excelente en condiciones de anclaje efectivo fuerte[8] (véase Fig. 2). Discutiremos cómo estas ideas pueden generalizarse para sustratos de forma general.

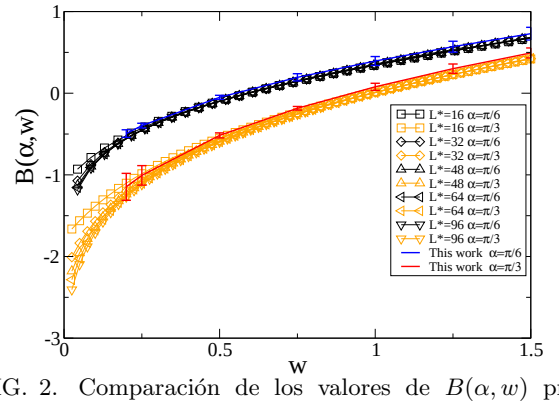


FIG. 2. Comparación de los valores de $B(\alpha, w)$ predichos por la Ec. (1) y los obtenidos mediante minimización numérica del modelo de Landau-de Gennes.

* oarojas@us.es
† enrome@us.es

[1] D. W. Berreman, Phys. Rev. Lett. **28**, 1683 (1972)
[2] P.G. de Gennes and J. Prost, *The Physics of Liquid Crystals*, 2nd ed. (Oxford University Press, Oxford, 1995)
[3] G. Barbero, A.S. Gliozzi, M. Scalerandi and L.R. Evangelista, Phys. Rev. E **77**, 051703 (2008)
[4] P. Patrício, N. M. Silvestre, C.-T. Pham and J. M. Romero-Enrique, Phys. Rev. E **84**, 021701 (2011).
[5] P. Patrício, C.-T. Pham and J. M. Romero-Enrique, Eur. Phys. J. E **26**, 97 (2008).
[6] P. Patrício, J. M. Romero-Enrique, N. M. Silvestre, N. R. Bernardino and M. M. Telo da Gama, Mol. Phys. **109**, 1067 (2011).
[7] J. M. Romero-Enrique, C.-T. Pham and P. Patrício, Phys. Rev. E **82**, 011707 (2010).
[8] O. A. Rojas-Gómez and J. M. Romero-Enrique, enviado a Phys. Rev. E (2012); arXiv: cond-mat/1205.2906 (2012).

# Spintronic Fluctuation Relations

David Sánchez*, Jong Soo Lim, Rosa López
*IFISC, Instituto de Física Interdisciplinar y Sistemas Complejos*
*CSIC-Universidad de las Islas Baleares 07122-Palma de Mallorca*

In quantum mesoscopic transport, higher-order fluctuation relations connect nonequilibrium current–current correlations to nonlinear response coefficients.[1–4] Their form is akin to extented fluctuation-dissipation theorems and they may be derived in some cases from nonequilibrium fluctuation theorems.[5] We investigate the role of a genuine quantum property such as the *spin* degree of freedom in the fluctuation relations.[6] Our motivation is not only fundamental since the electronic spin offers enormous advantages to create devices with unusual and extraordinary new functionalities.

Spins are sensitive to magnetic fields and also to electric fields via spin-orbit interactions. We derive the *spintronic fluctuation relations* when time-reversal symmetry is broken not only by external magnetic fields but also by the presence of ferromagnetic electrodes. We illustrate our findings with a quasi-localized level coupled to helical edge states which are partially polarized by the presence of polarized electrodes. This quantum spin Hall state consists of gapless excitations that exist at the boundaries in which its propagation direction is correlated with its spin due to the spin-orbit interaction.

Moreover, we show that the applicability of nonequilibrium fluctuation theorems when magnetic interactions are present is not *a priori* ensured. We illustrate this statement by using a quasi-localized level coupled to a chiral one-dimensional conducting channels. We demonstrate that local detailed balance condition is not satisfied when a magnetic field is included and the system is driven out of equilibrium. Our formalism is based on zero-frequency fluctuations and time-independent fields but in the presence of arbitrary interactions.

---

* david.sanchez@uib.es

[1] J. Tobiska and Y. V. Nazarov, Phys. Rev. B **72**, 235328 (2005).
[2] K. Saito and Y. Utsumi, Phys. Rev. B **78**, 115429 (2008).
[3] H. Förster and M. Büttiker, Phys. Rev. Lett. **101**, 136805 (2008).
[4] D. Sánchez, Phys. Rev. B **79**, 045305 (2009).
[5] M. Esposito and C. Van den Broeck, Phys. Rev. Lett. **104**, 090601 (2010).
[6] R. López, J.S. Lim, and D. Sánchez, Phys. Rev. Lett. (in print, 2012); arXiv:1205.2266

# Estudio de ángulos de contacto y fuerzas de retención de gotas líquidas sobre superficies inclinadas

Santos, M.J.* y White, J.A.†
*Departamento Física Aplicada. Facultad de Ciencias*
*Universidad de Salamanca*
*37008 Salamanca*

La ecuación de Young-Laplace determina que una gota sobre una superficie horizontal tiene una forma axisimétrica debido a la simetría cilíndrica del problema. Esta forma se convierte en no-axisimétrica cuando la superficie se inclina (o gira a una velocidad angular dada). Para ángulos de inclinación $\alpha$ por debajo de un valor crítico $\alpha_c$ se observa que la gota se mantiene adherida a la superficie debido a un cambio de forma: la gota se abomba en la dirección de inclinación por lo que los ángulos de contacto en la parte delantera de la gota son mayores que los de la parte posterior. La diferencia entre los ángulos de contacto de la gota se denomina histéresis del ángulo de contacto y ocasiona una fuerza de retención capilar que se compensa con la gravitatoria y evita el movimiento de la gota.

El objetivo del presente trabajo es analizar este problema por medio de simulaciones mediante un método recientemente desarrollado[1], para modelizar la histéresis del ángulo de contacto a través de Surface Evolver[2].

Los resultados de nuestras simulaciones tienen una gran dependencia con el ángulo de contacto inicial $\theta_{\rm i}$ de la gota. Por ello consideramos la evolución de una gota sobre una superficie horizontal que se inclina lentamente para dos situaciones iniciales diferentes: (i) $\theta_{\rm i} = \theta_{\rm av}$, y (ii) $\theta_{\rm i} = \theta_Y = (\theta_{\rm av} + \theta_{\rm re})/2$. Se analiza la evolución de la forma de la gota, los ángulos de contacto y las fuerzas de retención con un ángulo de inclinación en ambos casos. Y se compara además con datos experimentales para una aleación liquida de Sn-Ag-Cu sobre un substrato inclinado de Cu.

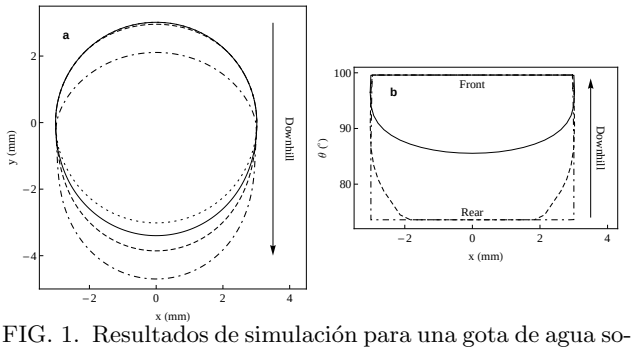


FIG. 1. Resultados de simulación para una gota de agua sobre PCTFE con un ángulo de contacto inicial igual a $\theta_{\rm av}$. (a) Línea de contacto triple. (b) Ángulos de contacto en función de la coordenada $x$ perpendicular a la inclinación. Línea de puntos: $\alpha = 0°$, línea continua: $\alpha = 10°$, línea a trazos: $\alpha = 20°$, línea punto-raya: $\alpha = 23°$.

La figura 1 muestra la evolución con la inclinación de la triple línea de contacto y los ángulos de contacto para una gota de agua sobre PCTFE con $\theta_{\rm i} = \theta_{\rm av}$. La forma de la gota va modificándose con $\alpha$ según los ángulos de contacto adoptados, sin caerse. Para $\alpha = 23°$ la gota está ya deslizándose y la anchura de la gota llega a ser ligeramente menor que la original.

La figura 2 muestra la evolución de $\cos\theta_{\rm min}$ y $\cos\theta_{\rm max}$ con $\alpha$ para una aleación líquida de Sn-Ag-Cu sobre un substrato inclinado de Cu. Este es un sistema con una histéresis pronunciada en la cual el ángulo de contacto inicial no es ni $\theta_{\rm av}$ ni $\theta_Y$. Para $\alpha$ pequeñas $\cos\theta_{\rm max}$ se aproxima a $\cos\theta_{av}$ de modo lineal mientras que $\cos\theta_{\rm min}$ aumenta linealmente hacia $\cos\theta_{\rm re}$, para $\alpha$ mayores, $\theta_{\rm max} = \theta_{\rm av}$ y $\cos\theta_{\rm min}$ aún aumenta linealmente hacia $\cos\theta_{\rm re}$ pero con una pendiente diferente. Es de destacar el excelente acuerdo con datos experimentales.

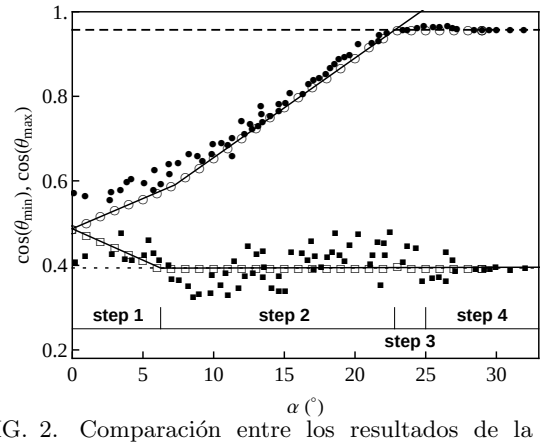


FIG. 2. Comparación entre los resultados de la simulación y los datos experimentales para una aleación líquida de Sn-Ag-Cu sobre un substrato inclinado de Cu. $\cos\theta_{\rm min}$ (círculos) y $\cos\theta_{\rm max}$ (cuadrados) frente al ángulo de inclinación $\alpha$. Las líneas discontinuas y las líneas de puntos indican $\cos\theta_{\rm re}$ y $\cos\theta_{\rm av}$ respectivamente. Los símbolos rellenos son los datos experimentales.

* smjesus@usal.es
† white@usal.es

[1] T. Young, Philos. Trans. R. Soc. London, 95 (1805) 65.
[2] M.J. Santos, J.A. White, Langmuir 27 (2011) 14868.
[3] Brakke, K.A., *Exp. Math.* 1(2), (1992) 141.
[4] M.J. Santos, S. Velasco, J.A. White. Enviado

# Crystallization versus vitrification in hard spheres

Eduardo Sanz(1,2)*, Chantal Valeriani(1,2), Emanuella Zaccarelli(3), Peter N Pusey(2), Wilson C K Poon(2), Michael E Cates(2)

*(1)Dep. Quimica-Fisica I, Universidad Complutense de Madrid, 28040, Madrid, Spain*
*(2)School of Physics and Astronomy, University of Edinburgh, EH9 3JZ, Edinburgh, UK*
*(3)CNR-ISC and Dip. di Fisica, Universita di Roma La Sapienza, P.le A. Moro 2, 00185, Roma, Italy*

A collective of hard spheres is, arguably, the simplest non-trivial system that displays a fluid-solid transition. This was discovered in pioneer computer simulations by Alder and Wainwright in the late 50s[1] and observed experimentally in suspensions of hard-sphere-like colloids by Pusey and van Megen about 30 years later[2]. Besides the solid and the fluid phases, Pusey and van Megen observed glassy samples, some of which were able to become crystalline after some time. This motivated our studies during the past few years on the relation between the glass transition and crystallization in hard-sphere systems.

We started by establishing the location of the dynamical glass transition in size monodisperse hard-sphere systems. Since crystallization in this system readily occurs before the dynamics shows any signature of arrest there has been some debate on whether or not there is a true glass transition for this system. By comparing the dynamics of monodisperse and polydisperse systems we concluded that there is indeed a glass transition and that crystallization occurs with no diffusion for densities larger than that corresponding to the dynamic transition[3,4].

More recently, we have focused our efforts in understanding and characterizing the regime in which crystals appear and grow with no particle diffusion[5]. We observed that particles are able to rearrange gradually into a crystalline environment by rattling motion alone, following a crystallization pathway that is nonetheless chaotic and unpredictable from the configuration. The chaotic and gradual nature of the mechanism is illustrated in the figure. This mechanism is self-sustained because the emergence of crystals increases the mobility of neighboring particles by free volume release. We have also analyzed the structural properties of the crystalline clusters growing via this mechanism, concluding that beyond the density at which crystallization times are shorter than diffusion times the structural properties of the growing clusters do not change with density[6].

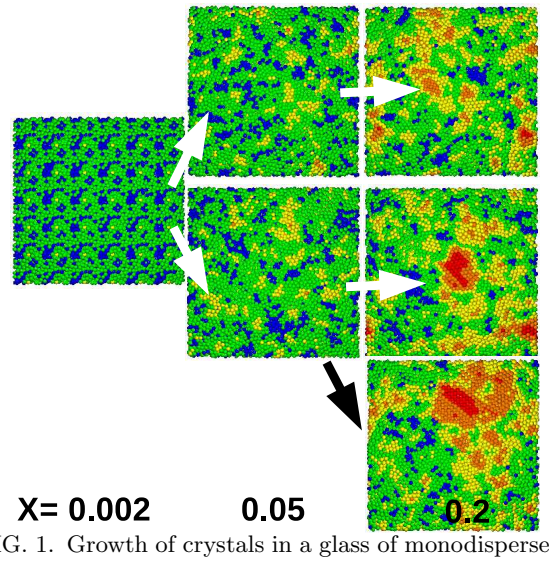


FIG. 1. Growth of crystals in a glass of monodisperse hard spheres at volume fraction 0.61.

* esa01@quim.ucm.es

[1] BJ Alder and T. E. Wainwright, J. Chem. Phys. 27, 1208 (1957).
[2] P. N. Pusey and W. van Megen, Nature 320, 340 (1986).
[3] E. Zaccarelli, C. Valeriani, E. Sanz, W. C. K. Poon, M. E. Cates and P. N. Pusey, Phys. Rev. Lett., 103, 135704, (2009).
[4] P. N. Pusey, E. Zaccarelli, C. Valeriani, E. Sanz, W. C. K. Poon and M. E. Cates, Phil. Trans. Royal Soc. A., 367, 4993, (2009).
[5] E. Sanz, C. Valeriani, E. Zaccarelli, W. C. K. Poon, P. N. Pusey and M. E. Cates, Phys. Rev. Lett., 106, 215701, (2011).
[6] C. Valeriani, E. Sanz, W. C. K. Poon, P. N. Pusey, M. E. Cates and E. Zaccarelli Soft Matter 8, 4960, (2012).

# Passive and Active Transport in Turbulent Fluid Flow caused by Faraday Waves

A. von Kameke, F. Huhn, V. Pérez-Muñuzuri, A.P. Muñuzuri
*Group of Nonlinear Physics, Faculty of Physics, University of Santiago de Compostela, E-15782 Santiago de Compostela, Spain.*

The study of passive and active transport in turbulent fluid flow is crucial for the understanding of a large variety of phenomena, e.g. the spread of oil spills, the patchiness and growth of plankton blooms, the distribution of larvae or the mixing in industrial reactors[1]. Therefore it is important to find model flows that allow to investigate turbulent transport on laboratory scales. We experimentally observe Richardson dispersion and a double cascade in a thin horizontal fluid flow induced by Faraday waves. The energy spectra and the mean spectral energy flux obtained from Particle Image Velocimetry data suggest an inverse energy cascade with Kolmogorov type scaling $E_k \propto k^\gamma, \gamma \approx -5/3$ and an $E_k \propto k^\gamma, \gamma \approx -3$ enstrophy cascade. Particle transport in this flow is studied analyzing absolute and relative dispersion as well as the Finite Size Lyapunov Exponent (FSLE) via the direct tracking of real particles and numerical advection of virtual particles. Richardson dispersion with $\langle R^2(t)\rangle \propto t^3$ is observed and is also reflected in the slopes of the FSLE ($\Lambda \propto \Delta R^{-2/3}$) for virtual and real particles[2]. Further we use active media in form of a Belousov-Zhabotinsky Reaction and study its behaviour in this experimental model flow. The behaviour of active and passive media is compared concerning its spreading and patterning behaviour[3].

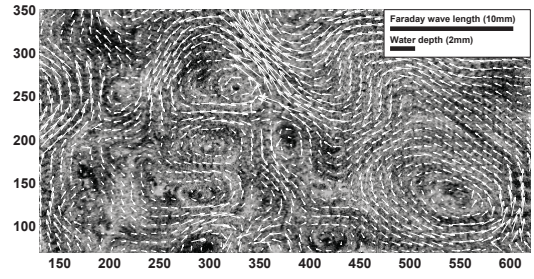


FIG. 1. The horizontal surface fluid flow induced by the Faraday waves at a forcing frequency of $\omega = 50$ Hz and acceleration $a = 1.5\, g_0$. Every second velocity arrow is shown. RMS velocity is $v_{rms} \approx 1.15$ cm/s. Reynolds number based on the Faraday wavelength and $v_{rms}$ is $Re \approx 100$.

* alexandra.vonkameke@usc.es

[1] Neufeld, Z. and Hernández-García, *E. Chemical and Biological Processes in Fluid Flows*, Imperial College Press, London, 2010.

[2] von Kameke, A.; Huhn, F.; Fernández-Garcia, G.; Muñuzuri, A. P. and Pérez-Muñuzuri, V.; *Double Cascade Turbulence and Richardson Dispersion in a Horizontal Fluid Flow Induced by FaradayWaves* Phys. Rev. Lett., American Physical Society, 2011, 107, 074502

[3] von Kameke, A.; Huhn, F.; Fernández-Garcia, G.; Muñuzuri, A. P. and Pérez-Muñuzuri, V.; *Propagation of a chemical wave front in a quasi-two-dimensional superdiffusive flow* Phys. Rev. E, American Physical Society, 2010, 81, 066211

# Parte III
# Paneles

# Modeling dynamical T-cell cross-regulation in a mouse model of multiple sclerosis

Elena Abad[1], Sara M. Pasamar[2], Nieves de Mendizábal[2], Pablo Villoslada[2], and Jordi García-Ojalvo[1,3]
[1] *Department of Physics and Nuclear Engineering, Universitat Politecnica de Catalunya, 08222 Terrassa, Spain*
[2] *Neuroimmunology group, IDIBAPS, Hospital Clínic, 08028 Barcelona, Spain*
[3] *Department of Experimental and Health Sciences, Universitat Pompeu Fabra, Barcelona Biomedical Research Park, 08003 Barcelona, Spain*

The autoimmune disease known as Multiple Sclerosis (MS) is characterized by a degeneration of the myelin sheath of neurons in the central nervous system. The basis of autoimmunity in MS is still unclear, but different possible mechanisms for this pathology have been proposed, including the existence of an imbalance of effector ($T_{eff}$) and regulatory ($T_{reg}$) CD4 T cells. Naive T cells are in a quiescent state and become activated by antigens, and subsequently migrate to the infection site. At same time this activity is downregulated by $T_{reg}$ cells. The main goal of this work was to test experimentally a recent theoretical model of $T_{eff}$ ant $T_{reg}$ cell population dynamics proposed for humans[1] to experimental data in an animal model of MS in mice (induced experimental autoimmune encephalomyelitis, EAE). T cells were extracted from spleen tissue (blood filter) and specific T cells for EAE (MOG-specific T cells) were counted by flow cytometry, measuring cell size populations for several days, which allowed us to obtain activation kinetics. We use a predator-prey-like model to describe the interactions between four cell populations (active and resting effector and regulatory cells), supplied by stochastic pulsed inputs representing naïve T cells. Results show that the experimentally monitored active $T_{eff}$ and $T_{reg}$ cell populations qualitatively agree with the model, showing irregular and coordinated spikes in the form of a remitting-relapsing dynamics typical of autoimmune diseases. This model should help us improve our understanding of cell population dynamics in the immune system.

[1] N. de Mendizábal et al., 'Modeling the effector-regulatory T cell cross-regulation reveals the intrinsic character of relapses in Multiple Sclerosis', BMC Systems Biology **5**, 114 (2011).

# Flocking and coherence emergence on active particle suspensions.

F. Alarcón and I. Pagonabarraga*
*Departament de Física Fonamental*
*Facultat de Física, Universitat de Barcelona*
*Carrer Martí i Franqués, 1, 08028 Barcelona.*

The emergence of collective motion is a ubiquitous self-organization phenomenon, which is interesting in several fields, from the biological perspective to the technological one, and observable at all scales. We can find from macro-scales, for example animals moving en masse to even molecular scale, where we can find novel results from experimental groups[1], they observed motional patterns associated with polar interactions using actin filaments and more recently another group have reported coordinated motion of hundreds of thousands of subcellular structures known as microtubules, which spontaneously self-organize into a lattice-like structure of vortices[2]. The non-living world has systems where collective motion appears also. From molecules to metallic rods, or even robots[3]. Just in the middle of these two extremal scales we mentioned above, we found the unicellar living organisms, such bacteria and algae, which propel themselves through a medium via cyclic strokes involving the motion of cilia and flagella. Hence, this micro-organisms can be classified by its characteristic propulsion, in pullers, pushers, movers and shakers[4]. Using this terminology we have fully characterized the collective motion since flocking to coherence in the orientation of swimm that emerge for this kind of micro-organism suspensions. Using a simple model in which the effect of the internal metabolism of the micro-organism can be described through the effective fluid flow the particle generates on its surface[5], and adding a Lenard-Jones (LJ) interaction between the swimmers as a model of the communication between the micro-organisms.

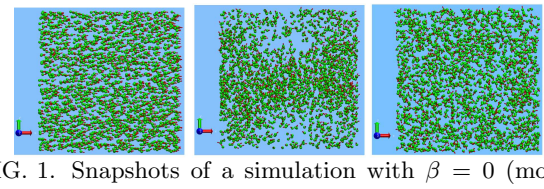

FIG. 1. Snapshots of a simulation with $\beta = 0$ (movers), $\beta = 0.5$ (pullers) and $\beta = -0.5$ (pushers) respectively at $t = 6 \cdot 10^5$. The snapshots have been done using the VMD software[6] with the Normal Mode Wizard (NMWiz) plugin[7].

The mechanism of how collective motion is created can be remarkably varied, so the search for possible universal features becomes a paramount issue. As it can be the stresslet parameter $\beta$, in which different values produce different collective phenomena as we depicted in Fig. 1. Where we can see three states of the active particle suspension: a completly coherent fluid, a fluid in a flocking state and an homogeneous and isotropic fluid.

---

* ipagonabarraga@ffn.ub.es

[1] Schaller, V. et al. *Nature* **467**, 73 (2010).
[2] Sumino, Y. et al. *Nature* **483**, 448 (2012).
[3] A. Snezhko, I.S. Aranson, *Nature Mater* **10**, 698 (2011).
[4] A. Baskaran and M.C. Marchetti, *Proc. Natl Acad. Sci.* **106**, 37 (2009).
[5] R. Blake, *Journal of Fluid Mechanics* **46**, 01 (1971).
[6] W. Humphrey, A. Dalke, K. Schulten, *J. Molec. Graphics* **14**, 33 (1996).
[7] A. Bakan, LM. Meireles, I. Bahar, *Bioinformatics* **27**, 1575 (2011).

# A phase-field approach to actin-based motility of lamellar fragments

Sérgio A. Lira*+, Carles Blanch-Mercader, and Jaume Casademunt
*Departament d'Estructura i Constituents de la Matèria, Universitat de Barcelona, Av. Diagonal 647, Barcelona, Spain*

Lamellar fragments are pieces of lamellipodia, the actin-based locomotion machinery of crawling cells. These fragments have been shown to exhibit spontaneous, sustained motion if properly deformed[1]. Despite its relative simplicity, a theoretical understanding of the minimal ingredients to explain this phenomenon is still lacking. A challenging question is how the treadmilling dynamics of actin, which polymerizes at the boundary, is coupled to the shape of the fragment to sustain motion, in particular in the absence of molecular motors. Recently, it has been shown that in an appropriate approximation, the flow of actin satisfies Darcy's law in an effectively two-dimensional geometry[2], thus reducing the dynamics to a free-boundary problem similar to that of viscous-fingering in Hele-Shaw cells, but with different boundary conditions[3].

Here we present a phase-field description of this free-boundary problem, as a tool to numerically integrate the fully nonlinear dynamics of this problem, aiming at a systematic study of the different families of steady propagating solutions, their stability and their basins of attraction. Such a diffuse-interface method is known to have important advantages with respect to sharp-interface methods (boundary-integral methods or confomal mapping techniques) in laplacian problems, in particular when interfaces adopt complex shapes. Most importantly, their advantage is most substantial when the viscosity of the displaced fluid is not neglected, a common approximation that may have to be relaxed in order to gain a more quantitative understanding of the problem and its biological relevance.

A phase-field strategy has already been used before within more complicated models[5,6]. The model we present concentrates on the effects of polymerization forces combined with friction on the substrate and with membrane tension. The absence of molecular motors in the description makes the model simpler and more amenable to theoretical discussion. Appropriate convergence tests have been performed showing that the model is quantitatively accurate and competitive with respect to other techniques. Our results in the fully nonlinear regime confirm that actin polymerization alone can sustain motion, and provide not only the families of stable steady shapes, but also a first characterization of their relative basins of attraction.

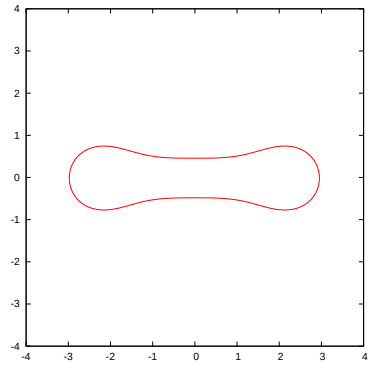


FIG. 1. Steady shape of a lamellar fragment obtained after the instability of a perturbed circle, using the phase-field model.

* sergiolira@df.ufpe.br
+ Departamento de Física, Universidade Federal de Pernambuco, Recife, Pernambuco 50670-901 Brazil.

[1] A. B. Verkhovsky, T. M. Svitkina, and G. G. Borisy, Curr. Biol. 9, 11 (1999).
[2] A. C. Callan-Jones, J.F. Joanny, and J. Prost, Phys. Rev. Lett. 100, 258106 (2008).
[3] J. Casademunt, Chaos 14, 809 (2004).
[4] R. Folch, J. Casademunt, A. Hernández-Machado, and L. Ramrírez-Piscina, Phys. Rev. E 60, 1724 (1999).
[5] F. Ziebert, S. Swaminathan and I. S. Aranson, J. R. Soc. Interface, 2011.
[6] D. Shao, H. Levine and W-J Rappel, PNAS, vol. 109, no. 18, 2012.

# Experimental free energy measurements of kinetic molecular states using fluctuation theorems

[1]Anna Alemany, [2]Alessandro Mossa, [3]Ivan Junier, [1,4*]Felix Ritort

[1]*Small Biosystems Lab, Departament de Física Fonamental, Universitat de Barcelona, Avda. Diagonal 647, 08028 Barcelona, Spain*

[2]*Department of Physics and Astronomy, University of Aarhus, Aarhus C, Denmark*

[3]*Centre de Regulació Genòmica (CRG), C/ Dr. Aiguader 88, 08003 Barcelona, Spain*

[4]*CIBER-BBN de Bioingeniería, Biomateriales y Nanomedicina, Instituto de Salud Carlos III, Madrid, Spain*

Recent advances in non-equilibrium statistical mechanics and single molecule technologies make it possible to extract free energy differences from irreversible work measurements[1–3]. To date, free energy recovery has been focused on native or equilibrium states, whereas free energy measurements of kinetic states (i.e. finite lifetime states that are generated dynamically and are metastable) have remained unexplored. Kinetic states can play an important role in various domains of physics, such as nanotechnology or condensed matter physics. In biophysics, there are many examples where they determine the fate of molecular reactions: protein and peptide-nucleic acid binding, specific cation binding, antigen-antibody interactions, transient states in enzymatic reactions or the formation of transient intermediates and non-native structures in molecular folders. Here we demonstrate that it is possible to obtain free energies of kinetic states by applying extended fluctuation relations[4,5]. This is shown by using optical tweezers to mechanically unfold and refold DNA structures exhibiting intermediate and misfolded kinetic states[6].

* fritort@gmail.com

[1] Ritort, F. Nonequilibrium fluctuations in small systems: from physics to biology. *Adv. Chem. Phys.* **137,** 31–123 (2008).

[2] Woodside M.T., García-García, C., Block, S.M. Folding and unfolding single RNA molecules under tension. *Curr. Opin. Chem. Biol.* **12,** 640-646 (2008).

[3] Jarzynski, C. Equalities and inequalities: Irreversibility and the second law of thermodynamics at the nanoscale. *Annu. Rev. Condens. Matter Phys.* **2,** 329–Â51 (2011).

[4] Maragakis, P., Spichty, M. & Karplus, M. A Differential Fluctuation Theorem. *J. Phys. Chem. B* **112,** 6168–6174 (2008).

[5] Junier, I., Mossa, A., Manosas, M. & Ritort, F. Recovery of free energy branches in single molecule experiments. *Phys. Rev. Lett.* **102,** 070602 (2009).

[6] Alemany, A., Mossa, A., Junier, I. & Ritort, F. Experimental free energy measurements of kinetic molecular states using fluctuation theorems. Accepted in *Nat. Phys.*

# Transition State Susceptibility in Single Molecule Force Spectroscopy

[1,*]Anna Alemany, [1,2]Felix Ritort

[1] *Departament de Física Fonamental, Universitat de Barcelona, Diagonal 647, 08028 Barcelona, Spain.* [2] *CIBER-BBN de Bioingeniería, Biomateriales y Nanomedicina, Instituto de Sanidad Carlos III, Madrid, Spain.*

Single molecule experiments allow to investigate with unprecedented detail the kinetics of biomolecules, such as DNA, RNA and proteins. Much information can be estimated from phenomenological models like the Bell-Evans theory[1]. However, a lot of theoretical work still needs to be done in order to unravel, form experimental measurements, ac- curate details of the molecular free energy landscape[2,3]. Here we use the Kramers theory to show that even in molecules with a unique unfolding pathway under the action of a mechanical force, the transition state location has a strong impact on data interpretation[4]. The concept of a transition state susceptibility is introduced in order to identify abrupt transitions in the location of the transition state and to detect specific binding of magnesium ions to nucleic acids[5].

* aalemany@ffn.ub.es

[1] Evans, E., and Ritchie, K. Dynamic Strength of Molecular Adhesion Bonds. Biophys. J. (1997).

[2] Schlierf, M. and Rief, M. Single-Molecule Unfolding Force Distributions Reveal a Funnel-Shaped Energy Landscape. Biophy. J. (2005).

[3] Manosas, M., Collin, D. and Ritort, F. Force-Dependent Fragility in RNA Hairpins. Phys. Rev. Lett. (2006)

[4] Kuo, T. L., et. al. Probing static disroder in Arrhenius kinetics by single-molecule force spectroscopy. Proc. Natl, Acad. Sci. USA (2010).

[5] Bizarro C.V., Alemany A. and Ritort F. Non-specific binding of Na+ and Mg2+ to RNA determined by force spectroscopy methods. Nucl. Acids Res. (2012)

# El efecto ratchet en la partícula relativista

Renato Alvarez-Nodarse, J. Cuesta y N. R. Quintero
*Departamentos de Análisis Matemático, IMUS (Universidad de Sevilla), Departamento de Matemáticas, GISC (Universidad Carlos III de Madrid) y Departamento de Física Aplicada I, IMUS (Universidad de Sevilla)*

El transporte ratchet es conocido en los sistemas no-lineales como el movimiento de partículas[1] sometidas a fuerzas de promedio nulo. En esta contribución estudiamos la velocidad promedio de la partícula relativista amortiguada y forzada con dos tipos de fuerzas que rompen las simetrías temporales del sistema, una de ellas es la fuerza biarmónica y la otra una onda rectangular asimétrica[3]. A través de la caracterización funcional de la velocidad ratchet[2] y utilizando el desarrollo de Taylor funcional[4] derivamos las expresiones para la velocidad en ambos casos. En este ejemplo, cuando la fuerza temporal es simétrica y no hay disipatición la velocidad es cero. Sin embargo, si introducimos disipación en el sistema comprobaremos que, contrariamente a lo que se podría esperar, se induce una corriente ratchet.

* renato@us.es

[1] P. Reimann, Phys. Rep., **361**, 57 (2002).
[2] Niurka R. Quintero, José Cuesta and Renato Alvarez-Nodarse. Phys. Rev. E, **81**, 030102(R) (2010).
[3] Niurka R. Quintero, Renato Alvarez-Nodarse and José Cuesta. J. Phys. A: Math. and Theoretical **44**, 425205 (2011).
[4] R. F. Curtain and A. J. Pritchard, *Functional Analysis in Modern Applied Mathematics, Academic Press, London), 1977.*

# Modelo con retardo temporal para la infección por Hantavirus

J.A. Reinoso* F. Javier de la Rubia
*Departamento de Física Fundamental, Universidad Nacional de Educación a Distancia (UNED), Paseo Senda del Rey 9, E-28040 Madrid, Spain*

A raíz del descubrimiento en 1993 de la enfermedad Hantavirus Pulmonary Syndrome (HPS) capaz de causar la muerte en humanos, se identificó al virus SinNombre, como el causante de dicha enfermedad, y al ratón ciervo, el mamífero más extendido de Norte America, como su portador. Sin embargo hasta la fecha, no ha sido posible encontrar una vacuna que combata eficazmente la acción del virus. Como vía alternativa es posible estudiar la dinámica poblacional del ratón ciervo. Un factor que juego un papel relevante en la dinámica a largo plazo es el clima, y más en concreto variaciones climáticas como el Niño, la Niña o los monzones que se pueden asociar con los distintos fenómenos transitorios de aparición y desaparición de la infección[1]. En esta línea introducimos una nueva descripción basada en un modelo originalmente propuesto por Abramson y Kenkre[2], para tener en cuenta la división por edades entre jóvenes inmunes al virus y adultos susceptibles (ecuaciones 1, 2 y 3). En él, un mecanismo de maduración, caracterizado por un término de retardo $\tau$, indica el tiempo que tarda en pasar de una etapa a otra. Estudiamos el modelo de forma analítica y numérica atendiendo al parámetro que describe las variaciones climáticas. De las simulaciones numéricas, se observa como el brote (la desaparición) de la infección tiene lugar un tiempo después, al aumento (descenso) de la población total de ratones debido a la mejora (el empeoramiento) de las condiciones climáticas (fig. 1).

$$\frac{dM_Y}{dt} = bM - cM_Y - \frac{M_Y M}{K} - be^{-\gamma\tau}M(t-\tau) \quad (1)$$

$$\frac{dM_{As}}{dt} = be^{-\gamma\tau}M(t-\tau) - cM_{As} - \frac{M_{As}M}{K} - aM_{As}M_{Ai} \quad (2)$$

$$\frac{dM_{Ai}}{dt} = -cM_{Ai} - \frac{M_{Ai}M}{K} + aM_{As}M_{Ai} \quad (3)$$

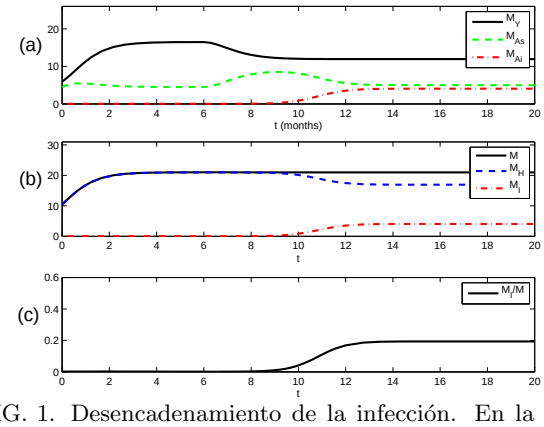


FIG. 1. Desencadenamiento de la infección. En la figura se observa la evolución temporal de la población de ratones, para los siguientes valores de los parámetros: $a = 0.4$, $b = 2$, $c = 0.6$, $\tau = 6$, $K = 15$ and $\gamma = 0.14$. La condición inicial es: $M_Y = 5.96$, $M_{As} = 4.50$, $M_{Ai} = 0.02$. En (a) estudiamos la evolución de las tres variables: jóvenes, $M_Y$, adultos susceptibles, $M_{As}$ y adultos infectados, $M_{Ai}$. En (b) se aprecia como el conjunto de todos los ratones, $M$, sigue la ecuación logística que se relaja rápidamente a un punto fijo después de un transitorio. A partir de entonces el sistema evoluciona dejando constante el número de ratones. $M_H$ se refiere al los ratones no infectados, $M_Y + M_{A_S}$, y $M_I$ a los infectados. La aparición de la infección se observa claramente en (c), donde se representa la relación entre ratones infectados y el total, iniciándose después de un tiempo que coincide con el tiempo de maduración $\tau$.

* jmaparicio@bec.uned.es

[1] T. L. Yates, J. N. Mills, C. A. Parmenter, T. G. Ksiazek, R. R. Parmenter, J. R. Vande Castle, C. H. Calisher, S. T. Nichol, K. D. Abbot, J. C. Young, et al., BioScience 52, 989 (2002).
[2] G. Abramson and V. Kenkre, Phys. Rev. E 66, 011912 (2002).

# Ordinal time-series analysis of low-frequency fluctuations in semiconductor lasers with optical feedback

A. Aragoneses*, N. Rubido**, T. Sorrentino, J. Tiana-Alsina, M. C. Torrent, C. Masoller
*Departament de Física i Enginyeria Nuclear, Universitat Politècnica de Catalunya, Colon 11, Terrassa, 08222, Barcelona, Spain.*

We study experimentally the dynamics of a semiconductor laser with time-delayed optical feedback in the regime of low-frequency fluctuations, where the laser intensity displays sudden and irregular power dropouts, that resemble excitable neuronal spikes. We show that, by using the ordinal methodology of nonlinear, simbolic time-series analysis, we can distinguish signatures of determinism and stochasticity in the sequence of intensity dropout events.

Deterministic nonlinearities and noise are present in many natural systems and there is often the need to distinguish their relative influence in observations of a system variable. In the case of time-delayed systems, this is particularly challenging as time delays results in a infinite-dimensional phase space that can make very tricky to distinguish high-dimensional deterministic dynamics from stochastic dynamics.

A semiconductor laser subjected to optical feedback is a well known example of this situation, as it can display complex dynamics in its output intensity that results from the interplay of deterministic, nonlinear light-matter interactions, spontaneous emission noise and time-delayed feedback effects. Close to the laser threshold the laser dynamics, referred to as Low Frequency Fluctuations (LFFs), consists of suden, irregular power dropouts, followed by gradual recoveries: the sequence of intensity dropouts resembling a sequence of excitable neuronal spikes.

We study the LFF dynamics employing a symbolic methodology of time series analysis known as Ordinal Analysis[1]. We have previously used this method for characterizing the complexity of the laser spikes[2,3] . In this work we show that this method can also yield light into the underlying structure of the laser spiking activity and distinguishes signatures of determinism and stochasticity.

We analyze experimentally measured time traces of the laser intensity, when the laser is biased close to threshold and thus stochastic effects are expected to play a crucial role in the LFF dropouts. More specifically, we analyze the sequence of time-intervals, $\Delta T_i$ , between consecutive dropouts (referred to as inter-dropout intervals or IDIs) and transform the sequence of IDIs into a sequence of or dinal patterns, or words. We then study the statistics and the transition probabilities among these words. To further analyze the underlying structure in the sequence of spikes we select a threshold $\Delta T_{th}$ that separates the IDI sequence into trains (or bursts) of consecutive short interdropout intervals, that are separated by longer intervals that are assumed to correspond to stable, fixed point (FP) behavior. For adequate values of the threshold $\Delta T_{th}$ the differences in the statistics of the words formed by the bursts intervals and by the fixed point intervals allow to interpret the full sequence of LFF dropouts as composed by bursts of consecutive spiking events with a deterministic underlying dynamics, that are separated by stochastic spiking events, associated to noise-induced fixed-point escapes. In addition, the comparison of the statistical distribution of the bursts intervals with recent numerical simulations of transient LFF dynamics based on the Lang-Kobayashi time-delayed model[4] allows interpreting the LFFs observed experimentally as a noise-sustained, deterministic transient spiking dynamics.

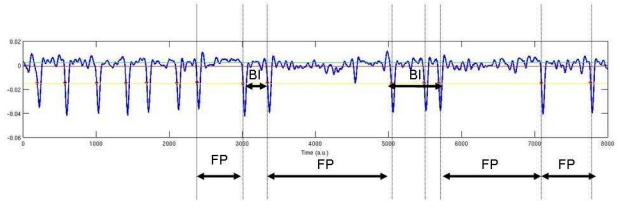


FIG. 1. Experimental time trace of the laser output intensity displaying power dropouts events. The timeintervals between consecutive power dropouts are classified as Fix Point (FP) intervals or Burst Intervals (BI) if they are longer or shorter than a given threshold ($\Delta T_{th}$).

* andres.aragoneses@upc.edu
** School of Natural and Computing Sciences, University of Aberdeen, King's College, Old Aberdeen, AB24 3UE, UK

[1] C. Bandt and B. Pompe, Phys. Rev. Lett. 88, 174102 (2002).
[2] J. Tiana-Alsina et al, Phys. Rev. A 82, 013819 (2010).
[3] N. Rubido et al, Phys. Rev. E 84, 026202 (2011).
[4] J. Zamora-Munt, Phys. Rev. A 81 033820 (2010).

# Collective modes of coupled phase oscillators with delayed coupling

Saúl Ares*†, Luis G. Morelli†‡¶, David J. Jörg, Andrew C. Oates‡, and Frank Jülicher
*Max Planck Institute for the Physics of Complex Systems*
*Nöthnitzer Str. 38, 01187 Dresden, Germany*

We study the effects of delayed coupling on timing and pattern formation in spatially extended systems of dynamic oscillators. Starting from a discrete lattice of coupled oscillators, we derive a generic continuum theory for collective modes of long wavelength[1].

The discrete lattice of coupled oscillators can be described by an evolution equation for the phase $\theta_{\mathbf{i}}$ of the oscillator $\mathbf{i}$, coupled to its nearest neighbors $\mathbf{j}$:

$$\frac{d\theta_{\mathbf{i}}(t)}{dt} = \omega_{\mathbf{i}} + \frac{\varepsilon_{\mathbf{i}}}{2d} \sum_{|\mathbf{j}-\mathbf{i}|=1} h(\theta_{\mathbf{j}}(t-\tau) - \theta_{\mathbf{i}}(t)) \ , \qquad (1)$$

where $\omega_{\mathbf{i}}$ is the intrinsic frequency of the oscillator $\mathbf{i}$, $\varepsilon_{\mathbf{i}}$ denotes the coupling strength of this oscillator to its neighbors, and $\tau > 0$ is a time delay in the coupling. The coupling is described by the $2\pi$-periodic function $h$. Introducing the continuum phase $\theta(x,t)$ and functions $\omega(x)$ and $\varepsilon(x)$ we show that the collective modes of long wavelength of Eq. (1) can be described by:

$$\frac{\partial\theta(x,t)}{\partial t} = \omega(x) + \varepsilon(x) h(\theta(x,t-\tau) - \theta(x,t)) \qquad (2)$$

$$+\frac{\varepsilon(x)a^2}{2} h''(\theta(x,t-\tau) - \theta(x,t)) \left(\frac{\partial\theta(x,t-\tau)}{\partial x}\right)^2$$

$$+\frac{\varepsilon(x)a^2}{2} h'(\theta(x,t-\tau) - \theta(x,t)) \frac{\partial^2\theta(x,t-\tau)}{\partial x^2} \ ,$$

where the prime denotes the derivative of $h$ with respect to its argument.

We use this approach to study spatial phase profiles of cellular oscillators in the segmentation clock, a dynamic patterning system of vertebrate embryos[2,3]. Collective wave patterns result from the interplay of coupling delays and moving boundary conditions[4,5]. We show that the phase profiles of collective modes depend on coupling delays, and derive experimental features of the segmentation clock starting from a very general framework.

---

* saul.ares@csic.es Also member of Grupo Interdisciplinar de Sistemas Complejos (GISC). Present address: Logic of Genomic Systems Laboratory, Centro Nacional de Biotecnología - CSIC. Calle Darwin 3, 28049 Madrid, Spain.
† These authors contributed equally to this work.
‡ Max Planck Institute of Molecular Cell Biology and Genetics, Pfotenhauerstr. 108, 01307 Dresden, Germany.
¶ CONICET, Departamento de Física, UBA, Ciudad Universitaria, 1428 Buenos Aires, Argentina.

[1] S. Ares, L.G. Morelli, D.J. Jörg, A.C. Oates and F. Jülicher, *Phys. Rev. Lett.* **108** 204101 (2012).
[2] D. Roellig, L.G. Morelli, S. Ares, F. Jülicher and A.C. Oates, *Cell* **145**, 800 (2011).
[3] A.C. Oates, L.G. Morelli and S. Ares, *Development* **139**, 625 (2012).
[4] L.G. Morelli, S. Ares, L. Herrgen, C. Schröter, F. Jülicher and A.C. Oates, *HFSP J.* **3**, 55 (2009).
[5] L. Herrgen, S. Ares, L.G. Morelli, C. Schröter, F. Jülicher and A.C. Oates, *Curr. Biol.* **20**, 1244 (2010).

# Optimal oscillator mobility for synchronization arising from the gradual recovery of oscillator coupling

Koichiro Uriu[†‡], Saúl Ares[*‡], Andrew C. Oates and Luis G. Morelli[‡¶]
*Max Planck Institute of Molecular Cell Biology and Genetics*
*Pfotenhauerstr. 108, 01307 Dresden, Germany*

Systems of moving oscillators that can interact between them are common in nature and in artificial systems. Previous theoretical works have shown that faster movement favors synchronization across populations of coupled oscillators[1–3]. An important assumption in these studies is that oscillators can immediately interact with their new neighbors after arriving at a new location. However, restoring coupling may not be instantaneous, an example being cellular systems where intercellular interactions may need some time to become fully established. How movement affects synchronization in this situation has not been examined. Here, we develop a coupled phase oscillator model in which we consider oscillator movement and the gradual recovery of coupling experienced by an oscillator after movement, characterized by a moving rate and a coupling recovery rate, respectively[4]. We find (1) an optimal moving rate for synchronization and (2) a critical moving rate above which achieving synchronization is not possible. These results indicate that the extent to which movement enhances synchrony is limited by a gradual recovery of coupling, suggesting that the ratio of time scales of movement and signaling recovery is critical for information transfer between moving oscillators.

* saul.ares@csic.es Also member of Grupo Interdisciplinar de Sistemas Complejos (GISC). Present address: Logic of Genomic Systems Laboratory, Centro Nacional de Biotecnología - CSIC. Calle Darwin 3, 28049 Madrid, Spain.
† Theoretical Biology Laboratory, RIKEN Advanced Science Institute, 2-1 Hirosawa, Wako, Saitama, 351-0198, Japan.
‡ Max Planck Institute for the Physics of Complex Systems, Nöthnitzer Str. 38, 01187 Dresden, Germany
¶ Departamento de Física, FCEyN, UBA, Ciudad Universitaria, 1428 Buenos Aires, Argentina

[1] K. Uriu, Y. Morishita and Y. Iwasa, *Proc. Natl Acad. Sci.* USA **107**, 4979 (2010).
[2] F. Peruani, E.M. Nicola and L.G. Morelli, *New J. Phys.* **12** 093029 (2010).
[3] N. Fujiwara, J. Kurths and A. Díaz-Guilera,*Phys. Rev.* E **83** 025101 (2011).
[4] K. Uriu, S. Ares, A.C. Oates and L.G. Morelli, *Phys. Biol.* **9**, 036006 (2012).

# Estados hidrodinámicos no estacionarios en el flujo longitudinal uniforme de un gas granular. Cumulantes y función de distribución

Antonio Astillero* y Andrés Santos†,‡
*Departamento de Tecnología de Computadores y Comunicaciones*
*Universidad de Extremadura, 06800 Mérida*

Un gas granular es un tipo particular de sistema complejo en el que una de las características más sobresalientes que lo definen es la disipación de energía que se produce cuando tiene lugar una colisión entre partículas. Además de su interés en aplicaciones industriales y tecnológicas, los gases granulares son importantes desde un punto de vista fundamental, teniendo en cuenta que se trata de sistemas físicos inherentemente alejados del equilibrio y, por tanto, mostrando un rico comportamiento complejo.

Una de las maneras más sencillas de modelizar un gas granular es suponer que está formado por un conjunto de esferas duras inelásticas lisas con un coeficiente de restitución normal $\alpha$. En el régimen diluido, una aproximación a este tipo de sistemas físicos utilizando la teoría cinética (basada en las ecuaciones de Boltzmann y Enskog convenientemente adaptadas a la inelasticidad de las colisiones entre partículas) ha resultado ser muy eficaz[1].

En este trabajo, partimos de un gas granular sometido a condiciones de flujo longitudinal uniforme[2] (ULF) y estudiamos la evolución temporal de la función de distribución de velocidades de una partícula y de sus momentos en la etapa *hidrodinámica*[3], que comienza una vez que la etapa cinética inicial (muy sensible por cierto a las condiciones iniciales) ha comenzado a decaer. Los elementos básicos que definen este flujo[2,3] son un campo de velocidades longitudinal y lineal $u_x(x,t) = a(t)x$, donde $a(t) = a_0/(1 + a_0 t)$ es el gradiente de velocidad, una densidad uniforme $n(t) \propto a(t)$ y una temperatura granular $T(t)$ también uniforme. En un gas granular caracterizado por un coeficiente de restitución normal constante $\alpha$, el parámetro de control relevante del problema es el gradiente de velocidad reducido $a^*(t) = a(t)/\nu(t)$ (que representa el papel de número de Knudsen), donde $\nu(t) \propto n(t)\sqrt{T(t)}$ es una frecuencia de colisión efectiva.

En un trabajo reciente[3], se presentaron resultados de simulaciones DSMC[4] correspondientes a la evolución hidrodinámica de la viscosidad tangencial no newtoniana (reducida) $\eta^*(a^*) = \frac{3}{4}\left(1 - T_x/T\right)/a^*$, donde $T_x$ es la temperatura parcial a lo largo de la dirección $x$, en función de $a^*$. El objetivo del presente trabajo es extender aquel análisis a los momentos de orden superior, tales como el segundo ($a_2$) y tercer ($a_3$) cumulantes, así como a la función de distribución de velocidades.

A modo de ejemplo, en la figura 1 se representa $a_2$ frente a $a^*$ para $\alpha = 0.5$. El círculo abierto representa el estado estacionario, el cual juega el papel de atractor en la evolución cuando $a^* < 0$. El punto negro en $a^* = 0$ corresponde al estado de enfriamiento homogéneo, que hace de repulsor en la evolución, tanto para $a^* < 0$ como para $a^* > 0$. Observamos que tras la etapa cinética, que dura apenas unas pocas colisiones por partícula, las curvas correspondientes a condiciones iniciales diferentes tienden a colapsar todas en una curva común.

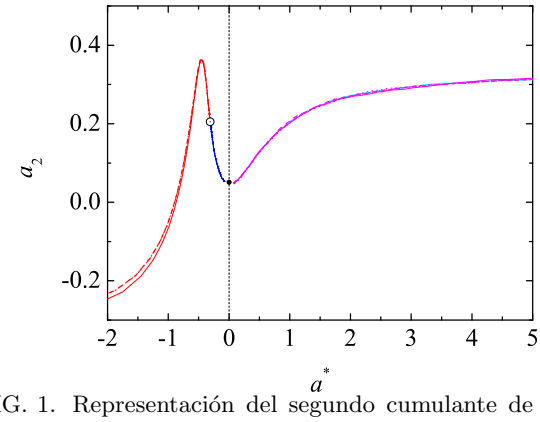


FIG. 1. Representación del segundo cumulante de la velocidad $a_2(t)$ frente al gradiente de velocidad reducido $a^*(t)$ para $\alpha = 0.5$.

* aavivas@unex.es
http://www1.unex.es/eweb/fisteor/antonio_astillero
† Departamento de Física, Universidad de Extremadura, 06071 Badajoz
‡ andres@unex.es
http://www1.unex.es/eweb/fisteor/andres

[1] N. Brilliantov and T. Pöschel, *Kinetic theory of granular gases* (Oxford University Press, Oxford, 2004).
[2] A. Santos, in *Rarefied Gas Dynamics: Proceedings of the 26th International Symposium on Rarefied Gas Dynamics*, Takashi Abe, ed. (AIP Conference Proceedings, vol. 1084, Melville, NY, 2009), pp. 93-98.
[3] A. Astillero and A. Santos, *Phys. Rev. E* **85**, 021302 (2012).
[4] G. A. Bird, in *Molecular gas dynamics and the direct simulation of gas flows*, Oxford Science Publications, Oxford (1994).

# Avalanches in the 3D-Gaussian Random Field Ising Model

Jordi Baró*, Eduard Vives†
*Departament d'Estructura i Constituents de la Matèria. Facultat de Física. Universitat de Barcelona. Diagonal, 647, E-08028 Barcelona, Catalonia.*

The 3D-Gaussian Random Field Ising Model[1] is widely used as a prototype model for the study of avalanche dynamics. For a critical amount of disorder $R_c$, this model reproduces the scale-free behaviour present in many natural systems[2]. However, numerical simulations tend to show a distorted distribution of avalanches because of the finite size of the lattice and the persistence of the effects caused by the discrete nature of the simulation[3]. We can identify these effects with the presence of small non-critical avalanches –known as lattice-animals in percolation theory[5]– and large spanning avalanches in the critical and subcritical regime. In order to avoid the presence of the non-critical spanning avalanches different techniques[6] and methods of classification[3,4] have been proposed. We have developed a technique[7] that allows to improve the classification of the avalanches. We will also discuss the effect of the lattice animals from the analysis of the interevent times[8] and avalanche rates.

* jordibaro@ecm.ub.es
† eduard@ecm.ub.es

[1] James P. Sethna, Karin Dahmen, Sivan Kartha, James A. Krumhansl, Bruce W. Roberts, and Joel D. Shore, Phys. Rev. Lett. **70**, 3347 (1993).
[2] O.Perkovic, K.A.Dahmen and J.P.Sethna, Phys. Rev. B **59**, 6106 (1999).
[3] F.J.Pérez-Reche and E.Vives, Phys. Rev. B **67**, 134421 (2003).
[4] F.J.Pérez-Reche and E.Vives, Phys. Rev. B **70**, 214422 (2004).
[5] D.Stauffer and A.Aharony, *Introduction to percolation theory* 2nd ed. Taylor and Francis UK (1994).
[6] Y.Liu and K.A.Dahmen, Phys. Rev. E **79**, 061124 (2009).
[7] J.Baró, E. Vives, e-print (arXiv:1202.2043)
[8] B.Cerruti and E.Vives, Phys. Rev. B **77**, 064114 (2008).

# Structure and fluctuations of adsorbed liquid films close to a first order wetting transition

Jorge Benet†, Luis G. MacDowell†, Eva M. Fernández‡, Enrique Chacón‡, Pedro Tarazona§‡
†*Departamento de Química Física, Facultad de Ciencias Químicas, Universidad Complutense de Madrid* ‡ *Instituto de Ciencia de Materiales de Madrid, CSIC, Madrid* § *Departamento de Física Teórica de la Materia Condensada, Universidad Autónoma de Madrid*

The concept of interface potential is a very convenient tool for the rationalization of wetting behavior. This potential is defined as the free energy, $g(\ell)$ of an adsorbed liquid film of height $\ell$ above the substrate[1] (a related quantity that is more familiar in some related communities is the concept of "disjoining pressure" which is actually obtained as the derivative of the interface potential). However, a careful analysis of this concept soon reveals important difficulties, that have their origin in the mean field approximation which is usually implied.[2] On the one hand, a continuous function of $\ell$ assumes explicitly that films or arbitrary thickness may be built, while in practice, the concave part of the thermodynamic potential should be ruled out as unstable. Secondly, due to thermal fluctuations, a film described by means of an average thickness is a poor description of its actual shape, which is actually rough as a result of capillary waves. Furthermore, the proper location of the films interface is also difficult and requires a careful analysis.[3] In this communication we will attempt to find a proper order parameter that is suitable to describe the corrugated nature of the adsorbed film and allows one to properly describe its related free energy. Stemming from this analysis,[4] one can determine the structure of the adsorbed film as seen from the liquid–vapor interface, rather than from the usual perspective that results when one places the origin at the substrate. The results are striking and reveal almost as much layering at the liquid-vapor interface than is observed at the substrate.

Within the "Surface Hamiltonian" approximation, the interface potential may be exploited in order to describe the shape of condensates on complex or structured substrates. The total free energy is then considered as a surface integral over $g(\ell(x,y))$, with the extra cost of bending the interface weighted by the surface tension.[5] In this paper, we will also consider the feasibility of extracting a meaningful $g(\ell)$, from the study of interfacial fluctuations of adsorbed flat films. i.e., we test whether one can calculate from simulations a continuous function, $g(\ell)$, which will simultaneously describe the wetting behavior of flat films and the deformations of such films away from planarity.

---

* luis@ender.quim.ucm.es

[1] M. Schick. In *Liquids at Interfaces*, Les Houches Lecture Notes, 1–89 (Elsevier Science Publishers, Amsterdam, 1990).

[2] L. G. MacDowell. Computer Simulation of Interface Properties: Towards a First Principle Description of Complex Interfaces? *Euro. Phys. J. ST*, **197**, 131–145 (2011).

[3] P. Tarazona, R. Checa and E. Chacon. Critical Analysis of the Density Functional Theory Prediction of Enhanced Capillary Waves. *Phys. Rev. Lett.*, **99**,

[4] E. M. Fernández, E. Chacón and P. Tarazona. Thickness and Fluctuations of Free and Adsorbed Liquid Films. *Phys. Rev. E*, **84**, 205435 (2011).

[5] S. A. Safran. *Statistical Thermodynamics of Surfaces, Interfaces and Membranes* (Addison-Wesley, Reading, 1994), first edition.

[6] E. M. Fernández, E. Chacón and P. Tarazona. Capillary Waves Spectrum at Adsorbed Liquid Films. *Phys. Rev. B* (2012).

# Collective migration of cells in spreading epithelia

Carles Blanch-Mercader* and Jaume Casademunt.
*Departament Estructura i Constituents de la Matèria, Universitat de Barcelona, Av. Diagonal 647, Barcelona, Spain*

Collective cell migration is present in many biological processes. It requires a guidance mechanism to coordinate mechanical stresses in large groups of cells. An example that has received intensive attention recently is the free advance of the front of a confined epithelial tissue when the confinement is removed. Cells are able to transmit forces through cell-cell junctions and through adhesion on the substrate, and tend to modify their trajectories in order to minimize the local intracellular stress[1]. Recently, it has been possible to measure quantitatively for the first time the mechanical stresses exerted at the cell-cell junctions, and on the substrate within single-cell resolution[1]. A detailed theoretical modeling of this process and the mechanical stresses involved, however, is still lacking.

Inspired by the above experiments, in this work we focus on understanding the collective migration of an advancing tissue of epithelial cells, considering the internal flow of actin in the crawling of cells, and the generation of traction forces applied on the substrate through focal adhesions. It has been pointed out[2] that during the spreading process of a tissue made up of Madin-Carby kidney epithelial cells, each individual cell in the sheet is not selfpropelling, whereas the traction force distribution on the cell sheet reveals that a single cell in the tissue does exert a net force on the substrate.

In this study we model an epithelial tissue as an active polar nematic gel[3,4]. Momentum and mass conservation then read

$$\begin{aligned} \partial_a \left(\sigma^{tot}_{\alpha,\beta} - P\delta_{\alpha,\beta}\right) &= \xi v_\alpha - f_c p_\alpha \\ \partial_t \rho + \partial_\alpha \left(v_\alpha \rho\right) &= \gamma \end{aligned}$$

where $p_\alpha$ is a polarization field which measures the degree of orientation of a patch of cells, $v_\alpha$ is the macroscopic velocity field of the tissue, $P$ stands for the pressure field and $\sigma^{tot}_{\alpha,\beta}$ is the total stress tensor. Due to the spreading process the thickness of the quasi-twodimensional tissue may vary along the cell sheet and consequently it might modify locally the density of cells. In order to take this into account in our model phenomenologically, we assume a certain function $\gamma$ which for simplicity will be considered homogeneous[5]. There are two different external friction forces from the substrate: the term $\xi v_\alpha$, coming from the macroscopic displacement of a group of cells relative to the substrate and the term $f_c p_\alpha$, which is due to internal actin flux from the lamellipodia.

The proposed framework is a coarse-grained description that treats the tissue as a continuous active material. We expect that different phenomenology already observed in experiments[1,2] may be understood within this approach. As a first step, we have studied the morphological instability of the advancing front of cells to transversal modulations, a phenomenon that is observed to lead to fingering patterns. The growth rate of a transversal perturbation on the leading edge is shown in the figure for two different biological values of the shear viscosity. The dominant transversal scale of the fingering of the leading edge is seen to be consistent with the dominant transversal wavelength obtained from experimental data, and provides an indirect way to obtain effective parameters of the model that cannot be easily accessed directly. The mechanism of destabilization of the front can be understood in terms of the microscopic friction force of the leading cells, provided that the strength of this physical element is above a critical value. Note that this term depends crucially on the nematic order of the cells. These results set the basis for a more detailed and quantitative understanding of a variety of experimental phenomena[2].

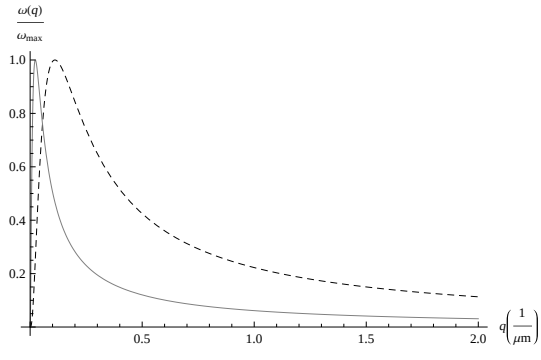


FIG. 1. Linear growth rate of a transversal perturbation on a rectangular steady configuration under biologically parameters normalized by its maximum positive value. The dashed curve corresponds to a shear viscosity of $10^4 Pa \cdot s$ and the solid curve to one of $10^7 Pa \cdot s$.

* blanch@ecm.ub.es

[1] D. T. Tambe, C. C. Hardin, T. E. Angelini, K. Rajendran, C. Y. Park, X. Serra-Picamal, E. H. Zhou, M. H. Zaman, J. P. Butler, D. A. Weitz, J. J. Fredberg and X. Trepat, Nature Materials, vol. 10, (2011)
[2] X. Trepat, M. R. Wasserman, T. E. Angelini, E. Millet, D. A. Weitz, J. P. Butler and J. J. Fredberg, Nature Physics, vol 5, (2009)
[3] J. Ranft, M. Basan, J. Elgeti, J.F. Joanny, J. Prost and F. Jülicher, PNAS, vol. 107, no. 49 (2010)
[4] K. Kruse, J.F. Joanny, F. Jülicher, J. Prost, and K. Sekimoto, Eur. Phys. J. E, 16, 5 (2005)
[5] B. I. Shraiman, PNAS, vol. 102, no. 9 (2005)

# Free energy calculations of molecular inclusions in short capped nanotubes: Targeted Molecular Dynamics and Grand Canonical Monte Carlo Calculations

C. Bores[1*], E. Lomba[1], H. Dodzyuk[2] and T. Korona[3]
[1] *IQFR-CSIC, Serrano 119, E-28006 Madrid*
[2] *Institute of Physical Chemistry, PAN, Warsaw, Poland*
[3] *Faculty of Chemistry, University of Warsaw, Poland*

Short capped nanotubes are hemispherical polyarene formed of 50 carbon atoms ($C_{50}H_{10}$) that comprise a complete end-cap and the beginnings of the sidewalls of a carbon nanotube. These structures can be used as small hydrocarbon templates for uniform growth of nanotubes.

Crystallization of these structures has been achieved by slow evaporation of a solution in $CS_2$, and the crystal structure obtained reveals that the cavity of every nanotube is occupied by a carbon disulfide molecule. The target of this research is to estimate the free energy of the $CS_2$ inclusion into the short nanotube, showing the tendency of these nanotubes to host molecules and estimate the estability of the resulting system in the presence of the solvent and without it. Molecular inclusion free energy is calculated by Targeted Molecular Dynamics simulation[2] and by Monte Carlo simulation in the Grand Canonical Ensemble[3].

Firstly, Targeted Molecular Dynamics Method considers spontaneous transitions between known end structures in order to estimate profiles of free energy and transition rates along the reaction coordinate. To this end, suitable defined distances are necessary to provide a first conjecture for the reaction coordinates of desired activated processes[2]. Finally, the required transitions are carried out by decreasing the constrained distance during a molecular dynamics simulation.

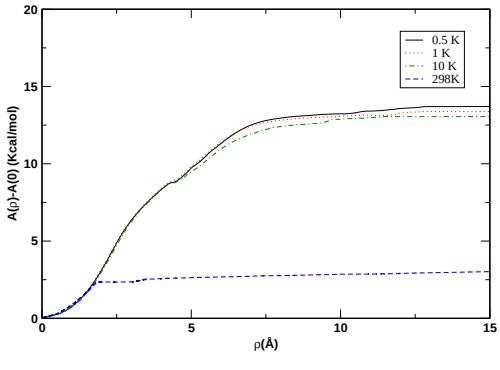


FIG. 1. Capped nanotube - $CS_2$ molecule binding free energy by Targeted Molecular Dynamics. The free energy profile has been given for different temperatures and belongs to vacuum conditions

In this case, we have taken the $CS_2$ molecule from the inside of the capped nanotube until a point far enough to avoid interaction between the nanotube and the $CS_2$ molecule. This is controlled by means of a reaction coordinate $\rho$, which measures the root mean square separation from the equilibrium positions of the $CS_2$ molecule inside the nanotube.

Figure 1 corresponds to the work (free energy) needed to drag the $CS_2$ molecule from the cage in vacuum. In Figure 2 we represent the corresponding work for a system at 298K, in presence of $Cl_3CH$ as solvent, which stabilizes the inclusion. As a reference we also plot the work required to drag a single $CS_2$ molecule in the bulk solvent.

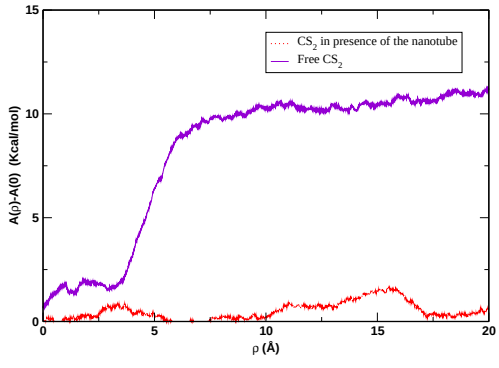


FIG. 2. Capped nanotube - $CS_2$ molecule binding free energy by Targeted Molecular Dynamics. The free energy profile has been given for T=298K and corresponds to the presence of solvent.

We will illustrate that the choice of a proper simulation length is crucial in the TMD calculations, so as to minimize kinetic energy effects in the corresponding free energy calculations.

Free energies will also be calculated by Monte Carlo simulation in the Grand Canonical Ensemble[3]. This second method has some benefits such as the independece of the simulation with the starting and ending positions, and with the nature of the binding site.

* Email address: cbores@iqfr.csic.es.

[1] L.T. Scott, E. A. Jackson, Q. Zhang, B.D. Steinberg, M. Bancu, and B. Li, J.Am.Chem.Soc., 134, 107 (2012)
[2] J. Schlitter, W. Swegat adn T. Mülders, J. Mol. Model., 7, 171 (2001)
[3] M. Clark, S. Meshkat, and J.S. Wiseman, J. Chem. Inf. Model. 49, 934 (2009)

# Theoretical study of the H-NMR relaxation times in aqueous ionic solutions

Carles Calero*, Elvira Guàrdia and Jordi Martí
*Departament de Física i Enginyeria Nuclear, Universitat Politècnica de Catalunya, B4-B5 Campus Nord 08034 Barcelona*

Understanding the relaxation of the nuclear spin in fluids is of fundamental interest and related to important applications such as nuclear magnetic resonance (NMR). The chemical shift spectra and the relaxation times ($T_1$ and $T_2$) obtained from NMR experiments are among the most reliable techniques to determine the molecular structure and chemical properties of a given substance.

In fluid samples, the relaxation properties of the nuclear spin are different from those observed in solids. This is due to the existence of rapid molecular motions of large amplitude and random character. These motions include rotational tumbling of individual and groups of molecules, relative translational motion of molecules and, in some cases, even migrations of atoms from one molecule to another. In molecular fluids, the relaxation time for the nuclear spin is determined by its interaction with other spins through dipolar and quadrupolar coupling and also by the sudden changes of the chemical shift local field due to mechanical rotations. In treating the relaxation of the nuclear spin of the protons of water, quadrupolar interacions are irrelevant, since they are only important for particles with spin $S \geq 1$, and the relaxation due to dipolar coupling is dominant. The relaxation due to dipolar coupling can be decomposed into two contributions: a dominant contribution, determined by molecular reorientation and caused by the interaction with the other hydrogen of the same molecule (intramolecular coupling), and another less important contribution caused by the interaction with hydrogens of other molecules (intermolecular coupling) which is mainly determined by the relative translations between molecules[1].

To compute the NMR relaxation times $T_1$ and $T_2$ in a fluid it is necessary to faithfully describe the rapid random motions that particles undergo due to collisions with other particles. Traditionally, assumptions on the nature of the Brownian motions were made to simplify the problem. The most extended treatment, due to Debye, assumes that both the rotations of a molecule and the relative translations of two molecules could be described by a diffusion equation. In that picture, the angular Brownian motion of the water molecules are given by very small regular angular steps. In recent years, however, a combination of theoretical and experimental breakthroughs has provided consistent evidence suggesting a dominant reorientation of water via a mechanism involving large-amplitude sudden angular jumps[2]. Consequently, many of the interpretations of experiments and theoretical predictions based on Debye's picture, in particular those regarding the relaxation properties of nuclear spin of protons in water, need to be revised.

In the present work we have devised a way to calculate the NMR relaxation times $T_1$ and $T_2$ for molecular fluids directly from the trajectories of MD simulations, with no assumptions made regarding the nature of the molecular motions. In particular, we have computed $T_1$ and $T_2$ for the nuclear spins of protons of bulk liquid water as described by different water models (TIP3P, TIP4P, and TIP4P/2005). Also, we have studied the dependence of such relaxation times on the concentration of different chaotropic and kosmotropic ions, reproducing the behaviour obtained in experiment: an increase (decrease) of the NMR relaxation times as the concentration of chaotropic (kosmotropic) ions is increased[3]. Furthermore, the mechanisms hypothesized in the literature responsible for such behaviour are quantitively analyzed. Under several simplifying assumptions, we have also obtained analytical results for the NMR relaxation times $T_1$ and $T_2$ based on Ivanov's model of water reorientation[4] and compared them with the results obtained from the MD simulations' trajectories.

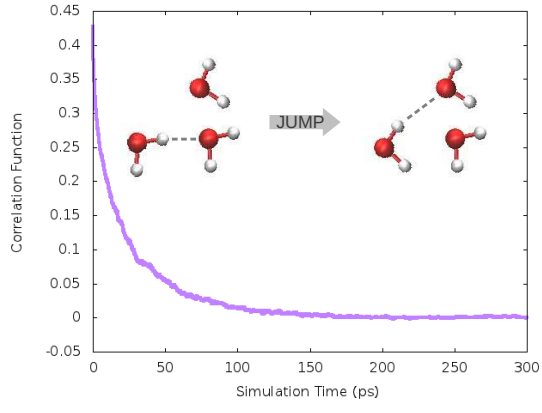


FIG. 1. The reorientation of water molecules occurs via large-amplitude sudden angular jumps. Such mechanism governs the time dependence of the different correlation functions which determine the H-NMR relaxation times.

* carles.calero@upc.edu

[1] A. Abragam, The principles of nuclear magnetism, Clarendon Press, Oxford (1961).
[2] D. Laage, J. T. Hynes, Science **311**, 832 (2006).
[3] H. J. Bakker, Chem. Rev. **108**, 1456 (2008); K. J. Tielrooij, N. Garcia-Araez, M. Bonn, H. J. Bakker, Science **328**, 1006 (2010).
[4] E. N. Ivanov, Sov. Phys. JETP **18**, 1041 (1964); K. A. Valiev and E. N. Ivanov, Sov. Phys.-Usp. **16**, 1 (1973).

# Force Fields Parametrization of Ion-Water Interactions via the Force Matching Algorithm

Ausias-March Calvo[†*], Marco Masia[‡] and Elvira Guàrdia[†]
[†] *Departament de Física i Enginyeria Nuclear, Universitat Politécnica de Catalunya, Campus Nord, B4-B5 08034 Barcelona, Spain*
[‡] *Dipartimento di Chimica, Università degli Studi di Sassari, Sardinian Laboratory for Computational Materials Science SLACS (INFM-CNR) and INSTM, Via Vienna 2, 07100 Sassari, Italy*

Ion solvation constitutes a central topic in chemical physics and theoretical chemistry; up to now a huge quantity of classic Molecular Dynamics studies have been performed to look into different aspects of Ion solvation. One crucial point lies in the choice of parameters of the interaction model, the so-called force-field. In most refined approaches, they are usually found by fitting hundreds of points on the ab initio potential energy surface (PES) for relatively small clusters, (cf. Ref. 1). Although being accurate, the main drawback of this approach is that the PES explored is not the one for the condensed phase and some points included in the fit could be physically unimportant, while at the same time missing some points that are important. To overcome this problem, a new method has been recently introduced, which is based on a least-square fitting to forces obtained from ab initio calculations of the condensed phase of interest[2,3]. In this contribution the focus is on the parameters for the interaction between ions and water. To this end, Car Parrinello Molecular Dynamics simulations[4] have been used to compute the reference forces; then, we fitted ion-solvent interaction parameters in conjunction with the most widespread classical force fields for water. The ions studied include $F^-$, $Cl^-$,$Br^-$, $I^-$, $Li^+$, $Na^+$, $K^+$, $Mg^{2+}$ and $Ca^{2+}$. Fig. 1 shows some representative scatter plots of the ion-water force fields derived in combination with the SPC water model. The slope $b$ of the fitted forces versus the ab initio forces is also included.

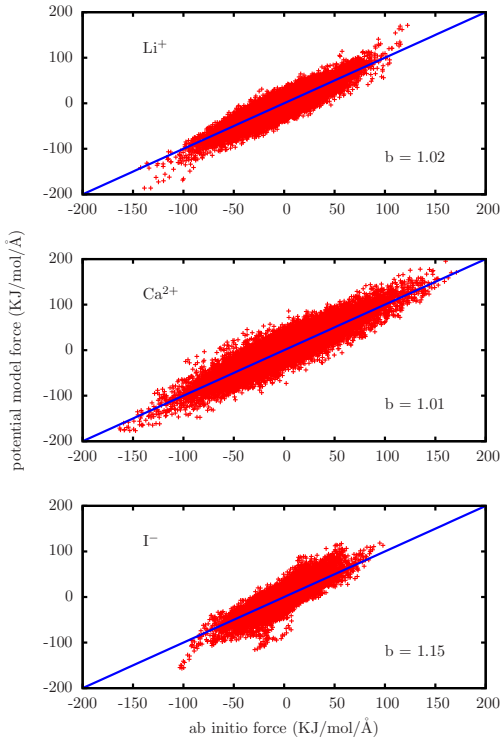


FIG. 1. Scatter plots of ion-water atomic forces: The potential model force vs. the ab initio Car-Parrinello force for the force fields derived in combination with the SPC water model. The line corresponds to a perfect match, i. e. $b = 1$. Top: $Li^+$, Medium: $Ca^{2+}$, Bottom: $I^-$

* ausias.march@upc.edu

[1] D. Spångberg and K. Hermansson, J. Chem. Phys. **120**, 4829 (2004).
[2] S. Izvekov, M. Parrinello, C. J. Burnham and G. A. Voth, J. Chem. Phys. **120**, 10896 (2004).
[3] D. Spångberg, E. Guardia, and M. Masia, Comput. Theor. Chem. **982**, 58 (2012).
[4] E. Guardia, I. Skarmoutsos, and M. Masia, J. Chem. Theory Comput. **5**, 1449 (2009).

# Affinity measurements of ligands binding nucleic acids using fluctuation theorems

J. Camunas-Soler[1,2*],A. Alemany[1,2], I. Tinoco Jr.[3], F. Ritort[1,2]
*1) Small Biosystems Lab, Departament de Física FonamentalFacultat de Física Universitat de Barcelona, Barcelona, Spain*
*2) CIBER de Bioingeniería, Biomateriales y Nanomedicina, Instituto de Salud Carlos III, Madrid, Spain*
*3) Department of Chemistry, University of California, Berkeley, CA 94720, USA.*

Fluctuation theorems allow to relate the work performed along non-equilibrium trajectories to thermodynamic free-energy differences. In the past years, fluctuation theorems have been used to obtain the free-energy of formation of DNA and RNA structures from force-spectroscopy measurements[1]. More recently, an extended version of the Crooks fluctuation relation has been used to recover free-energies of intermediate and misfolded structures[2,3]. However, so far this method has only been applied to unimolecular reactions. In this work, we have measured the binding affinity of a set of ligands to DNA and RNA structures using the Crooks fluctuation relation. We have measured the affinity of binding of single DNA intercalators, DNA restriction enzymes, and an RNA binding protein, finding good agreement with bulk measurements. We have measured the binding energy of low solubility compounds difficut to characterize with bulk techniques. The use of fluctuation theorems to obtain binding affinities in bimolecular reactions is also of interest to characterize protein-protein affinities.

* joan.camunas@gmail.com

[1] F. Ritort, *Nonequilibrium fluctuations in small systems: from physics to biology*, Advances in Chemical Physics, **137**, 31-123 (2008). Ed. Stuart. A. Rice, Wiley publications
[2] I. Junier, A. Mossa, M. Manosas and F. Ritort, *Recovery of free energy branches in single molecule experiments*, Physical Review Letters, **102** (2009) 070602
[3] A. Alemany, A. Mossa, I. Junier and F. Ritort, *Experimental free energy measurements of kinetic molecular states using fluctuation theorems*, Accepted Nature Physics

# Unraveling the kinetics of aggregation of single peptide-DNA complexes using force spectroscopy

J. Camunas-Soler[1,2*],S. Frutos[1,2], C.V. Bizarro[1,2], S. de Lorenzo[1,2],M.E. Fuentes-Perez[3], R. Ramsch[4,2], S. Vilchez[4,2], C. Solans[4,2], F. Moreno-Herrero[3], F. Albericio[5,2], R. Eritja[4,5,2], E. Giralt[5,2], S.B. Dev[5], F. Ritort[1,2]

*1) Small Biosystems Lab, Departament de Física FonamentalFacultat de Física Universitat de Barcelona, Barcelona, Spain*

*2) CIBER de Bioingeniería, Biomateriales y Nanomedicina, Instituto de Salud Carlos III, Madrid, Spain*

*3) Centro Nacional de Biotecnologia, CSIC, Cantoblanco, Madrid, Spain*

*4) Institut de Química Avançada de Catalunya Consejo Superior de Investigaciones Científicas (IQAC-CSIC), Barcelona, Spain*

*5) Institute for Research in Biomedicine(IRB Barcelona), Barcelona Science Park Baldiri Reixac 10-12,08028, Barcelona, Spain*

The knowledge of the mechanisms of interaction between hydrophobic molecules and essential cellular components is key to the understanding of many aggregation processes underlying several human diseases. Kahalalide F (KF) is an hydrophobic marine-derived peptide with a strong anticancer activity which contains a positively charged residue (L-Orn). KF is an ideal model to elucidate the mechanisms by which self-aggregation competes with binding to a strongly charged polyelectrolite such as DNA. Here we carry out mechanical stretching and unzipping experiments of single DNA molecules (in double and single stranded form) complexed with KF using optical tweezers. We show that KF and DNA interact forming large aggregate complexes promoted by the recruitment and binding of DNA to the aggregate surface that are further stabilized by hydrophobic interactions. These experiments reveal unique features of the aggregation process, and the proposed methodology might be useful to quantitatively characterize other compounds or proteins in which the formation of aggregates is of relevance.

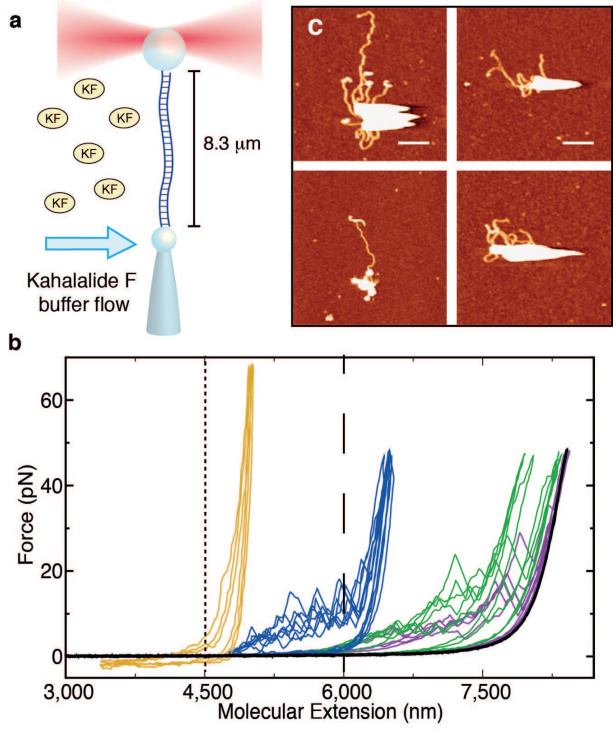


FIG. 1. **(a)** Optical tweezers experimental setup. **(b)** DNA pulling curves before (black) and after flowing KF at different waiting times: 5 min (purple), 15 min (green) and 30 min (blue). The sawtooth pattern observed indicates that KF induces the compaction of DNA. Pulling cycles reaching end-to-end distances lower than 4 $\mu$m are shown in yellow. v=500 nm/s. **(c)** AFM images of reactions of 1.65 ng linearized pGEM plasmid (2743-bp) and 100 $\mu$M KF obtained at 30 min incubation times at room temperature. The number of free DNA molecules decrease with the incubation time and large compaction blobs are observed.

* joan.camunas@gmail.com

# Estocasticidad y exclusión competitiva en comunidades ecológicas

José A. Capitán, Sara Cuenda, José A. Cuesta y David Alonso
*Centro de Astrobiología, INTA-CSIC y Grupo Interdisciplinar de Sistemas Complejos (GISC)*
*Ctra. de Ajalvir, km. 4. 28850 Torrejón de Ardoz, Madrid*

¿Qué factores determinan la coexistencia de especies en comunidades ecológicas? Una regla clásica en ecología nos dice que la coexistencia estable de especies se mantiene gracias a que la competición por recursos *dentro* de la propia especie (competición intraespecífica) es siempre más fuerte que la competición entre especies distintas (competición interespecífica.)[1] Este hecho se basa en el llamado principio de exclusión competitiva o ley de Gause,[2] que esencialmente establece que dos especies no pueden coexistir de forma estable si compiten por los mismos recursos. Por tanto, tener una coexistencia estable equivale a limitar la similitud entre especies. Si dos especies son ecológicamente muy similares, la selección natural actuará diferenciándolas de forma que consuman distintos recursos. Aunque bajo ciertas hipótesis este resultado clásico adquiere el rango de teorema matemático,[3] múltiples estudios posteriores han demostrado que este principio no es válido en general.[4] Entre ellos, destacan distintos resultados empíricos, así como modelos matemáticos que incluyen restricciones espaciales explícitamente.

Sin embargo, la mayoría de las excepciones al principio de exclusión competitiva están basadas en modelos dinámicos deterministas. En esta contribución mostraremos que, cuando la competición se formula en términos estocásticos, la exclusión competitiva surge de forma natural. Veremos que una nueva forma de exclusión competitiva aparece incluso en el caso más contrario a la intuición en el que las especies interaccionan de forma equivalente (competición simétrica.)[5] En este caso, el cociente $\rho$ entre la competición interespecífica y la intraespecífica debe ser menor que un cierto umbral para permitir la coexistencia estable de las especies (ver Fig. 1 y 2.) En la aproximación determinista, el umbral aparece solamente en el caso límite $\rho = 1$. Es precisamente la estocasticidad quien impone un umbral que limita la similitud entre especies. Por encima de este umbral, un colapso en la biodiversidad (es decir, en el número de especies que la comunidad es capaz de sostener) necesariamente tiene lugar.

Apoyando estos resultados encontramos una bifurcación estocástica que no tiene análogo en la aproximación determinista (ver Fig. 1.) Por otro lado, demostraremos que esta nueva forma de exclusión estocástica es aplicable a otros modelos de comunidades ecológicas en competición. Finalmente analizaremos la relevancia de estos resultados en comunidades ecológicas reales.[6]

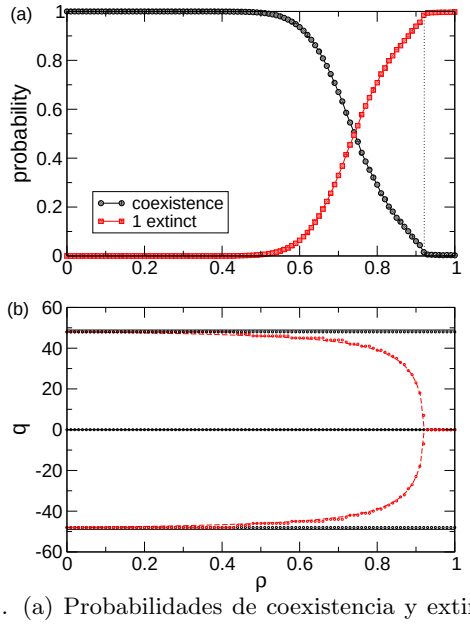


FIG. 1. (a) Probabilidades de coexistencia y extinción de una especie en función del cociente $\rho$ entre competición interespecífica e intraespecífica, para una comunidad de dos especies. (b) Parámetro de orden de la transición, $q = n_1 - n_2$, siendo $n_1$ and $n_2$ las poblaciones de cada especie.

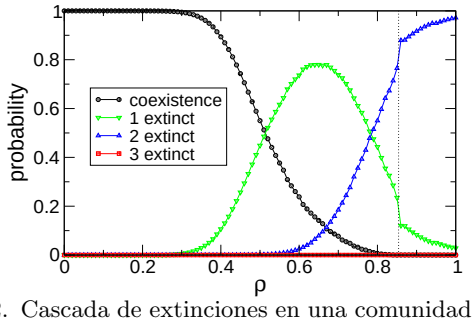


FIG. 2. Cascada de extinciones en una comunidad de 3 especies. En la aproximación determinista, la bifurcación tiene lugar en $\rho = 1$ y da lugar a la extinción simultánea de $S - 1$ especies en comunidades de $S$ especies. De esta forma, la cascada de extinciones es propia del modelo estocástico.

* joseangel.capitan@cab.inta-csic.es

[1] P. L. Chesson. Ann. Rev. of Ecol. and Syst., **31**:343, 2000.
[2] G. F. Gause. The Struggle for Existence. Hafner Press, 1934.
[3] J. Hofbauer and K. Sigmund. Evolutionary Games and Population Dynamics. Cambridge University, 1998.
[4] M. Gyllenberg y G. Meszna. J. Math. Biol., **50**:133, 2005.
[5] B. Haegeman and M. Loreau. J. Theor. Biol., **269**:150, 2011.
[6] J. A. Capitán et al. In preparation.

# The role of noise and initial conditions in the asymptotic solution of a continuous opinion dynamics model

Adrián Carro*, Raúl Toral, Maxi San Miguel
*IFISC, Instituto de Física Interdisciplinar y Sistemas Complejos*
*CSIC-Universidad de las Islas Baleares*
*07122-Palma (Mallorca)*

The models of "opinion dynamics" focus on the processes of opinion formation within a society consisting of an ensemble of interacting individuals with diverse opinions. A wide variety of models, mostly inspired by statistical mechanics and nonlinear physics, has been developed in order to deal with the different phenomena observed in real societies[1]: emergence of fads, minority opinion survival and spreading, collective decision making, emergence of extremism and so on. One of the main problems addressed by some of these models is whether the opinion formation processes within a society will eventually lead to the emergence of a consensus, with a vast majority of the agents adopting a similar opinion, or to the fragmentation of its constituent individuals into different opinion groups.

A model was introduced in 2000 by Deffuant, Weisbush and others[2], in the context of a European Union project for the improvement of agri-environmental policies, in order to describe the dynamics of continuous opinions under bounded confidence. In this model, each agent is therefore characterized by an opinion which is a continuous variable taken from a given interval. In its original version, these agents meet in random pairwise encounters and, if the difference between their continuous-value opinions is less than a certain confidence level, they interact, that is, they adjust their opinion towards the opinion of the other agent.

While most of the existing literature has focused on the important role played by the bound of confidence parameter, a topic that has received much less attention is the dependence of the model on the initial conditions, that is, on the initial distribution of opinions among the agents. As a first and naïve argument, we could notice that the model, as has been presented, conserves the mass and the mean opinion of the population, so the position of the final clusters will depend on the mean of the initial distribution. However, also different initial conditions with the same mean opinion could give rise to different final configurations. In fact, any combination of delta-functions is a steady state solution of the master equation describing the model, provided these delta-peaks are separated by more than a distance $\epsilon$ and they conform to the mean opinion conservation[4]. This has been the object of our study, and we have shown that it is perfectly possible to force or avoid a consensus by varying the initial distribution of opinions. Thus, we have sketched the structure of attractors of the dynamical system, by means of the numerical computation of the time evolution of the agents density. In particular, we have used a discrete density-based reformulation of the model as discussed by J. Lorenz[3].

In order to avoid having perfect consensus within each cluster, i.e., all the participant agents sharing exactly the same opinion, Toral, Pineda and Hernández-García have recently presented an extension of the original Deffuant-Weisbush model taking into account some additional randomness[4]. Thus, a noise is introduced in the dynamics as a *free will*, which allows for the agents to change their opinion from time to time to a randomly chosen value. For a uniform opinion distribution of the noise, this is equivalent to a quenched noise —as contrary to some other more adaptive noise approaches[5]—, that is, to allowing each agent to go back to a certain preferred opinion from time to time. As a result of this extension, there exists a transition between an organized and a disoganized phase at a critical value of the noise intensity. In the disordered state, corresponding to quite high noise rates, there is no cluster formation, as noise is stronger than nucleation processes; on the other hand, in the ordered state, corresponding to lower noise rates, we can still clearly observe the formation of clusters, even if they broaden with respect to the noiseless case. An interesting feature of this extension is that the average opinion of the system tends to the average of the noise opinion distribution, independent of that of the initial condition. Therefore we have also studied the influence of the initial distribution of opinions in this noisy case. There, we have shown that, even if the importance of the initial distribution regarding the average opinion is replaced by that of the noise distribution, the former has still some influence in determining the bifurcation patterns.

---

* adrian.carro@ifisc.uib-csic.es

[1] C. Castellano, S. Fortunato, and V. Loreto. *Statistical physics of social dynamics*. Rev. Mod. Phys. 81, 591 (2009).
[2] G. Deffuant, D. Neau, F. Amblard, and G. Weisbuch. *Mixing Beliefs among Interacting Agents*. Advances in Complex Systems, 3: 87-98, 2000.
[3] J. Lorenz. *Heterogeneous bounds of confidence: Meet, discuss and find consensus!* Complexity, 15: 43-52, 2010.
[4] M. Pineda, R. Toral, and E. Hernández-García. *Noisy continuous-opinion dynamics*. J. Stat. Mech. Theory Exp. P08001, 2009.
[5] M. Mäs, A. Flache, and D. Helbing. *Individualization as Driving Force of Clustering Phenomena in Humans*. PLoS Comput. Biol. 6, e1000959 (2010).

# Stochastic resonance and diversity in an agent-based herding model

Adrián Carro*, Raúl Toral, Maxi San Miguel
*IFISC, Instituto de Física Interdisciplinar y Sistemas Complejos*
*CSIC-Universidad de las Islas Baleares*
*07122-Palma (Mallorca)*

The mainstream approach to economics has traditionally neglected the study of two of the most relevant and universal features of the economic activity: the diversity among the economic actors, and the interplay and connections between them. Indeed, the overall systemic features of the present crisis could be understood as emergent phenomena arising from the micro-activity of strongly interacting economic units.

Recent years, however, have witnessed the appearance of a growing number of contributions, by heterodox economists and physicists, based on heterogeneous interacting agents. The fundamental attribute of these agent-based models is the behavioral heterogeneity among agents, i.e. their capability to choose from a set of different market strategies or trading rules. Furthermore, most of these models involve some interaction mechanism between market participants, whether direct or indirect, global or local. We will focus on a series of stochastic models of information transmission inspired by Kirman[1], and whose main ingredient is their emphasis on the processes of social interaction among agents, based on herding behavior or a tendency to follow the crowd.

Inspired by a series of entomological experiments with ant colonies, Kirman[1] proposed a stochastic herding formalism to model decision making among financial agents. In the experiments, entomologists observed asymmetric macroscopic patterns emerging from an apparently symmetric situation: when ants were faced with two identical food sources, a majority of the population tended to exploit only one of them at a given time, switching its foraging attention focus to the other source every once in a while. In order to explain this behavior, Kirman developed a stochastic model where the probability for an ant to change its foraging source is a combination of two terms, one related to pairwise herding interactions or recruitment probability, and the other as an autonomous switching tendency. This very simple model can also be interpreted in terms of market behavior by just replacing an ant's binary choice between food sources by a market agent's choice between trading strategies, particular rules for the formation of his expectations, or differences in access and interpretation of information.

A series of subsequent papers have focused on explaining some of the stylized facts observed in empirical data from financial markets[2],[3]. Those features are explained as the macroscopic outcome emerging from the internal dynamics of an ensemble of heterogeneous interacting agents. Some of the universal features of financial time series which have been reproduced in the framework of herding models of the Kirman type are: the non-Gaussian or leptokurtic character of the unconditional distribution of returns, the temporal bursting behavior of the volatility, and the positive autocorrelation of absolute and squared returns.

The main purpose of the present contribution is the study of some possible stochastic resonance effects in the framework of an agent-based herding model of the Kirman type. A stochastic resonance is basically a maximum in a suitably defined response of the system to an external forcing as a function of the intensity of some noise or fluctuations. It generally requires only a bistable system, an additive noise term and a sub-threshold periodic forcing[4]. The two former being already included in the original Kirman model, we just need to add an external periodic signal which will, at regular time intervals, induce a modification of the potential helping the transitions in one direction or the other alternatively. This external forcing can be interpreted, in terms of financial markets, as an advertising or a public perception in favor or against one of the two possible trading behaviors, thus periodically breaking the symmetry of the system. The conditions for the ensemble of agents to more accurately follow the periodicity of the signal are studied. In particular, we computed the response of the system as a function of the tendency of the agents to randomly change their behavior (switch the food source in the case of ants or the trading strategy in the case of financial markets), and also as a function of the diversity of the agents[5]. To this latter end, we introduced another source of heterogeneity in the model by allowing the agents to have different individual preferences for one or the other possible market strategies.

It is also worth mentioning that the method we used to solve the model is slightly different from those used in the previous literature. We applied a Gillespie algorithm in order to generate statistically correct trajectories of the stochastic equation.

---

* adrian.carro@ifisc.uib-csic.es

[1] A. P. Kirman. Quarterly Journal of Economics, 108: 137–156, 1993.
[2] S. Alfarano, M. Milaković. Journal of Economic Dynamics and Control, 33: 78–92, 2009.
[3] S. Alfarano, M. Milaković, M. Raddant. Munich Personal RePEc Archive, 2011.
[4] L. Gammaitoni, P. Hänggi, P. Jung, F. Marchesoni. Reviews of modern physics, 70: 223–287, 1998.
[5] C. J. Tessone, R. Toral. The European Physical Journal B, 71: 549–555, 2009.

# Shape and motility of actin lamellar fragments

Carles Blanch-Mercader and Jaume Casademunt*
*Departament Estructura i Constituents de la Matèria, Universitat de Barcelona, Av. Diagonal 647, Barcelona, Spain*

Lamellar fragments of keratocytes are pieces of the actin-based motile machinery extracted from those cells. These fragments lack nucleus, microtubules and most organelles, but retain the minimal ingredients to generate motion. Experimental observations[1] show that such fragments are capable to generate and sustain spontaneous directional motion if the circular symmetry is externally or spontaneously broken. A theoretical understanding of this phenomenon is still lacking. In particular, an interesting open question is whether actin polymerization forces plus friction, without the action of molecular motors, are sufficient to sustain motion.

We base our study on a physical model that was recently introduced by Callan-Jones et al[2]. It assumes a polar nematic continuous description[3] of the gel of actin and assumes that the dynamics of the polymerization can be slaved to the slow membrane dynamics. Assuming that actin treadmilling is controlled by polymerization at the membrane with velocity $v_p$ and uniform depolymeriztion in the bulk, the velocity field can be shown to satisfy Darcy's law and therefore be reduced to a laplacian pressure field with appropriate boundary conditions at the moving boundary. The dynamics is then reduced to a free-boundary problem which is similar to the classic problem of viscous fingering in Hele-Shaw cells[4]. Similarly, the laplacian nature of the problem allows to take advantage of conformal mapping techniques.

One of the central results of this work is the proof of an exact expression for the instantaneous velocity of the center of mass ($R_A$) that establishes and interesting connection between shape and motility,

$$\dot{R}_A = \frac{v_p L}{A}\left(R_L - R_A\right), \qquad (1)$$

where $R_A$ and $R_L$ are the center of masses of the area and of the contour, respectively. $A$ stands for the area and $L$ for the perimeter. This identity establishes a direct connection between the instantaneous velocity of the center of mass and simple geometrical properties of the contour. In other words, regardless of the actual evolution of the shape, at any time we can obtain the instantaneous velocity of the center of mass from the shape. This reduces the controversial question on the existence of steady motile shapes in this problem to the existence of asymmetric steady shapes, a problem that is more amenable to analytical and numerical treatment. With the help of conformal mapping techniques, we prove numerically that such solutions exist and some of them are stable.

Extending a previous linear stability analysis of the circular shape[2], we also show that the mechanism to initiate motion through symmetry breaking is necessarily nonlinear. To pursue the nonlinear character of the motility mechanism we also perform the center manifold reduction of the dynamics close to different bifurcation points, unraveling a rather complex mathematical structure. In particular, we find that there is an infinity of branches of traveling solutions that can be accessed analytically. Remarkably, the velocity of these solutions vanishes in the center manifold. With the help of high-precision arithmetics (64 digits), we have shown numerically that the velocity of these solutions as one approaches the bifurcation point is actually exponentially small, with the general form $\dot{R}_A \propto \exp(-a/g_i^n)$, where $g_i$ is the distance to the bifurcation point of the $i-th$ mode. For $i=2$, we have $a \approx 20.6$, and $n \approx 1/6$. This is a remarkable example of asymptotics beyond all orders that is reminiscent of the one associated to the steady-state selection mechanism in viscous fingering[4]. Whether this analogy entails a deeper connection is yet to be elucidated.

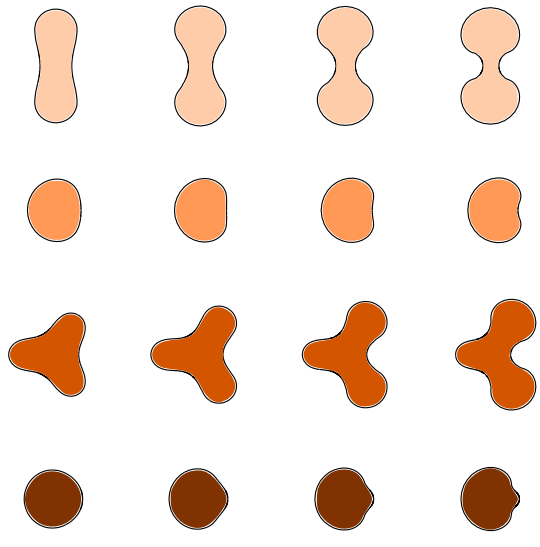

FIG. 1. Sample of motile steady shapes.

* jaume.casademunt@ub.es

[1] A. B. Verkhovsky, T. M. Svitkina, and G. G. Borisy, Curr. Biol. 9, 11 (1999)
[2] A. C. Callan-Jones, J.F. Joanny, and J. Prost, Phys. Rev. Lett. 100, 258106 (2008)
[3] K. Kruse, J.F. Joanny, F. Jülicher, J. Prost, and K. Sekimoto, Eur. Phys. J. E 16, 5 (2005)
[4] J. Casademunt, Chaos 14, 809 (2004)
[5] F. Ziebert, S. Swaminathan and I. S. Aranson, J. R. Soc. Interface, 2011.

# Phase diagram of a single magnetic filament in bulk, an approach via numerical simulations and theory.

Joan J. Cerdá*, Pedro A. Sànchez†, Tomàs Sintes
*IFISC, Instituto de Física Interdisciplinar y Sistemas Complejos*
*CSIC-Universidad de las Islas Baleares 07122-Palma (Mallorca)*

Magnetic filaments constitute a novel type of unconventional magnetic materials. Basically, magnetic filaments can be conceived like supramolecular polymers at the scale of tenths of nanometers that may exhibit permanent magnetic properties at room temperatures in contrast with chemical 1D polymers which are magnetic only at $T < 100K$[1].

Despite the idea of magnetic filaments is not new at all, since the Cretaceous nature has been using systems very similar to the magnetic filaments inside magnetostatic bacterias to help them to orientate[2], the humankind has only very recently begun to caress its potential for novel applications[3,4]. Among the many new plausible applications there is the chance of using them as an improved substitute for current ferrofluids or magnetorheological fluids. In turn, these new magnetic systems pose an interesting case of research for Soft Matter community due to the non-isotropic character of the magnetic interaction combined with the physics of traditional polymers.

The current state of the art in which still very little is known about the physical behavior of such novel magnetic systems is the perfect scenario for the use of numerical simulations which can contribute in a decisive way to unravel and understand how such filaments may behave under different experimental conditions. Furthermore, numerical simulations can help in assessing the usefulness or not of the magnetic filaments for certain kinds of technologies.

After the study of the properties of a single magnetic filament close to an adsorptive wall[5], in this contribution we will present our recent advances in the characterization of magnetic filaments in bulk. In particular we will focus in the phase diagram of such magnetic filaments as a function of the temperature, the value of the magnetic moment of the beads that constitute the magnetic filament, the length of the chain, and the intensity of the interaction (attractive or repulsive) among those beads of the magnetic filaments. Furthermore, the dependence of the phase diagram with the value of an applied external magnetic field will be also studied in detail.

As we will show, our results predict a very complex phase diagram which includes many types of structural transitions ranging from globular and pseudo-helicoidal states till the case of rings and rods. In addition to our numerical simulations we will present a simple theoretical statistical-mechanics model which will be compared stringently with our simulations in order to validate it. The new theoretical model will help us to explain the physics behind the phase transitions we have observed, and it will contribute to pave the way in the study of solutions containing magnetic filaments as solutes.

---

† Institute for Computational Physics, Universität Stuttgart,Pfaffenwaldring 27, 70569, Stuttgart.
* joan@ifisc.uib-csic.es

[1] M. Kamachi, *J. Macromol. Sci.* **C42**, S41 (2002)
[2] A. Komeili *et al*, *Science* **311**, 242 (2006)
[3] S. J. Blundell *et al*, *J. Phys. Condens. Matter* **16**, R771 (2004)
[4] J.J. Benkoski, R.M. Deacon, *et al*, *Soft Matter* **6**, 602 (2010).
[5] P.A. Sànchez, J.J. Cerdà, V. Ballenegger, T. Sintes, O.Piro, C.Holm *Soft Matter* **7**, 1809 (2011).

# Compressible Cell Gas Models and Yang-Yang Critical Anomalies

Claudio A. Cerdeiriña
*Departamento de Física Aplicada, Universidad de Vigo − Campus del Agua, Ourense 32004, Spain*

Gerassimos Orkoulas
*Department of Chemical and Biomolecular Engineering, University of Califormia, Los Angeles, California 90095, USA*

Michael E. Fisher*
*Institute for Physical Science and Technology, University of Maryland, College Park, Maryland 20742, USA*

Asymmetry features of liquid-gas criticality in pure fluids are analyzed with the aid of exactly soluble lattice gas models in which individual cell volumes are allowed to fluctuate. Such *compressible cell gases* CCG's obey *complete scaling* theory with pressure mixing,[1,2] and thereby display, in accord with experimental evidence,[1,3] Yang-Yang anomalies. This means that, in the exact thermodynamic relation for the isochoric heat capacity $C_V$[4]

$$C_V = \tilde{C}_p + \tilde{C}_\mu, \tag{1}$$

$$\tilde{C}_p = \frac{T}{\rho}\Big(\frac{\partial^2 p}{\partial T^2}\Big)_V, \tilde{C}_\mu = -T\Big(\frac{\partial^2 \mu}{\partial T^2}\Big)_V, \tag{2}$$

not only $\tilde{C}_p$ diverges at criticality like $|t|^{-\alpha}$ [where $t \equiv (T - T_c)/T_c$, with $T_c$ denoting the critical temperature and $\alpha \simeq 0.109$] but so also $\tilde{C}_\mu$ does, that is,

$$\tilde{C}_p(T) \sim \tilde{A}_p|t|^{-\alpha}, \tilde{C}_\mu(T) \sim \tilde{A}_\mu|t|^{-\alpha}, \tag{3}$$

with $\tilde{A}_p \neq 0$ and $\tilde{A}_\mu \neq 0$. Complete scaling also predicts that the coexistence-curve diameter in the density-temperature plane, $\rho_d \equiv (\rho^{liq} + \rho^{gas})/2$, behaves like

$$\rho_d(T) = \rho_c\{1 + A_{2\beta}|t|^{2\beta} + A_{1-\alpha}|t|^{1-\alpha} + A_1|t| + ...\}, \tag{4}$$

where $\beta \simeq 0.326$. The existence of the $|t|^{2\beta}$ singularity, which is supported by simulations[5] and experiments,[6,7] is intimately related to the Yang-Yang anomaly. Specifically, $\tilde{A}_\mu \neq 0$ and $A_{2\beta} \neq 0$ as long as the *crucial* pressure mixing coefficient $j_2$ is nonzero, and so the Yang-Yang ratio $\mathcal{R}_\mu \equiv \tilde{A}_\mu/(\tilde{A}_p + \tilde{A}_\mu) = -j_2/(1 - j_2)$.

Complete scaling remains a phenomenological theory with no physical insights regarding microscopic origins, signs, or magnitudes. Here we show that for the models under consideration $\mathcal{R}_\mu$ ranges from $-\infty$ to $1/2$. When cell volumes fluctuate independently, nonvanishing $\mathcal{R}_\mu$ values emerge as a result of *local free volume fluctuations*. Among the various decorated CCG's explored, simple versions in which energies and cell volumes are coupled reveal *local void volume fluctuations* associated to interactions as another source of Yang-Yang and related anomalies. A previously reported model for hydrogen bonding in water[8] appears as a relevant example.

* xpectnil@umd.edu

[1] M. E. Fisher and G. Orkoulas, Phys. Rev. Lett. **85**, 696 (2000).
[2] Y. C. Kim, M. E. Fisher, and G. Orkoulas, Phys. Rev. E **67**, 061506 (2003).
[3] G. Orkoulas, M. E. Fisher, and C. Üstün, J. Chem. Phys. **113**, 7530 (2000).
[4] C. N. Yang and C. P. Yang, Phys. Rev. Lett. **13**, 303 (1964).
[5] Y. C. Kim and M. E. Fisher, Chem. Phys. Lett. **141**, 185 (2005).
[6] M. A. Anisimov and J. T. Wang, Phys. Rev. Lett. **97**, 025703 (2006).
[7] J. T. Wang and M. A. Anisimov, Phys. Rev. E **75**, 051107 (2007).
[8] S. Sastry, P. G. Debenedetti, F. Sciortino, and H. E. Stanley, Phys. Rev. E **53**, 6144 (1996).

# Statisical features of the global velocity of imbibition fronts in disordered media

Xavier Clotet*[a,b], Stéphane Santucci[b], Jordi Ortín†[a]
[a] Dept. d'Estructura i Constituents de la Matèria, Fac. de Física, Universitat de Barcelona, Catalonia, Spain
[b] Lab. de Physique, CNRS UMR 5672, Ecole Normale Supérieure de Lyon, France

Imbibition is a process of fluid transport in a medium in which the resident fluid is displaced by a second immiscible invading fluid that preferentially wets this medium. When this process occurs in a disordered medium the system develops long range correlations along the interface due to the competing forces acting on different length scales: fluctuations in capillary forces, heterogeneities in the permeability, viscous pressure drop and surface tension. As a result, the system evolves out of equilibrium towards a statistically stationary state with critical fluctuations of the interface. The dynamics is highly heterogeneous both in space and time.

Our experimental system consists on large Hele-Shaw models of disordered media (described in detail in Ref.[1] and Refs. within). The gap spacing between the two plates of the cell takes two values randomly distributed in space. The invading fluid is a silicone oil. It is injected into the system at constant flow rate, displacing the resident air. The advancing of the oil-air front is recorded using a fast camera, allowing us to capture the local motion of the interface, $h(x,t)$. Therefore we can obtain the waiting time matrix, $wt(x, y = h(x,t))$, computed as the amount of time the front has spent on each position. Taking the inverse of $wt(x,t)$ we obtain the local velocity map, $v(x,t)$. This method was developed by Måløy et al.[2] for studying the intermittent dynamics of crack fronts.

In this work we analyse the average velocity of the invading front as a function of time. This global signal is given by $V_l(t) = \frac{1}{l}\int_l v(x,t)dx$ for an observation window of size $l$. It exhibits burst-like dynamics, with power-law distributed avalanches[3].

The shape of these avalanches is studied as a function of both the imposed mean velocity (v) and the size of the averaging window ($l$). We observe that the shape is asymmetric, particularly for short durations. In addition, an evolution of avalanche shape as a function of its duration, $T$, is noticed. The larger the duration, the flatter the shape and the larger the values of $V_l(t) - V_c$, where $V_c$ is a clip velocity.

We also study the increments of the global velocity, $\Delta V_l(\tau) = V_l(t+\tau) - V_l(t)$. Distributions of $\Delta V_l$ show an evolution through time scales, $\tau$, from fat tail distributions at small time increments to almost Gaussian distributions. In Fig. 1 we show this variation in the shape of the pdf as a function of $\tau$ for a given injection velocity v. It seems reasonable to define a critical increment, $\tau_c$, to distinguish the Gaussian from the non-Gaussian behaviour. The statistical properties of the $\Delta V_l$ distributions have been analysed in order to determine this critical increment. Specifically, the skewness and the kurtosis of the pdf have been computed. The skewness (proportional to the third moment) gives information about the asymmetry of the pdf. It is different from 0 for the non-Gaussian distributions, i.e. for small $\tau$. The degree of asymmetry depends systematically on the size of the observation window, $l$: the larger $l$, the smaller the asymmetry. The kurtosis (proportional to the fourth moment) measures the flatness of the pdf. For a Gaussian pdf the kurtosis is 3. In our experiments the kurtosis takes values larger than 3 at small $\tau$. This effect is more evident at small $l$.

Statistics of global observables in correlated systems can be related to extreme value problems and to fat tail pdfs statistics[4]. In our case the temporal correlation in the $\Delta V_l$ arises from the long range correlations along the front interface. The characteristic length of these spatial correlations ($l_c$) together with v determines $\tau_c$. The dependence of $\tau_c$ on $l$ comes from the definition of $V_l$. When considering $l < l_c$ all the local velocities considered in the average are correlated, while for $l > l_c$ non-correlated $v(x,t)$ are also added.

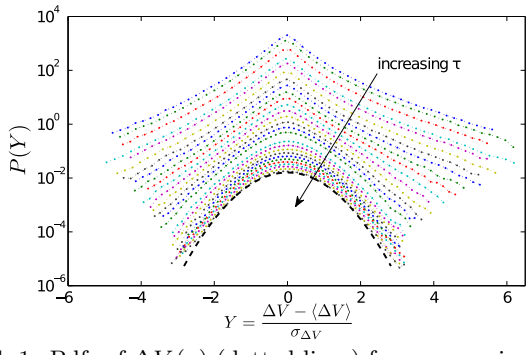


FIG. 1. Pdfs of $\Delta V_l(\tau)$ (dotted lines) for an experiment at v = 0.131 mm/s and $l = L/8$, where $L = 136$ mm is the system size. The pdfs are shifted in the vertical direction for clarity. $\tau$ ranges from 0.06 s to 33 s and changes logarithmically. A Gaussian pdf is also plotted as a guide to the eye (dashed line).

* xclotet@ub.edu
† jordi.ortin@ub.edu

[1] S. Santucci et al., Europhys. Lett., **94**, 46005 (2011).
[2] K.J. Måløy et al., Phys. Rev. Lett. **96**, 045501 (2006).
[3] R. Planet et al., Phys. Rev. Lett. **102**, 94502 (2009).
[4] E. Bertin, Phys. Rev. Lett. **95**, 170601 (2005).

# Adler synchronization of spatial laser solitons pinned by defects

P.V. Paulau[1], C. McIntyre[2], Y. Noblet[2], N. Radwell[2], W.J. Firth[2], P. Colet[3], T. Ackemann[2], and G.-L. Oppo[2]
[1] *TU Berlin, Institut für Theoretische Physik, Hardenbergstr. 36, Sekr EW 7-1, 10623 Berlin, Deutschland*
[2] *SUPA and Department of Physics, University of Strathclyde, 107 Rottenrow, Glasgow G4 0NG, UK*
[3] *Instituto de Física Interdisciplinar y Sistemas Complejos, IFISC (CSIC-UIB), Campus Universitat de les Illes Balears, 07122-Palma (Mallorca)*

Laser cavity solitons (LCS) are transverse, nonlinear, self-localized and dissipative states which have the potential for massive parallelism and the formation of complex arrays. Phase-locked bound states with solitons have been predicted in mode-locked lasers for the temporal case[1] and in lasers with saturable absorbers for the spatial case[2]. Corresponding phase-quadrature states have been observed in fiber lasers[3]. Here we present a different kind of soliton locking. We demonstrate experimentally and theoretically Adler-type locking and synchronization of spatial LCS in a vertical-cavity surface-emitting laser (VCSEL) with an external Bragg grating that provides frequency- selective feedback[4].

The dynamics of LCS in a semiconductor laser with feedback is well captured by a generic cubic complex Ginzburg-Landau equation coupled to a linear filter[6]:

$$\partial_t E = g_0 E + g_2|E|^2 E - i\partial_x^2 E + F + in(x)E,$$
$$\partial_t F = -\lambda F + \sigma E \qquad (1)$$

where $E(x)$ is the intra-cavity field, $F(x)$ the filtered feedback field, $g_0$ the linear gain and detuning, $g_2$ the nonlinear gain and dispersion, $\sigma$ the feedback strength and $\lambda$ the filter bandwidth. The reference frequency is set to the filter peak. $n(x)$ describes background defects that perturb the material refractive index.

For $n(x) = 0$, Eqs. 1 have exact solutions corresponding to stable single-frequency chirped-sech solitons[6] with two free parameters: location and phase. The interaction of two solitons makes them spiral slowly to fixed relative distances and phase differences around $\Phi = \pi/2$ unless merging takes place. $\Phi = 0, \pi$ are also possible but correspond to saddles that are either phase or distance unstable.

Small variations of $n(x)$ lead to pinning and small changes in the LCS frequency. If defects are located close enough, solitons interaction locks their frequencies to a common value. The phase difference $\Phi$ relaxes to stationary values that depend on the defect detuning $\Delta\omega = \omega_2 - \omega_1$ generated by $n(x)$. The dependence of $\Phi$ on $\Delta\omega$ for numerical simulations of (1) is shown in Fig. 1 (dots) for $|x_2 - x_1| = 1.5$ space units. Locking and synchronization occur only in the range $|\Delta\omega| < \Delta\omega_{th}$. Very similar results (triangles) have been obtained from numerical simulations of LCS in models of VCSELs with frequency-selective feedback that include the dynamics of the carriers[5]. The solid line refers to the results from the Adler model for synchronization between two coupled oscillators with different bare frequencies[7],

$$\dot{\Phi} = \Delta\omega - \varepsilon \sin(\Phi)\,. \qquad (2)$$

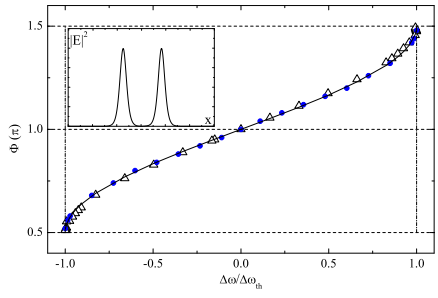


FIG. 1. Locked phase differences $\Phi$ of pinned LCS for different frequency detunings. The inset shows the spatial profile of the intensity.

The experiment was performed with a VCSEL and a volume Bragg grating (VBG) in a self-imaging configuration[6]. A piezo-electric transducer was used to minutely tilt the VBG with respect to the optical axis leading to a differential change in the feedback phase and allowing the tuning of $\Delta\omega$. When performing such a scan, a region of frequency and phase locking appears, identified in Fig. 2 by the region of high fringe visibility in the far field. As expected for the Adler scenario, in the locking region, the fringe phase varies smoothly and quasi-linearly with the detuning of the external cavity. The width of the locking range is close to the expected value of $\pi$ and the transitions to and from frequency and phase-locking are rather abrupt

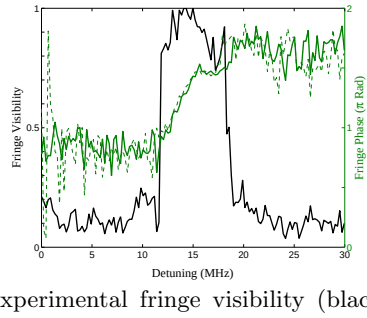


FIG. 2. Experimental fringe visibility (black) and fringe phase (green/gray)

[1] P. Grelu and N. Akhmediev, Nature Photon. **6**, 84 (2012).
[2] A.G. Vladimirov, G.V. Khodova, and N.N. Rosanov, Phys. Rev. E, **63**, 056607 (2001).
[3] Ph. Grelu, F. Belhache, F. Gutty, and J.-M. Soto-Crespo, Opt. Lett. **27**, 966 (2002).
[4] P.V. Paulau *et. al.* Phys. Rev. Lett. to appear.
[5] A.J. Scroggie, W.J. Firth, and G.-L. Oppo, Phys. Rev. A **80**, 013829 (2009).
[6] P.V. Paulau, *et. al.* Phys. Rev. E **84**, 036213 (2011).
[7] R. Adler, Proc. IRE **34**, 351 (1946); reprinted in Proc. IEEE **61**, 1380 (1973).

# Phase Noise Performance of Double-Loop Optoelectronic Microwave Oscillators

Romain Modeste Nguimdo[1], Yanne Kouomou Chembo[2], Pere Colet[1] and Laurent Larger[2]
[1] *Instituto de Física Interdisciplinar y Sistemas Complejos, IFISC (CSIC-UIB), Campus Universitat de les Illes Balears, E-07122 Palma de Mallorca, Spain.*
[2] *UMR CNRS FEMTO-ST 6174/Optics Department, Université Franche-Comté, 16 Route de Gray, 25030 Besançon, France*

In applications such as radar, time-frequency metrology and lightwave technology, microwaves with exceptional purity are needed. Optoelectronic oscillators (OEOs) are useful for these applications because they can convert continuous light energy into stable and spectrally pure microwave signals[1–3]. In such systems, the purity of microwave signal is achieved thanks to an optical fiber delay-line inserted into the feedback loop. The role of the delay is to store the energy providing a quality factor equal to $Q = 2\pi f_m T$, where $f_m$ is the microwave frequency and $T$ the delay induced by the optical fiber. A convenient way to evaluate the purity in systems is to measure its phase noise spectrum, which is directly connected to the oscillator performance. The main advantage of the OEO is its capability to generate ultra-stable, spectrally pure microwaves with frequencies as large as 75 GHz, and with a phase noise lower than −160 dBc/Hz at 10 kHz[4]. Later, these studies were complemented with a nonlinear and stochastic dynamics approach which enabled to investigate theoretically the stability properties of OEOs, and also to predict phase noise performance[5–7].

Theoretical studies predict that the use of a long delay line plays a key role in improving the phase noise performance. However, in the single loop configuration, the possibility of using long delays is limited because the delay is also responsible to the appearance of very strong parasite ring-cavity peaks, which appear at the integer multiples of the round-trip frequency $\Omega_T = 2\pi/T$. Thus, the increase of delay line reduces the region of low phase noise because of these ring-cavity peaks.

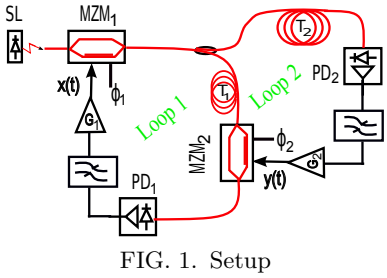


FIG. 1. Setup

Here, we consider a double-loop optoelectronic delay system in which the output of one of the loops is used to modulate the other (Fig. 1). A semiconductor laser (SL) injects light into a Mach-Zehnder ($MZM_1$). One part of the optical output is delayed by $T_2$ , detected by photodiode $PD_2$, fed to a narrow-band filter with a central frequency $\Omega_0$ and bandwidth $\Delta\Omega_2$, amplified, and used to modulate $MZM_2$. The other part is delayed by $T_1$, optically fed to $MZM_2$, detected by $PD_1$, filtered by an RF filter of central frequency $\Omega_0$ and bandwidth $\Delta\Omega_1$, amplified and finally fed to the $MZM_1$ RF electrode to close the loop. Proceeding as in ref.[5], the system can be described by the dimensionless amplifier outputs $x(t)$ and $y(t)$

$$x + \tfrac{1}{\Delta\Omega_1}\tfrac{dx}{dt} + \tfrac{\Omega_0^2}{\Delta\Omega_1}u_1 =$$
$$= \tfrac{G_1}{4}\Big[F(x_{T_1},\phi_1) + F(y,\phi_2) + F(x_{T_1},\phi_1)F(y,\phi_2) + 1\Big],$$
$$y + \tfrac{1}{\Delta\Omega_2}\tfrac{dy}{dt} + \tfrac{\Omega_0^2}{\Delta\Omega_2}u_2 = \tfrac{G_2}{2}[F(x_{T_2},\phi_1) + 1]$$

where $x_{t_0} = x(t - t_0)$, $F(x,\phi) = \cos[2x(t) + 2\phi]$, $du_1/dt = x(t)$, $du_2/dt = y(t)$ and $G_1$ and $G_2$ are the overall loop gains.

We derive an amplitude equation to investigate the stability properties and study the noise performance. We show that by carefully setting the parameters of the second loop, a significant improvement of performance can be achieved comparatively to the single-loop configuration, as the detrimental effect of the multiplicative phase noise can be reduced up to about 18 dB close to the carrier, while delay-induced spurious peaks can be strongly damped.

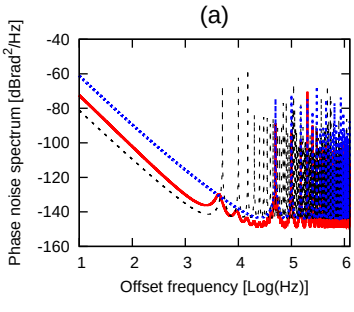


FIG. 2. Phase noise spectrum of a single loop OEO with $T = 20\ \mu$s (dotted line) and with $T = 200\ \mu$s (dashed line) and of a double loop OEO (solid line) ($\phi_1 = \phi_2 = 0.5$, $T_1 = 20\ \mu$s, $T_2 = 200\ \mu$s, $G_1 = 2.0$ and $G_2 = 0.5$)

[1] X.S. Yao and L. Maleki, *Electron. Lett.*, **30**, 1525 (1994).
[2] X.S. Yao and L. Maleki, *J. Opt. Soc. Am. B* **13**, 1725, (1996).
[3] X.S. Yao and L. Maleki, *IEEE J. Quantum Electron.* **32**, 1141 (1996).
[4] See www.oewaves.com.
[5] Y.K. Chembo, L. Larger, H. Tavernier, R. Bendoula, E. Rubiola, and P. Colet, *Opt. Lett.*, **32**, 2571 (2007).
[6] Y.K. Chembo, L. Larger, P. Colet, *IEEE J. Quantum Electron.* **44** 858 (2008).
[7] Y.K. Chembo, K. Volyanskiy, L. Larger, E. Rubiola, and P. Colet, *IEEE J. Quantum Electron.*, **45**, 178 (2009).

# Clustering of random scale-free networks

Pol Colomer-de-Simón* and Marián Boguñá
*UB, Universitat de Barcelona, Departament de Física fonamental*
*Martí i Franquès 1 08028 Barcelona, Spain*

We derive the finite size dependence of the clustering coefficient of scale-free random graphs generated by the configuration model with degree distribution exponent $2 < \gamma < 3$. Degree heterogeneity increases the presence of triangles in the network up to levels that compare to those found in many real networks even for extremely large nets. We also find that for values of $\gamma \approx 2$, clustering is virtually size independent and, at the same time, becomes a *de facto* non self-averaging topological property. This implies that a single instance network is not representative of the ensemble even for very large network sizes.

In the absence of high degree nodes the Clustering coefficient of the resulting network is given by [1]:

$$C \sim \frac{(\langle k(k-1)\rangle)^2}{\langle k\rangle^3} \tag{1}$$

That vanishes very fast for large system sizes. However in the case of a scale-free networks it predicts a behaviour

$$C \sim N^{\frac{7-3\gamma}{\gamma-1}} \tag{2}$$

that diverges for $\gamma < 7/3$. This is because this derivation does not account for the structural correlations among degrees of connected nodes that appear in order to be able to close the network for degree distributions with $\gamma < 3$ [2].
Here we explain how to derive the correct scaling behaviour of clustering for scale-free random graphs with $2 < \gamma < 3$. We also show that when clustering is very high and becomes nearly size independent.
Using a Canoncial version of the configuration model (hidden variables) we were able to derive that the Clustering coefficient depends with the size of the system as follows:

$$C \sim N^{2-\gamma} \ln N \tag{3}$$

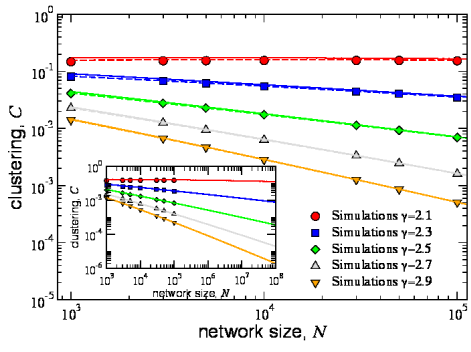


FIG. 1. Clustering coefficient as measured in numerical simulations for different values of $\gamma$ and size $N$ with $\bar{k}_{min} = 2$ and $\kappa_c = N^{1/(\gamma-1)}$. Each point is an average over $10^4$ different network realizations. Dashed lines are the numerical solution and solid lines are the approximate solution. The inset shows an extrapolation up to size $N = 10^8$.

* polcolomerdesimon@gmail.com

[1] M.E.J. Newman, Random graphs as models of networks. In Handbook of graphs and Networks,S.Bornholdt and H.G. Shuster (eds.) (Wiley-VCH, Berlin, 2003)
[2] M. Boguñá, R.Pastor-Satorras, and A. Vespignani, Eur. Phys. J. B 38, 205 (2004)

# Delay identification in semiconductor lasers with optical feedback

Miguel C. Soriano*, Romain Modeste Nguimdo, and Pere Colet
*IFISC (CSIC - UIB), Instituto de Física Interdisciplinar y Sistemas Complejos, Campus Universitat Illes Balears, E-07122 Palma de Mallorca, Spain*

Semiconductor lasers (SLs) with optical feedback have attracted a lot of attention in the chaos cryptography community due to its capability to develop broadband chaos within which giga-bit message can be encoded[1]. The security of laser-based chaos communications relies mainly on the difficulty of identifying the emitter parameters necessary to build an adequate receiver which can synchronize with it.

In chaos communication schemes based on SLs with delayed optical feedback, the delay time can be identified from time series using standard techniques in most parameter regimes. However, the efforts to enhance the security in these schemes have led to the characerization of a regime in which the delay time appears to be concealed, namely when it is closer to the relaxation period of the laser operating with moderate feedback[2]. These results were obtained exclusively by computing the quantifiers from intensity time series. Taking into account that, in addition to the intensity, the phase information is also transmitted through the public channel, it is mandatory to check if the delay time can be concealed when computing different quantifiers from the phase of the field.

Here, we show results for the analysis of time series that originate from a numerical realization of a SL with delayed optical feedback. The model is based on the Lang and Kobayashi rate equations, which are described in terms of the complex electric field $E(t)$ and the carrier number $N(t)$ inside the active layer (see[3] for details). The laser exhibits chaotic intensity pulsations in our numerical realization of a laser with optical feedback. In order to identify the time delay, we employ the autocorrelation function (ACF) and delayed mutual information (DMI) quantifiers. The time delay present in the system dynamics can then detected through the presence of clear extrema of the quantifiers when they are calculated as a function of a time lag.

In Fig. 1 we plot the autocorrelation function and the delayed mutual information obtained by analyzing the intensity time series, $|E(t)|^2$, for two different feedback strengths ($\kappa$) when the delay time $T$ is close to the relaxation oscillation period $\tau_{RO}$. The quantifers are not able to identify the delay time at $T = 1$ ns for $\kappa = 5$ ns$^{-1}$, see Fig 1 (a) and (c). In contrast, a clear peak at $T = 1$ ns can be observed for $\kappa = 10$ ns$^{-1}$, see Fig 1 (b) and (d).

The delay time can be concealed in the intensity time series when the laser is subject to a low feedback strength and $T \sim \tau_{RO}$. However, the phase information contained in the optical field emitted by the laser also needs to be analyzed. We present in Fig. 2 the autocorrelation function and the delayed mutual information obtained by analyzing time series from the phase and the real part of the electric field. Remarkably, the delay time can be identified both for low and moderate feedback strengths.

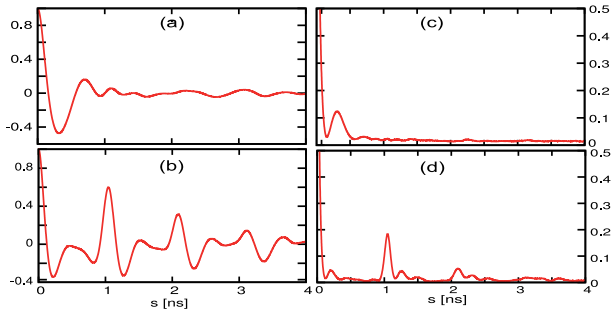


FIG. 1. ACF (left) and DMI (right) for $T = 1$ ns and $\tau_{RO} = 0.75$ ns (a, c) $\kappa = 5$ ns$^{-1}$, (b, d) $\kappa = 10$ ns$^{-1}$, obtained by analyzing the intensity time series.

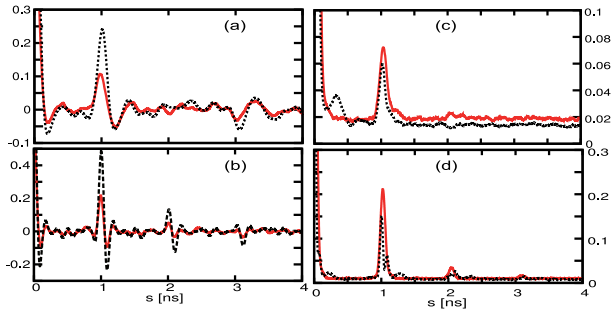


FIG. 2. ACF (left) and DMI (right) for $T = 1$ ns and $\tau_{RO} = 0.75$ ns (a, c) $\kappa = 5$ ns$^{-1}$ , (b, d) $\kappa = 10$ ns$^{-1}$, obtained by analyzing time series from the phase (solid line) and the real part (dot line) of the complex electric field, respectively.

We have illustrated by means of the autocorrelation function and the delayed mutual information that, in semiconductor lasers with optical feedback, the time-delay signature can be better retrieved from the phase of the complex electric field rather than the intensity. Interestingly, not only the time delay peak is always distinguishable when computing the quantifiers from the phase, but its precise location is also considerably improved compared to the quantifiers obtained by analyzing the intensity time series[3].

* miguel@ifisc.uib-csic.es

[1] A. Argyris et al., Nature **438**, 343 (2005).
[2] D. Rontani, A. Locquet, M. Sciamanna, D. S. Citrin, and S. Ortin, IEEE J. Quantum Electron. **45**, 879 (2009).
[3] R. Modeste Nguimdo, M. C. Soriano, and P. Colet, Opt. Lett., **36**, 4332 (2011).

# Brownian dynamics and dynamic Monte Carlo simulations of isotropic and liquid crystal phases of anisotropic colloidal particles: a comparative study

Alejandro Cuetos[1], Alessandro Patti[2]
[1] *Department of Physical, Chemical and Natural Systems, Universidad Pablo Olavide, 41013 Sevilla, Spain*
[2] *Institute of Advanced Chemistry of Catalonia (IQAC-CSIC) and CIBER de Bioingeniería, Biomateriales y Nanomedicina (CIBER-BBN), Jordi Girona 18-26 - 08034 Barcelona, Spain*

We report on the diffusion of merely repulsive and freely rotating colloidal rods in the isotropic, nematic and smectic liquid crystal phases, to probe the agreement between Brownian and Monte Carlo dynamics under the most general conditions. By properly rescaling the Monte Carlo time step, being related to any elementary move via the corresponding self-diffusion coefficient, with the acceptance rate of simultaneous trial displacements and rotations, we demonstrate the existence of a unique Monte Carlo time scale that allows for a direct comparison between Monte Carlo and Brownian dynamics simulations. To estimate the validity of our theoretical approach, we compare the mean square displacement of rods, their orientational autocorrelation function, and the self-intermediate scattering function, as obtained from Brownian dynamics and Monte Carlo simulations. The agreement between the results of these two approaches, even under the condition of heterogeneous dynamics generally observed in liquid crystalline phases, is excellent.

# Spatiotemporal Bounded Noises in the Ginzburg-Landau model

Sebastiano de Franciscis*

Alberto d'Onofrio

*European Institute of Oncology, Department of Experimental Oncology, Via Ripamonti 435, I20141 Milano (Italy)*

first important result of these investigations has been the emergence of noise-induced phase transitions "disorder to order" in spatially extended systems: in those cases a key bifurcation parameter is the force of strength of the spatial coupling (e.g. in the case of Laplace coupling, the diffusion coefficient). The most of the works in the field of noise-induced phase transitions are based on Gaussian noise (GN) or, more in general, white noises, in which is absent any spatiotemporal correlation or structure. This kind of fluctuations is appropriate when modelling system internal "hidden" degrees of freedom, of microscopic dynamical nature. On the contrary, fluctuations originating externally to the system in study may exhibit both temporal and spatial structure. Zero dimensional systems with colored Ornstein-Uhlenbeck noise (OU) showed to possess correlation-dependent properties that are missing in case of null autocorrelation, such as the emergence of stochastic resonance and re-entrant phase transitions[1]. Spatially extended systems exhibit even more striking effects when they are perturbed by spatially white but temporally colored noises: a complex interplay between noise intensity, spatial coupling and autocorrelation time[1].

Garcia-Ojalvo *et al* introduced in the spatial version of the OU noise, characterized by both a temporal scale $\tau$ and by a spatial scale $\lambda^2$. Later, in a study on additive spatiotemporally colored perturbations in the Ginzburg-Landau field, they showed the existence of a nonequilibrium phase transition controlled by both the correlation time and the correlation length[3].

Recently a vast body of research focused on an important class of non-Gaussian stochastic processes: the bounded noises. The interest on bounded noises is motivated by the fact that in many applications noise models are inadequate because of their infinite domain: this should preclude their use to model stochastic fluctuations affecting parameters which must be bounded by physical constraints, especially in biology, where some parameters and quantities must be strictly positive. As a title of example, a GN-based modelling of the fluctuations affecting the pharmacokinetics of an antitumour drug delivering could lead to the paradox that the probability that the drug increases the number of tumour cells may become nonzero[4].

In our contribution we define two simple families of spatiotemporally bounded noises, which extend two kinds of temporal bounded noises frequently employed in literature: the Tsallis-Borland noise and the Cai-Lin noise[5,6,2]. These can be characterized in terms of the spatial coupling parameter $\lambda$ and of the temporal correlation parameter $\tau$ on the distribution of the noise with suitable statistical observables and distributions. Differently from unbounded noise, bounded noises preserve their equilibrium distribution under tuning in $\tau$, while in some noise cases $\lambda$ modulation changes their shape. These characterization could be determinant when bounded noise are applied to dynamical systems, in particular in the presence of noise induced phase transitions.

Then we employed these two kinds of noises to study the phase transitions of the Ginzburg-Landau model, which under bounded perturbations resulted to exhibit a phenomenology quite different from the one induced by colored unbounded noises. Here, an increasing of noise temporal correlations enhances the "quenchedness" of noise, eventually producing an order to disorder transition, in an inverse manner with respect to what previously observed in former works with unbounded noise. On the other hand spatial coupling induces competitive effect on noise spatiotemporal fluctuations, resulting for some kind of noises a GL reentrant transition (order/disorder/order).

We point out finally that there is a dependence of the transitions or of stochastic resonance on the specific model of noise that has been adopted, and then in absence of experimental data on the distribution of the stochastic fluctuations for the problem in study, it is often necessary to compare multiple kinds of possible stochastic perturbations models.

---

* sebastiano.defranciscis@ifom-ieo-campus.it

[1] H.S. Wio and K. Lindenberg, Modern Challenges in Statistical Mechanics, AIP Conference Proceedings, Vol. 658, pp. 1-60 (2003).

[2] J. Garcia-Ojalvo, J.M. Sancho and I. Ramirez-Piscina, Phys. Rev. E 46, 4670 (1992)

[3] J. Garcia-Ojalvo, J.M. Sancho, Phys. Rev. E 49, 2769 (1994)

[4] A. dÓnofrio and A. Gandolfi, Phys Rev E 82 (6), 061901 (2010)

[5] L. Borland, Phys. Lett. A 245 (1-2), 67 (1998)

[6] C.Q. Cai and Y.K. Lin, Phys Rev E 54 (1), 299 (2004)

# Métodos de discretización para ecuaciones fluctuantes

J. A. de la Torre[1*], P. Español[1] y D. Duque[2]
[1] *Dept. Física Fundamental UNED. Senda del Rey 9, 28040 Madrid*
[2] *Dept. Enseñanzas Básicas de la Ing. Naval UPM. Avda. Arco de la Victoria, 28040 Madrid*

La simulación de procesos hidrodinámicos multiescala es a menudo abordada con mallados arbitrarios que permiten resolver con precisión aquellas regiones en la que los campos cambian más fuertemente en ciertas regiones de interés. Cuando estas regiones tienen tamaños mesoscópicos, empiezan a ser importantes las fluctuaciones térmicas.

En este trabajo[1] proponemos la elaboración de algoritmos de simulación en mallados arbitrarios que incluyan fluctuaciones térmicas de manera consistente. A partir de la definición formal de unos ciertos operadores de continuación y discretización (que verifican propiedades de *localidad* y *consistencia lineal*), elaboramos según el esquema de residuos pesados un algoritmo de elementos finitos basados en la teselación de Delaunay.

Tomando como ejemplo paradigmático una ecuación de difusión no lineal,

$$\frac{\partial c(\mathbf{r},t)}{\partial t} = \nabla\mu(c(\mathbf{r},t))\nabla\frac{\delta\mathcal{F}}{\delta c(\mathbf{r},t)}\left[c(\mathbf{r},t)\right] + \nabla\tilde{J}\,, \qquad (1)$$

consideramos dos ejemplos para el funcional de energía libre $\mathcal{F}[c(\mathbf{r},t)]$: un modelo gaussiano cuadrático en la concentraciones y un modelo correspondiente a la energía libre de Cahn-Hilliard[2]. En ambas situaciones comprobamos que la parte determinista de la ecuación de difusión discreta respeta los dos ingredientes fundamentales de dicha ecuación: conservación del número de partículas y existencia de un teorema H. Que el algoritmo discreto respete este último requisito es fundamental para la formulación termodinámicamente consistente de las fluctuaciones térmicas. Éstas se formulan de tal manera que se satisface el teorema de fluctuación–disipación. Se observa que, mientras que las variables hidrodinámicas están definidas en los nodos de la malla arbitraria, los ruidos térmicos están definidos en los simplex de la red (triángulos en 2D, tetraedros en 3D). Estos resultados generalizan a mallados arbitrarios frente a resultados previos para la discretización de la ecuación de difusión en mallados regulares[3].

---

* jatorre@bec.uned.es

[1] J. A. de la Torre, D. Duque, P. Español, *en preparación* (2012)
[2] J. W. Cahn, J. E. Hilliard, J. Chem. Phys **28**, 258 (1958)
[3] J. A. de la Torre, P. Español, J. Chem. Phys **135**, 114103 (2011)

# Unified Model for thermal transport in bulk, thin films and nanowires

C. de Tomas*, A. F. Lopeandia, F. X. Alvarez
*Physics Department*
*Autonomous University of Barcelona 08193 Bellaterra, (Catalonia)*

A. Cantarero
*Materials Science Institute*
*University of Valencia 22085, E-46071 Valencia*

A general model able to explain the thermal conductivity for macro, micro and nanostructured systems is still an open challenge. Experimental measurements on these systems have shown a drastic size-dependent reduction of the thermal conductivity compared to bulk values. Much effort has been devoted to the development of models to provide an accurate understanding of this behavior[7,6,5,3]. At the moment, we can only confirm that when the size of the sample is reduced, classical boundary effects are expected, and below some nanometers in size, quantum confinement should also start to influence the thermal conductivity through the modification of the dispersion relations (folding phonons and aperture of gaps in the dispersion relations). However, it is still under debate which are the most important effects at the different length scales since most of the proposed models do not agree in the origin of the thermal conductivity reduction, if it is a classical or quantum effect, especially at the 10-100 nanometer scale. In order to obtain a thermal transport model valid at all ranges of sizes and temperatures, it is necessary to have some certainty about the limits of applicability of the classic and quantum approaches. As a consequence, it is essential to study in detail every contribution independently. We have explore the limits of validity of the approaches based on the classical Boltzmann transport equation (BTE). This should lead us to establish the classical to quantum thermal transport frontier when the thermal conductivity behavior in reduced size systems is addressed. Eventually, we obtain a thermal conductivity expression that provides results in good agreement with published data on bulk silicon, thin films and nanowires, with characteristic sizes above 30 nm and show that quantum confinement effects above these sizes are not needed to understand the thermal transport.

Our thermal conductivity expression is based on the Guyer-Krumhansl model[1], conversely to previous attempts, which are based on the more usual Callaway model[2]. The provided expression accounts for hydrodynamic effects in the thermal transport equations, and it is obtained after a more rigorous treatment of normal scattering processes than that described in the Callaway model. This allows to reproduce the predicted values of the thermal conductivity in the region where the Callaway model over-predicts them. In order to provide a general analytical expression valid for the different geometries (three dimensional, two dimensional and one dimensional materials), the form factor of the Guyer-Krumhansl model is replaced by an expression given by the Extended Irreversible Thermodynamics model[4]. The results fit very accurately to experimental values of bulk silicon, thin films at the micro and nanoscale and silicon nanowires.

---

* carla.tomas@uab.cat

[1] R. A. Guyer, and J. A. Krumhansl, Phys. Rev. **148** 778 (1966)
[2] J. Callaway, Phys. Rev. **113** 1046 (1958)
[3] D. T. Morelli, J. P. Heremans and G. A. Slack, Phys. Rev. B **66** 195304 (2002)
[4] D. Jou and J. Casas-Vazquez and G. Lebon, *Extended Irreversible Thermodynamics*, Springer, Berlin (1993)
[5] P. Martin, Z. Aksamija, E. Pop and U. Ravaioli, Phys. Rev. Lett. **102** 125503 (2009)
[6] J. Zou and A. Balandin, J. App. Phys. **89** 2932 (2001)
[7] N. Mingo, Phys. Rev. B **68** 113308 (2003)

# Detecting long-range teleconnections in the climate network via ordinal pattern time-series analysis

J. Ignacio Deza[†*], Marcelo Barreiro[‡] y Cristina Masoller[†]

[†] *Departament de Física i Enginyeria Nuclear, Universitat Politècnica de Catalunya, Colom 11. E-08222, Terrassa, Barcelona.*

Complex networks appear in almost all fields of science, examples being the internet, social interactions, food webs, biochemical reactions, brain functional networks, etc. For the purpose of modeling and forecasting, many systems lead naturally to the concept of networks of interacting elements, where one can define nodes and assign links among them depending on the (in principle, very complex) features of the system under study. It is by now well known that the Earth's climate is not only based on local factors, as the atmosphere connects far away regions through waves and advection of heat and momentum. This long-range coupling makes the network modeling approach of the Earth's climate extremely attractive and promissing[1,2]. By covering the Earth' surface with a regular grid of nodes, and by assigning links to connections between two different nodes via an analysis of their climate interdependency, the network approach has been shown to be able to extract novel and meaningful information.

Mutual information (MI) is a nonlinear measure, function of the probability density functions (PDF) that characterizes the time series in two different nodes $p_i(m)$ and $p_j(n)$, as well as of the joint probability function $p_{ij}(m,n)$. It can be defined as

$$M_{ij} = \sum_{m,n} p_{ij}(m,n) \log \frac{p_{ij}(m,n)}{p_i(m)p_j(n)}. \qquad (1)$$

where the PDF needed for computation can be approximated by means of histograms. Besides that method, it has been proposed the use of ordinal patterns (OP). These are used in symbolic calculus and are first calculated from the time series by noting the value of a given point relative to its neighbors (see figure 1). Ordinal patterns do not constrain us to choose immediately adjacent points in order to make the patterns. We can construct them letting a time interval between points, and in this way we can consider different time scales.

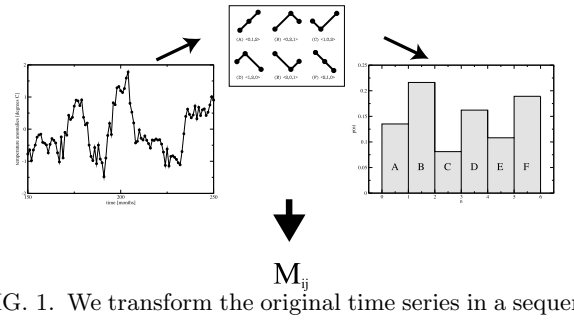


FIG. 1. We transform the original time series in a sequence of OPs (shown for n=3), then compute the PDFs of the OPs and finally compute the Mutual Information using Eq. 1.

We analyze monthly averaged surface air temperature anomalies (SAT field) from the NCEP/NCAR reanalysis[1].

We have calculated Mij from the PDFs of the OPs constructed from consecutive months and from consecutive years. We have used OPs of length 4 and thus there are 4! = 24 different possible OPs. Afterwards we construct the elements $A_{ij}$ of the network with the elements of $M_{ij}$ over a threshold of significancy (calculated using surrogate data). In figure 2 we graphically represent our networks showing the Area Weighted Connectivity: $AWC_i = \sum_j^N A_{ij}\cos(\lambda_i)/\sum_j^N \cos(\lambda_j)$ over the world map.

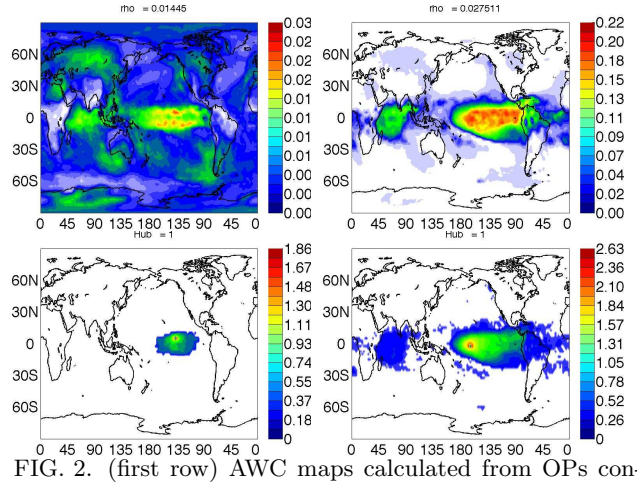


FIG. 2. (first row) AWC maps calculated from OPs constructed with adjacent months (left) and OPs constructed with adjacent years (right). On the second row we show the corresponding most connected node (hub) in the network: the color code indicates the mutual information of the hub with the other nodes. We observe tele-connections in the inter-anual time scale (left) but not in the intra-season time scale (right).

We have shown that these techniques are useful for constructing climate networks on different time scales. This provides a novel approach to climate network analysis that can be extended to other, shorter or longer timescales, such as those in meteorology or in paleoclimatology.

* juan.ignacio.deza@upc.es

‡ Instituto de Física, Facultad de Ciencias, Universidad de la República, Iguá, 4225, Montevideo, Uruguay.

[1] M. Barreiro, A. C. Marti y C. Masoller. *Chaos*, **21**:013101(2011).

[2] J. F. Donges, Y. Zou, N. Marwan and J. Kurths. Eur. Phys. J. Spec. Top.**174**:157 (2009).

# Cosecha de energía de espectro amplio con osciladores alineales monoestables: mejora con potenciales de paredes finitas y ruidos tipo Lévy

J. Ignacio Deza†, Roberto R. Deza* y Horacio S. Wio
*IFCA, Instituto de Física de Cantabria, CSIC-Universidad de Cantabria 39005-Santander (Cantabria)*

Recientemente se estudió la aptitud de osciladores alineales monoestables con potencial polinómico, para la cosecha de energía de espectro amplio mediante piezoelectricidad. El sistema es descrito por las ecuaciones[1]

$$m\ddot{x} = -U'(x) - \gamma\dot{x} - K_v V + \sigma\eta(t), \quad (1)$$

$$\dot{V} = K_c\,\dot{x} - \frac{1}{\tau_p}V, \quad (2)$$

donde $K_v$ y $K_c$ son los acoplamientos piezoeléctricos, $\tau_p$ la constante de tiempo del circuito de carga, $\gamma$ la de amortiguación del oscilador monoestable, y $\sigma$ la de acoplamiento al ruido coloreado $\eta(t)$, cuyo tiempo de autocorrelación es $\tau$. Se observa $V_{rms}$, ya que la potencia entregada a la resistencia de carga $R$ es $P = V_{rms}^2/R$.

En este trabajo investigamos la aptitud del potencial de Woods–Saxon[2]

$$U(x) = -\frac{V_0}{1+\exp\left(\frac{|x|-r}{a}\right)} \quad (3)$$

cuya forma, controlada por $a$, va desde un pozo cuadrado con paredes de altura $V_0$ y ancho $2r$ hasta confundirse en la zona de interés con un oscilador armónico (Fig. 1).

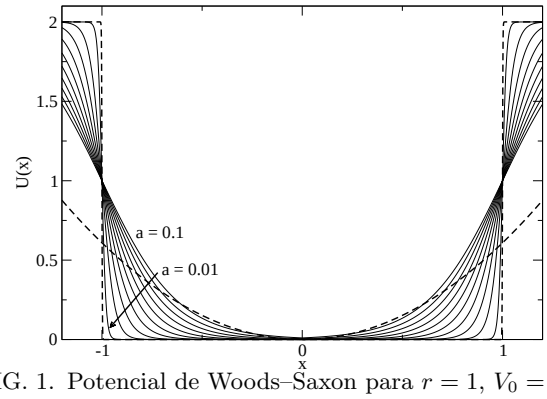


FIG. 1. Potencial de Woods–Saxon para $r = 1$, $V_0 = 2$ y $a$ entre 0,01 y 0,1.

Pero además permitimos que el ruido coloreado $\eta(t)$ sea *no Gaussiano*, al generalizar la ecuación dinámica del ruido de Ornstein–Uhlenbeck a

$$\dot{\eta} = -\frac{1}{\tau}\frac{d}{d\eta}V_q(\eta) + \frac{1}{\tau}\xi(t), \quad (4)$$

donde

$$V_q(\eta) = \frac{1}{\beta(q-1)}\ln\left[1+\beta(q-1)\frac{\eta}{2}\right] \quad (5)$$

con $\beta = \tau/D$, y $\xi(t)$ es un ruido blanco Gaussiano de media nula y varianza $D$. $\eta$ es de Ornstein–Uhlenbeck para $q = 1$, de intensidad acotada para $q < 1$ y cualitativamente similar al de Lévy para $q > 1$. Las figuras 2 y 3 muestran (además del efecto de variar $V_0$ y $a$) que $V_{rms}$ tiende a crecer con $q$. Se concluye que el rendimiento energético del sistema depende de la estadística del ruido, y aumenta si éste es de tipo Lévy.

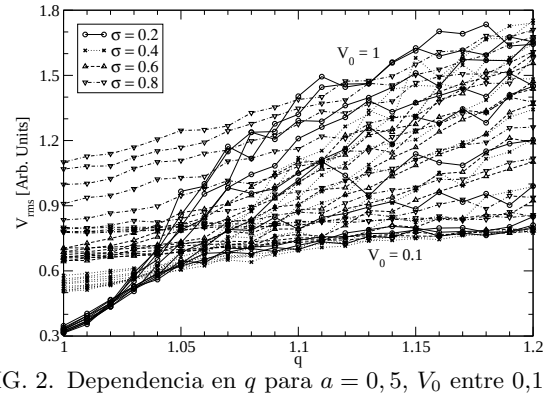


FIG. 2. Dependencia en $q$ para $a = 0,5$, $V_0$ entre 0,1 y 1 y varios $\sigma$ (indicados en el recuadro).

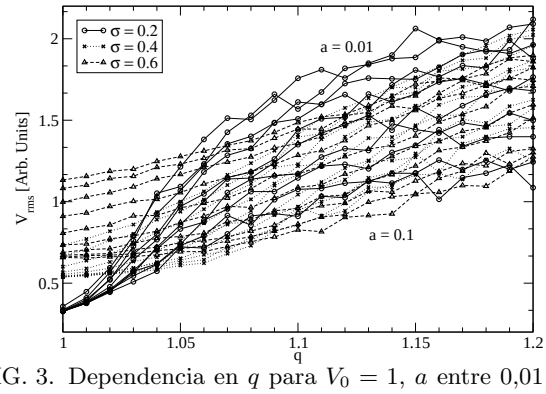


FIG. 3. Dependencia en $q$ para $V_0 = 1$, $a$ entre 0,01 y 0,1 y varios $\sigma$ (indicados en el recuadro).

† Departament de Física i Enginyeria Nuclear, Universitat Politècnica de Catalunya, 08222-Terrassa (Barcelona).
* IFIMAR, Mar del Plata, Argentina. deza@mdp.edu.ar

[1] L. Gammaitoni, I. Neri y H. Vocca, Chem. Phys. Lett. **375**, 435 (2010).
[2] A. Bohr y B. R. Mottelson, *Nuclear structure* v.1 (Benjamin, NY, 1975).
[3] J. I. Deza, R. R. Deza y H. S. Wio, enviado a Europhys. Lett. (2012).

# Los parámetros mecánicos de la Membrana controlan la Fisión mediada por Dinamina

S.Morlot[†,◁], V.Galli[†], M.Klein[◁], J.Manzi[◁], F.Humbert[†], L.Dinis[*], M.Lenz[⊙], G.Capello[◁], A.Roux[†,‡]
*Dpto. Física Atómica, Molecular y Nuclear (UCM) y GISC*

La dinamina es una proteína helicoidal con actividad GTPasa que constriñe el cuello de las invaginaciones cubiertas de clatrina hasta conseguir su fisión.

Aunque la bioquímica de la dinamina está mejor caracterizada que para otros sitemas de fisión, la física de la fisión no se conoce bien. En particular, las condiciones mínimas para la fisión todavía son controvertidas ya que la presencia de dinamina es necesaria pero no suficiente, como muestran varios experimentos[1,2]. Estos resultados apuntan además a una más que probable influencia de los parámetros mecánicos de la membrana en el proceso de fisión.

Para estudiar cómo la mecánica de la membrana controla la fisión, se diseñó un experimento en el que a partir de una Vesícula Unilamelar Gigante (GUV) se extrae un nanotubo de membrana mediante pinzas ópticas (figura 1). La tensión $\sigma$ se controla mediante la aspiración en la micropipeta que mantiene la GUV. Finalmente, el valor del módulo de flexión $\kappa$ se puede controlar modificando la composición lipídica de la membrana utilizada en el experimento. Para iniciar la reacción de fisión, se inyectan simultáneamente una dinamina marcada con Alexa488 y GTP. El tiempo de fisión se mide controlando la fluorescencia de la dinamina-Alexa488.

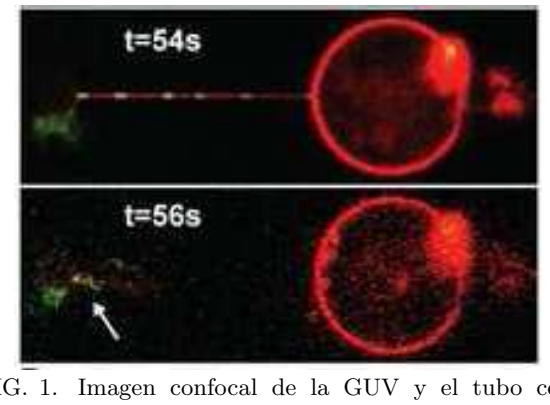


FIG. 1. Imagen confocal de la GUV y el tubo con la membrana en rojo y de la dinamina en verde, marcada con Alexa488. Arriba, nanotubo parcialmente cubierto con dinamina. Abajo, fisión del nanotubo tras 56 segundos.

Los datos muestran los tiempos de fisión se distribuyen exponencialmente y que el tiempo promedio disminuye con la tensión aplicada y crece con el módulo de flexión. Por otra parte, el logaritmo del tiempo medio de fisión decrece linealmente con el logaritmo de la concentración de GTP.

En este trabajo mostramos cómo, a pesar de la complejidad de la maquinaria biológica involucrada, las tendencias observadas pueden explicarse mediante la física de la deformación de la membrana. Para ello, modelamos la fisión como una transición entre dos estados controlada por una barrera energética que se puede sobrepasar mediante fluctuaciones térmicas espontáneas. Dicha barrera tiene su origen en la energía necesaria para constreñir el cuello de membrana que une el nanotubo recubierto de dinamina con el resto de la membrana y puede evaluarse una vez conocida la forma de la membrana. Para calcular la forma de la membrana se ha de minimizar el Hamiltoniano de Canham-Helfrich[3] que representa la energía de la membrana en función de su curvatura y tensión superficial. La teoría predice un comportamiento del tiempo medio de fisión:

$$\langle t_f \rangle \simeq \tau e^{\frac{bk^{3/2}}{\sqrt{\sigma}kT}}, \qquad (1)$$

expresión que puede utilizarse para ajustar todos los datos experimentales, como se muestra en la figura 2.

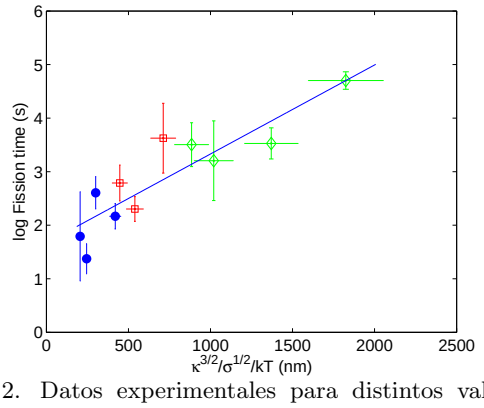


FIG. 2. Datos experimentales para distintos valores de tensión y módulos de flexión y ajuste a la expresión teórica. Puntos azules: EggPC + PI(4,5)$P_2$, cuadrados rojos: EggPC + Cholesterol + PI(4,5)$P_2$, rombos verdes: Esfingomielina + PI(4,5)$P_2$

* ldinis@fis.ucm..es
† Biochemistry Department, University of Geneva, CH-1211 Geneva, Switzerland.
‡ Swiss National Centre for Competence in Research Programme Chemical Biology, CH-1211 Geneva, Switzerland.
◁ Institut Curie, Centre de Recherche; CNRS, UMR 168; y UPMC, F-75248 Paris, France.
⊙ James Franck Institute, University of Chicago, IL-60637 Chicago, U.S.A.

[1] Danino, D., Moon, K.H., and Hinshaw, J.E., J Struct Biol **147**, 259 (2004)
[2] Roux, A., Uyhazi, K., Frost, A., and De Camilli, P., Nature **441**, 528 (2006).
[3] Helfrich, W., Zur Naturforschung **28c**, 693 (1973)

# Colapso gravitatorio y descomposición espinodal: ¿es lo mismo?

Alvaro Domínguez*
*Física Teórica, Universidad de Sevilla, Apdo. 1065, E–41080, Sevilla*

Un gas de Yukawa bidimensional consiste en esferas duras (diámetro $\sigma$) que se atraen según el potencial

$$V_{\rm atr}(d) = -V_0 K_0(d/\lambda) \qquad (V_0, \lambda > 0) \qquad (1)$$

en términos de la función de Bessel modificada $K_0$. Esta exhibe un decaimiento exponencial para $d \gg \lambda$ (correspondiente a una interacción de corto alcance), pero un comportamiento logarítmico para $d \ll \lambda$ (formalmente análogo a la gravitación newtoniana bidimensional y por tanto no integrable en el sentido de la mecánica estadística del equilibrio). Los estudios previos del gas de Yukawa han considerado invariablemente $\sigma \approx \lambda$; nuestro objetivo es estudiar el caso $\sigma \ll \lambda$, de forma que el efecto del comportamiento logarítmico sea patente.

Aparte de su interés fundamental intrínseco, este modelo es de importancia práctica porque describe la interacción por fuerzas capilares de partículas coloidales atrapadas en una interfase fluida. Se trata de un sistema que hoy en día se genera y estudia rutinariamente en el laboratorio, para los cuales $V_0$ y $\lambda$ dependen de parámetros experimentalmente controlables con relativa facilidad. En particular, una configuración típica involucra $\sigma \approx 1$ $\mu$m (partículas coloidales) y $\lambda \approx 1$ mm (longitud capilar). Debido a esta separación de escalas, el sistema exhibe características tanto de un fluido autogravitante como de un fluido de van der Waals.

Nos hemos centrado en el estudio de la dinámica de este modelo, prestando particular atención a la dependencia con el rango $\lambda$ de la interacción: si $\lambda$ es muy grande se espera que una distribución inicialmente homogénea sufra un colapso colectivo de tipo gravitatorio (efectos globales dominantes), mientras que si $\lambda$ es muy pequeño se puede esperar una descomposición espinodal de separación de fases (efectos locales dominantes). El modelo teórico empleado[1] describe la evolución, en la aproximación de campo medio, del campo densidad de partículas debida a la competición entre la atracción (1) y la difusión térmica. El análisis teórico se ha complementado con simulaciones numéricas, incluyendo la medición de cuantificadores particularmente sensibles a la formación de estructuras en el régimen no lineal (inhomogeneidad grande)[2], así como condiciones iniciales inhomogéneas (disco finito) que realzan la influencia del contorno sobre la evolución[3]. Las conclusiones se pueden resumir como sigue:

- Cuando se dispone de predicciones teóricas (usualmente resultados perturbativos en diferentes regímenes), éstas son confirmadas por las simulaciones.
- Se aprecia una transición continua entre colapso gravitatorio (formación de cúmulos densos inmersos en una distribución muy diluída de partículas) y descomposición espinodal (separación de fases líquida y gaseosa) como función del alcance $\lambda$ de la interacción.
- En el colapso gravitatorio se aprecia una evolución en dos etapas ("separación de fases" y "crecimiento de dominios") reminiscentes de las de descomposición espinodal.
- Durante la descomposición espinodal se aprecian rasgos globales (formación de cúmulos preferentemente sobre una "onda de choque" viajera inducida por el contorno del disco finito) reminiscentes del colapso gravitatorio.

La siguiente figura resume el tipo de evolución según los dos parámetros adimensionales relevantes del estado inicial de un disco finito: $\lambda/L$ en la abscisa, con $L$ = tamaño inicial del disco, y el cociente entre la energía térmica y la energía de atracción según (1) en la ordenada.

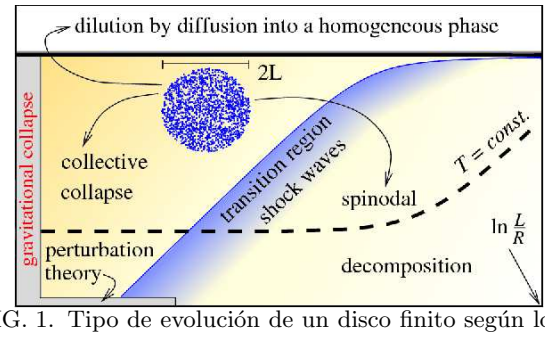


FIG. 1. Tipo de evolución de un disco finito según los dos parámetros adimensionales relevantes del estado inicial: la abscisa representa $\lambda/L$, con $L$ = radio inicial del disco, y la ordenada corresponde al cociente entre la energía térmica y la energía de atracción según (1). (Figura en escala log–log).

* dominguez@us.es

[1] Domínguez, Oettel, and Dietrich, *Phys. Rev. E* **82**, 011402 (2010).
[2] Bleibel, Domínguez, Oettel, and Dietrich, *Eur. Phys. J. E* **34**, 125 (2011).
[3] Bleibel, Domínguez, Oettel, and Dietrich, *Phys. Rev. Lett.* **107**, 128302 (2011).

## The meaning of niche: Cause or consequence of food-web structure?

Virginia Domínguez García* [1], Sam Johnson [2] and Miguel A. Muñoz [1]
[1] *Departamento de Electromagnetismo y Física de la materia, and instituto carlos I de Física Teórica y Computacional, universidad de Granada,18010 Granada,Spain.*
[2] *Oxford Centre for Intrgrative Systems Biology, and Department of Physics, University of Oxford, clarendon Lab, OX1 3QU, United Kingdom*

The research in the field of ecological networks is becoming more and more relevant given the increasing pressure the ecosystems are facing, which makes the study of their topology specially interesting due to its interconnectance with the dynamical processes taking place in it.

Food webs - networks of predators and prey - have long been known to exhibit intervality: species can be ordered along a single axis in such a way that the prey of any given predator tend to lie on unbroken intervals. Although the meaning of this niche dimension has remained a mystery, it is widely assumed to be the reason behind the highly non-trivial structure of food webs. For decades, therefore, most food-web modelling has been based on assigning species a niche value by hand, with the niche model, one of their main exponents, becoming a kind of a benchmark for the study of food-webs.

However, going on empirical evidence and a simple self-assembling network model, in which species are added sequentially to the network and prey are selected according to their trophic level, a purely structural property, it can be shown that realistic intervality - and other features of general insterest in the study of trophic networks - can come about as a consequence of biologically plausible mechanisms that do not require an a priori ordering.

With this is mind we can conclude therefore that the niche dimension is probably an artefact, which calls for a fundamental change in perspective as to how ecosystems arise and persist.

* virginia@onsager.ugr.es

# Nonlinear methods in modified gravities and the corresponding cosmologies

Emilio Elizalde*
*Consejo Superior de Investigaciones Científicas, ICE/CSIC and IEEC*
*Campus UAB, Facultat Ciències, Torre C5-Par-2a pl, 08193 Bellaterra (Barcelona) Spain*

Dark Friedman-Robertson-Walker fluids governed by non-linear inhomogeneous equations of state (EoS) have been considered that can be viewed as a conveniently simple paradigm for a whole class of models that exhibit phase transitions from a non-phantom towards a phantom era in the universe evolution. Such dark fluid models may also describe quintessence-like cosmic acceleration. Thermodynamical considerations for the processes involved are of great importance in the characterization of the global evolution of the corresponding universe. In particular, viscous cosmology models have been increasingly popular lately. From a hydrodynamical viewpoint this is quite a natural development, as the inclusion of the viscosity coefficients (shear and bulk) means physically that one departs from the case of an ideal fluid and incorporates the deviations from thermal equilibrium to first order. The case of an ideal (nonviscous) fluid is, after all, quite an idealized model. Also, under boundary-free conditions—such as in free turbulence—viscosities are physically most important. In a cosmological context, as the cosmic fluid is assumed to be spatially isotropic the shear viscosity is usually left out. One place where the appearance of bulk viscosity in the cosmic fluid should be expected to play an important role, is in the Big Rip phenomenon, i.e. the singularity of the universe in the future This means that one or more of the physical quantities go to infinity at a finite time $t$ in the future. Mathematically this implies divergent integrals, typically met when one uses the Friedmann equations to express $t$ as an integral over the density $\rho$. A novel scenario has been proposed, the so-called Little Rip, models in which the nonviscous dark energy density increases with time (EoS parameter $w < -1$), but $w \to -1$ asymptotically, in that way avoiding the future singularity. Typically, this was found to occur when the scale factor increases rapidly with time, like $a(t) \sim \exp[\exp(t)]$ or higher exponentials. And this brings us to the topic, namely to examine the consequences of endowing the fluid with a bulk viscosity.

Actually, dark energy of phantom or quintessence nature with an equation of state parameter $w$ almost equal to $-1$ often leads the universe evolution to a finite-time future singularity. An elegant solution to this problem has been recently proposed under the form of this Little Rip cosmology which appears to be a realistic alternative to the ΛCDM model[1]. Whereas generically bulk viscosity tends to promote the Big Rip, we find that there are a number of situations where this is not the case and where the formalism nicely adjusts itself to the Little Rip scenario. In particular, a viscous fluid (or, equivalently, one with an inhomogeneous (imperfect) equation of state) is actually able to produce a Little Rip cosmology as a purely viscosity effect. The possibility of its induction as a combined result of viscosity and a general (power-like) equation of state is investigated in detail. A physical interpretation of the dissolution of bound structures in the Little Rip cosmology is presented too.

In a related cosmological context, let us mention the known fact that, once the initial inflationary stage in the universe evolution, which originated a supercooling effect, ended up, temperature started to increase until, eventually, a recombination of elementary particles to create bound structures, in particular the first atoms, took place. This increase in the temperature is called re-heating, which also gives name to this period in the evolution of the universe, which subsequently led to the formation of the first stars, galaxies and much bigger structures, typical of the present universe at large scale.

One of the problems which appears in this process, when one tries to go the details of a feasible fundamental theory, as superstring theory, is the so-called field moduli problem. Field moduli can be considered, at first instance, as additional degrees of freedom corresponding to, say 'pulsations' of the universe when it was very small. They are a remnant of the compactification processes of superstrings, in going from the 11 dimensions of the mother theory to the 4 dimensional space-time we observe now.

In a seminal paper published a decade ago, Felder, Kovman and Linde[2] used a model of light particle production during and after the inflation process and where able to prove that, when implementing the model in string theory, a large amount of moduli fields were produced, what was in contradiction with astronomical observations. This is the so-called 'moduli problem.' In an attempt at trying to solve this issue, they obtained a reheating temperature of the universe that was abnormally small, far from the one predicted in theoretical models. On the contrary, in a more recent paper[3], trying to solve the same problem by using a different argumentation, an abnormally too high reheating temperature has been postulated. Recently, we have given a solution to the moduli problem by a different method, which in the end nicely reconciles the above discrepancies and yields a very reasonable value for the reheating temperature[4].

---

* elizalde@ieec.uab.es, elizalde@math.mit.edu.

[1] I. Brevik, E. Elizalde, S. Nojiri, and S.D. Odintsov, Phys. Rev. D84, 103508 (2011).
[2] G. Felder, L. Kovman and A. Linde, JHEP 0002, 027 (2000).
[3] F. Finelli, A. Gruppiso, F. Paci, and A.A. Starobinsky, Phys. Rev. D79, 044007 (2009)
[4] J. de Haro and E. Elizalde, PRL 108, 061303 (2012).

# Modeling the interaction of DNA with Terahertz fields.

A. E. Bergues-Pupo[1], J. M. Bergues[2], F. Falo[3*]
[1] *Dpto de Física, Universidad de Oriente, 90500 Santiago de Cuba, Cuba.*
[2] *Universidad San Jorge, 50830 Villanueva de Gállego, Zaragoza, Spain.*
[3] *BIFI and Dpto de Física de la Materia Condensada, 50009 Universidad de Zaragoza, Spain.*

Today the use of non-ionizing radiation sources with frequencies on the THz range has spread in everyday life. The effects of this radiation on biological systems are interesting issues because biological functions may be altered and genotoxic effects may be generated. Particularly, the vibrational modes of DNA and others biomolecules are on the cited frequency range. Since THz photons do not carry enough energy to directly alter chemical reactions, nonlinear resonance effects may cause local changes of dynamics breathing in these systems. Motivated by this fact, Alexandrov et al. studied the influence of a THz field into dynamics of a homogeneous poly (A) DNA molecule with 64 base pairs (bp)[1,2]. To model the interactions of dsDNA with THz field, they used the Peyrard-Bishop-Dauxois (PBD) model citePBD. For this purpose, they studied periodic driving and frictional terms in the absence of thermal noise. It was found that breather modes (localized separations of the double strand) can be observed under certain conditions. Hence, it was concluded that the main effect of THz radiation is to resonantly influence into dynamical stability of the dsDNA. Later, Swanson showed that these breather modes can be eliminated changing the PBD model parameters or by including thermal noise[4]. He admitted that under assumptions concerning drag and drive forcing, breather modes can be generated at certain resonant frequencies.

On the other hand, Tapia et al. studied a homogeneous A-T sequence and the P5 virus promoter in the framework of the PBD model without applied external field and including thermal noise[5]. They enhanced this model with the inclusion of the solvent interaction through the addition of a Gaussian barrier to the Morse potential. They set suitable parameter values for the model and studied the formation and stabilities of bubbles in the system. They focused on the application of the principal component analysis (PCA) of the trajectories for P5 virus promoter under equilibrium conditions.

For these reasons we study the effect of the THz field in the dynamics of a heterogeneous sequence that has been widely studied in the framework of the PBD model[6], the P5 virus promoter. We included thermal noise to see the field influence under this condition. We use the PBD model with a solvation barrier. This barrier accounts for solvent interactions in the system and modifies the melting transition and the dynamics of molecule.

In this work we analyze the response of the system at different frequencies and field amplitudes. After that, we show the influence under some specific parameters of THz field in the melting transition and in the denaturation bubbles formation.

---

* fff@unizar.es

[1] B. S. Alexandrov, V. Gelev, A.R. Bishop, A. Usheva, and K.O. Rasmussen, Phys. Lett. A 374, 1214 (2010).
[2] P. Maniadis, B. S. Alexandrov, A. R. Bishop, and K. O. Rasmussen, Phys. Rev. E 83(1), 011904 (2011).
[3] T. Dauxois, M. Peyrard, and A.R. Bishop, Phys. Rev. E 47, R44 (1993).
[4] Eric S. Swanson, Phys. Rev. E 83, 040901 (R) (2011).
[5] R. Tapia-Rojo, J. J. Mazo, and F. Falo, Phys. Rev. E 82, 031916 (2010).
[6] G. Kalosakas, K. O. Rasmussen, A. R. Bishop, C. H. Choi, and A. Usheva. Europhys. Lett. 68, 127-133 (2004).

# Trees as Representation of human-like adaptive systems

Miguel A. Fernandez*, Hector Corte, Elka Korutcheva
*Departamento de Fisica Fundamental, UNED, c/ Senda del Rey,No 9, 28080 Madrid.*

Dynamic networks are systems in which the number of nodes and connexions are not constant, they undergo an evolution in which new nodes and connexions appear and existing ones are deleted. In this paper we study a kind of growing networks which defines a collaborative software development by pieces built by different persons or teams. We focus on the growing dynamics of systems driven by stimulus-response, like chatbots and AI games.

Chatbots are programs which imitate the responses a human would produce in a chat. Several approaches are used and we focus in the storage of stimuli-responses[1].

Stimuli are inputs to the bot and responses are outputs. The overall interaction is described by a generalized directed tree graph in which nodes are stimuli and branches are responses. A conversation can then be represented as a path along the tree.

Similar mechanism is found in some AI turn-based games, where the machine must react to human inputs with a new move. Again, this can be represented by a directed tree graph in which new branches correspond to new strategies, linking two existing nodes equals to using the same strategy when the situation is similar and where specific game is a path across the tree. A word of caution here: this linking of two existing nodes is not always desired, it happens because some lack of coordination between builders, and can originate unpredicted behaviour like an absurd answer.

These systems are particularly interesting due to several reasons. They are widespread and useful, and they are capable of either mimicking (passing a Turing test) or beat humans in strategy games. It is very interesting to ascertain whether a qualitative change is produced at some point in their evolution which enables their success in such tasks and we approach it as a phase transition[3], in some ways similar to the manifestation of the "small world" behaviour.

Our complex network model, which matches the building process of a chatbot, is based on a recursive tree starting from a root node, which is an initial seed or test conversation. Then the process consists in adding subtrees: in each step an existing node is selected by a probability based on its clustering coefficient[2] -higher probability for lower clustering coefficients- and spans new nodes with a non constant branching factor, selected between 1 and k by a Poisson distribution. Additionally, in each step two existing nodes i,j are selected randomly and linked together. The Nodes with higher clustering coefficient have more chances of being linked. This is behaviour is found in chatbots where general topics are linked together much more easily than very specific topics. This kind of growing model has never been explored to our knowledge. All the work we are aware of considers linking a new node to existing nodes by different preferential schemas. Yet to be explored is also the effect of linking existing nodes. The goal is to have a "world" as big as possible, for it enables longer paths. The resulting structure is like in the following figure:

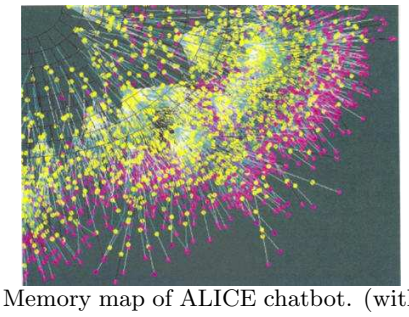

FIG. 1. Memory map of ALICE chatbot. (with permission of ALICE foundation for Artificial Intelligence)

We use a bottom top approach, vary the spanning probability which determines each step branching factor and the probability of linking existing nodes. We use a generating function approach to derive the rate equations for the population of layers and to derive the dynamics of node in-component and out-component, where in-component of a node is the set of all nodes from which current node can be reached and out-component is the set of all nodes reachable from current[4].

* miguel_a_fernandez@hotmail.com

[1] R.Wallace, "Be your own botmaster", ALICE A.I. Foundation, 2n edition (2005)
[2] T. Antal, P.L. Krapivsky, "Weight-driven growing networks", 71 Physical Review E, 2 (2008).
[3] S.N. Dorogovtsev, A.V. Goltsev, "Critical phenomena in complex networks", Arxiv Cond-mat 0705.0010
[4] M. E. J. Newman, S. H. Strogatz, "Random graphs with arbitrary degree distribution and their applications" 64, Physical Review E, 2 (2001).
[5] S. Maslov, K. Sneppen, A. Zaliznyak, "Detection of Topological Patterns in Complex Networks: Correlations Profile of the Internet", Physica A, 333, 539-540, (2004).
[6] P.L. Krapivsky, S. Redner, F. Leyvraz, "Connectivity of growing random networks", Arxiv Cond-mat 0005139v2

# Interdependent choices, individual preferences and social influence

Ana Fernández del Río*, Elka Korutcheva and Javier de la Rubia
*Departamento de Física Fundamental*
*Universidad Nacional de Educación a Distancia (UNED)*
*Facultad de Ciencias, Paseo Senda del Rey 9*
*28040-Madrid (Spain)*

Mean-field Ising equilibrium dynamics can be used to describe the collective properties of certain choice or decision making processes when we want to mimic a generic tendency of individuals to *conform to the norm*, understood in this case as the accurately perceived average behaviour of the group. This can be a useful approach for a wide range of problems covered by the social sciences, from political science to demand contexts or the incidence of any particular social trait or habit.

Even very simple models already have interesting interpretations in social contexts[1] and direct parallelisms can be drawn between them and some utility maximising scenarios from *traditional* discrete choice theory in the social sciences literature[2]. In particular, even when considering completely homogeneous populations (in their individual preferences and interaction), first and second order phase transitions provide mechanisms for abrupt changes in the aggregate state of the system with no parallelled changes in the parameters. Metastability and hysteresis appear as collectively reinforced opinion states which persist even when individual preferences would be best satisfied by a change in option, but to which there is no going back by reversing the changes once it is abandoned.

Furthermore, these setups provide a framework in which to naturally introduce heterogeneity, characterising the group through probability distributions describing individual attitudes towards the particular choice[3,4]. These are considered fixed in time (*quenched disorder*), which is equivalent to a Random Field Ising model. The study of the system at finite temperature allows for the consideration of fluctuations varying in time (*annealed disorder*), which can encode lack of information or a more fundamental uncertainty on human nature concerning *free will*.

The type of opinions or decisions under study can seldom be considered to be isolated, as these are normally deeply interrelated. As a first approximation, two variables modelled as described above, can be coupled explicitly through a term in the Hamiltonian. Coupled Ising models have been considered in the literature before, in particular for their interest in the study of plastic phase transitions[5,6]. When understood as discrete choice models, even in simple cases of homogeneous populations[7] or zero temperature RFIMs[8], these show that interdependence promotes polarisation, enriches the stability landscape and can qualitatively change the aggregate outcome from that of the uncoupled case.

We will discuss the use of two coupled Random Field Ising models to describe a group where individuals have to make two choices which affect each other. The population's preferences can be then characterised by two probability distributions (or a single bivariate one), one for each decision. We study the dependence of the aggregate outcome on the parameters (which measure strength of choice interdependence and social influence and characterise the joint probability distribution for individual preferences) and describe the system's phase diagrams for some particular cases in the light of binary interdependent decisions.

This work has been financially supported by the Ministerio de Ciencia e Innovación (Spain), Project No. FIS2009-09870.

---

* ana.fernandez@invi.uned.es

[1] S. Galam, Y. Gefen and Y. Shapir. *Sociophysics: A new approach of sociological collective behaviour. I. mean-behaviour description of a strike*, The Journal of Mathematical Sociology, 9:1-13, 1982.

[2] S. N. Durlauf. *How can statistical mechanics contribute to social science?*, Proceedings of the National Academy of Science, 96:10582-10584, 1999.

[3] S. Galam, *Rational group decision making: A random field Ising model at $T = 0$*, Physica A: Statistical and Theoretical Physics, 238:66-80, 1997.

[4] M. B. Gordon, J.-P. Nadal, D. Phan and V. Semeshenko. *Discrete Choices under Social Influence: Generic Properties*, Mathematical Models and Methods in Applied Sciences, 19:1441-1481, 2008.

[5] S. Galam, S. R. Salinas and Y. Shapir. *Randomly coupled Ising models*, Physical Review B, 51:2864-2871, 1995.

[6] E. Korutcheva and D. I. Uzunov. *Ising models and coupled order parameters*, Preprint Joint Inst. Nuclear Research Dubna, E-17-88-467, 1988.

[7] A. Fernández del Río, E. Korutcheva and J. de la Rubia, *Interdependent binary choices under social influence: Phase diagram for homogeneous unbiased populations*, Complexity, DOI: 10.1002/cplx.21397, 2012.

[8] A. Fernández, E. Korutcheva and J. de la Rubia. *Deterministic interdependent choices in populations with limited heterogeneity*, work in progress.

# CHARACTERIZATION OF DELAY PROPAGATION IN THE AIRPORT NETWORK

P Fleurquin*, J J. Ramasco, V M. Eguíluz, M. San Miguel
*IFISC Instituto de Física Interdisciplinaria y Sistemas Complejos (CSIC-UIB), CSIC-Universidad de las Islas Baleares 07122-Palma (Mallorca)*

Complex networks[1,2] provide a suitable framework to model air traffic. Previous works[3–5] described the world air-traffic network as a graph with direct flights between airports as edges and passenger commercial airports as vertices.

In this work we characterize the US airport network, in the time period 2005-2011, as a weighted graph where the accumulated delay in each airport and the average delay per flight is, respectively, the node and edge strength. We observe that the dynamical behaviour of clusters[6–8], representing groups of delayed connected airports, is very volatile; in particular, the largest cluster has an explosive growth. Motivated by this empirical result, we propose a queuing model based on delay propagation between single company flights and airport congestion due to over-scheduling, which reproduces the empirical observations. Furthermore, we analyze the implementation of different operations protocol and the impact over the flight schedules.

This investigation is expected to help devise more efficient strategies for delay management, both from the point of view of ATM (e.g., flight prioritization criteria) and of airline planning (e.g., robust scheduling).

* pfleurquin@ifisc.uib-csic.es

[1] DJ Watts, SH Strogatz, Nature 393, 440 (1998)
[2] AL Barabasi, R Albert, Science 286, 509 (1999)
[3] A Barrat, R Pastor-Satorras, A Vespignani,Proc. Natl. Acad. Sci. USA 101, 3747 (2004)
[4] R Guimera, S Mossa, M Sales-Pardo, LAN Amaral,Proc.Natl. Acad. Sci. USA 102, 7794 (2005)
[5] M Sales-Pardo, R Guimera, AA Moreira, LAN Amaral,Proc. Natl. Acad. Sci. USA 104, 15224 (2007)
[6] J Hopcroft, O Khan, B Kulis, B Selman, PNAS 101, 5249 (2004)
[7] G Palla, A Barabasi, T Vicsek, Nature 446, 664 (2007)
[8] S. Asur, S. Parthasarathy, D. Ucar,TKDD 3, 913 (2009)

# Mercados Internacionales de Comercio: Una analogía con las redes mutualistas

Maximiliano Fernández*, Javier Galeano y Cesar Hidalgo†
*Grupo de Sistemas Complejos de la UPM*
*E.T.S. de Ingenieros Agrónomos*
*Universidad Politécnica de Madrid.*
*Ciudad Universitaria s/n, 28040, Madrid*

Adam Smith está considerado el padre de la Economía moderna. Su investigación sobre *Wealth of Nations* fue el primer trabajo científico[1], donde se hablaba de manera teórica sobre la complejidad de los sistemas económicos y de como una mano invisible auto-regulaba los mercados y su comportamiento. En este sentido, nuestro trabajo se engloba en el estudio de los mercados internaciones de comercio como una red compleja[2].

En nuestro trabajo analizamos las propiedades tipológicas, la estructura y dinámica temporal de datos reales de comercio Internacional obtenidos en la base de datos de libre acceso UN COMTRADE[3]. La premisa principal en la que se basa el trabajo es que la red de comercio es una red *bipartite* ya que los grupos de importadores y exportadores juegan diferentes papeles en el sistema global. Así pues, aplicamos la metodología desarrollada para redes ecológicas de tipo mutualistas, tanto en el caso de que sean redes no-pesadas[4] y pesadas[5].

Los resultados obtenidos muestran una fuerte analogía entre los mercados y los ecosistemas mutualistas. Además, hemos desarrollado y aplicado algunas herramientas de visualización para una mejor comprensión del comportamiento de las redes de mercado internacional.

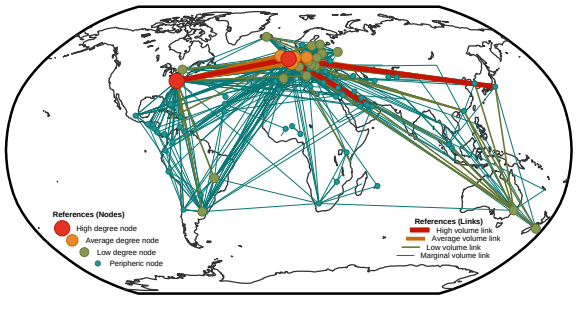


FIG. 1. Desarrollamos una herramienta para visualizar las redes de los mercados internacionales sobre un Mapa mundial. Este ejemplo representa el mercado de caballos pura sangre en 1995.

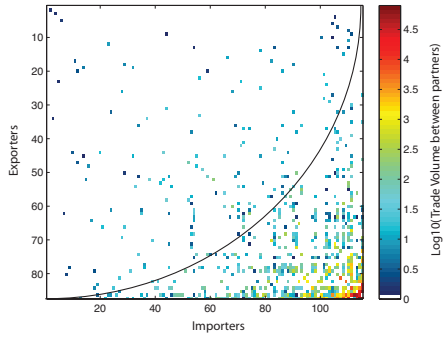


FIG. 2. Realizamos el análisis de la red sobre una matriz *bipartite*, beneficiándonos de los trabajos ya realizados para ecosistemas mutualistas.

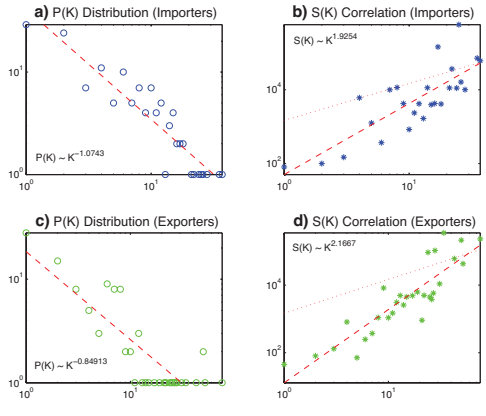


FIG. 3. La primera part del trabajo se realizó calculando los parámetros tradicionales de la estructura de la red pesada. Esta figura muestra las distributiones de grado y de *strength* vs. grado, para importadores y exportadores.

---

† The Media Laboratory (MIT, USA)
* maximiliano.fernandez@alumnos.upm.es, javier.galeano@upm.es, chidalgo@mit.edu

[1] Adam Smith, *An Inquiry into the Nature and Causes of the Wealth of Nations*, (London: Methuen and Co., Ltd., ed. Edwin Cannan. Fifth edition), (1904).
[2] C. Hidalgo et al., Science **317**, 5837 (2007).
[3] UN COMTRADE `http://comtrade.un.org/`
[4] U. Bastolla et al., Nature **458**, 7241 (2009).
[5] L. Gilarranz et al., Oikos (2012).

# Medida de la robustez de redes de polinización a partir del k-shell.

Juan Manuel Pastor* and Javier Galeano+
*Depto. Ciencia y Tecnología Aplicada a la I.T. Agrícola*
*y Grupo de Sistemas Complejos*
*Universidad Politécnica de Madrid*
*28040 Madrid*

En las redes ecológicas es importante conocer el papel que juega cada especie en el conjunto, especialmente en el contexto de cambios exógenos (fundamentalmente andrógenos) en los ecosistemas.

La desaparición de las interacciones planta-polinización supone una amenaza tanto para las especies de plantas como para la comunidad en general. Este problema es potencialmente muy importante en algunos ecosistemas de condiciones más específicas, como los de alta montaña, donde las interacciones planta-polinizador juegan un papel clave[1].

Los estudios ecológicos clásicos sobre robustez exploran la tolerancia de las redes a la eliminación de sus nodos[2]. La secuencia de extinción de nodos se hace de manera aleatoria y de manera sistemática, siguiendo orden creciente y decreciente de grado. Los resultados aparecidos hasta el momento únicamente se limitan a representar la tasa de supervivencia en función del porcentaje de extinciones primarias producidas. Hasta ahora, las únicos parámetros utilizados para caracterizar la *robustez* de la red son el valor $R_{50}$ , que indica cuándo se ha producido un 50% de las extinciones secundarias, y el valor de la integral de la curva de supervivencia (conocido como $R$).

Para redes pequeñas, como las ecológicas, la caracterización de los procesos de ataques y errores no puede hacerse en función del tamaño y número de clusters. Sin embargo, podemos analizar la curva de extinción para determinar cuándo y cómo se desintegra la red. Como primer paso, cambiamos la representación mostrando las extinciones secundarias frente a las primarias. Al tratarse de redes muy anidadas, con bastante redundancia entre *generalistas* (especies con gran número de enlaces), tanto los errores como los ataques dan lugares a extinciones secundarias puntuales hasta que se produce la cascada final de extinciones. Como aproximación a una secuencia de extinción en cascada podemos ajustar las curvas de extinción secundaria a una función de la forma:

$$f(x) \sim \left(\frac{x - x_0}{1 - x_0}\right)^{\alpha}, \qquad (1)$$

de modo que sea la unidad cuando se ha producido el 100% de las extinciones primarias y consideramos despreciable las extinciones secundarias hasta un determinado momento ($x_0$) en el que comienza a producirse la cascada de extinciones. En la figura se observa una representación de la secuencia de extinciones para una red real de polinizadores[3]. Haciendo un ajuste con esta función podemos obtener los parámetros $x_0$ y el exponente $\alpha$ de la curva, para caracterizar la secuencia de extinciones secundarias.

Otra forma empírica de encontrar este valor de inicio de la cascada de extinción ($x_0$) es a partir del *k-shell*. Para este tipo de redes el inicio de la cascada ocurre cuando se elimina el *núcleo*, es decir, el *k-shell* máximo. Además, podemos usar como criterio para la secuenciación en las extinciones primarias el grado de k-shell, tanto en orden creciente como decreciente de conexión.

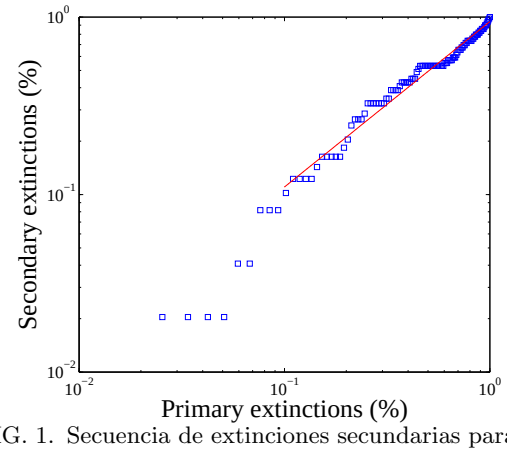


FIG. 1. Secuencia de extinciones secundarias para una red real de polinizadores. El ajuste por mínimos cuadrados nos da el exponente característico de la curva de extinción.

* juanmanuel.pastor@upm.es
+ javier.galeano@upm.es

[1] R. May, *Stability and Complexity in Model Ecosystems*, Princeton Univ. Press., 2001.
[2] J. Memmott, N. M. Waser and M.V. Price, *P.N.A.S.* **271** 2004.
[3] R.B. Primack, *New Zeal. J.Bot.* **21** 1983.

# Evolución temporal de la dinámica de poblaciones en redes mutualistas.

Javier García-Algarra , Javier Galeano, Juan Manuel Pastor, José J. Ramasco† y José María Iriondo*
*Grupo de Sistemas Complejos de la UPM*
*E.T.S. de Ingenieros Agrónomos*
*Universidad Politécnica de Madrid.*
*Ciudad Universitaria s/n, 28040, Madrid*

El uso de las redes complejas para el estudio de las interacciones ecológicas ha generado una gran cantidad de trabajos en los últimos años. Los primeros estudios se centraron en estudiar las interacciones ecológicas de tipo depredador-presa, siendo conocida su representación gráfica, como Food-webs[1]

Posteriormente, la aplicación de las técnicas de redes complejas se ha centrado en otro tipo de interacción ecológica conocida como *mutualista*. Las redes mutualistas en Ecología muestran las interacciones entre especies que obtienen un beneficio mutuo en su relación. En este tipo de redes hay dos conjuntos de especies (por ejemplo, animales y plantas) y las relaciones sólo ocurren entre especies pertenecientes a los distintos conjuntos. Los dos grupos de redes mutualistas más estudiados representan interacciones entre polarizadores-plantas y dispersores de semillas-plantas. Estas interacciones ecológicas se han representado mediante redes *bipartitas*[2].

El estudio de estas redes mutualistas ha revelado una estructura en la matriz de interacciones. Existen especies, llamadas especialistas, que interactúan con pocas especies del otro conjunto de nodos. Se ha observado que dichos especialistas siempre interactúan con especies que llamamos generalistas, que se relacionan con un gran número de especies. A esta propiedad se la denomina *anidamiento*. Sobre estas redes mutualistas se han realizado ya diferentes estudios de la topología de las redes[3], pero hasta la fecha existen muy pocos estudios que proporcionen una perspectiva dinámica. En este trabajo presentamos un modelo que muestra la evolución de la dinámica de poblaciones en redes mutualistas.

Se ha modificado un modelo de dinámica de poblaciones que introduce el término más sencillo no trivial de interacción mutualista[4]. Nuestra versión con dos especies es la siguiente:

$$\frac{dN_1}{dt} = r_1 N_1 \left(1 - \frac{N_1}{K_1}\right)\left[1 + \beta_1 b_{12}\frac{N_2}{K_1}\right] \qquad (1)$$

$$\frac{dN_2}{dt} = r_2 N_2 \left(1 - \frac{N_2}{K_2}\right)\left[1 + \beta_2 b_{21}\frac{N_1}{K_2}\right], \qquad (2)$$

siendo $N_1$ y $N_2$ las poblaciones de las especies 1 y 2 de los subgrupos de animales y plantas, respectivamente. Los parámetros $r_1$ y $r_2$ son las respectivas tasas de crecimiento, que en nuestro modelo son constantes positivas. Al igual que los parámetros $K_1$ y $K_2$ que se conocen como parámetros de la capacidad de carga. Por último los coeficientes $b_{12}$ y $b_{21}$ son los coeficientes que expresan la interacción mutualista y los parámetros $\beta_1$ y $\beta_2$ que la modulan.

Para resolver las ecuaciones, se han realizado simulaciones estocásticas en las cuales se ha tenido el cuenta el carácter discreto de los números de individuos en las poblaciones de cada especie. Esta cuestión es relevante cuando la cantidad de individuos en una especie particular es baja, ya que mantener las ecuaciones continuas puede llevar a resultados espurios y ha sido discutida y solucionada en el marco de trabajos en epidemiología computacional[5].

Los primeros resultados de las simulaciones muestran que la extinción de especies en un grupo, nos permite ver la evolución hacia la extinción de especies altamente dependientes pertenecientes al otro grupo.

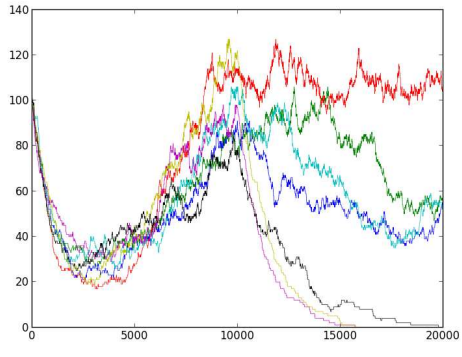


FIG. 1. Evolución temporal del tamaño de las poblaciones de plantas obtenidas en una matriz de interacción mutualista al eliminar la especie de mayor grado.

† Instituto de Física Interdisciplinar y Sistemas Complejos IFISC (CSIC-UIB), Palma de Mallorca, Spain
* Área de Biodiversidad y Conservación, Depto. Biología y Geología, Universidad Rey Juan Carlos.

[1] R. J. Williams and N. D. Martinez, Nature, **404** (9), 2000.
[2] J. Bascompte, Science, **329**, (2010).
[3] L. J Gilarranz, et al., Oikos 000: 001–009, (2012).
[4] R.M. May. *Stability and Complexity in model Ecosystems.* Princeton Univ. Press. Princeton, 1975.
[5] D. Balcan et al., Proc. Natl. Acad. Scie. (USA) **106**, 21484 (2009).

# Granular fluids driven by a scochastic bath with friction

M. G. Chamorro, F. Vega Reyes and V. Garzó
*Departamento de Física, Universidad de Extremadura, E-06071 Badajoz, Spain*

Granular systems are constituted by macroscopic grains that collide inelastically so that the total energy of the system decreases with time. Thus, in order to maintain the granular medium in a fluidized state, an external energy input is needed to compensate for the collisional loss of energy and achieve a *steady* nonequilibrium state. In most of the experiments, energy is supplied through the boundaries causing spatial gradients in the system. To avoid the difficulties associated with inhomogeneous states, it is usual in computer simulations to heat the system by the action of an external driving force (thermostat). Nevertheless, in spite of its practical importance, little is known about the influence of the thermostat on the properties of the system[1].

The goal of this contribution is to analyze the homogeneous steady state of a driven granular fluid described by the Enskog-Boltzmann kinetic equation. In order to reach a steady state, the particles are assumed to be under the action of an external thermostat composed by two different forces: (i) a stochastic force where the particles are randomly kicked between collisions[2] and (ii) a viscous drag force which mimics the interaction of the particles with an effective viscous "bath". One of the main advantages of using this kind of thermostat[3] with respect to others present in the literature[2] is that the temperature of the thermostat $T_b$ (different from the temperature $T < T_b$ of the granular fluid) is always well defined. In particular, for elastic collisions, the fluid equilibrates to the bath temperature ($T = T_b$). Moreover, some recent results[4] suggest that this thermostat is the most appropriate to modelize some experiments.

Our study follows two complementary routes: (i) an analytical solution obtained from a Sonine polynomial expansion and (ii) a numerical solution of the Enskog-Boltzmann equation obtained by means of the direct simulation Monte Carlo (DSMC) method. Our results are also compared with recent molecular dynamics (MD) simulations performed by other authors[3]. Comparison at the level of the (steady) granular temperature $T_s$ and the fourth cumulant of the velocity distribution function shows in general a good agreement, even for strong values of dissipation. As an illustration, the (steady) temperature $T_s$ is plotted in Figure 1 as a function of the solid volume fraction $\phi$. It is quite apparent that the agreement between theory with MD simulations data from[3] is very good. In addition, as expected, at a given value of density, the granular temperature decreases as the gas becomes more inelastic.

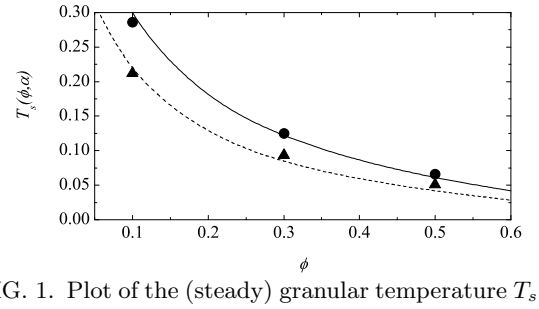


FIG. 1. Plot of the (steady) granular temperature $T_s$ (measured in units of the bath temperature $T_b$) versus the volume fraction $\phi$ for a two-dimensional system and two different values of the coefficient of restitution: $\alpha = 0.8$ (solid line) and $\alpha = 0.6$ (dashed line). The symbols are the simulation data (circles for $\alpha = 0.8$ and triangles for $\alpha = 0.6$) obtained by Gradenigo *et al.*[3].

## ACKNOWLEDGEMENTS

This work has been supported by the Spanish Government through Grants No. FIS2010-16587 and (only F. V. R.) No. MAT2009-14351-C02-02, partially financed by FEDER funds and by the Junta de Extremadura (Spain) through Grant No. GR10158.

[1] V. Garzó and A. Santos, *Kinetic Theory of Gases in Shear Flows. Nonlinear Transport* (Kluwer Academic, Dordrecht, 2003).

[2] D. R. M. Williams and F. C. MacKintosh, *Phys. Rev. E* **54**, R9–R12 (1996).

[3] G. Gradenigo, A. Sarracino, D. Villamaina, and A. Puglisi, *J. Stat. Mech.* P08017 (2011).

[4] G. Gradenigo, A. Sarracino, D. Villamaina, and A. Puglisi, *Europhys. Lett.* **96**, 14004 (2011)

## Ecuaciones fluctuantes de Navier-Stokes para esferas y discos duros inelásticos[1]

J.J. Brey, M.I. García de Soria*, and P. Maynar
*Física Teórica, Universidad de Sevilla*
*Apartado de Correos 1065, E-41080, Sevilla, Spain*

A partir de la ecuación de Boltzmann fluctuante para esferas o discos duros inelásticos, hemos derivado ecuaciones cerradas para los campos hidrodinámicos fluctuantes en el orden de Navier-Stokes. Esto requiere derivar las relaciones constitutivas para los flujos fluctuantes y las funciones de correlacion de las fuerzas. Los primeros se identifican de manera que tengan la misma forma que los flujos macroscópicos, involucrando los mismos coeficientes de transporte. Por otro lado, los términos de fuerza exhiben dos peculiaridades si los comparamos con el límite elástico para sistemas moleculares. En primer lugar, no son ruidos blancos, sino que presentan un tiempo de relajación finito. En segundo lugar, su amplitud no está determinada por los coeficientes de transporte macroscópicos, sino que involucran nuevos coeficientes.

---

* gsoria@us.es

[1] J.J. Brey, P. Maynar, and M.I. García de Soria, Phys. Rev. E **83**, 041303 (2011).

## Structure and Thermodynamics of Curved Interfaces

José G. Palanco†, Victor H. Elvira‡, Luis G. MacDowell‡
†*Departamento de Física y Química Aplicadas a la Técnica Aeronáutica, Escuela de Ingeniería Aeronáutica y del Espacio, Universidad Universidad Politécnica de Madrid* ‡*Departamento de Química Física, Facultad de Ciencias Químicas, Universidad Complutense de Madrid*

In this paper we present new analytical results for the structure and thermodynamics of curved interfaces. Starting from a density functional formalism, we show that the square gradient approximation is fully consistent with the capillary approximation for the thermodynamics of droplet formation, namely i) a meaningful droplet radius may be defined whose size is dictated by the Laplace pressure difference accross the interface, ii) provided the droplet is large, such pressure difference is accurately obtained from bulk equation of state data, iii) the work of formation is one third of the droplet's surface free energy. Using an approximate model which is asymptotically exact, we show that two different regimes exist depending on the droplet's size relative to the interfacial width. For large droplets, corrections to the clasical capillary approximation are exponentially small, and an asymptotically exact expansion for the Toman length in powers of the inverse droplet radius may be obtained. For droplets with size of the order of bulk correlation lengths, expressions for the Tolman length are still possible, but they no longer adopt a simple power law.

# Unzipping DNA at controlled force

Adan Garriga[1*], Josep Maria Huguet[2,3], and Felix Ritort[2,3]
*1)International Center for Numerical Methods in Engineering (CIMNE)*
*Bisbe Azara, 4, 07800, Ibiza (Spain)*
*2) Small Biosystems Lab, Departament Física Fonamental, Facultat de Física*
*Universitat de Barcelona, Diagonal 647, 08028 Barcelona (Spain)*
*3) CIBER-BBN, Centre of Bioengineering, Biomaterials and Nanomedicine, ISCIII, Madrid (Spain)*

Single molecule studies, at constant force (CF), of DNA unzipping may provide information relevant to the dynamics of DNA replication[1]. Controlled force experiments can be performed with optical tweezers by using a force feedback[2,3]. Here we show experimental data of the Force Distance Curve (FDC) at CF. The unzipping/rezipping curves show strong hysteresis, a typical feature of relaxation processes in non-equilibrium systems with rough free energy landscape. Also, the experimental data fits quite well with the scaling predictions of theoretical studies of mesoscopic models of DNA[4].

* adan.garriga@gmail.com

[1] C. Danilowicz, V.W. Coljee, C. Bouzigues, D.K. Lubensky, D.R.Nelson, M. Prentiss,*DNA unzipped under a constant force exhibits multiple metastable intermediates*, Proc Natl Acad Sci U S A, **100(4)**,1694-1699 (2003)

[2] J.M. Huguet, *Statistical and thermodynamic properties of DNA unzipping experiments with optical tweezers*, PhD thesis, University of Barcelona (2010).

[3] N. Forns, S. De Lorenzo, M. Manosas, K. Hayashi, J. M. Huguet and F. Ritort, *Improving Signal/Noise Resolution in Single-Molecule Experiments Using Molecular Constructs with Short Handles*, Biophysical Journal, **100** 1765-1774 (2011)

[4] D.K. Lubensky, D.R. Nelson, *Single molecule statistics and the polynucleotide unzipping transition*, Phys. Rev. E, **65**, 031917 (2002).

# Logical operations with Localized Structures

Adrian Jacobo*, Damià Gomila, Manuel A. Matías, and Pere Colet
*IFISC, Instituto de Física Interdisciplinar y Sistemas Complejos (CSIC-UIB),E-07122 Palma de Mallorca, Spain*

Localized structures (LS), also known as dissipative solitons, have been suggested as a potentially useful strategy for information storage. This application is specially attractive in nonlinear photonics after LS have been observed in semiconductor lasers, but the general concept of using LS to carry information is not restricted to optics. Within this approach a LS describes one bit of information. This idea can be taken a step further and discuss the potential of LS for carrying out computations beyond mere information storage. In this work we propose to use excitability mediated by LS to implement three basic logic gates, namely the AND, OR, and NOT gates, providing complete logic functionality[1], as by combination of them one can realize any other logical operation, including the NOR and NAND universal gates. In our scheme bits are represented by a dynamical state (an excitable excursion) rather than by a stationary solution. This provides a natural reset mechanism for the gates. The way computations are performed relays on the emergent properties of the LS, independently of the microscopic details of the underlying physical system.

We consider a nonlinear optical cavity as sketched in Fig. 1. Three narrow addressing beams $b_1$, $b_2$, and $b_3$ facilitate excitability by allowing to tune the threshold for the size of a perturbation necessary to trigger an excitable excursion. The positions in the transverse plane of these narrow beams define also the input and output ports of the logic gate. Alternatively the transverse plane of the device could be engineered to fix the positions of the ports. Here the bright spots created inside the cavity by $b_1$ and $b_2$ will act as input ports, while the spot at the position of $b_3$ will be the output port. The incoming bits $(\delta_1, \delta_2)$ will be superimposed to $b_1$, $b_2$.

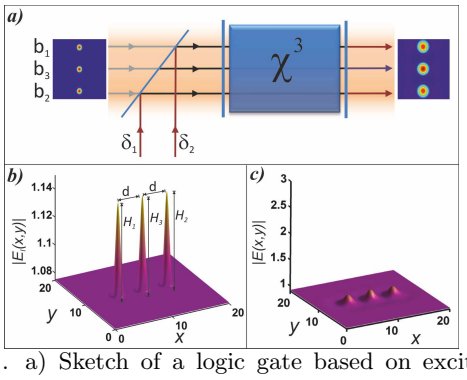


FIG. 1. a) Sketch of a logic gate based on excitable LS in a nonlinear optical cavity. b) Input of the cavity $E_I(x, y)$, including the holding beam (background) and the three localized beams with intensities $H_1$, $H_2$, and $H_3$. $d$ is the distance between ports. c) Intracavity field of the resting state of the system. Adimensional units are used in all figures.

In our proposal a bit '1' corresponds, internally, to the presence of an excitable excursion. Then, a super-threshold perturbation at an input port (i.e. causing an excitable excursion) will be considered as a bit '1', while sub-threshold (or absence of) perturbations will be considered as '0'. At the output port, the occurrence of an excitable excursion should be taken as a '1', and '0' otherwise.

For an OR gate, $d$ and $H_3$ are such that an excitable excursion of a single input is already enough to excite the output, as shown in Fig. 2. The bit '1' is introduced by setting $\delta_1 = 0.03$ during 1 time unit. After receiving the bit, the left input port exhibits an excitable excursion which, by the above mechanism, triggers an excitable excursion of the output port. Because of symmetry, the output would look exactly the same for the case (0,1). A double activated (1,1) input would give a very similar response, completing the truth table of the OR gate.

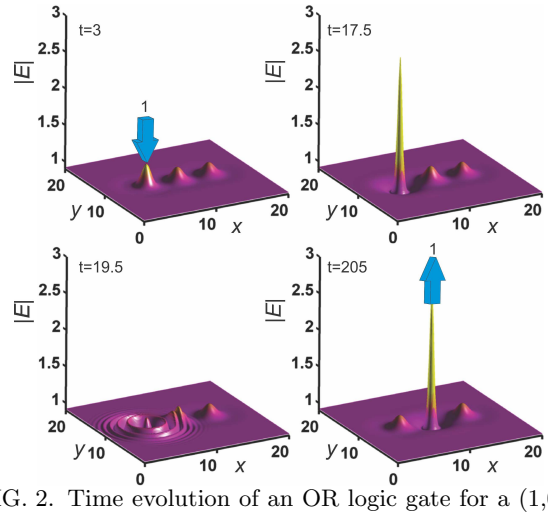


FIG. 2. Time evolution of an OR logic gate for a (1,0) input.

Similarly, AND logic can be implemented by increasing $d$ or decreasing $H_3$, such that the pulse of a single input is not enough to elicit a response of the output, but the combined action of two simultaneous excitations is. A NOT gate is also proposed, providing together with the OR and AND gates full logic functionality.

---

* Present address: Max Planck Institute for the Physics of Complex Systems, Nöthnitzer Straße 38, 01187 Dresden, Germany.

[1] A. Jacobo, D. Gomila, M.A. Matías, and P. Colet, New Journal of Physics **14**, 013040 (2012).

# Patterns and Domain Walls in Generalized Swift-Hohenberg Dynamics

Daniel Walgraef, Damià Gomila, Pere Colet, and Thorsten Ackemann
*IFISC, Instituto de Física Interdisciplinar y Sistemas Complejos (CSIC-UIB),E-07122 Palma de Mallorca, Spain*

Near a pitchfork bifurcation, where a uniform steady state becomes unstable towards two branches of equivalent uniform steady states, the dynamics may be reduced to the following order parameterlike dynamics, for two-dimensional systems with inversion and space-inversion symmetry:

$$\partial_t \sigma = [\epsilon + \mu\nabla^2 - \nabla^4]\sigma - \sigma^3 \quad (1)$$

where $\sigma(x, y, t)$ is the order parameterlike variable and $\nabla^2 = \partial_x^2 + \partial_y^2$. Fourth derivatives are relevant for $\xi_0^2 << 1$. The trivial state $\sigma = 0$ is stable for $\epsilon < 0$ and unstable for $\epsilon > 0$. For $\epsilon > 0$, this equation admits two branches of equivalent stable uniform steady states given by $\sigma_0(\pm) = \pm\sqrt{\epsilon}$. In some cases, though, nonlinearities may also depend on space derivatives of the order parameterlike variable. This is the case, for instance, in sodium vapor cells, where the two nontrivial equivalent solutions may become modulationally unstable[1]. A systematic expansion in powers of these derivatives gives, at lowest orders, in the case of space-inversion symmetry:

$$\partial_t \sigma = [\epsilon + \mu\nabla^2 - \nabla^4]\sigma - \sigma^3 - \gamma\sigma^2\nabla^2\sigma - \kappa\sigma(\vec{\nabla}\sigma)^2 \quad (2)$$

This dynamics admits the same steady states than (1), but the stability of the bifurcating states is different. In the case of the dynamics observe in optical systems[1], the bifurcation parameter also determines the strength of the nonlinearities, and the dynamics can be qualitatively described by the following model

$$\partial_t \sigma = -[\lambda_c - \mu\nabla^2 + \nabla^4]\sigma + \lambda[\sigma - \sigma^3 - \gamma\sigma^2\nabla^2\sigma - \kappa\sigma(\nabla^2\sigma)^2] \quad (3)$$

where $\lambda$ is the order parameter. For $\lambda < \lambda_c$, the trivial steady state $\sigma = 0$ is stable. For $\lambda > \lambda_c$, it becomes unstable, via a pitchfork bifurcation, versus the two equivalent uniform steady states $\sigma_0(\pm) = \pm\sqrt{\frac{\lambda-\lambda_c}{\lambda}}$ which tend to 1 for increasing $\lambda$. One also finds that uniform bifurcating states become unstable at

$$\lambda_p = \lambda_c + (\frac{\sqrt{2} + \sqrt{2 + \gamma\mu}}{\gamma})^2 \quad (4)$$

versus spatial modulations of wavenumber

$$|q_p| = \sqrt{\frac{\gamma(\lambda_p - \lambda_c) - \mu}{2}} \quad (5)$$

leading to hexagonal patterns around the two $\sigma_0(\pm)$ solutions.

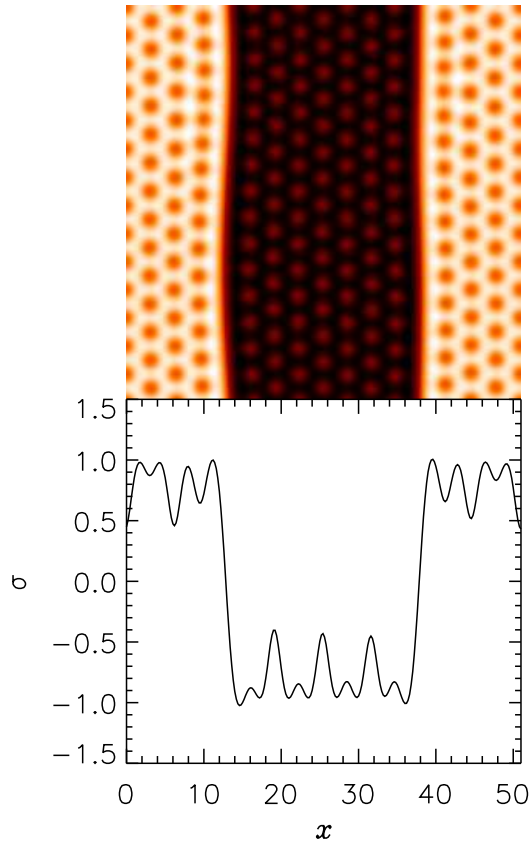


FIG. 1. Snapshot of the evolution of a two opposite domain walls between hexagonal patterns around the $\sigma_0(\pm)$ solutions. The bottom panel shows a transverse cut of the pattern shown at the top.

This leads to very complex dynamics including domain walls between patterned solutions (see Fig. 1). In this work we explore the dynamics of such general model and compare the results with experimental observations in an optical system.

[1] A.Aumann, E.Grosse Westhoff, R.Herrero, T.Ackermann and W.Lange, J.Opt.B: Quantum Semiclass. Opt. **1** 166 (1999); E.Grosse Westhoff, V.Kneisel, Yu. A.Logvin, T.Ackermann and W.Lange, J.Opt.B: Quantum Semiclass. Opt. **2** 386 (2000); M. Pesch, W. Lange, D. Gomila, T. Ackemann, W.J. Firth, and G.-L. Oppo, Phys. Rev. Lett. **99**, 153902 (2007).

# Técnicas numéricas para el estudio del mecanismo de nucleación de burbujas de vapor bajo presiones negativas.

Miguel Ángel González, Juan L. Aragones, Chantal Valeriani and José Luis F. Abascal*
*Departamento de Química-Física, Facultad de Ciencias Químicas, Universidad Complutense de Madrid, 28040 Madrid, Spain*

La nucleación homogénea, en ausencia de interfases preexistentes, se define como la formación de un núcleo crítico, el cual desembca en el crecimiento de una nueva fase dentro de una fase metaestable. Es un mecanismo vinculado a una transición de primer orden, que se se estudia principalmente por medio de la teoría de nucleación clásica (CNT). Esta teoría estudia en la nucleación de un líquido en un vapor sobreenfriado. Es posible utilizarla en otros sistemas como la nucleación de un sólido, la formación de una burbuja de gas... A partir de esta teoría han aparecido una serie de modificaciones y otros métodos para calcular los parámetros característicos del proceso de nucleación (tasa de nucleación, barrera de nucleación...).

El trabajo presentado se basa en la utilización del método *Mean first passage time*[1,2] (MFPT) para estudiar el mecanismo de nucleación de burbujas de vapor en el seno de agua líquida (cavitación). Se han llevado a cabo una serie de simulaciones de Dinámica Molecular de agua en condiciones metaestables. Las temperaturas y presiones de simulacion se encuentran en el intervalo 260-370 K y desde -2000 bar hasta 3000 bar. El potencial de agua utilizado es el TIP4P/2005[3] que ha demostrado excelentes resultados en la predicción de propiedades del agua en condiciones extremas.[4] Estas simulaciones permiten analizar el paso del líquido metaestable hasta la cavitación del sistema y el crecimiento de las burbujas en el seno del mismo. El método MFPT monotoriza el primer tiempo de aparición de la burbuja más grande durante la simulación para lo que es necesario examinar la evolución de un parámetro de orden local.

En nuestro, caso el parámetro de orden es el volumen de la burbuja más grande dentro del líquido metaestable y para determinar éste hemos utilizado dos vías diferentes. Por medio de los poliedros de Voronoi,[5,6] somos capaces de determinar el volumen de la burbuja y seguir su desarrollo de una forma precisa pero con un importante coste computacional. El otro método es la utilización de un grid más unos criterios de clasificación basados en el números de vecinos para diferenciar el líquido del vapor. Estos dos métodos convergen en valores comparables lo cual afianzan su utilización y la validez del MFPT como herramienta para estudiar el mecanismo de cavitación del agua.

Con esta información nos hemos embarcado en el estudio del mecanismo de nucleación del agua por debajo y por encima de la línea espinodal. Se ha comprobado que, tanto las barreras de nuclación como la física del proceso es diferente a ambos lados de la espinodal (Figura 1). Estas diferencias se podran comentar en la contribución.

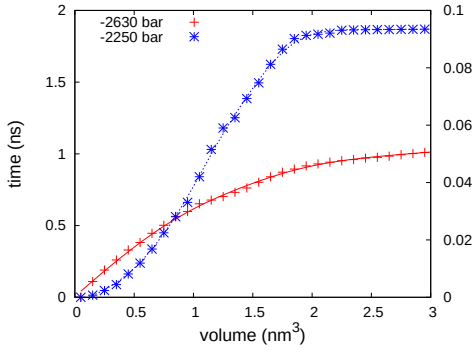


FIG. 1. MFPT en funcion del volumen para el model TIP4P/2005, calculado a T=280K y a dos presiones diferentes. p=-2630bar (cruces rojas), condiciones por debajo de la linea espinodal y p=-2250bar (asteríscos azules), valor de presión por encima de la espinodal.

* abascal@quim.ucm.es

[1] J. Wedekind, R. Strey, and D. Reguera, J. Chem. Phys. 126, 134103 (2007).
[2] L. S. Bartell, and D. T. Wu, J. Chem. Phys. 125, 194503 (2006).
[3] J. L.F. Abascal, and C. Vega, J. Chem. Phys. 123, 234505 (2005).
[4] C. Vega, and J. L.F. Abascal, Phys. Chem. Chem. Phys. 13, 19663 (2011).
[5] J. C. Gil Montoro, and J. L.F. Abascal, J. Chem. Phys. 99, 4231 (1993).
[6] J. C. Gil Montoro, F. Bresme, and J. L.F. Abascal, J. Chem. Phys. 101, 10892 (1994).

# A two-component mixture of Janus-like anisotropic sticky hard spheres

Miguel Ángel G. Maestre* and Andrés Santos**
*Departamento de Física, Universidad de Extremadura, E-06071 Badajoz, Spain*

Recently, the study of the physical properties of so-called Janus spheres (where half the surface is hard and the other half is sticky) has been the subject of much attention[1]. In the present work we study a closely related system composed by spheres of the same diameter but belonging to two different equimolar species. The surface of each particle is divided into fixed "North" and "South" hemispheres, one of them being stickier (North hemisphere for species 1, South hemisphere for species 2) than the other one. According to this, there are four possible forms of interaction between the particles and therefore four temperature-like stickiness parameters: $\tau_{11}$, $\tau_{12}$, $\tau_{21}$ and $\tau_{22}$. In the case of a common value $\tau_{11} = \tau_{12} = \tau_{21} = \tau_{22}$, we recover the well-known Baxter sticky-hard-sphere (SHS) model, which is known to present a vapor-liquid critical point.

In our system we want to preserve the Janus-like feature of the model and thus we keep $\tau_{12}$ (representing the interaction of a particle of species 1 being "below" a particle of species 2, so that the two respective stickier faces are in contact) different from $\tau_{21}$ (representing the interaction of a particle of species 2 being "below" a particle of species 1, so that the two respective less sticky faces are in contact). Next, by symmetry, it is assumed that $\tau_{11} = \tau_{22}$. Two classes of models are considered:

- **Model A:** $\tau_{12} = \tau$, $\tau_{11} = \tau_{22} = \tau_{21} = \tau/\mu$,
- **Model B:** $\tau_{12} = \tau_{11} = \tau_{22} = \tau$, $\tau_{21} = \tau/\mu$,

where $0 \le \mu \le 1$. The introduction of the parameter $\mu$ allows us to modify both the anisotropy of the system and the strength of the less sticky interaction, relative to the stickier interaction. Thus, both models A and B reduce to the conventional isotropic SHS model if $\mu = 1$. In the opposite limit $\mu = 0$, model A presents three HS and one SHS interactions, while model B presents one HS and three SHS interactions.

We have applied the rational-function approximation methodology[2] to generalize the analytical solution of the Percus–Yevick equation for a multi-component isotropic SHS system[3] to the anisotropic case. As a result, we get a closed quartic equation whose physical solution is identified as the one reducing to Baxter's solution in the special case $\mu = 1$. For a given value of $\mu$, it turns out that the physical solution ceases to be real if (a) $\tau$ is smaller than a certain critical value $\tau_c$ and (b) the packing fraction $\eta$ lies in a certain interval $\eta_1(\tau) < \eta < \eta_2(\tau)$. As $\tau$ tends to $\tau_c$ from below, both $\eta_1(\tau)$ and $\eta_2(\tau)$ tend to a common critical value $\eta_c$. Figure 1 shows the critical values $\tau_c$ and $\eta_c$ versus the ratio $\mu$ for models A and B. In both cases the critical values $\tau_c$ and $\eta_c$ monotonically decrease until vanishing in the limit $\mu \to 0$. This signals the absence of critical behavior as soon as one of the four possible interactions in the equimolar mixture becomes non-sticky.

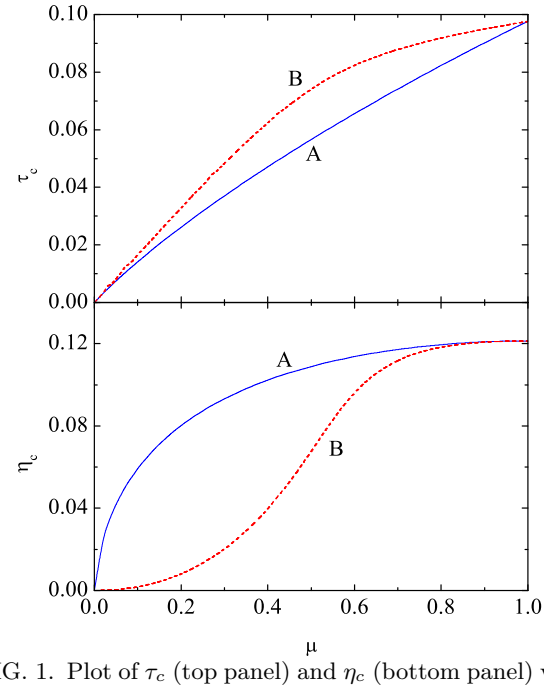


FIG. 1. Plot of $\tau_c$ (top panel) and $\eta_c$ (bottom panel) versus $\mu$ for models A (solid blue lines) and B (red dashed lines).

* maestre@unex.es
** andres@unex.es
http://www.unex.es/eweb/fisteor/andres

[1] R. Fantoni, A. Giacometti F. Sciortino, and G. Pastore, Soft Matter **7**, 2419 (2011).
[2] M. López de Haro, S. B. Yuste, and A. Santos, in *Theory and Simulation of Hard-Sphere Fluids and Related Systems*, Lectures Notes in Physics, vol. 753, A. Mulero, ed. (Springer, Berlin, 2008), pp. 183–245.
[3] J. W. Perram and E. R. Smith, Chem. Phys. Lett. **35**, 138 (1975).

# Simulación del diagrama de fases y autoensamblado de partículas coloidales anisótropas

Eva G Noya, Günther Doppelbauer, Emanuela Bianchi, Gerhard Kahl
*Instituto de Química Física Rocasolano, CSIC, Madrid, España*
*TU Wien, Wiedner Hauptstrasse 8-10/136, 1040, Wien, Austria*

En los últimos años se han producido grandes avances en la ciencia de coloides que han permitido la síntesis de partículas coloidales anisótropas con un elevado control tanto en la forma de las partículas como en el potencial de interacción[1]. Estos experimentos abren la posibilidad de fabricar materiales que se autoensamblan diseñando partículas con interacciones específicas que formen la estructura deseada. Sin embargo para ello es necesario conocer el comportamiento de fase en función de la anisotropía de las interacciones, para lo cual la simulación molecular se perfila como una herramienta de gran utilidad. Con este objetivo hemos abordado el estudio del diagrama de fases de un modelo sencillo de partículas coloidales esféricas decoradas con cuatro sitios de interacción atractivos cuya disposición viene determinada por un parámetro que nos permite ir de una geometría tretraédrica alargada a una más achatada[2–4]. El diagrama de fases de este sistema se ha calculado utilizando una combinación de varios métodos. Primero realizamos una búsqueda de las estructuras cristalinas más estables a T=0 con un algoritmo de optimización y posteriormente calculamos el diagrama de fases a temperatura finita mediante el cálculo de energías libres de dichas estructuras. Siguiendo este procedimiento hemos identificado una gran variedad de estructuras sólidas e investigado su estabilidad dependiendo de la geometría de los sitios atractivos en la superficie de las partículas[4,?].

[1] A.B. Pawar, I. Kretzschmar, Macromol. Rapid Commun. **31**, 150 (2010).
[2] J.P.K.Doye *et* al., Phys. Chem. Chem. Phys. **9**, 2197 (2007).
[3] E.G. Noya, C. Vega, J.P.K. Doye y A.A. Louis, J. Chem. Phys. **132**, 234511 (2010).
[4] G. Doppelbauer, E.G. Noya, E. Bianchi, y G. Kahl, enviado (2012).
[5] G. Doppelbauer, E.G. Noya, E. Bianchi, y G. Kahl, J. Phys.: Condens. Matt. (2012).

# 2D liquid crystal confined in a square cavity

M. González Pinto[1], Y. Martínez-Ratón[2] and E. Velasco[1]
[1] *Departamento de Física Teórica de la Materia Condensada, Universidad Autónoma de Madrid, 28049 Madrid*
[2] *Grupo Interdisciplinar de Sistemas Complejos (GISC), Departamento de Matemáticas, Universidad Carlos III de Madrid, 28911 Leganés, Madrid*

Nematic fluids in confined geometries are a subject of much interest from both fundamental and technological points of view. In these systems there is a competition between orientational ordering, anchoring (favoured director alignment at surfaces) and elasticity whose final outcome depends sensitively on imposed conditions. This interplay involves frustration and formation of defects.

3D studies of this problem, using different approaches and confinement geometries, are numerous. However, 2D fluids have not been explored in detail, and only a few simulation and theoretical works exist. Recently vibrated grains have been studied in quasimonolayers in circular cavities[1,2]. Similar behaviours to those found in thermal systems have been observed. Our recent theoretical work of this problem pointed to a rich phenomenology[3,4].

In this work we use density-functional theory, in its fundamental-measure version, to study the ordering properties of a fluid of rectangles of length $L$ and width $\sigma$ in a square cavity. The square geometry creates quite different conditions at the surfaces because of the presence of corners, and further frustration effects are expected with respect to the circular geometry.

In bulk conditions, our model fluid presents stable isotropic and nematic phases, with a continuous phase transition at a value of density which depends on the aspect ratio $\kappa = L/\sigma$. For a fixed value of $\kappa$, we study both the thermodynamics and structure of the fluid as the chemical potential is increased. Nematic ordering (capillary isotropic-nematic phase transition) is shifted in chemical potential with respect to the bulk transition and the confined nematic presents a defected structure. Changes in the structure in the nematic régime, associated with changes in the size of the square cavity, are discussed.

[1] V. Narayan, N. Menon and S. Ramaswamy, J. Stat. Mech. (2006) P01005.
[2] J. Galanis, R. Nossal, W. Losert and D. Harries, Phys. Rev. Lett. **105**, 168001 (2010).
[3] D. de las Heras, E. Velasco and L. Mederos, Phys. Rev. E **79**, 061703 (2009).
[4] D. de las Heras, L. Mederos and E. Velasco, Liq. Cryst. **37**, 45-56 (2010).

# Hierarchical screening of topological scales in complex networks

Clara Granell*, Sergio Gómez, and Alex Arenas
*Departament d'Enginyeria Informàtica i Matemàtiques*
*Universitat Rovira i Virgili*
*43007 Tarragona (Spain)*

The detection of the modular structure of networks is of utmost importance in the analysis of real networked systems. Most of the methods proposed to detect this strcutural organization, are based on the optimization of a quality function called modularity whose analogy with the minimization of the hamiltonian of a genralized Potts model has been previously reported. Optimizing modularity or minimizing the equivalent hamiltonian, poses an intrinsical drawback. In the presence of different topological scales of organization, the modularity function can not account for all them separately, incurring in an incorrect grouping of nodes, this effect has been called resolution limit. Here, we present a hierarchical method to unravel the modular structure of complex networks optimizing modularity. The method overcomes the resolution limit of modularity based schemes. The performance of the new method is proved in synthetic and real networks. The results are in good agreement with the real organization of networks at different topological scales.

* clara.granell@urv.cat

# Three is a crowd in iterated prisoner's dilemmas: experimental evidence on reciprocal behavior"

Jelena Grujić[1], Burcu Eke[2], Antonio Cabrales[3], José A. Cuesta[1,3], Angel Sánchez[1,3*]
[1] *GISC, Dpto. de Matemáticas, Universidad Carlos III de Madrid, 28911 Leganés, Spain*
[2] *Dpto. de Economía, Universidad Carlos III de Madrid, 28903 Getafe, Spain*
[3] *BIFI, Universidad de Zaragoza, Campus Río Ebro, 50018 Zaragoza, Spain*

Cooperation constitutes a key ingredient to understand the origins of animal societies and, in particular, of human ones. The reasons why this general prevalence of cooperation is not disrupted by cheaters or free-riders more often are not well understood yet. In spite of the fact that a number of mechanisms leading to the emergence and stability of cooperative behavior in social dilemmas have been proposed, experimental studies have shown that without additional enforcement mechanisms, human groups often fail to sustain a public resource, which every group member is free to overuse.

One of the most plausible explanations for the decay of cooperation in public goods settings is the fact that many individuals are willing to contribute only by reciprocating what their partners do. This behavior, called conditional cooperation, has been observed in many public goods experiments, often along with a large percentage of free-riders.

The most recent development on this issue arises from in the experiments by Grujić *et al.*[1]. Although in these experiments the players play Multiplayers Prisoner's dilemma on a network, which is not exactly equivalent to a public goods game, conditional cooperation is observed again. Interestingly, it was found that conditional cooperation may also depend on the individual's own past action, i.e., on the 'mood' in which the subject currently is. In this case, individuals behave as conditional cooperators if they cooperated in the past while they ignore the context and free-ride with high probability if they did not cooperate. These moody conditional cooperators are a majority of the population in the aforementioned experiments, but a large group of defectors is also seen. This is in contrast with theoretical results based on a replicator dynamics approach[2], that showed that in groups with five or more people the coexistence of moody conditional cooperators with free-riders (and possibly a few unconditional cooperators) is not possible.

Inspired by the predictions of this work, in this paper we advance the knowledge on this issue by reporting on a series of experiments with human subjects playing an iterated multiplayer Prisoner's dilemma in groups of different sizes. Our starting research question is whether individuals actually behave in a moody conditionally cooperative manner or not, and whether the behavior of real subjects changes with the group size. We have addressed this question by looking at very long IMPDs on groups of 2, 3, 4 and 5 subjects. In our experimental setup, human subjects played a Prisoner's Dilemma (PD) with each member of their group, taking only one action, either to cooperate (C) or to defect (D), the action being the same against all the opponents. After every round the players were shown how many of their partners cooperated and defected in their group and the payoffs of cooperators and defectors. The number of rounds was 100, which was unknown to the players.

The analysis of our results allowed us to confirm very clearly the existence of moody conditional cooperation in all group sizes, this being in fact the behavior of almost all subjects. There is a very clear difference between the probability of cooperating after having cooperated or having defected, highlighting the importance of relating the current action with the one in the previous round. As for the linear behavior of each one of those probabilities, they appear to have larger intercepts for groups of size 2, while those of larger groups are comparable, while slopes are similar in all cases. The groups of size two (i.e., pairwise interactions or usual 2 Prisoners Dilemma) are very different for the observations on the rest of groups (sizes three and higher). Pairwise interactions show very high cooperation levels with an increasing trend, whereas for the rest of groups we find that cooperation decays from initially large values (around 60% or larger) much in the same way as in most Public Goods or networked PD experiments. In addition, for the case of pairwise prisoner's dilemma the cooperation level decreases in the first rounds, just like in the previous experiments[4–6]. However, here we conducted the experiment much longer than that, and, although the cooperation level does decrease at the beginning, after that it starts increasing reaching 80% after 100 rounds.

---

* jgrujic@math.uc3m.es

[1] Grujic J, Fosco C, Araujo L, Cuesta JA, Sanchez A, PLoS ONE vol. 5, e13749 (2010).
[2] Grujic J, Cuesta JA, Sanchez A, Journal of Theoretical Biology vol. 300, pp. 299-308 (2012)
[3] Grujic J, Eke B, Cabrales A, Cuesta JA, Sanchez A in preparation.
[4] Dal Bo P, Am. Econ. Rev., vol. 95, pp. 1591-1604, 2005.
[5] Dal Bo P and Frechette GR, Am. Econ. Rev., vol. 101, pp. 411-429, 2011.
[6] Kuemmerli R, Colliard C, Fiechter N, Petitpierre B, Russier F and Keller L, Proc. R. Soc. B, vol. 274, pp. 2965-2970, 2007.

# On the Morphology of Turing Instability under Microscopic Transport

Jacobo Guiu-Souto, Jorge Carballido-Landeira, Alberto.P. Muñuzuri
*Group of Nonlinear Physics, Faculty of Physics, University of Santiago de Compostela, E-15782 Santiago de Compostela, Spain.*

One of the most important systems able to generate organization through pattern formation is the Turing instability[1], it is liable for morphogenesis in the living organisms, which explains, for example, the colour of pattern on fish skin or on the seashells. Usually in Nature pattern formation does not occurs in isolated reaction system but in presence of external forcing, as the influence of the temperature or density gradients, and even, in presence of certain types of periodical forcing or luminous flows.

In this work we study, theoretically and experimentally, the dynamical response of macroscopic Turing patterns subjected to a mechanical periodic forcing which implies a sinusoidal modulation of gravity. Theoretical predictions indicate that the extra energy due to the forcing, and the reactor characteristics (that prevent flows to occur) modifies the diffusion coefficient at a microscopic level[2], producing changes in the domain where Turing stability appears and also in pattern characteristics[3], as its configuration or wavelength.

In addition, Turing structures appear naturally under different configurations such as stripes and spots as well as mixed states. And the traditional tool to characterize these patterns is the Fourier transformation, which accounts for the spatial wavelength, but it presents difficulties in order to discriminate among the structures just cited previously (see Fig.1). Thus we propose a method based on the Minkowski functional[4] that, in a clearly way, differentiates all spatial configurations, giving a supplementary information about their transitions between each other. This method was successfully tested on a steady and temporally evolving Turing patterns[5].

The authors want to enhance the relevance of the study here presented. Since, on the one hand, it can be applied to other situations where external forcing influences transport in the system through diffusive mechanisms but when no flow or convection is allowed, and in the other hand, as our morphological method results an useful technique to identify the morphology and characterize possible transitions among a great diversity of dynamical spatiotemporal structures.

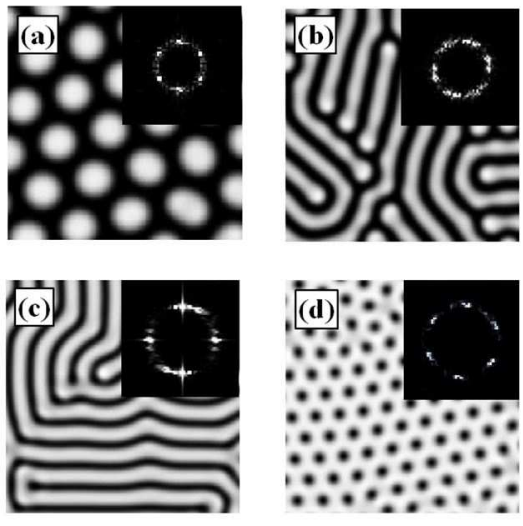


FIG. 1. Numerical simulation of Turing patterns using Oregonator model a) Hexagonal pattern (white spots). b) Direct labyrinth structure (white stripes). c) Reverse labyrinth structure (black stripes). d) Reverse hexagons (black spots).

* jacobo.guiu@usc.es

[1] A. M. Turing, Philos. Trans. R. Soc. London B 237, 37 (1952).
[2] J. Guiu-Souto, J. Carballido-Landeira, A. P. Muñuzuri, and V. Pérez-Villar, Phys. Rev. E 82, 066209 (2010).
[3] J. Guiu-Souto, J. Carballido-Landeira, and A. P. Muñuzuri, Journal of Physics: Conference Series 296, 0120156 (2011).
[4] K. R. Mecke, Phys. Rev. E 53, 4794 (1996).
[5] J. Guiu-Souto, Jorge Carballido-Landeira, and A. P. Muñuzuri, Phys. Rev. E 85, 056205 (2012).

# Statistical Analysis of Investors' Behaviour: Different Temporal Scales

Mario Gutiérrez-Roig* and Josep Perelló
*Departament de Física Fonamental*
*Universitat de Barcelona Diagonal 647, E-08028 (Barcelona)*

The human collective behaviour in society is becoming more and more empirically studied by scientists. Nowadays, globalization, internet and our ICT society let us provide very large amount of data ready to study empirically. Most of the challenges can be summarized along the question how microscopic interactions between agents trigger macroscopic phenomena in a large scale level. Inside the context of financial markets, the role of agents' statistical properties, for instance the expectation time studied here, it is crucial to understand the price formation at the macro-level.

We study a dataset containing more than 7 million of individual recordings from 29,930 non-experts professional investors (clients) of a particular investment firm. All of them had traded between 2000 and 2007 in Spanish stock market IBEX. Price, date, and number of shares traded are recorded for each transaction, so that we can track the performance for every individual.

In order to guess an approximate investor's strategy it is reasonable to hypothesize that most influence over investors' response is the price of the asset which they are trading with. Therefore we can study the cross-correlation between what people do and what market does[1] through the coefficient

$$\rho^i_{Sr}(L) = \frac{1}{T^i_L}\sum_{k=1}^{T^i_L} \frac{\left(S^i_k(L) - \bar{S}^i(L)\right)\left(r_k(L) - \bar{r}(L)\right)}{\sigma_S \sigma_r}, \quad (1)$$

where $T^i_L$ is the number of active periods of length $L$, $S^i_k(L)$ is the balance (shares bought minus shares sold) for investor $i$ in the time-window of length $L$ and $r_k(L)$ means the logarithmic price change in that time-window.

The mean of the distribution is found on negative region (FIG. 1), meaning that, on average, when market goes up investors sell and when the market falls down investors buy. One of the reasons to explain the dispersion of the points is because all agents does not base their strategy on the same time-horizon. This time-horizon can be heuristically determined by finding out which period $L$ maximises $\rho^i_{S-r}(L)$ function (FIG. 2).

The implications of these preliminary results can be important for testing and estimating parameters in agent-based models, like the expectation horizon for the price formation of a single agent[2].

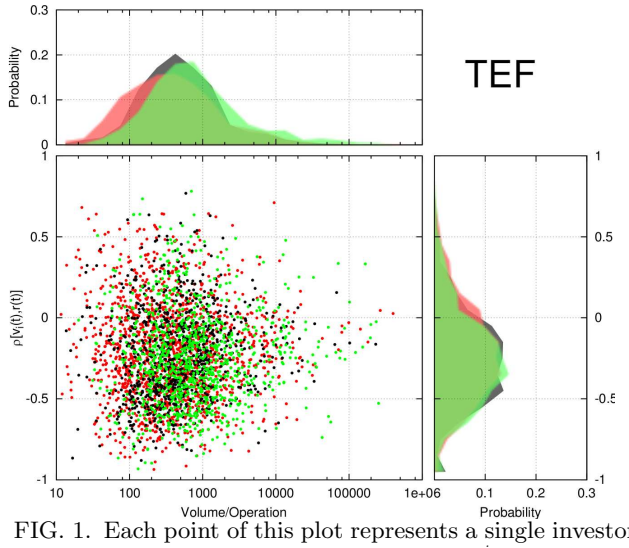


FIG. 1. Each point of this plot represents a single investor. The $y$ component represents the correlation $\rho^{i,a}_{S-r}$ using time windows of $L = 1$days, while the $x$ component represents total volume traded divided by the number of operations done. The color represents the "efficiency" (average income per operation); green for huge positive incomes, red for huge negative incomes and black for incomes in mid zone.

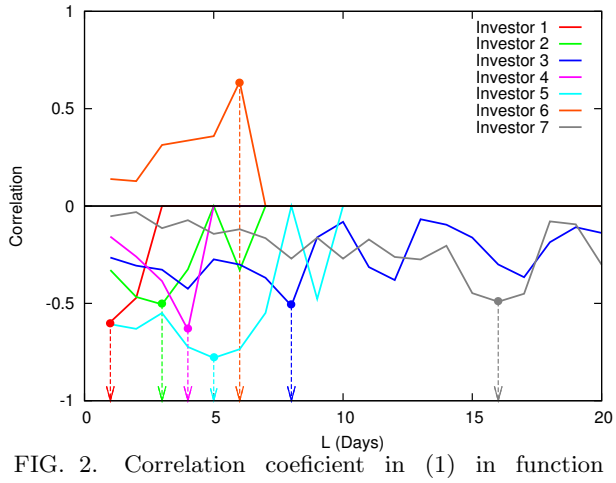


FIG. 2. Correlation coeficient in (1) in function of time-window length $L$ for different invesors, each one represented by colored solid line. Dashed arrows point to the value of $L$ which maximises the absolute value of the correlation for each investor and is expected to be the time-window length which the investor work with.

* mgutierrez@ffn.ub.es

[1] F. Lillo, E. Moro, G. Vaglica and R.N. Mantegna,*New Journal of Physics* **10**, 043019 (2008).
[2] C. Chiarella, G. Iori and J. Perelló,*Journal of Economic Dynamics and Control* **33**, 525-537 (2009).

# Predicting effects of structural stress in a genome-reduced model bacterial metabolism

Oriol Güell[1,*], Francesc Sagués,[1] and M. Ángeles Serrano[2]
[1] *Departament de Química Física, Facultat de Química, Universitat de Barcelona*
[2] *Departament de Física Fonamental, Facultat de Física, Universitat de Barcelona*

*Mycoplasma pneumoniae* is a human pathogen recently proposed as a genome-reduced model for bacterial systems biology. The response of its metabolic network to different forms of structural stress, including removal of individual and pairs of reactions and knockout of genes and clusters of genes with correlated coexpression, reveals a network architecture as robust as that of other model bacteria, despite its reduced genome and its greater metabolic linearity. Interestingly, metabolite motifs associated to reactions can predict the propagation of individual failures and strong non-linear damage amplification effects that may arise in double breakdowns. We also detect a significant correlation between gene essentiality and the damages produced by single gene knockouts, and find that genes controlling high-damage reactions tend to be expressed independently of each other, a functional switch mechanism that simultaneously acts as a genetic firewall to protect metabolism. Control of failure propagation is crucial for metabolic engineering or disease treatment.

---

* oguell@ub.edu

[1] Güell O, Sagués F, Serrano MA, 2012. Predicting effects of structural stress in a genome-reduced model bacterial metabolism. *arXiv:1202.5931v1 [q-bio.MN].*

# Neutron diffraction and computer simulation studies on the plastic phase of $C_2Cl_6$

A. Henao[1*], M. Rovira-Esteva[2], Sz. Pothoczki[2], G.J. Cuello[3], E. Guardia[1] and L.C Pardo[2].
[1] *Grup de simulació de materia condensada per ordinador, Departament de Física i Enginyeria Nuclear, Universitat Politècnica de Catalunya, Campus Nord B4-B5, Barcelona 08034, Spain.*
[2] *Grup de Caracterització de materials, Departament de Física i Enginyeria Nuclear, ETSEIB, Universitat Politècnica de Catalunya, Diagonal 647, Barcelona 08028, Spain.*
[3] *Institut Laue Langevin, 6 Rue Jules Horowitz, BP. 156, F-38042 Grenoble Cedex 9, France .*

Hexachloroethane ($C_2Cl_6$) is an interesting material with three different solid phases[1](orthorombic between 4 and 318K, monoclinic between 318 and 344K and a plastic phase (BCC) stable from 344K up to the melting temperature, 458K). In plastic or orientationally disordered phases[2] molecules conserve the translational order but they lose the orientational one, as can be seen from Fig. 1.

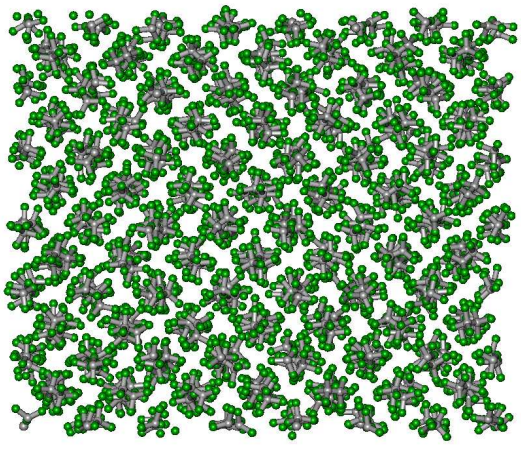

FIG. 1. Snapshot of an MD configuration of the plastic phase of $C_2Cl_6$.

In this contribution we report results (simulation and experiments) on the structure of $C_2Cl_6$ in the range of temperatures of the BCC phase (345-450K). Neutron diffraction experiments were carried out at the diffractometer dedicated to glasses and liquids D4c[3] at the Institute Laue Langevin (ILL, Grenoble, France). Molecular dynamics (MD) simulations were performed using the Gromacs[4] package. The potentials parameters were chosen from the Gromos53a6[5] forcefield. The simulations were carried out in the NPT ensemble using: $\Delta t = 2$fs, shifted cut-off from 16 to 17 Å for Lenard-Jones interactions and 20Å for coulomb pairs. We used the Particle-Mesh-Ewald method to deal with the long-range electrostatic forces. The system box contained 2000 molecules. Each run was extended up to 500 ps and properties were obtained from the last 300 ps. We compare the static structure factor resulting from MD with neutron scattering experiments at T = 400K in Fig.2.

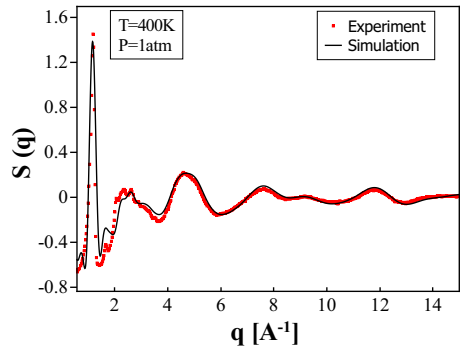


FIG. 2. Comparison between experimental (dots) and MD simulation (solid line) static structure factor at T = 400K and P = 1atm

* andres.henao@upc.edu

[1] A. Criado and A. Muñoz, Molecular Physics. **83**, 815 (1994).
[2] J.N. Sherwood, The Plastically Crystalline state, 1979 (Chichester: Wiley)
[3] H.E. Fischer, G.J. Cuello, P. Palleau, D. Feltin, A.C. Barnes, Y.S. Badyal and J.M. Simonson, Appl. Phys. A: Mater. Sci. Process. **74**, S160 (2002).
[4] B. Hess, C. Kutzner, D. Van der Spoel and E. Lindahl. Chem. Theory Comput. **4**, 435 (2008).
[5] C. Oostenbrik, A. Villa, A.E. Mark, and W.F. Van Gunsteren, J. Comp. Chem. **25**, 1656 (2004).

# Biological production and plankton dynamics in a turbulent ocean upwelling system

Ismael Hernández-Carrasco[a], Vincent Rossi[b], Emilio Hernández-García[a]*, Veronique Garçon[c], and Cristóbal López[a]
[a] *IFISC, Instituto de Física Interdisciplinar y Sistemas Complejos CSIC-Universidad de las Islas Baleares, E-07122 Palma de Mallorca, Spain*
[b] *University of New South Wales, School of Maths and Statistics, Applied, Coastal Oceanography, Sydney 2052, Australia*
[c] *Laboratoire d'Études en Géophysique et Océanographie Spatiale, CNRS, Observatoire Midi-Pyréenées, 14 avenue Edouard Belin, Toulouse, 31401 Cedex 9, France*

The interaction of fluid flow with the biology of organisms living in the water is a topic of confluence of hydrodynamics, statistical and nonlinear physics, ecological modelling, and Earth sciences[1]. Upwelling systems, i.e. ocean areas were vertical water motions bring nutrients towards the ocean surface were phytoplankton can combine them with light availability, are the most productive regions in the global oceans. They are generally located at the eastern boundaries of the different Earth oceans.

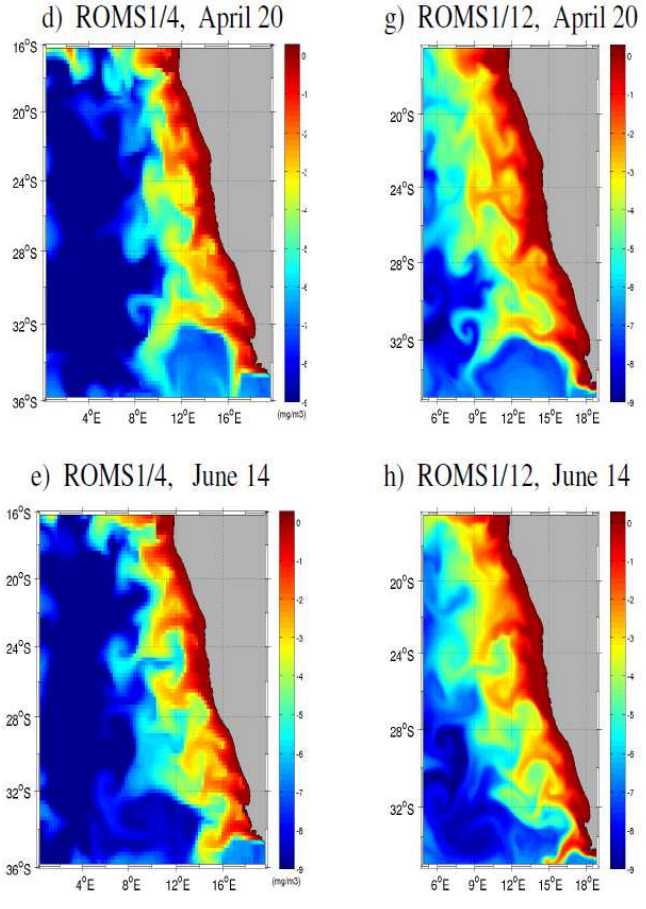


FIG. 1. Phytoplankton distributions obtained from the NPZ model of biological interactions coupled with the flow field from the ROMS model at 1/4 ° resolution (left) and 1/12 ° resolution (left). Colorbar in $mg/m^3$ (log scale).

Recent studies, both based on remote sensed data and coupled models, showed a reduction of biological productivity due to vigorous horizontal mixing in these upwelling regions[2–4]. This seems to contrast with other observations of productivity enhancement in open ocean areas much poorer in nutrients. In order to better understand this phenomenon, and in general the interplay between flow and biological growth, we have considered the oceanic flow in the Benguela area (West-South African coast) coupled with a simple biogeochemical model of Nutrient-Phyto-Zooplankton (NPZ) type. For the flow three different surface velocity fields are considered: one derived from satellite altimetry data, and the other two from a regional numerical model at two different spatial resolutions. We computed horizontal particle dispersion in terms of Lyapunov Exponents, and analyzed their correlations with phytoplankton concentrations. Our modelling approach confirms that in the south Benguela there is a reduction of biological activity when stirring is increased. Two-dimensional offshore advection seems to be the dominant process involved. In the northern area, other factors not taken into account in our simulation are in influencing the ecosystem. We provide explanations for these results in the context of studies performed in other Eastern Boundary upwelling areas.

* emilio@ifisc.uib-csic.es

[1] Z. Neufeld and E. Hernández-García, *Chemical and Biological Processes in Fluid Flows: A Dynamical Systems Approach* . Imperial College Press (2009). ISBN: 978-1-86094-699-8
[2] V. Rossi, C. López, J. Sudre, E. Hernández-García, V. Garçon, *Comparative study of mixing and biological activity of the Benguela and Canary upwelling systems*, Geophys. Res. Lett. **35**, L11602 (2008).
[3] V. Rossi, C. López, E. Hernández-García, J. Sudre, V. Garçon, Y. Morel, *Surface mixing and biological activity in the four Eastern Boundary upwelling systems*, Nonlinear Process. Geophys. **16**, 557–568 (2009).
[4] N. Gruber, Z. Lachkar, H. Frenzel, P. Marchesiello, M. Münnich, J.C. McWilliams, T. Nagai, G-K. Plattner, *Eddy-induced reduction of biological production in eastern boundary upwelling systems*, Nature Geoscience **4**, 787–792 (2011).

# Stochastic Amplification of Fluctuations in Neural Networks

Jorge Hidalgo*, Luís F. Seoane, Jesús M. Cortés, Miguel A. Muñoz
*Departamento de Electromagnetismo y Física de la Materia e Instituto de Física Teórica y Computacional Carlos I Universidad de Granada 18071 - Granada.*

The cerebral cortex exhibits complex patterns of oscillations even in the absence of external stimuli. Deciphering its nature, structure and function are challenging tasks. Cortical local field potentials are bistable and can fluctuate spontaneously between a quiescent (Down) and an active (Up) state, generating slow $\delta$ oscillations (also known as Up-and-Down States). Experimental evidence shows that spontaneous high oscillations (in the $\beta - \gamma$ band) emerge within Up states[1]; remarkably, similar oscillations do not appear in Down states. Moreover, this rhythm within Up states seems to be a collective phenomenon given that individual neurons do not lock to it. Our conclusion, supported by both theory and simulations, is that the collective phenomenon of "stochastic amplification of fluctuations" –previously described in other contexts such as Ecology[2] and Epidemiology– explains in an elegant manner, beyond model-dependent details, all this intriguing phenomenology described above[4].

One of the simplest model for Up and Down states describes the local field potential of the network, $v$, whose dynamics are regulated by a variable $u$, the synaptic utility, which measures the level of depression of the synaptic resources[3]:

$$\dot{v} = -\frac{v - V_r}{\tau} + \frac{w_{in}\mu u f(v)}{\tau}$$
$$\dot{u} = \frac{1-u}{\tau_R} - \mu u f(v), \qquad (1)$$

where $\tau$ and $\tau_R$ are the characteristic times of voltage leakage and synaptic recovery, respectively, $w_{in}$ is the amplitude of internal inputs, $V_r$ is the resting potential, and $\mu$ is the release fraction indicating the efficiency of synapses; the firing rate function, $f$, is assumed to depend on $v$ as $f(v) = \alpha(v - T)$ if $v \geq T$, where $T$ is a threshold value, and $f(v) = 0$.

This model presents two fixed points, which correspond to a high-activity level (Up state) and other quiescent (Down state). Adding noise to this equations, the system can switch between the two states.

To analyze fluctuations around a fixed point $(v^*, u^*)$ of the deterministic dynamics, a standard linear stability analysis can be performed. Defining $x = v - v^*$ and $y = u - u^*$, one can linearize the deterministic part of the dynamics, writing the Jacobian matrix $A$, evaluated at every fixed point for the dynamics presented in equation 1. Also, we compute the power spectra of fluctuations of $x$ and $y$, which both have a peak at

$$\omega_0 \simeq \sqrt{\det A - (\mathrm{Tr}A)^2/2}, \qquad (2)$$

A simple analysis of the characteristics of $A$ which give a peak in the power spectrum (positive argument of the square root) reveals that $A$ must have complex eigenvalues; in other words, the relaxation towards the stable fixed point should be in the form of damped oscillations (spiral trajectories) with a not too small damping frequency. Noise "kicks" the system away from the fixed point, and amplifies predominantly some frequency which –surprisingly enough– turns out to be *different* from the characteristic frequency of the deterministic damped oscillations. This is the mechanism of *stochastic amplification of fluctuations*.

Now, we can understand why this peak appears in the Up state but not in the Down: for the first one, eqs. 1 are strongly coupled –because of the high value of the firing rate $f$–, and eigenvalues turn out to be complex; for the Down state, the firing rate $f$ is almost zero, equations 1 are essentially independent and eigenvalues become real.

The same analysis can be performed in other models of Up-and-Down dynamics (as excitation-inhibition models), but the arguments remain the same. Also, the mechanism only applies for variables describing the mean-field level, whose values oscillate around one (or more) fixed points. In the case of neurons, their microscopic values are integrating and spiking all the time, so we cannot observe the same peak at this level. In other words, stochastic amplification has to be viewed as a collective phenomenon.

---

* jhidalgo@onsager.ugr.es

[1] Compte A, Sanchez-Vives MV, McCormick DA, Wang XJ. J Neurophysiol 89: 2707-2725.
[2] McKane AJ, Newman TJ (2005). Phys Rev Lett 94: 218102.
[3] Holcman D, Tsodyks M (2006). PLoS Comput Biol 2: e23.
[4] Pending publication

# Mixing and transport in chaotic flows analyzed with Lagrangian coherent structures

F. Huhn*, A. von Kameke, V. Pérez-Muñuzuri
*Grupo de Física No Lineal, Facultade de Física, Universidade de Santiago de Compostela, 15782 Santiago de Compostela, A Coruña, España*

Transport in time-dependent aperiodic velocity fields can be highly chaotic. The dynamical systems approach to fluid transport allows to find geometrical coherent structures in the flow that govern the transport[1,4]. They are related to the stable and unstable manifolds of hyperbolic regions in the flow and serve to separate different regions of the flow that contain dynamically different trajectories. These coherent structures can be extracted by analyzing the properties of fluid trajectories that are obtained by integrating the time-dependent velocity field. In particular, we compute spatial maps of the Finite-Time Lyapunov Exponents (FTLE) of trajectories to unveil the structures. We study these patterns, called Lagrangian Coherent Structures (LCS), in different two-dimensional chaotic flows in the ocean and in the laboratory. Velocity fields are obtained from satellite data, a hydrodynamic coastal model or direct measurements via Particle Image Velocimetry (PIV). In all cases the extracted LCS act as barriers to transport and determine the local mixing dynamics. We show how LCS influence the transport of continuous active tracers, e.g., plankton concentration in the ocean[2] or a chemical reaction in the laboratory. LCS also serve to understand the pathways of surface drifters in an estuary and give a footprint of the water exchange processes of the estuary with the shelf[3].

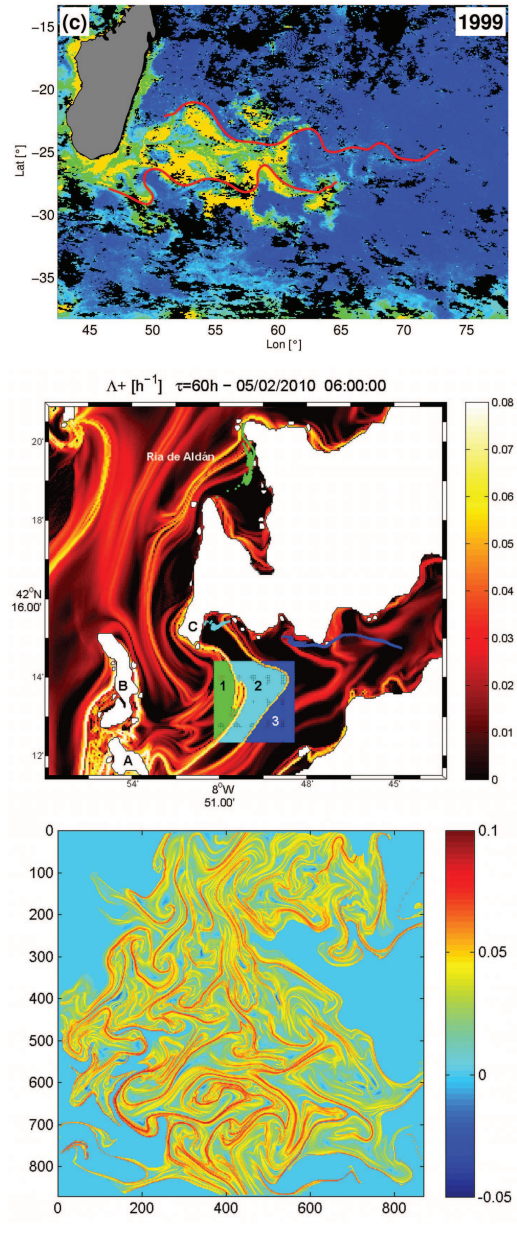


FIG. 1. Lagrangian Coherent Structures (LCS) from finite–time Lyapunov exponents (FTLE). (top) Madagascar plankton bloom between zonal jets. (middle) Virtual tracers in a tidal surface flow in the estuary Ria de Vigo. (bottom) Turbulent two-dimensional laboratory flow.

* florian.huhn@usc.es

[1] G. Haller, and G. Yuan, Physica D **147**, 352-370, (2000).
[2] F. Huhn, A. von Kameke, V. Pérez-Muñuzuri, M.J. Olascoaga, and F.J. Beron-Vera, Geophys. Res. Lett. **39**, L06602 (2012).
[3] F. Huhn, A. von Kameke, S. Allen-Perkins, P. Montero, A. Venancio, and V. Pérez-Muñuzuri, Cont. Shelf Res. **39-40**, 1-13 (2012).
[4] T. Peacock, and J. Dabiri, Chaos **20**, 017501, (2010).

# Robust Short-Term Memory without Synaptic Learning

Sam Johnson*,†,‡, J. Marro†, and Joaquín J. Torres†
*Department of Physics and Oxford Centre for Integrative Systems Biology, University of Oxford, OX1 3QU, United Kingdom*

Whenever an image is flashed briefly before your eyes, or you hear a sudden sound, you are usually able to recall the information presented for a few seconds thereafter.[1] In fact, it is most vivid at first but fades gradually. According to our current understanding of neural networks, memories are stored by strengthening and weakening the appropriate connections (synapses) between neurons.[2] But these biochemical processes take place on a timescale of minutes.[3] Most models of short-term memory get round this problem by assuming that the information in the stimulus is (sometimes inexplicably) already in the brain, which therefore has only to activate the correct pattern.[5] However, this clashes with everyday experience as well as with more rigorous observation.[4] Mechanisms of cellular bistability have also been proposed, such that each neuron has an individual memory.[6] But considering how noisy real neurons are, it seems difficult for these to be robust enough.[7]

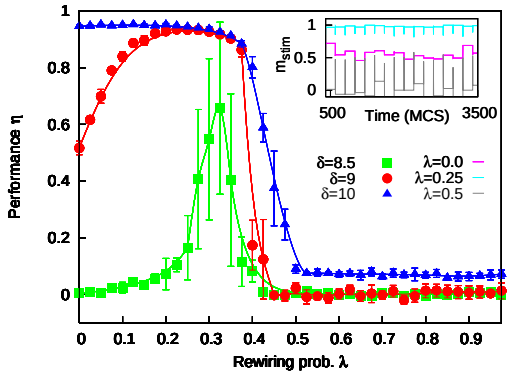


FIG. 1. Performance $\eta$ against probability of rewiring $\lambda$ for modular networks, from Monte Carlo (MC) simulations; patterns are "shown" to the system with different intensities $\delta$. For intensities similar to the input the average neuron receives from its neighbours, there is an optimal value of $\lambda$ (a measure of network modularity). Inset: Typical time series for $\lambda = 0.5$ (bad performance), 0 (intermediate), and 0.25 (near optimal).

Here we suggest an entirely different mechanism – Cluster Reverberation – whereby simple model neurons can store novel information for a short time (a few seconds) without previous learning or individual cellular memory[8] (Fig. 1). This is achieved thanks to metastable states of activity that arise from the clustered nature of the underlying network topology. We show that this mechanism is robust to the kind of model neuron used (which can be very noisy) and to network structure. Furthermore, we predict that forgetting will occur according to quasi-power laws (Fig. 2), in the same way as happens for nonequilibrium magnetic systems or Griffiths phases on networks; and that there will be local synchronization of synaptic inputs.[9] Both these results fit in with experimental findings from psychology[10] and neurobiology.[11]

We conclude by suggesting some *in vitro* and *in vivo* experiments that could be done to test whether the brain does indeed make use of this mechanism.

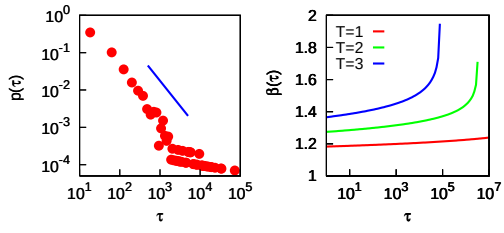


FIG. 2. Left panel: Distribution of escape times $\tau$ for $\lambda = 0.25$ and noise $T = 2$, from MC simulations. Slope is for the theoretical prediction at $\tau = 10^3$ ($\beta \simeq 1.35$). Other parameters as in Fig. 1. Right panel: Exponent $\beta$ of the quasi-power-law distribution $p(\tau)$ as obtained analytically, for noise $T = 1$, 2 and 3.

* Department of Mathematics, Imperial College London, SW7 2AZ, United Kingdom.
† Departamento de Electromagnetismo y Física de la Materia, and Institute *Carlos I* for Theoretical and Computational Physics, University of Granada, 18071 Granada, Spain.
‡ samuel@onsager.ugr.es

[1] Baddeley, A. D., *Essentials of Human Memory*, Psychology Press, London, 1999.
[2] Amit, D.J., *Modeling Brain Function*, Cambridge Univ. Press, Cambridge, 1989.
[3] A.Y. Klintsova and W.T. Greenough, *Current Opinion in Neurobiology* **9**, 203 (1999).
[4] D. Durstewitz, J.K. Seamans, and T.J. Sejnowski, *Nature Neuroscience* **3**, 1184–91 (2000).
[5] G. Mongillo, O. Barak, and M. Tsodyks, *Science* **319**, 1543–1546 (2008).
[6] E. Tarnow, *Cognitive Neurodynamics* **3**, 263–9, (2008).
[7] A. Compte, C. Constantinidis, J. Tegnér, *et al.*, *J. Neurophysiol.* **90** 3441-54 (2003).
[8] S. Johnson, J. Marro, and J.J. Torres, *Submitted.*
[9] M.A. Muñoz, R. Juhasz, C. Castellano, G. Odor, *Phys. Rev. Lett.* **105**, 128701 (2010).
[10] S. Sikström, *Cognitive Psychology* **45**, 95–152 (2002).
[11] N. Takahashi, K. Kitamura Naoki Matsuo, M. Mayford, *et al.*, *Science* **335**, 353–6 (2012).

# Threshold phenomenon in the *Countdown* game

Lucas Lacasa, Bartolo Luque
*Dpto. de Matemática Aplicada y Estadística, ETSI Aeronáuticos*
*Universidad Politécnica de Madrid, Spain*

In combinatorial optimization problems, a large amount of literature points out to the occurrence of a so called threshold phenomenon in the performance of search algorithms: there exists a phase in parameter space where the search algorithm can easily find a solution to the aforementioned combinatorial problem (as the number of available solutions is exponentially large with the system size), and a phase where such solution typically (i.e. almost surely) does not exist[1]. The transition between both phases is sharp in some situations, mimicking in several aspects the phenomenon of a phase transition in statistical physics problems. Some classical problems evidencing such phenomenon include combinatorial problems in random graphs or the satisfaction of (random) boolean clauses, generically gathered under the umbrella of random constraint satisfaction problems (rCSP)[1]. Many of these concrete problems can indeed by interpreted under a statistical physics formalism[2], the general idea being the following: in a combinatorial optimization problem, is some cases one can formalize a cost function to be minimized. In satisfaction problems, this is for instance the number of violated constraints. Within statistical physics of disorders systems, such as in spin glasses, one indeed proceeds in the same manner if the system is studied in the limit of low temperature (in that situation, the system tries to adopt the ground state or minimal energy configuration). Thereby, the cost function of a combinatorial optimization problem can be related to the Hamiltonian of a disordered system at zero temperature (for instance, finding a minimum partition within the so-called partitioning problem is equivalent to finding the ground state of a infinite range Ising spin glass with Mattis-like, antiferromagnetic couplings[3]).

In this work we present a random decision problem, called the *countdown game*, which is inspired in a celebrated british TV quiz show called Countdown (based itself on the French game show *Des chiffres et des lettres*, one of the longest-running game shows in the world, and receiving other names in several countries[5]). This show is separated in several games, one of which incorporates the combinatorial problem of arithmetically combining some numbers to produce another one. Concretely, the contestants must use arithmetic to reach a given target number from six other numbers. Here we formalize a random version of this decision problem and explore its solvability as a function of the parameter space. After defining the game in a similar fashion as random constraint satisfaction problems, we numerically explore the ability of a search algorithm to solve it, and show that this probability drops sharply from typically one to zero (where typically is synonymous to almost surely in the thermodynamic limit). This suggests that that the game evidences the threshold phenomenon. At odds with standard decision problems evidencing sharp algorithmic transitions either in physics or computer science, we show that within this problem such behavior is genuinely of a number-theoretical garment. We take advantage of this fact to characterize the transition, which is of a purely algorithmic nature, in terms of combinatorial number theory. Some discussions regarding possible relations of this problem to more general questions in random group theory, and other alternative approaches are also presented.

---

[1] C. Moore and S. Mertens, The Nature of Computation, Oxford University Press (2011).
[2] M. Mezard, G. Parisi, and M. Virasoro, Spin glass theory and beyond (World Scientific, Singapore, 1987).
[3] S. Mertens, A Physicist's Approach to Number Partitioning. Theoret. Comput. Sci. 265, 79-108 (2001).
[4] S. Kirkpatrick and B. Selman, Critical Behavior in the Satisfiability of Random Boolean Expressions,Science 264, 5163 pp. 1297-1301 (1994).
[5] Wikipedia entry for Countdown game show: http://en.wikipedia.org/wiki/Countdown_(game_show)

# Collective effects of heterogeneity and stochasticity in interacting particle systems

L. F. Lafuerza*, R. Toral
*IFISC, Instituto de Física Interdisciplinar y Sistemas Complejos*
*CSIC-Universidad de las Islas Baleares 07122-Palma (Mallorca)*

Systems studied traditionally in physics are made of identical (some times even indistinguishable) units (molecules, atoms, electrons). In recent years, methods and ideas developed in statistical physics have been applied to other disciplines (such as ecology, epidemic spreading, economy...), and systems outside the traditional realm of physics have been studied by physicists, focusing on collective and emergent phenomena in what is known as complexity science. This kind of systems are typically characterized by a large degree of heterogeneity among their units, and very often they can be modeled only at a stochastic level (since complete knowledge of all the variables, the precise dynamics of the units and the interaction with the environment is not available). One way to include the heterogeneity of the system is by considering that the interactions of the particles are not homogeneous but given by some connectivity network; an approach that has attracted enormous attention in the last years. An issue that has been less studied systematically is the role played by particle heterogeneity in the overall behavior of stochastic systems.

In this work, we show that the combined effect of stochasticity and heterogeneity can give rise to non-trivial results, and develop a general formulation to study systems of heterogeneous stochastic interacting particles.

For systems of 2-state independent particles, we show that the fluctuations of the collective variable decrease as the degree of heterogeneity is increased. Moreover, one can obtain precise information about the degree of heterogeneity in the system, by measuring only the collective variable ($n$) and its fluctuations:

$$\sigma_p^2 \equiv \langle p^2\rangle - \langle p\rangle^2 = \frac{\langle n\rangle - \langle n\rangle^2/N - \sigma_n^2}{N}, \qquad (1)$$

with $p_i$ some intrinsic parameter of the particle, that is distributed over the population. This expression is universal, regardless the specific form in which $p_i$ is distributed, and an equivalent result is obtained for $k$-state systems for $k > 2$. Higher moments of the heterogeneity distribution are also related to higher moments of the collective variable.

We develop an approximated method to analytically study systems of heterogeneous interacting particles, and apply it to study the effect of heterogeneity in various models, such as the Kirman model[1].
We find that heterogeneity can amplify or reduce the fluctuations of the collective variable, depending on the way it is introduced and the particular form of the system.

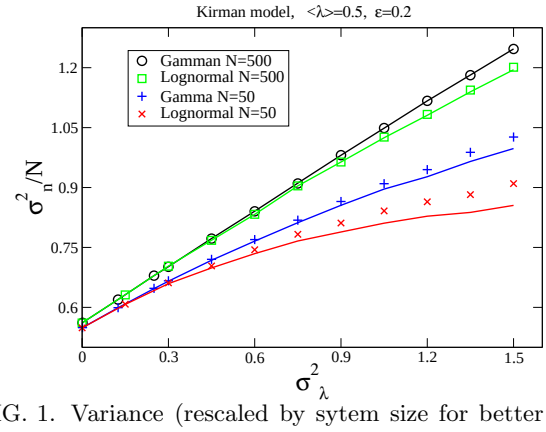


FIG. 1. Variance (rescaled by sytem size for better comparison) of the number of particles in state 1 as a function of the variance of the distribution of "influence" in Kirman model. Results coming from numerical simulations (symbols) and theoretical analysis (solid lines), for different system sizes and forms of the distribution.

* luis@ifisc.uib-csic.es

[1] A. Kirman, The Quarterly Journal of Economics, **108**, 137 (1993). This model was proposed to study herding behaviour in the context of stock markets and collective behavior in ant colonies. It corresponds to particles changing their states trough two mechanisms: spontaneous transitions at a rate $\epsilon$, and induced transitions at a rate $\sum \frac{\lambda_j(1-\delta_{n_i,n_j})}{N}$, so that $\lambda_j$ is the "influence" of agent $j$ towards his current opinion.

# Large Fluctuations of the Dissipated Energy in a Simple Model System

Antonio Lasanta*, Antonio Prados* and Pablo I. Hurtado†
*Física Teórica, Universidad de Sevilla, Apdo. de Correos 1065, Sevilla 41080, Spain
†Instituto Carlos I de Física Teórica y Computacional, Universidad de Granada, Granada 18071, Spain

We analyze the fluctuations of the dissipated energy in a simple and general model where dissipation, diffusion and driving are the key ingredients. The large deviation function for the dissipation follows from hydrodynamic fluctuation theory and an additivity conjecture. This function is strongly non-Gaussian and has no negative branch, thus violating the fluctuation theorem as expected from the irreversibility of the dynamics. It exhibits simple, universal scaling forms in the weak- and strong-dissipation limits, with large fluctuations favoured in the former case but strongly suppressed in the latter. The typical path associated to a given dissipation fluctuation is also analyzed in detail. Our results, confirmed in extensive simulations, strongly support the validity of hydrodynamic fluctuation theory to describe fluctuating behavior in driven dissipative media.[1]

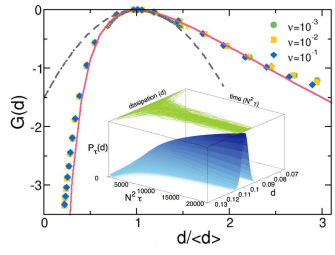


FIG. 1. Scaling of the dissipation LDF in the quasielastic limit ($\nu \ll 1$) for $N = 50$, $T = 1$, and varying $\nu$. The solid and dashed lines are the HFT prediction and Gaussian estimation, respectively. Small points around the peak were obtained in standard simulations. Inset: Convergence of time- averaged dissipation and sketch of the probability concentration associated with the large deviation principle.

* alasanta@us.es

[1] A. Prados, A. Lasanta and P. I. Hurtado, Phys. Rev. Lett. **107**, 140601 (2011)

# Magnetoasymmetric transport in a quantum dot Aharonov-Bohm interferometer

Jong Soo Lim*, David Sánchez, Rosa López
*IFISC, Instituto de Física Interdisciplinar y Sistemas Complejos*
*CSIC-Universidad de las Islas Baleares 07122-Palma de Mallorca*

Away from linear response, screening effects can lead to a breakdown of microreversibility in mesoscopic systems. In nonequilibrium, the internal potential of the conductor is, quite generally, an uneven function of the magnetic field, implying a magnetoasymmetry of the differential conductance.[1] Recent theoretical developments relate the asymmetry of the noise to the asymmetry of the differential conductance in the leading order of a voltage expansion.[2] As a consequence, a higher-order fluctuation relation is established between the two magnetoasymmetries even when fluctuation theorem is not obeyed.

Here we discuss magnetoasymmetries in quantum-dot Aharonov-Bohm interferometers when strong electron-electron interactions are taken into account beyond the mean-field approach.[3] With the aid of the electron occupation at the dot, we demonstrate that its nonequilibrium component is an asymmetric function of the flux even to lowest order in voltage. We also calculate the magnetoasymmetry of the noise and find that it is given, to a good extent, by the magnetoasymmetry of the weakly nonlinear conductance term. Therefore, both magnetoasymmetries (noise and conductance) are related to each other via a higher-order fluctuation relation.

---

* lim.jongsoo@gmail.com

[1] D. Sánchez and M. Büttiker, Phys. Rev. Lett. 93, 106802 (2004); B. Spivak and A. Zyuzin, Phys. Rev. Lett. 93, 226801 (2004).
[2] H. Förster and M. Büttiker, Phys. Rev. Lett. 101, 136805 (2008); Y. Utsumi and K. Kaito, Phys. Rev. B 79, 235311 (2009); D. Sánchez, Phys. Rev. B 79, 045305 (2009).
[3] J.S. Lim, D. Sánchez, and R. López, Phys Rev. B 81, 155323 (2010).

# Lagrangian Coherent Structures in three-dimensional flows

Joao B. Bettencourt, Cristóbal López, Emilio Hernández-García*
*IFISC, Instituto de Física Interdisciplinar y Sistemas Complejos*
*CSIC-Universidad de las Islas Baleares 07122-Palma (Mallorca)*

Coherent Structures are known to drive biological dynamics, from plankton to top predators, thus it is very important to be able to characterize them in realistic three dimensional flows. The FSLE is a measure of particle dispersion in fluid flows and the ridges of this scalar field locate regions of the velocity field where strong exponential separation between particles occur. These regions are referred to as Lagrangian Coherent Structures (LCS). We have identified LCS in two different 3d flows: a canonical turbulent velocity field that is the turbulent flow between two parallel stationary plates driven by a pressure gradient in the mean flow direction and a primitive equation model (ROMS) simulation of the oceanic flow in the Benguela region[1].

* clopez@ifisc.uib-csic.es

[1] J. Bettencourt, C. López,E. Hernández-García, Ocean Modelling **51**, 73-83 (2012).

# La Estabilidad de los Arcos en un Medio Granular

C. Lozano*, I. Zuriguel, A. Garcimartín y G. Lumay‡
*Departamento de Física y Matemática Aplicada*
*Facultad de Ciencias, Universidad de Navarra*
*31080 Pamplona*

Un medio granular es un conjunto numeroso de partículas de similares características que manifiestan comportamientos colectivos. Una de las propiedades características de los medios granulares es su capacidad para formar arcos. Se puede definir *arco* como una estructura espacial de partículas que se sostienen entre si. Como los arcos son mecánicamente estables, provocan atascos, que detienen el movimiento ordenado de los granos o al menos lo dificultan.

El trabajo consiste en el estudio experimental de la estabilidad de los arcos formados en un silo en 2D aplicando una vibración vertical. El objetivo es encontrar algún tipo de relación entre la estabilidad de los arcos y la geometría de los mismos.

El sistema experimental está formado por un silo bidimensional, en el cual hay un orificio que deben atravesar los granos. Este tipo de montaje permite observar cada arco individualmente. El silo se coloca encima de un vibrador electromecánico. Con ello se pretende analizar el efecto de la vibración sobre cada arco en particular, y buscar parámetros característicos (como puede ser una amplitud característica, o una frecuencia, o un tiempo de espera). Además, si se emplean recipientes bidimensionales se pueden observar directamente los arcos, lo cual permite caracterizarlos geométricamente mediante análisis de imágenes[1].

El principal factor que determina la estabilidad de un arco frente a vibraciones externas es el ángulo máximo que se forma entre cualquier partícula del arco y sus dos vecinas (véase el *inset* de la Figura 1). Denominamos *defecto* a la partícula que tenga un ángulo con sus vecinas superior a $180^o$. El principal resultado que se ha obtenido es que cuanto mayor sea este ángulo, más fácil es romper el arco (véase la Figura 1). Con base a un análisis del balance de fuerzas involucrado en un defecto, se ha dado una explicación sencilla para esta dependencia. De este análisis se puede extraer información del valor de las fuerzas normales y los coeficientes de fricción de estas partículas.

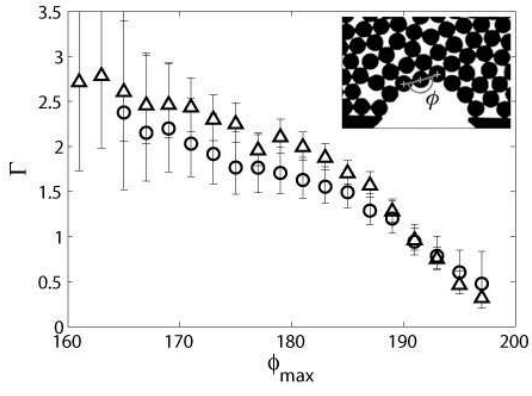


FIG. 1. Aceleración a la que se rompe un arco Γ en función del ángulo máximo $\phi_{max}$. Donde los triángulos corresponden a bolas de acero y los círculos a bolas de latón. Se representa la media y las barras de error corresponden a los intervalos de confianza del 95%. *Inset:* Una fotografía de un arco, indicando el ángulo $\phi$ de una partícula.

* clozano@alumni.unav.es
`http://fisica.unav.es/granular`
‡ GRASP, Universitè de Liège, B-4000 Liège, Bélgica.

[1] A. Garcimartín, I.Zuriguel, L. A. Pugnaloni, A. Janda, *Phys. Rev. E* **8**2, 031306 (2010).

# Spatial correlation of concentration fluctuations in reaction diffusion problems by the Gillespie algorithm

Jorge Luis Hita, José María Ortiz de Zárate*
*Departamento de Física Aplicada I, Universidad Complutense de Madrid*

During the last decades the spectrum of thermal fluctuations in non-equilibrium systems has been widely studied. It has been shown that static correlations have generically long range behavior, while the fluctuations around equilibrium states are, except in the neighborhood of critical points, short ranged. These investigations may be helpful to elucidate whether or not there exist thermodynamic potentials out of equilibrium, and could exclude the local potentials.

Among the non-equilibrium states that have been studied theoretically, there are examples of reaction-diffusion systems in which the inverse chemical reaction and the direct chemical reaction occur through different paths, avoiding chemical equilibrium. It is hard to devise an experimental set up to verify the theoretical conclusions in this case, because it is difficult to find a two-component system whose kinetics is as simple as the ones theoretically studied. A numerical simulation could be a better way to confirm the theory for this kind of problems. More over, there are so far very few simulations that focus on non-equilibrium fluctuations. This is why a simulation of equilibrium and non-equilibrium reaction-diffusion problem is of current interest.

The Gillespie algorithm[1] is a Montecarlo method that simulates efficiently a system of chemical reactions through the chemical master equation. Although it was developed in 1976, the interest in this algorithm has grown during the last years, particularly because of its proven utility in Biophysical problems. The Gillespie algorithm was originally conceived to describe a large network of coupled chemical reactions, but it can be applied to diffusion processes as well, by assuming that the diffusion of one particle from one domain of the system to other can be handled as a chemical reaction with a certain probability[2].

We have developed a computer code to simulate, via the Gillespie algorithm, isothermal reaction-diffusion problems in one dimension. We have performed extensive simulations to numerically study the statistical correlations of the concentration fluctuations at different spatial spots, in order to verify that such correlations are shot-ranged if the chemical reactions are in equilibrium and long-ranged if they are not in equilibrium. We studied the system with an equilibrium chemical reaction (a simple association-dissociation)

$$A \underset{k_2}{\overset{k_1}{\rightleftharpoons}} B, \tag{1}$$

while, as an example of a non-equilibrium reaction, we studied the nonzero stationary state of the WOH model[3]:

$$\begin{aligned} A &\xrightarrow{k_1} B, \\ A + B &\xrightarrow{k_2} 2A. \end{aligned} \tag{2}$$

As an example of our results, we show in Fig. 1 the real-space correlation functions of concentration fluctuations in reaction-diffusion problems corresponding to the chemical kinetics of Eq. (1) (equilibrium, top panel) and of Eq. (2) (nonequilibrium, bottom panel). Short-ranged behavior in the first case and long-ranged in the second case, as predicted by the theory, are obvious. Diffusion coefficients are the same in both cases.

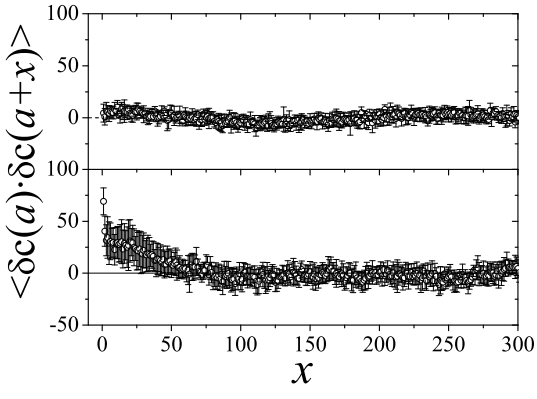


FIG. 1. Real-space correlation function of concentration fluctuations in equilibrium (top panel) and outside of equilibrium (bottom panel).

In addition, we have studied the validity of the van Kampen approach in an homogeneous reacting system, and estimated the number of particles $N$ at which the probability distribution of the fluctuations can be assumed as gaussian. We have applied the Gillespie algorithm to a pure diffusion problem as well, and checked its validity by verifying that the variance of the fluctuations are, as expected, equal to the square root of the mean number of particles at every spot.

* jmortizz@fis.ucm.es

[1] D.T. Gillespie. Exact stochastic simulation of coupled chemical reactions. *J. Phys. Chem.*, 81(1977), p. 2340.

[2] D. Bernstein. Simulating mesoscopic reaction-diffusion systems using the Gillespie algorithm. *Phys. Rev. E*, 71(2005), 041103.

[3] F. van Wijland, K. Oerding and H. J. Hilhorst, Wilson renormalization of a reaction-diffusion process, *Physica A*, 251(1998), p. 179.

# Power Laws and Scaling in the Waiting Time Distribution of Speech

J. Luque[1,2*], L. Lacasa[2], B. Luque[2]
[1] *Dept. de Teoria del Senyal i Comunicacions, TALP Research Center, Universitat Politècnica de Catalunya (UPC), Barcelona, (Spain)*
[2] *Dept. de Matemática Aplicada y Estadística, ETSI Aeronáuticos, Universidad Politécnica de Madrid (UPM), Madrid, (Spain)*

Speech is a distinctive feature of human capabilities. Knowledge of the speech amplitude-squared density, which constitutes an estimation of the released energy, provides basic data concerning statistics of the continuous speech waveform and understanding of the physics of speech production. In this work we present and investigate the statistics of intra-phoneme waiting time distributions in several human speech databases with sufficient size to describe the longtime speech energy density. We find that the waiting time statistics evidence a robust power-law shape, which suggests long-range temporal correlations in the energy of speech. Whereas long-range correlations have been previously reported in several human activities[1], we emphasize that statistics addressed in this work restrict to the intra-phoneme range (characteristic time $t < 10$ ms). This suggests that the responsible of this complex phenomenon is not cognitive[2], but resides on the physiological speech production mechanism by itself.

Furthermore, we show that these waiting time distributions follow a scaling law in the sense that they are invariant under a renormalization group transformation[3,4]. Such a result suggests that the speech production process is indeed critical, at odds with standard approaches in speech processing which rely on linear stochastic approaches[5,6].

Results are robust and independent of the communication language, the number of speakers or the speech style, pointing towards an universal pattern and a hint of the complexity of human speech that evokes an explanation in terms of a critical phenomenon.

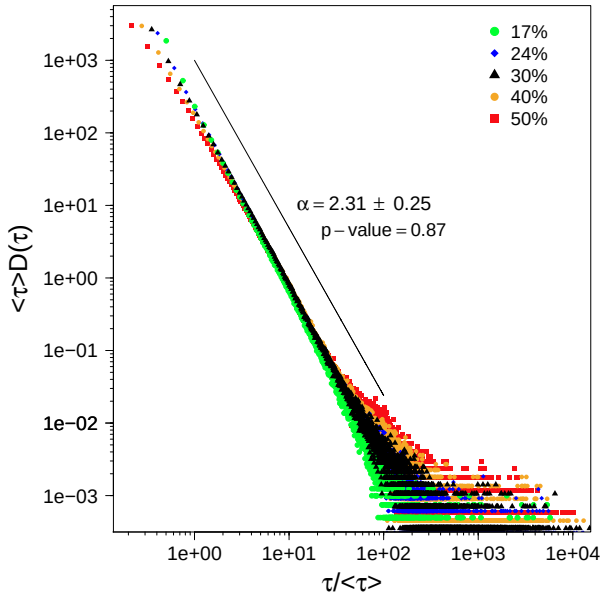


FIG. 1. **Rescaled power-law distributions of speech waiting times for different energy thresholds.** The speech waveform corresponds to an excerpt, from Catalonian broadcast news television, lasting four hours and sampled at 16 KHz. Waiting times distributions – $D(\tau)$ – are calculated for different energy thresholds, ranging in $17\% - 50\%$ of the maximum of the speech amplitude-squared. It is worth to mention that energy speech values below that threshold are discarded from the waiting time computation. In all cases the data can be fitted by a power law distribution with plausible evidence. The maximum likelihood power-law fit obtained setting the energy threshold to 30% is also depicted. It yields $\alpha = 2.31 \pm 0.25$ with a p-value around 87%.

* jorge.luque@upc.edu

[1] Barabasi, A. The origin of bursts and heavy tails in human dynamics. *Nature* **435**, 207 (2005)
[2] Kello, C.T., Brown, G.D.A., Ferrer-i-Cancho, R., Holden, J.G., Linkenkaer-Hansen, K., Rhodes, T. and Van Orden, G.C., Scaling laws in cognitive sciences, *Trends in Cognitive Sciences* **14**, 5 (2010).
[3] Corral, Álvaro. Long-Term Clustering, Scaling, and Universality in the Temporal Occurrence of Earthquakes. *Phys. Rev. Lett.* **92**, 108501 (2004).
[4] Corral, A., Ossó, A. and Llebot, J. E. Scaling of Tropical Cyclone Dissipation. *Nature Phys.* **6**, 693-696 (2010).
[5] Taylor, P., Text-to-Speech Synthesis, (Cambridge University Press, 2009).
[6] Flanagan, J. L., Allen, J. B. and Hasegawa-Johnson, M. A., Speech analysis synthesis and perception, (Springer-Verlag, 3rd edition, 2008).

# Signal integration shapes the dynamics of neuronal networks

Leonardo L. Gollo*, Claudio Mirasso, Víctor M. Eguíluz
*IFISC, Instituto de Física Interdisciplinar y Sistemas Complejos*
*CSIC-Universidad de las Islas Baleares 07122-Palma de Mallorca, Spain*

Cognition and consciousness emerge from the outcome of a multitude of interconnected neurons. In this scenario, the integration of incoming inputs from neighboring neurons plays a crucial role. We find that this integration shapes the macroscopic dynamics of the neuronal network[1].

Taking advantage of general aspects of phase transitions and critical phenomena, several features (including distinction of external stimulus[2], transmission and storage of information[3,4], etc.) become optimized near the critical state. Supported by some experimental evidences, the critical brain hypothesis conjectures that the brain operates at a critical point of a continuous phase transition[5].

We address how the features of the neuronal process of signal integration affects the critical brain hypothesis, the dynamic range, and in general the collective behavior of a network of excitable units. By means of numerical simulations and a mean-field approach, we explore the nonequilibrium phase transition in the presence of integration. We show that the firing rate in random and scale-free networks undergoes a continuous or a discontinuous phase transition depending on both the integration time ($\tau$) and the density of integrator units ($d$), as depicted in Fig. 1. Moreover, in the presence of external stimuli, we find that a system of excitable integrator units operating in a bistable regime largely enhances its dynamic range.

These results are compatible with bi- and multi-stable dynamics (which represent an important part of the brain's dynamic repertoire), and constitute a challenge to the conceptual framework of the critical brain hypothesis.

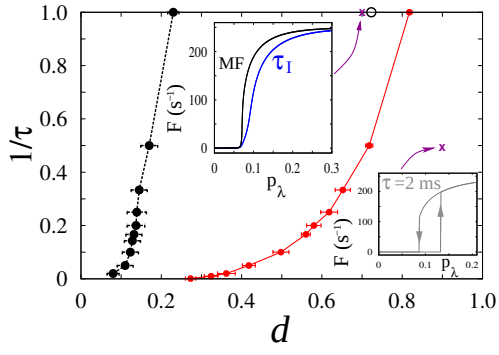


FIG. 1. Dependence of the nature of the phase transition order on the integration time $\tau$ for networks (N = 5000) composed of a mixture of both integrators, which have a density $d$ of nodes with integration threshold $\theta = 2$, and nonintegrators ($\theta = 1$). The red solid (black dashed) line corresponds to the random (scale-free) network. The left-hand side of the curve corresponds to a continuous phase transition whereas the right-hand side corresponds to a discontinuous phase transition. The black open symbol depicts the mean-field shift in the order of the phase transition.

* leonardo@ifisc.uib-csic.es

[1] L. L. Gollo, Claudio Mirasso, Víctor M. Eguíluz, Phys. Rev. E, 85, 040902 (2012).
[2] O. Kinouchi and M. Copelli, Nat. Phys. 2, 348 (2006).
[3] D. Plenz and T. C. Thiagarajan, Trends Neurosci. 30, 101 (2007).
[4] J. M. Beggs, Philos. Trans. R. Soc. London A 366, 329 (2008).
[5] D. R. Chialvo, Nat. Phys. 6, 744 (2010).

# A non local spatial model for savannas.

Ricardo Martínez-García*, Cristóbal López.
*IFISC, Instituto de Física Interdisciplinar y Sistemas Complejos*
*CSIC-Universidad de las Islas Baleares 07122-Palma (Mallorca)*

Savannas are very important ecosystems. They appear in a wide range of climatic and encological conditions, and are mainly characterized by a long time coexistence between a continuous grass layer and dispersal clusters of trees. Their spatial structure, resilience and adaptation capacity have awaken a great interest among ecologists[1], however, despite extensive study, the mechanisms regulating savanna tree populations are not well understood.

In this work, we propose a stochastic nonlocal macroscopic equation to model savannas which takes into account two of the factors that are thought to be crucial to structure semiarid savannas: tree-tree competition and fire[2].

We study the spatial structures in the mean field limit of the model, where fluctuations vanish. Later the impact of fluctuations on them is studied. We consider both intrinsic fluctuations (demographic) as a consequence of the stochastic nature of the model and extrinsic fluctuations (environmental), whose origin lies in the temporally heterogeneous distribution of precipitations.

Also, the phase transition from an active phase where grass and trees coexist, to an absorbing one, characterized by the absence of trees, is analyzed in detail in both situations[3].

---

* ricardo@ifisc.uib-csic.es

[1] M. Sankaran et al., Nature, **438**, 846-849, (2005).
[2] J.M. Calabrese et al. The Am. Nat., **175**, 3, (2010)
[3] R. Martínez-García and C. López, (In preparation).

# A long range communication model for foragers.

Ricardo Martínez-García[1,2,*], Cristóbal López[1], Justin M. Calabrese[2].
[1] *IFISC, Instituto de Física Interdisciplinar y Sistemas Complejos CSIC-Universidad de las Islas Baleares 07122-Palma (Mallorca).*
[2] *Smithsonian Conservation Biology Institute, 1500 Remount Road, Front Royal, VA 22630.*

We present a random walk model for the movement of a population of interacting individuals looking for resources. The problem is studied using numerical simulations of the microscopic stochastic dynamics as well as a macroscopic advection-diffusion equation for the density of foragers.

The dynamics of the particles is governed by two mechanisms which induce biases in the random movement. On the one hand they move following local gradients of resources. On the other hand, we assign to each walker a *calling function* which switches on whenever it finds a good patch of resources. This term models the communication process observed in some ungulates, as gazelles in the Mongolian eastern steppe.

We use the mean first passage time of the population of individuals through the boundaries of the patches of resources as a measurement of the efficiency of the search. We focus our interest in its behavior with the length of the communication range, finding an optimal value at intermediate scales. Other dynamics properties, as the distributions of first passage times, and statics, as the stationary distributions of individuals are also studied[1].

---

* ricardo@ifisc.uib-csic.es

[1] R. Martínez-García et al. (In preparation).

# A Complex Network Model for Mild Cognitive Impairment Subject Characterization

Johann H. Martínez[*,†•], Javier M. Buldú[‡,§], Massimiliano Zanin[§,ι,⊕], Juan Manuel Pastor[*]
*Universidad Politécnica de Madrid [*], Universidad Rey Juan Carlos [‡], Centro de Técnología Biomédica de Madrid - (UPM) [§]*
*Universidad del Rosario de Colombia [†], Universidade Nova de Lisboa [ι], The INNAXIS Research Institute [⊕]*

Mild Cognitive Impairment (MCI) is a brain syndrome[1] that eventually could lead to Alzheimer disease. One important MCI medical issue is the classification problem between healthy and unhealthy individuals, therefore the ways to make descriptional inferences about which neurological features are involved in such a medical condition.

The aim of this work is to apply an innovative methodology[2] to build neurological networks, based on statistical analysis of brain time series, to characterize differences between MCI patients and control individuals. Brain data is collected from individuals divided into two groups: controls and patients, using magnetoencephalographic (MEG) recordings of fourteen subjects for each group. We measure the activity of 147 channels, whose record time series of brain activity during a memory task (Sternberg's test). Time series were analysed using the Synchronization Likelihood algorithm (SL) to detect the consistency (ability to respond in the same way facing same stimulus) of each brain site[3]. Consistency per channel and subject is the feature analyzed in this work.

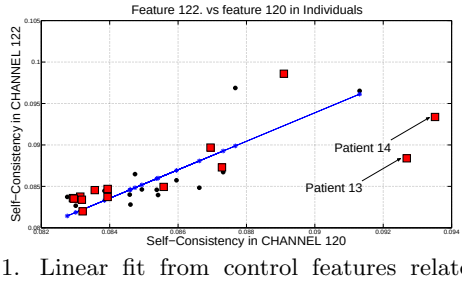


FIG. 1. Linear fit from control features related to the consistency in channels (nodes) 122 and 120, in black dots. Equivalent patient features values are plotted in red squares. Note how feature values in patient 13 and 14 are far from the equivalent information in control fit.

Controls features associated to each pair of different channels, are fitted to get standard deviations (SD). Patient features are related with controls comparing control SD and patient feature values (Fig. 1). The former method is accomplished for all combinations among 147 control and patient features. Patient features, those who have larger values (almost 3 times SD) than its respective control SD, are taken into account to build the patient network edges.

Control networks are built up in similar way avoiding self redundancy. Thence, networks obtained are weighted graphs and it is possible to use several complex network parameters[4] to find more interesting differences among the consistency networks. This methodology unveils topological differences between both groups, in fact, control networks reveal structures with more random configuration, in contrast to star-like shape in patients (Fig. 2).

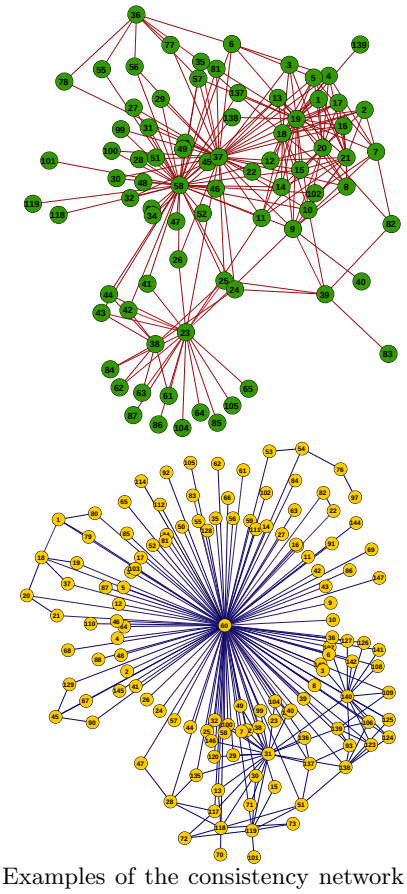

FIG. 2. Examples of the consistency network of a control (top) and MCI patient (down). Networks have different structures: MCI patients have a star-like configuration while controls have a more homogeneous structure.

• jh.martinez@alumnos.upm.es

[1] American Psychiatric Association, Diagnostic and statistical manual of mental disorders, Task Force on DSM-IV, Washington DC, IV, 2006
[2] Zanin M., Boccaletti S., Complex networks analysis of obstructive nephropathy data, Chaos: An Interdisciplinary Journal of Nonlinear Science, 21, 3, 2011
[3] Buldú Javier M., et al, Reorganization of Functional Networks in Mild Cognitive Impairment, PLoS ONE. Public Library of Science, 6, 5, 2011
[4] Boccaletti S., et al, Complex networks: Structure and dynamics, Physics Reports, 424, 4-5, 175-308, 2006

# Synchronization in delayed mutually coupled optoelectronic oscillators

Jade Martínez-Llinàs*, Pere Colet
*Instituto de Física Interdisciplinar y Sistemas Complejos IFISC (CSIC-UIB)*
*Campus Universitat de les Illes Balears, E-07122 Palma, Spain*

In this work we study the synchronization between two delayed mutually coupled optoelectronic oscillators with intrinsic delay. In particular we consider the interplay of the different delays in achieving synchronized behavior. We analyze the stability of the synchronized solutions computing the spectrum of Lyapunov exponents.

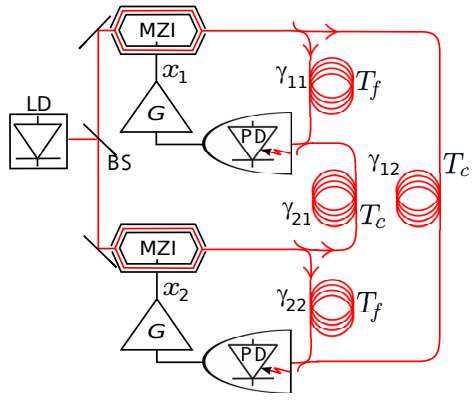


FIG. 1. Setup.

The setup is based on two electro-optical delay systems mutually coupled as shown in FIG. 1. Light from a cw semiconductor laser (LD) is splitted into two beams, each of which enters a system[1] with a Mach-Zender Interferometer (MZI). A fraction of light $\gamma_{ii}$ enters the electro-optical loop of oscillator $i$ with self-feedback delay $T_{ii} = T_f$, while a fraction $\gamma_{ij,j\neq i}$ is coupled to oscillator $j$ with coupling delay $T_{ij,j\neq i} = T_c$. Light is detected by a photo-diode (PD) and the electrical signal goes through a band-pass amplifier of gain $G_i$ and low and high cut-off characteristic times $\theta_i = 5\mu s$ and $\tau_i = 25ps$, respectively. The dynamics of the electrical signal $x_i$ is:

$$x_i(t) + \tau_i \frac{dx_i}{dt}(t) + \frac{1}{\theta_i}\int_{t_0}^{t} x_i(s)ds = \beta C_i,$$
$$C_i = \gamma_{ii}^2 \cos^2(z_{ii}) + \gamma_{ji}^2 \cos^2(z_{ji}) + \\ + 2\gamma_{ii}\gamma_{ji}\cos(z_{ii})\cos(z_{ji})\cos(z_{ii} - z_{ji}),$$

where $i, j = 1, 2$, $z_{ji} = x_j(t - T_{ji}) + \phi_j$, $\phi_i$ is an offset phase and $\beta$ is proportional to the pump power.

Here we keep fixed $\gamma_{11} = \gamma_{12} = 0.5$ and $\phi_i = 0.25\pi$. For very low values of $\gamma_{22}$ and $\gamma_{21}$ (a configuration similar to unidirectional coupling) increasing $\beta$ we find steady states, periodic solutions of period $2T_f$ and chaotic solutions. For intermediate values of $\gamma_{22}$ or $\gamma_{21}$, the $2T_f$ periodic solutions become unstable, but we find other periodic solutions in certain cases. More precisely, when $T_c$ and $T_f$ satisfy the ratio $T_c/T_f = (2m + 2)/(2m + 1)$ for any integer $m \geq 0$, there are multiple stable periodic solutions with period $T_m = 2T_l/(2m + 1)$, being $T_l = T_c - T_f$. In these solutions, $x_1$ and $x_2$ are anitisynchronized with zero lag: $x_2(t) = -x_1(t)$. An example is shown in FIG.2, where almost square waveforms arise for $\tau_i << T_c = 40ns$, $T_f = 30ns << \theta_i$. From the Lyapunov spectrum shown in FIG.3, one can identify a region in the parameter space of $\gamma_{22} = \gamma_{21}$ where two exponents are zero and the rest are negative; this reveals that this solutions exhibit stability and double periodicity. Further increasing the pump or the coupling, periodic solutions become unstable and the system gets chaotic.

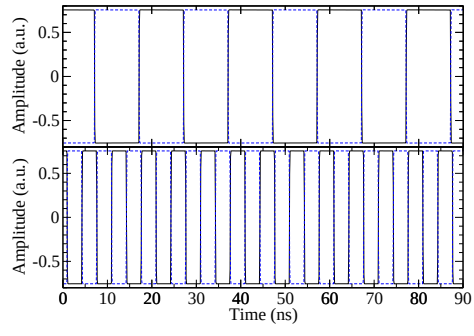


FIG. 2. Stable periodic solutions synchronized in antiphase with fundamental frequency (top panel, $m = 0$) and first harmonic (lower panel, $m = 1$). We have taken $\beta = 5$ and $\gamma_{22} = \gamma_{21} = 0.05$.

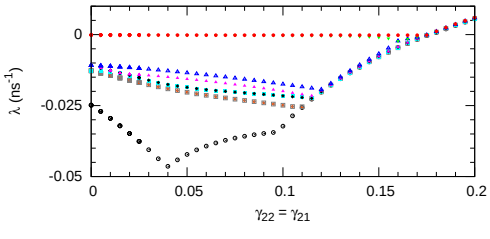


FIG. 3. First nine Lyapunov exponents of trajectories with periodicity shown in top panel in FIG.2, $\beta = 5$ and coupling $\gamma_{22} = \gamma_{21}$. Stability is lost around $\gamma_{22} = \gamma_{21} = 0.175$, where one Lyapunov exponent becomes positive.

[1] J. P. Goedgebuer, P. Levy, L. Larger, C.-C. Chen, and W.T. Rhodes, IEEE J. Quantum Electron. **38**, 1178 (2002).

* jade@ifisc.uib-csic.es

# Calculation of surface tension in a confined hard cut spheres liquid crystal using Monte Carlo simulation

Martín Pérez-Rodríguez, Manuel M. Piñeiro*
*Departamento de Física Aplicada, Universidade de Vigo*

**Introduction**. Monte Carlo simulations of slab confined hard cut spheres (HCS) have been performed to investigate the liquid crystal structure behavior and the confinement influence, by means of order parameter (OP), radial distribution function (RDF) and surface tension ($\gamma$).

The system definition was inspired by a previous work[1], and consisted of hard cut spheres of aspect ratio $L/D = 0.1$ (being $D = 1$ the particle diameter, considered as length scaling unit). The particles were confined between two fixed parallel walls separated by 6 length units in the $z$ direction. In addition, two types of confining walls were considered: hard walls, which exclude the particle completely and adsorbent walls, which exclude only the center of mass. $6 \cdot 10^6$ cycles were considered for final simulations, after testing pressure and density results from $2 \cdot 10^6$ to $8 \cdot 10^6$, being the first half of the simulation considered as stabilization and the remaining as production steps. Simulations were performed first in the $NPT$ ensemble, at pressures in the range $[0.5-9.0] \cdot 10^{-19}$ (reduced units) in steps of $0.5 \cdot 10^{-19}$ to asses the transition regions. Further simulations were performed from $1.5 \cdot 10^{-19}$ to $6.0 \cdot 10^{-19}$ in steps of $0.1 \cdot 10^{-19}$ to better determine the system behavior. To quantitatively characterize the system structure, the usual[2] order parameters were calculated in each simulation. Confinement effects were investigated by means of surface tension, which was calculated using the classical mechanical route, by determining the components of the pressure tensor, and in this case a recent method to compute either expansive and contractive contributions was applied[3]. When the expansion term is considered separately, an interesting result emerges: in a non confined system, an isotropic expansion produces some overlap only in concave particles; but in a confined one, a planar surface can effectively produce overlap, resulting in a non negligible contribution that may even change the surface tension sign.

**Results**. Expected isotropic ($I$) and nematic ($N$), and three additional higher pressure mesophases[4], disordered columnar ($C_D$), ordered hexatic columnar ($C_H$), and columnar solid ($C_S$), have been identified in the pressure range under consideration. Different order parameters account for the corresponding transitions, being the nematic order parameter main probe for $I - N$ transition, while the transitions between the columnar phases are determined by the appearance of order in the plane $xy$, parallel to the confining walls. $P^*(\rho^*)$ trend was useful to register the existence of all transitions. However it was not useful to asses neither the type of phase nor the internal structure of the system. The nonlinearity at higher pressures gave us a clue about the possibility of the last phase to be (almost) solid. Interestingly enough, surface tension expansion contribution has been observed to be a good descriptor of all the transitions in the bulk. Moreover, this capability of the expansion term could be easily generalized to non confined systems through the use of anisotropic expansions, considering the expansion in a $z$ confined slab to be equivalent to an anisotropic expansion limited to the plane $(x, z)$.

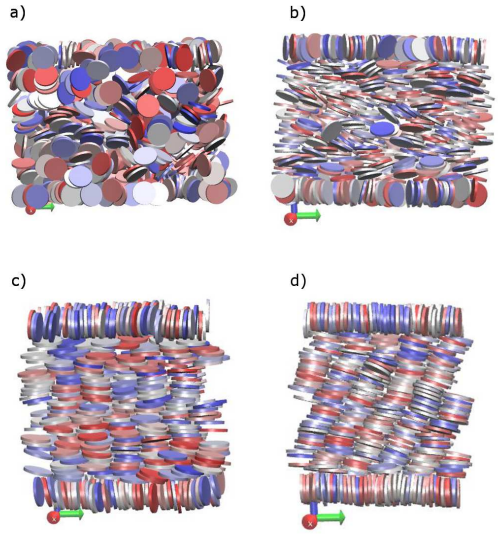


FIG. 1. Illustrative examples of observed mesophases in the adsorbent walls case. a) Isotropic ($P^* = 2.0 \cdot 10^{-19}$), b) Nematic ($P^* = 3.0 \cdot 10^{-19}$), c) Columnar hexatic ($P^* = 5.0 \cdot 10^{-19}$), d) Columnar solid ($P^* = 6.0 \cdot 10^{-19}$). Note that in d) the columns are tilted, arguably due to the effect of spherical surface on the particle rim, which causes the contact angle between a pair of particles to be greater than 0 at such high pressures. This effect was observed in all simulations above the $C_H - C_S$ transition.

* mmpineiro@uvigo.es

[1] M. M. Piñeiro, A. Galindo, A. O. Parry, *Soft Matter*, **3**, 768, (2007).
[2] E. M. del Río, E. de Miguel, *Phys. Rev. E*, **55**, 2916 (1997).
[3] P.E. Brumby, A. J. Haslam, E. de Miguel, G. Jackson, *Mol. Phys.*, **1**, (2010).
[4] Comparable but not equivalent structures to previously reported for unconfined hard cut spheres in: A. Cuetos, B. Martínez-Haya, *J Chem. Phys.*, **1**29, 214706, (2009).

# Efecto de la polidispersidad y asimetría de partículas oblatas en los diagramas de fases de emulsiones coloidales

Y. Martínez-Ratón[1] y E. Velasco[2]

[1] *Grupo Interdisciplinar de Sistemas Complejos (GISC). Departamento de Matemáticas, Universidad Carlos III de Madrid, Leganés, Madrid.*

[2] *Departamento de Física Teórica de la Materia Condensada, Universidad Autónoma de Madrid, 28049 Madrid.*

Es de sobra conocido que un fluido de partículas anisótropas discoidales que interaccionan con potenciales de corto alcance y extremadamente repulsivos presenta un diagrama de fases que incluye a las fases fluidas isótropa y nemática[1]. Resultados experimentales recientes de suspensiones discoidales polidispersas del mineral $\alpha$-zirconium fosfato previamente exfoliado muestran unos diagramas de fases muy peculiares. En dichas suspensiones las partículas son muy asimétricas (la relación de aspecto suele ser muy alta), poseen un grosor fijo y son altamente polidispersas en diámetro. Dichas peculiaridades se pueden resumir en dos: (i) Para algunas relaciones de aspecto la coexistencia isótropo-nemático presenta un enorme ensanchamiento de su zona de inestabilidad. (ii) La fracción de volumen que ocupa el nemático en función de la densidad total de partículas presenta un comportamiento altamente no lineal cuando la polidispersidad es relativamente alta[2,3].

En este trabajo presentamos un modelo teórico basado en la técnica del funcional de la densidad en el que se incluye la polidispersidad de las partículas oblatas. Con este modelo logramos explicar las peculiaridades anteriormente mencionadas dilucidando sus causas fundamentales. Aparte de la relación de aspecto y del grado de polidispersidad, la forma específica de la función de distribución en diámetros (como su grado de asimetría, su bimodalidad y su decaimiento) es crucial a la hora de predecir adecuadamente los resultados experimentales.

---

[1] J. A. C. Veerman and D. Frenkel, Physical Review A 45 5632-5648 (1992)

[2] D. Sun, H.-J. Sue, Z. Cheng, Y. Martínez-Ratón y E. Velasco.

[3] A. F. Mejia, Y.-W. Chang, R. Ng, M. Shuai, M. S. Mannan and Z. Cheng, preprint (2012).

## Universal reference state in a driven homogeneous granular gas

María Isabel García de Soria, Pablo Maynar*, and Emmanuel Trizac
*Física Teórica, Universidad de Sevilla, Apartado de Correos 1065, E-41080, Sevilla, Spain*

We study the dynamics of a homogeneous granular gas heated by a stochastic thermostat, in the low density limit. It is found that, before reaching the stationary regime, the system quickly "forgets" the initial condition and then evolves through a universal state that does not only depend on the dimensionless velocity, but also on the instantaneous temperature, suitably renormalized by its steady state value. We find excellent agreement between the theoretical predictions at Boltzmann equation level for the one-particle distribution function, and Direct Monte Carlo simulations. We conclude that at variance with the homogeneous cooling phenomenology, the velocity statistics should not be envisioned as a single-parameter, but as a two-parameter scaling form, keeping track of the distance to stationarity[1].

* maynar@us.es

[1] M. I. García de Soria, P. Maynar, and E. Trizac, Phys. Rev. E **85**, 051301 (2012)

# Sobre el oscilador logarítmico como termostato

Marc Meléndez Schofield*
*Dpto. Física Fundamental UNED. Senda del Rey, 9, 28040 Madrid*

Campisi, Zhan, Talkner y Hänggi han propuesto el uso del oscilador logarítmico como termostato, tanto en simulaciones numéricas como en sistemas experimentales pequeños, tales como clusters de átomos[1]. Un oscilador logarítmico no es más que una masa puntual $m$ en el seno de un potencial central logarítmico. El hamiltoniano del sistema es

$$H(q,p) = \frac{p^2}{2m} + k_B T \ln\left(\frac{\|q\|}{b}\right)$$

donde $k_B T$ y $b$ son parámetros arbitrarios del sistema. El factor que multiplica al logaritmo se escribe como $k_B T$ debido a que el promedio temporal de la energía cinética resulta ser para este sistema

$$\left\langle \frac{p^2}{2m} \right\rangle_t = \frac{1}{2} k_B T,$$

(siendo $k_B T$ *precisamente* el valor introducido en el hamiltoniano). Esto significa que la "temperatura" del oscilador es igual a $T$ independientemente de su energía $E$. Basándose en esta propiedad, Campisi y sus colaboradores han demostrado que, si el oscilador interacciona de manera débil con un sistema de interés, entonces acaba induciendo en éste una dinámica que muestrea los estados de la colectividad canónica. Este "termostato" presenta, por tanto, dos características muy atractivas: primero, tiene una dinámica hamiltoniana determinista[2] relativamente sencilla, y, segundo, se pueden diseñar en principio experimentos en los que una partícula física se comporta de forma parecida a un baño térmico[1].

En las simulaciones numéricas, se puede evitar la singularidad en el potencial aproximando el hamiltoniano expuesto más arriba mediante

$$H(q,p) = \frac{p^2}{2m} + \frac{1}{2} k_B T \ln\left(\frac{\|q\|^2 + b^2}{b^2}\right),$$

que da lugar a trayectorias en el espacio de fases como las que se muestran en la figura.

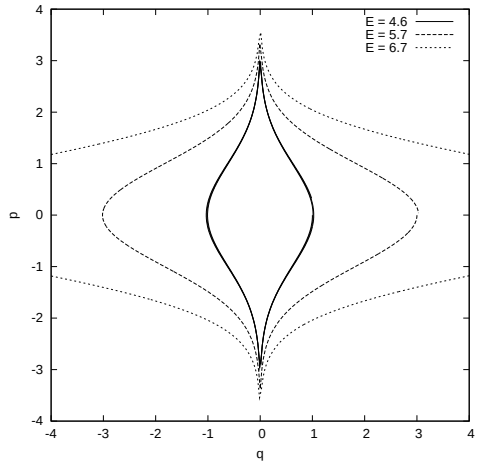


FIG. 1. Trayectorias aproximadas del oscilador logarítmico en el espacio de fases para diferentes valores de la energía $E$ ($k_B T = 1$ y $b = 10^{-2}$).

Sin embargo, nuestro análisis revela que el oscilador logarítmico no puede utilizarse en la práctica como termostato debido a que las elongaciones máximas $q_{max.}$ y los periodos entre dos estados de máxima elongación $\Delta t$ dependen exponencialmente de la energía $E$ del oscilador.

$$q_{max.} \propto b e^{\beta E},$$

$$\Delta t \propto b e^{\beta E},$$

donde $\beta = (k_B T)^{-1}$. Por lo tanto, cuando el oscilador absorbe energía del sistema que se desea simular, se aleja progresivamente de él y realiza revoluciones cada vez más lentas, lo cual provoca una convergencia extremadamente lenta a la temperatura de equilibrio deseada.

* mmelendez@fisfun.uned.es

[1] M. Campisi, F. Zhan, P. Talkner and P. Hänggi, *Logarithmic oscillators: Ideal Hamiltonian Thermostats*, arχiv 1203.5968v3 (2012) [cond-mat.stat-mech].

[2] M. Campisi, F. Zhan, P. Talkner and P. Hänggi, *Reply to Hoover [arXiv: 1204.0312v2]*, arχiv 1204-4412v1 (2012) [cond-mat.stat-mech].

# El intercambio de energía entre sistemas hamiltonianos desde la teoría del coarse-graining

Marc Meléndez Schofield*
*Dpto. Física Fundamental UNED. Senda del Rey, 9, 28040 Madrid*

Pep Español Garrigós
*Dpto. Física Fundamental UNED. Senda del Rey, 9, 28040 Madrid*

Cuando varios sistemas hamiltonianos intercambian energía mediante una interacción débil, se produce una tendencia al equilibrio térmico si la dinámica presenta la propiedad de *mixing*[1]. Utilizando la técnica de operadores de proyección de Zwanzig[2] se puede escribir una ecuación de evolución para la probabilidad $P(e,t)$ de que cada uno de los sistemas en interacción tenga una energía dada.

En el caso de que se cumpla además la *hipótesis de variables lentas*, esta ecuación para la probabilidad se convierte en una *ecuación de Fokker-Planck*.

$$\frac{\partial P(e,t)}{\partial t} = \frac{\partial}{\partial e_j} v_j(e) P(e,t) + \frac{\partial}{\partial e_j} \Omega(e) D_{jk}(e) \frac{\partial}{\partial e_k} \frac{P(e,t)}{\Omega(e)},$$

donde las funciones $\Omega(e)$, $v_j(e)$ y $D_{jk}(e)$ están definidas en términos de la dinámica microscópica. Las predicciones de esta ecuación se ajustan a las simulaciones de dinámica molecular si los sistemas cumplen la hipótesis antes mencionada (véase el ejemplo de la figura 1).

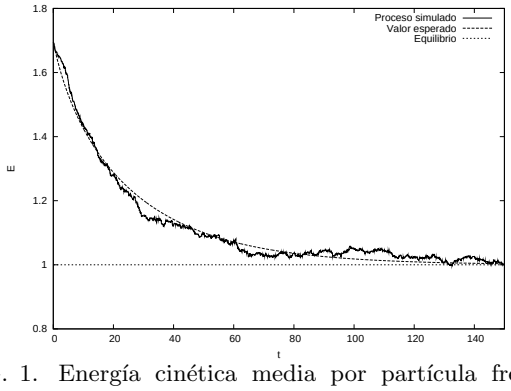


FIG. 1. Energía cinética media por partícula frente al tiempo de un gas de esferas duras que se equilibra con otro de las mismas características pero menor temperatura (*línea continua: simulación de dinámica molecular; línea discontinua: valor esperado calculado con la ecuación de Fokker-Planck; puntos: energía correspondiente al estado de equilibrio*).

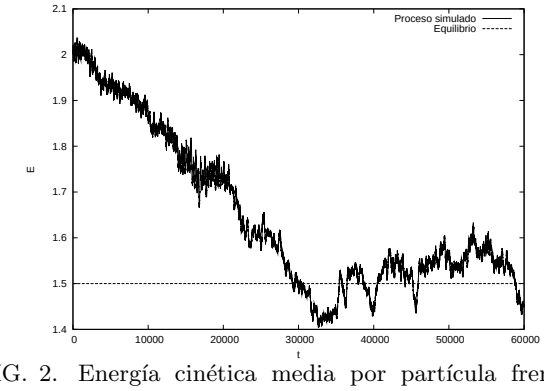


FIG. 2. Energía cinética media por partícula frente al tiempo de una cadena de osciladores no lineales que se equilibra con otra de las mismas características pero menor temperatura. La dinámica difiere apreciablemente de la que predice la ecuación de Fokker-Planck.

Sin embargo, si existen gradientes térmicos apreciables en el seno de los sistemas en interacción o si unos sistemas realizan trabajo macroscópico sobre otros, es decir, si no se cumple la hipótesis de variables lentas, entonces no se puede derivar la ecuación de Fokker-Planck mencionada antes y se deben tener en cuenta los efectos de memoria. Incluso si los sistemas han alcanzado el equilibrio térmico por separado y se permite que intercambien energía con un acoplamiento global y débil, es posible que aparezcan dinámicas no markovianas en la tendencia al equilibrio térmico. Nuestro análisis del equilibrado térmico entre dos sistemas de Fermi-Pasta-Ulam reveló este tipo de proceso no markoviano debido al intercambio de energía entre los modos de vibración más lentos de ambos sistemas (figura 2).

* mmelendez@fisfun.uned.es

[1] J. Español, F.J. de la Rubia, and J.M. Rubí, *Mixing and Equilibrium Probability Densities in Classical Statistical Mechanics*, Physica A 187, 589 (1992).

[2] Grabert, H. *Projection Operator Techniques in Nonequilibrium Statistical Mechanics*. Springer Tracts in Modern Physics, 95 (1982).

# The evolution of communication ties

Giovanna Miritello[1,2], Rubén Lara[2], and Esteban Moro[1,3,4]
[1] *Departamento de Matemáticas & GISC, Universidad Carlos III de Madrid, 28911 Leganés, Spain*
[2] *Telefónica Research, Madrid, Spain*
[3] *Instituto de Ciencias Matemáticas CSIC-UAM-UCM-UC3M*
[4] *Instituto de Ingeniería del Conocimiento, Universidad Autónoma de Madrid, 28049 Madrid, Spain*

The dynamics of social networks is highly articulated and evolves as a result of the joining and leaving of nodes and the creating, reinforcing, weakening and dissolution of ties[1–4]. Understanding the evolution of social ties is not only useful to characterize human behavior, but also to understand and model its impact on dynamical processes such as diffusion of information, passage of opinions, community formation. In recent years, there has been a large interest in characterizing the structure and dynamical triggers of link formation and decay. However, little is known about how to model the dynamical process of tie evolution. In most studies it is assumed that a tie forms at the moment the communication is observed[5]. However, the dynamics of ties formation/decay is entangled with the very dynamics of communication, which is characterized by bursts of events and heavy-tailed distributed inter-event times[6]. If many efforts have been spent to characterize the burstiness of communication events and understand the underlying mechanism leading to such a human activity pattern, much less is known about the dynamics of ties formation/decay. The main reason for this lack of understanding is based on the believe that tie formation/decay is a much slower process than tie interactions and that available data is restricted to small networks or short periods of time.

Here we address the problem of how ties form/decay by studying the mobile phone communication network of about 20 million people over a long period of 19 months. This long database allows us to consider three time windows, focus on the links evolution in the window in the middle and use the right and left intervals to assess whether a tie exists before and after the observation window. By doing this we are able to disentangle the links formation/decay from the burstiness of communication thus analyze the temporal evolution of social ties with high precision. Our results show that most people form/remove communication ties almost constantly in time with a given rate $\alpha_i$. More interestingly, we find that users tend to balance the formation/deletion of edges which yields to a steady number of open relationships maintained by people over time. This suggest that people have finite social capacity $\kappa_i$ and that the number of interactions (the connectivity $k_i$) observed in a time window is a function of both the social capacity $\kappa_i$ and the rate of formation of edges. Finally, we find that the evolution of communication ties affects information diffusion. In particular the turnover of the social network over time due to the evolution of ties hinders the propagation.

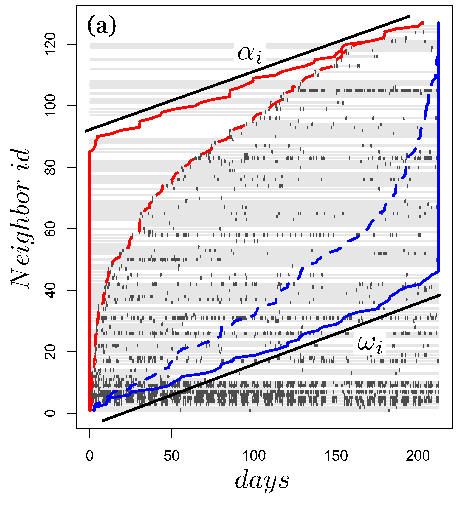


FIG. 1. Schematic view of the dynamics of tie formation/decay and the interplay between tie communication patterns and tie dynamics for a single user and a given observation time window $T = 7$ months. Each black vertical line is a communication event. Solid red/blue curves are the aggregated open/closed links at a given time (including those open/close outside the time window), while dashed lines are the observed open/closed links only within the time window.

[1] Grindrod, P. & Higham, D.J., 2011. Models for evolving networks: with applications in telecommunication and online activities. IMA Journal of Management Mathematics, 23(1), pp.1-15.
[2] Holme, P., 2003. Network dynamics of ongoing social relationships. Europhys. Lett., 64(cond-mat/0308544. NORDITA-2004-28), pp.427-433.
[3] Modeling the evolution of continuously-observed networks: Communication in a Facebook-like community, T. Opsahl, B. Hogan, arXiv:1010.2141v2 (2011).
[4] J. Leskovec, *et al.*, *Microscopic evolution of social networks.* In KDD '08: Proceeding of the 14th ACM SIGKDD international conference on Knowledge discovery and data mining. (2008).
[5] M. Karsai *et al.* Correlated dynamics in egocentric communication networks arXiv:1202.3062v1 (2012).
[6] G. Miritello, E. Moro, and R. Lara, Dynamical strength of social ties in information spreading. Phys. Rev. E (2011) vol. 83 (4) pp. 045102.

# Stability of Boolean Multiplex Networks

Emanuele Cozzo, Alex Arenas, Yamir Moreno*
*Instituto de Biocompytación y Física de Sistemas Complejos*
*Universidad de Zaragoza*
*Zaragoza 50018, Spain*

Nearly four decades ago, Random Boolean Networks (RBNs) were introduced as a way to theoretically address several scientific challenges regarding the description and dynamics of biochemical networks[1]. Since then, this framework has been successfully applied to model theoretically and computationally the biochemical and genetic control of cells[2]. RBNs consider that each gene of a genetic regulatory network is a node of a directed graph, the direction corresponding to the effect of one gene on the expression of another. Additionally, the nodes can be in one of two states: they are either *on* (1) or *off* (0) - i.e. in the case of a gene its target protein is expressed or not. The system so composed evolves at discrete time steps. At each time step nodes are updated according to a boolean rule assigned to each node that is a function of its inputs. Notwithstanding the high simplicity of RBNs models, they can capture the behavior of some real regulatory networks[3] allowing for the study of several dynamical features, above all their critical properties. However, although some coupled Boolean networks have been recently investigated[4,5], the vast majority of existent works have considered RBNs as *simplex* networks, in which a single graph is enough to represent all the interactions a given gene is involved in.

The previous description implicitly assumes that all biochemical signals are equivalent and then collapses information from different pathways. Actually, in cellular biochemical networks, many different signaling channels do actually work in parallel, i.e., the same gene or biochemical specie can be involved in a regulatory interaction, in a metabolic reaction or in another signaling pathway. Therefore, a more realistic set up will be obtained by considering the participation in different pathways as different interconnected layers of interaction, something more consistent with a multiplex network[6,7] representation (see Fig. 1). Namely, each level in the multiplex would represent the different signaling pathways or channels the element participates in.

In this work, we study the stability of Boolean networks defined at multiple topological layers. In particular, we inspect a Boolean multiplex network model, in which each gene is a node that participates in one or more layers of interactions. Moreover, we focus on the case of canalizing rules, which has been shown to be relevant to genetic networks. Boolean functions are canalizing if whenever the canalizing variable takes a given value, the canalizing one, the function always yields the same output. Capitalizing on a semi-annealed approximation, we analytically and numerically study the conditions defining the stability of the aforementioned system and show that the interplay between the different layers can be enough to stabilize different levels or the whole system even for parameter values where the sub-systems, if isolated, were unstable.

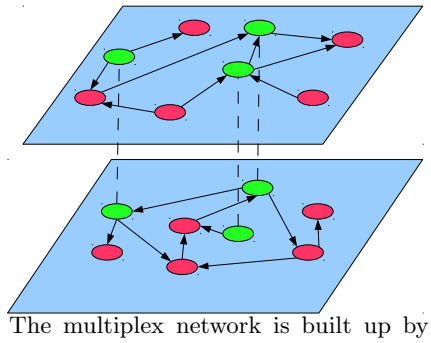

FIG. 1. The multiplex network is built up by randomly connecting $N$ nodes per layer. With probability $\sigma$, each of the $N$ nodes can be present in both layers. Therefore, the total number of *different nodes* in the system is $\tilde{N} = (2-\sigma)N$. In the example of the figure, the whole system is made up of $\tilde{N} = 13$ nodes, of which 3 are present in the two layers and there are 5 additional nodes per layer, therefore $N = 8$ and $\sigma = 3/8$.

* yamir.moreno@gmail.com

[1] S. Kauffman, *Curr. Top. Dev. Biol.*, **6**: 145-182, (1971).
[2] L.P. Kadanoff M. Aldana, S. Coppersmith. *Boolean dynamics with random couplings.* Springer, 2003.
[3] Y. Lu Q. Ouyang C. Tang F. Li, T. Long. *Proc. Natl. Acad. Sci. USA*, **101**, 4781 (2004).
[4] R. Serra *at. al*, In: *Proceedings of the European Conference on Complex Systems*, Dresden, October 1-5 (2007).
[5] R. Serra, M. Villani, C. Damiani, A. Graudenzi, A. Colacci, in *Lectures Notes Complex Systems* Vol. 5191, 315-322, Springer, Heidelberg (2009).
[6] P. J. Mucha, T. Richardson, K. Macon, M. A. Porter, J.-P. Onnela, *Science* **328**, 876 (2010).
[7] K.-M. Le *et. al.*, *N. J. Phys.* **14**, 033027 (2012).

# Simulación multiescala de la formación de patrones por irradiación

Ana Moreno*, Mario Castro†, Javier Muñoz-García‡ y Rodolfo Cuerno‡
*Instituto de Investigación Tecnológica, Universidad Pontificia Comillas, Madrid E-28015.*

Una de las promesas de la nanotecnología reside en la capacidad de producir estructuras ordenadas con al menos una escala del orden del nanómetro[1]. La erosión por bombardeo iónico es una técnica utilizada desde los años 60 y que es capaz de producir este tipo de estructuras de manera autoorganizada[2].

A pesar de que el proceso se conoce y se ha utilizado durante décadas, la Física que da lugar al tamaño y organización de estos patrones es controvertida. Recientemente se ha visto que el paradigma comúnmente aceptado (el llamado modelo de Bradley-Harper[3]) no es capaz de explicar las transiciones morfológicas rugoso-patrón ni, cuantitativamente, las escalas observadas en los experimentos.

Recientemente, Castro y Cuerno[4] han propuesto una teoría en la que el material bombardeado se puede modelar como un fluido (altamente) viscoso cuyo movimiento se debe al stress residual creado por los impactos de los iones y la consiguiente producción de defectos. Así, los iones crean una *capa amorfa* cerca de la superficie debido a las colisiones que ocurren en tiempos del orden de picosegundos. Esta capa amorfa *fluye* debido a la reorganización de defectos en escalas de tiempo varios órdenes de magnitud superiores.

En la Fig. 1 se muestra la capa amorfa producida tras el bombardeo de 200 iones de Xe de 100 eV de energía sobre una cristal de Si incidiendo a 45° con respecto a la superficie.

Una dificultad del sistema experimental es, precisamente, determinar de manera precisa el valor del stress. Por otra parte, los modelos teóricos tienen coeficientes macroscópicos que son difíciles de estimar a partir de primeros principios.

En este trabajo proponemos un método multiescala para conectar la física de la colisión y la hidrodinámica del flujo viscoso. Para ello, proponemos utilizar una descripción basada en la teoría de lubricación (en este caso justificada porque la capa amorfa es del orden de 1 nm para estas energías y los patrones del orden de 50 nm) utilizando medidas de stress a partir de simulaciones de dinámica molecular. Así, la altura de la superficie de silicio, $H(X,T)$, se describe mediante la ecuación (adimensionalizada)[4]

$$\partial_T H = -\partial_X \left[ (\tilde{\sigma}\partial_X^3 H + \partial_X \Sigma_n^{(ext)}) \frac{H^3}{3} + \Sigma_t^{(ext)} \frac{H^2}{2} \right], \quad (1)$$

donde $\Sigma_{n,t}^{(ext)}$ son, respectivamente, las proyecciones superficiales en la dirección normal y tangencial del tensor stress residual.

De este modo, midiendo dicho stress residual a partir de las simulaciones, se determinan numéricamente los coeficientes de la ecuación (1), lo que permite, *de facto*, abordar las escalas diversas involucradas en el problema. La ecuación resultante se puede integrar numéricamente utilizando esquemas de discretización adaptados a ecuaciones que obedecen leyes de conservación[5].

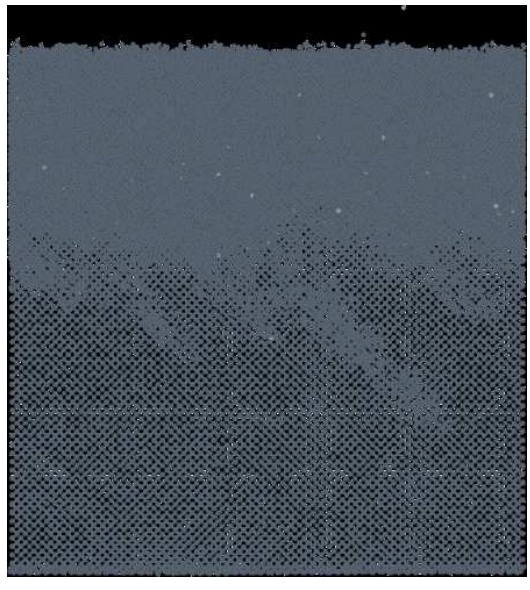

FIG. 1. Morfología de un cristal de silicio tras 100 impactos de iones de Xe de 100 eV de energía en incidencia a 45°. El potencial utilizado es un Tersoff interpolado mediate un potencial ZBL para tener en cuenta el efecto colisional a altas energías.

* ana.moreno@iit.upcomillas.es
† Grupo Interdisciplinar de Sistemas Complejos (GISC), Universidad Pontificia Comillas, Madrid E-28015.
‡ Departamento de Matemáticas y GISC, Universidad Carlos III de Madrid, Leganés E-28911.

[1] R. Cunningham, P. Haymann, C. Lecomte, W. Moore, and J. Trillat, Journal of Applied Physics **31**, 839 (1960).
[2] M. Navez, C. Sella, and D. Chaperot, Comptes Rendus. Académie des Sciences **254**, 240 (1962).
[3] R. Bradley and J. Harper, J. Vac. Sci. Technol. A **6**, 2390 (1988).
[4] M. Castro and R. Cuerno, Appl. Surf. Sci. **258**, 4171 (2012).
[5] L. Kondic, SIAM Review **45**, 95 (2003).

# Rare region effects in hierarchical networks

Paolo Moretti* and Miguel Ángel Muñoz
*Departamento de Electromagnetismo y Física de la Materia*
*Universidad de Granada. Fuentenueva s/n, E-18071, Granada*

Spreading processes on networks represent the paradigm for a broad variety of propagation phenomena taking place on non-trivial topologies. The way epidemics, computer viruses, rumors or cortical signals propagate is known to be affected by the topology of their underlying contact patterns, which often exhibit pronounced community structures. Communities rarely are interconnected at random. Instead, they are often organized in a hierarchical fashion, as it is commonly observed in cerebral networks[1,2].

Here we study the dynamics of spreading processes on hierarchical modular networks and discuss the emergence of rare-region effects due to the non-trivial topology of such contact patterns. We find that deep hierarchical structures are able to sustain network activity on rare regions for extremely long times. We relate this phenomenology to the degree-heterogeneity of the networks, their predicted epidemic threshold and their fractal nature. Our results are relevant for neurophysiological studies, which have recently highlighted the emergence of persistent sustained activity in cerebral cortical networks. In order to provide predictions for such systems, we discuss the complex interplay between the network topology and the dynamics implemented on it, showing to which extent simple dynamical processes are sufficient to capture the physics of rare-region effects and if a more realistic description of neuronal dynamics requires more specialized dynamical rules.

---

* pmoretti@onsager.ugr.es

[1] S. J. Wang, C. C. Hilgetag and C. Zohu, Frontiers in Computational Neuroscience, **30** 1 (2011)
[2] M. Rubinov, O. Sporns, J. P. Thivierge and M. Breakspear, PLoS Computational Biology, **7** e1002038 (2011)

# Pattern formation of nitrogen fixing cells in filamentous cyanobacteria

Javier Muñoz-García* and Saúl Ares†

* *Departamento de Matemáticas and Grupo Interdisciplinar de Sistemas Complejos (GISC), Universidad Carlos III de Madrid, 28911 Leganés, Spain*

† *GISC and Logic of Genomic Systems Laboratory, Centro Nacional de Biotecnología - CSIC, 28049 Madrid, Spain*

In the study of the transition between unicellular and multicellular forms of life with differentiated cell types, an important model organism are cyanobacteria. Cyanobacteria were the first organisms to use oxygenic photosynthesis and are currently one of the most successful living groups, occupying a broad range of habitats across all latitudes and producing 20-30% of Earth's photosynthetic activity. These cyanobacteria may form colonies consisting of a one-dimensional filament composed under normal conditions only of vegetative cells. However, as a response to different environmental stresses they can differentiate into specialized cell types that perform important functions for the survival of the colony[1].

Here we will focus on the case of heterocyst differentiation. Heterocysts are specialized cells able to fix atmospheric nitrogen into a chemical form usable by vegetative cells. Bacteria and archea are the only forms of life able to fix atmospheric $N_2$, making them crucial for all living forms on Earth. When external N-sources are scarce heterocysts appear in regular patterns, with intervals of around 10 vegetative cells between consecutive heterocysts, representing a paradigmatic example in pattern formation of developing biological systems[2]. Since a continuous outer membrane covers the whole filament, the fixed nitrogen produced by heterocysts can diffuse through the periplasm and reach the vegetative cells. In turn, nutrients produced by photosynthesis in vegetative cells are also shared and reach the heterocysts.

The biology of this differentiation process has been the subject of several studies (for recent reviews see for example Refs. 1, 3). Most of these genetic studies have been focused on a particular species named Anabaena sp. PCC 7120 (also known as Nostoc sp. PCC 7120), which has become a prototypical organism in this field. However, theoretical models are scarce and the inclusion of recently discovered genetic regulations is still lacking.

In this study we formulate a theoretical description of heterocyst pattern formation that includes the genetic regulations between the main genes identified in the process, such as hetR, patS, and hetN. This description has been coded using an object-oriented platform based on systems of stochastic reaction-diffusion differential equations for each cell, with variables representing the concentration of each molecular species. We reproduce qualitatively and quantitatively some of the main features of the observed differentiation process, including the appearance of heterocysts forming a quasi-regular pattern. Our results are in good agreement with experimental observations in wild type and mutants of Anabaena sp. PCC 7120, adding support for the regulatory relations in our model and allowing to make predictions on the role of recently described genes.

---

* javiermunozgarcia@gmail.com
`http://gisc.uc3m.es/~javier`

[1] E. Flores and A. Herrrero, *Nat. Rev. Microbiol.* **8**, 39 (2010).
[2] L. G. Morelli, K. Uriu, S. Ares, and A. C. Oates, *Science* **336**, 187 (2012).
[3] K. Kumar, R. A. Mella-Herrera, and J. W. Golden, *Cold Spring Harb. Perspect. Biol.* **2**, a000315 (2010).

# Microscopic tip fluctuations drive the morphology of macroscopic Fisher fronts

Svetozar Nesic[1], Rodolfo Cuerno[1], Esteban Moro[1,2,3]
[1] *Departamento de Matemáticas & GISC, Universidad Carlos III de Madrid, 28911 Leganés, Spain*
[2] *Instituto de Ciencias Matemáticas CSIC-UAM-UCM-UC3M*
[3] *Instituto de Ingeniería del Conocimiento, Universidad Autónoma de Madrid, 28049 Madrid, Spain*

We have investigated the dynamics of the morphology of Fisher waves subjected to small intrinsic noise, as described by the Fisher-Kolmogorov-Petrovsky-Piscounov (FKPP) equation,[1]

$$\frac{\partial \rho}{\partial t} = D\Delta\rho + \rho - \rho^2 + \sqrt{\rho/N}\ \eta(x,t), \qquad (1)$$

where $\eta(x,t)$ is a Gaussian white noise and $N$ is approximately the number of particles per unit volume.[2] For $N = N_c$, equation (1) undergoes a phase transition between an active phase ($\rho \neq 0$) and an absorbing state ($\rho = 0$).[4–6] In addition, for very large $N \gg N_c$ the FKPP equation displays *pulled fronts* in which the active phase invades the absorbing state.[3] Although intrinsic noise is really small for large $N$, it produces strong corrections to the velocity of the front when compared to the deterministic $N \to \infty$ equation.[8]

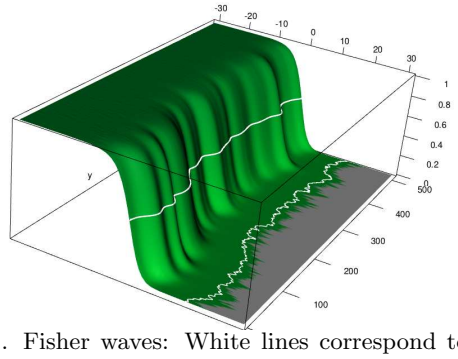


FIG. 1. Fisher waves: White lines correspond to equipotential lines at $\rho = 1/2$ (front) and $\rho = 1/N$ (cut-off). The light gray color represents the area where $\rho = 0$.

In this communication we study whether those strong corrections also happen in the kinetic roughening of the front. Using a non-negativity preserving algorithm to integrate equation (1),[5,6] we have found that the large-scale fluctuations in the morphology of the front line, see Fig. 1, belong to the 1D Kardar-Parisi-Zhang (KPZ) universality class.[7] As in the zero-dimensional case,[9] we find that the dynamics of the front in the cut-off microscopic line where $\rho \simeq 1/N$ (see Fig. 1) drive the dynamics of the macroscopic system (see Fig. 2). On the left panel of this figure, we show the time evolution of the roughness for both the front and the cut-off lines. Although the small-scale behavior is strictly different (see zoom in inset), the large-scale properties are indistinguishable. Hence, the 1D KPZ asymptotic behavior of the cut-off line is inherited by the front line, see right panel in the same figure, where the power spectral density function (PSD) is shown for both lines at long times. Notice that the strong short-scale fluctuations in the cut-off line are suppressed for the front, that looks much smoother at such scales, see Fig. 1. Morever we have also found that the 1D dynamics of the cut-off line propagates back to the front line (see inset of Fig. 2) and that it happens with a time ag that depends logarithmically on $N$.

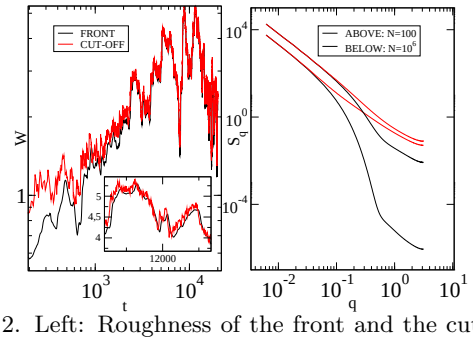


FIG. 2. Left: Roughness of the front and the cut-off lines vs time (single realiaztions). Inset: Zoom of main panel. Right: PSD functions of front (lower curves) and cut-off (upper curves) lines vs wave-vector $q$ for times $t > 10^4$, for two values of $N$. For small $q$ (long-rage correlations), the front and cut-off display the same behavior, which is not the case for small $q$.

We have thus found that the large-scale dynamics of the macroscopic front is determined by the evolution of the region that is driven by microscopic fluctuations, which is an unusual effect in front dynamics and creates macroscopic observable effects from microscopic noise.

[1] R. A. Fisher, Ann. Eugenics VII, 355 (1936); A. Kolmogorov, I. Petrosvky, and N. Piscounov, Moscow Univ. Bull. Math. A **1**, 1 (1937).
[2] N. G. van Kampen, *Stochastic Processes in Physics and Chemistry* (North-Holland, 1992); C. W. Gardiner, *Handbook of Stochastic Methods*, (Springer-Verlag, Berlin 1985).
[3] W. van Saarloos, Phys. Rep. **386**, 29 (2003); D. Panja, *ibid.* 393, 87 (2004).
[4] H. Hinrichsen, Adv. Phys. **46**, 815 (2000).
[5] E. Moro, Phys. Rev. E **70**, 045102(R) (2004)
[6] I. Dornic, H. Chate, and M. A. Muñoz, Phys. Rev. Lett. **94** 100601 (2005).
[7] A.-L. Barabási and H. E. Stanley, *Fractal Concepts in Surface Growth* (Cambridge University Press, Cambridge, England, 1995).
[8] E. Brunet and B. Derrida, Phys. Rev. E **56**, 2597 (1997); J. Stat. Phys. **103**, 269 (2001).
[9] E. Brunet, B. Derrida, A. H. Muller, and S. Munier, Phys. Rev. E **73**, 056126 (2006).

# A reaction-diffusion system to model symmetry-breaking in the C. elegans worm

Ernesto M. Nicola[†*], N.W. Goehring[‡], P. Khuc Trong[§‡], J.S. Bois[§‡], D. Chowdhury[§‡], A.A. Hyman[‡] and S.W. Grill[§‡]

[†] *IFISC, Instituto de Física Interdisciplinar y Sistemas Complejos CSIC-Universidad de las Islas Baleares 07122-Palma de Mallorca, Spain*

[‡] *Max-Planck Institute of Molecular Cell Biology, Dresden, Germany*

[§] *Max-Planck Institute of the Physics of Complex Systems, Dresden, Germany*

The main aim of a signaling pathways in cells is the transduction of a signal. These pathways regulate the cellular response to external cues. Such a situation occurs for example during cell polarization, where the cell undergoes a symmetry-breaking process in response to a weak external cue. Most cells have polarity and consequently have two different sides. A case where this is evident is for the cells that form the skin, which have an inside and outside. The study of the mechanisms by which cells become polarized is very important. These mechanisms are actually very similar for all animals[1].

A standard model organism where cell polarization has been studied extensively[1] is the nematode worm *Caenorhabditis elegans*. A group of genes (called the PAR genes) are in charge of the regulation of cell polarity in *C. elegans* and many other organisms. Prior to the first unequal cell division in the *C. elegans* embryo, the PAR proteins become distributed asymmetrically in distinct anterior and posterior domains[2,3].

A possible way of describing mathematically this problem is with a two-variable reaction-diffusion system. In this model each variable describes the concentration of a group of PAR proteins. The model accounts for the segregation of the PAR proteins and this separation can be triggered either convectivelly by cortical flows or spontaneously by random perturbations. In a recent publication appeared in *Science*[4], we have shown that the spontaneous symmetry-breaking leading to the polarization of the cell is induced by a mechanism similar to a Turing instability. However, in our model the fastest growing spatial perturbation's wavelength is equal to the system size. Many features of this model are in agreement with experimental observations in *C. elegans*. In Ref.[4], we have been also able to experimentally measure many of the model's parameters.

---

* ernesto.nicola@ifisc.uib-csic.es

[1] Pellettieri and Seydoux, Science **298**, 1946 (2002).

[2] Grill, Gonczy, Stelzer and Hyman, Nature **409**, 630(2001).

[3] Grill, Howard, Schaffer, Stelzer and Hyman, Science **301**, 518 (2003).

[4] N.W. Goehring, P. Khuc Trong, J.S. Bois, D. Chowdhury, E.M. Nicola, A.A. Hyman and S.W. Grill, *Polarization of PAR proteins by advective triggering of a pattern forming system*; **Science 334**, 1137-1141 (2011).

# Image Analysis of the Cavitation Process in Pressure Sensitive Adhesives

Matteo Nicoli*, François Tanguy†, Costantino Creton†
*Physique de la Matière Condensée, École Polytechnique, CNRS, 91128 Palaiseau, France.*

Pressure sensitive adhesives (PSAs) are viscoelastic or viscoplastic materials that adhere to a substrate upon the application of light pressure[1]. A well known example of a PSA is the sticky layer on Scotch® tape. A good PSA is obtained when the material has a liquid-like behavior to create easily a molecular contact and dissipate energy upon debonding, and an elastic behavior to resist shear forces over long times. This dual property is especially important on rough surfaces and low energy surfaces.

Although recent advances in mesoscale modeling of the rheological properties of PSAs have greatly improved our knowledge about the bulk behavior of such materials[2], the debonding mechanism is essentially an interfacial process and it is still poorly understood. In fact, the detaching of PSAs is due to different phenomena, such as the creation of cavities and fibrils, the propagation of interfacial cracks and the lateral invasion of air fingers into the sample.

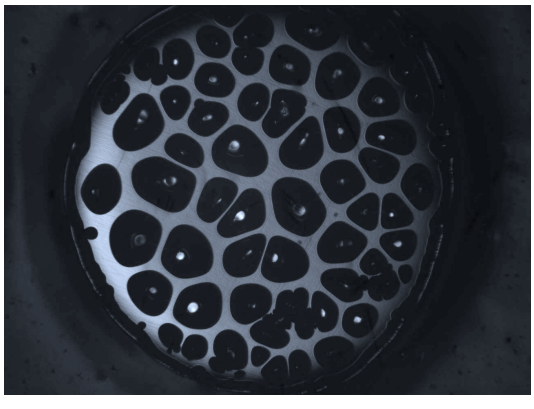

FIG. 1. Top view of the probe tack experiment. The PSA material is transparent and the black regions are the interface of the cavities.

The studies of adhesive performances of these materials are efficiently carried out through the so-called probe tack tester. In this test a flat ended probe (of a diameter of 10 mm) is brought in contact with a thin adhesive layer and is then removed at a controlled velocity[3]. Typically, force versus displacement curves are measured and the adhesion energy is calculated as integral of these curves in the debonding phase. Besides, taking advantage of the transparency of the PSA, additional information regarding the interfacial events occurring during the debonding phase can be obtained by inspecting the sample with a standard optical microscope and a digital video camera, see Figure 1. This imaging technique allows one to detect curved interfaces between trapped gas in cavities (or air in fingers) and the PSA from a top view perspective (a two-dimensional projection of the real three-dimensional space).

Here we have developed a boundary recognition algorithm in order to analyze the digitalized frames from probe tack experiments. This methodology allowed us to detect the nucleation of cavities, track their growth during the detachment process and measure various geometrical quantities, such as the equivalent area, the eccentricity, and so on. We have verified the reproducibility of our measurements over different experiments under the same conditions. From the data of the projected cavities we can obtain the load bearing area and estimate the magnitude of the shear stress from the nominal force measured during the experiment and the knowledge of the uniaxial tensile stress.

We have analyzed the images from the probe tack test of three PSAs with different viscoelastic features, ranging from a more liquid to a more elastic behavior, at two pulling velocities (1 and $10\,\mu m s^{-1}$). For each material we have characterized the growth law of the radius of individual cavities as function of time. Moreover, we have been able to test the validity of the assumption of spherical cavities after the onset of each nucleation events by comparing the overall probe displacement (i.e. a change in the total volume of the PSA) with the growth of the projected area of each cavity.

To conclude, we have shown that the probe tack experiment combined with our image analysis technique can provide valuable data for the understanding of the interfacial processes that lead to the debonding of pressure sensitive adhesives.

---

* matteo.nicoli@polytechnique.edu
† Laboratoire de Physico-chimie des Polymères et des Milieux Dispersés, ESPCI, 75005 Paris, France.

[1] C. Creton, *MRS Bull.* **28**, 434 (2003).
[2] J. T. Padding, L. V. Mohite, D. Auhl, W. J. Briels, and C. Bailly, *Soft Matter* **7**, 5036 (2011).
[3] H. Lakrout, P. Sergot, and C. Creton, *J. Adhesion* **69**, 307 (1999).

# Classical force fields for water from density functional theory based molecular dynamics simulations and force matching algorithm

Paolo Nicolini[†*], Jonàs Sala[†], Marco Masia[‡] and Elvira Guàrdia[†]
[†] *Departament de Física i Enginyeria Nuclear, Universitat Politècnica de Catalunya, Campus Nord B4-B5, Barcelona 08034, Spain.*
[‡] *Dipartimento di Chimica, Università degli Studi di Sassari, Istituto Officina dei Materiali del CNR, UOS SLACS, Via Vienna 2, 07100 Sassari, Italy.*

Water is one of the most abundant substances and is essential for all life on Earth. Therefore, it has been the subject of numerous studies but, despite all this effort, water clusters and condensed phases are still not fully understood. The main way to achieve this aim is represented by *ab initio* molecular dynamics (MD), particularly in the Car-Parrinello (CP) implementation[1]. Density functional theory (DFT) is the method often employed to simulate this kind of system. Despite advances in this so called first principle simulations field, only system size from few tens up to one hundred molecules are now approachable.

In this scenario, classical force fields (FFs) still play an important role. Basic ingredients of this kind of pairwise potentials are repulsive-dispersive (*i.e.,* Lennard-Jones potential) and Coulombian interactions. Polarization effects and flexible geometry of the water molecules can be also included. Several models are developed in the last decades[2] and are continuously object of refinement, in order to reproduce majority of physical properties of water (density, heat of vaporization, radial distribution function, critical parameters and so on).

The parametrization approaches could be gathered into two classes: fit of experimental properties or fit of *ab initio* potential energy surface. A recently proposed method, that belongs to the latter class, is the so called *force matching algorithm*[3]. It is based on a least-squares fitting of the potentials to force data obtained from reference calculations at a higher level of description. This approach has been used successfully in the development of new families of FFs[4].

In this contribution we present the results of the force matching application. The least-squares fitting is performed on both *ab initio* forces and molecular dipoles. Reference data were obtained from a 15 ps CP simulation of 96 water molecules with DFT level of theory. The teperature was set to 330 K and the density was held fixed to 0.997 g cm$^{-3}$. Standard periodic boundary were applied. Wannier centers[5] were computed along the simulation to calculate molecular dipole moments.

The force matching algorithm led to parameterize new classical FFs in which polarization is taken into account explicitly by using polarizable point dipoles method and damping functions[6]. Structural and dynamical properties have been computed for the water models here presented and these properties show a good agreement with the *ab initio* ones.

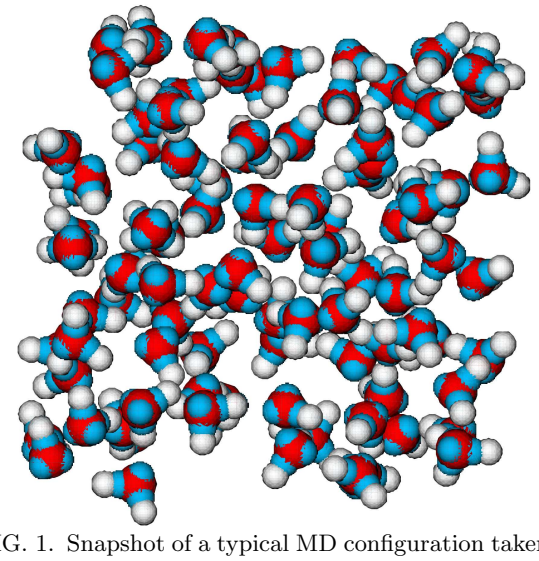

FIG. 1. Snapshot of a typical MD configuration taken from the CP dynamics. H atoms are in white, O atoms in red and Wannier centers are in cyan.

* paolo.nicolini@upc.edu

[1] R. Car and M. Parrinello, *Phys. Rev. Lett.* **55**, 2471 (1985).
[2] B. Guillot, *J. Mol. Liq.* **101**, 219 (2002).
[3] F. Ercolessi and J. B. Adams, *Europhys. Lett.* **26**, 583 (1994).
[4] J. Sala, E. Guàrdia, J. Martí, D. Spångberg and M. Masia, *J. Chem. Phys.* **136**, 054103 (2012).
[5] N. Marzari and D. Vanderbilt, *Phys. Rev. B* **56**, 12847 (1997).
[6] J. Sala, E. Guàrdia, M. Masia, *J. Chem. Phys.* **133**, 234101 (2010).

# Quasiperiodic graphs: structural design, scaling and entropic properties

B. Luque, A. M. Núñez and J. P. Gómez
*Dept. Matemática Aplicada y Estadística. ETSI Aeronáuticos, Universidad Politécnica de Madrid, Spain.*

A novel class of graphs, here named quasiperiodic, are constructed via application of the Horizontal Visibility algorithm to the stationary trajectories of the universality class of low-dimensional nonlinear iterated maps with a cubic inflexion point, as represented by the circle map

$$\theta_{t+1} = f_{\Omega,K}(\theta_t) = \theta_t + \Omega - \frac{K}{2\pi}\sin(2\pi\theta_t), \text{ mod } 1 \quad (1)$$

along the quasiperiodic route to chaos. We show how the hierarchy of mode-locked regions represented by the Farey tree is inherited by their associated graphs. We are able to establish, via Renormalization Group (RG) theory, the architecture of the quasiperiodic graphs produced by irrational winding numbers with periodic continued fractions. And finally, we demonstrate that the RG fixed-point degree distributions are recovered via optimization of a suitably defined graph entropy.

[1] Lacasa L., Luque B., Ballesteros F., Luque J., Nuño J.C., *Proc. Natl. Acad. Sci. USA* **105**, 4972 (2008).
[2] Luque, B., Lacasa, L., Ballesteros, F.J., Robledo, A., *PLoS ONE* **6**, e22411 (2011).
[3] Luque, B., Lacasa, L., Ballesteros, F.J., Robledo, A., *Chaos*, **in press**, 2012.
[4] Luque B., Ballesteros F., Núñez A. M., Robledo A., *arXiv*:1203.3717v1.

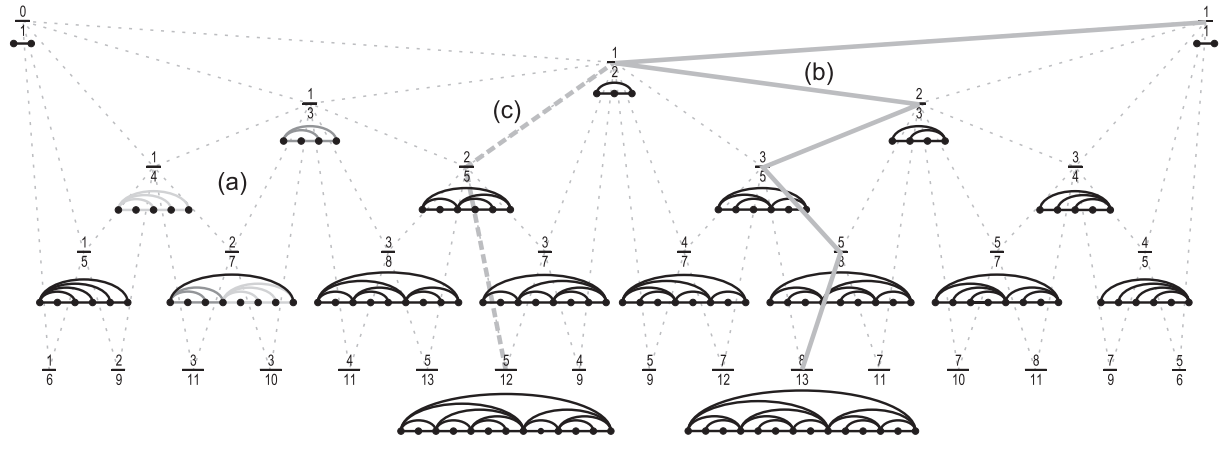


FIG. 1.: Six levels of the Farey tree and the periodic motifs of the graphs associated with the corresponding rational fractions $p/q$ taken as dressed winding numbers $\omega$ in the circle map (for space reasons only two of these are shown at the sixth level).

# The role of hydrolysis kinetics on the collective performance of single-headed kinesins

David Oriola* and Jaume Casademunt
*Departament d'Estructura i Constituents de la Matèria, Universitat de Barcelona*
*Avinguda Diagonal 647, 08028-Barcelona (Spain)*

Intracellular traffic is mainly enabled by molecular motors that transport a large variety of organelles along microtubule filaments. One of the most remarkable examples of intracellular transport is found in neurons. Large vesicles that contain synaptic precursors need to be carried from the cell body over long distances along the axon in order to supply dendrites. The collective performance of these motors is essential for the proper transport in the axon since intracellular traffic disorders have been associated to neurodegenerative diseases such as Alzheimer. Kinesins are a large family of processive molecular motors which play a fundamental role in anterograde transport in the axon. Most of them are dimeric motors composed of two motor "heads" which walk in a hand-over-hand fashion by alternating sequentially the motor domains attached to a microtubule filament. However, this model fails to describe the dynamics of KIF1A[1], a monomeric kinesin motor which moves processively by "hopping" along the microtubule track and it is able to freely diffuse while still weakly bound to the filament, without detaching during many steps. Strikingly, *in-vitro* experiments have shown KIF1A is very inefficient acting individually compared to conventional dimeric kinesins. The current open question is why KIF1A is specific of such a demanding task in spite of its clear inefficiency acting individually. We propose KIF1A motors could have an unusual and remarkable adaptation to cooperative action, which could largely compensate their individual inefficiency.

Recent studies on Brownian ratchets have revealed non-trivial dynamics leading to a dramatic enhancement of the efficiency of motor clusters with respect to the expected behaviour of a pure superposition of individual motors[2,3]. We develop a quantitatively realistic model by performing Langevin dynamics of KIF1A motors on a two-state noise-driven ratchet. We find a surprising enhancement on the stall force of the system which is mediated by hydrolysis kinetics. Moreover, the effect becomes more dramatic as the number of motors increases (Fig 1). This mechanism could be of special importance in the axon in order to overcome possible traffic jams and ensuring the proper transport of large vesicles against large forces. The underlying cooperativity which triggers the growth of the stall force relies on the presence of the weakly bound state which allows force transmission between motors. This state is a hallmark of KIF1A which differentiates this motor from its dimeric counterpart. Hence, single-headed kinesins could cooperate achieving much larger forces than dimeric kinesins. Also, we develop a simplified version of the model on a lattice by taking into account the main ingredients used in the previous description. The lattice description successfully describes the main phenomenology found in the Langevin description and it can be specially useful on the study of density waves, traffic jams and non-equilibrium phase transitions. Finally, simple experiments could be proposed to study the cooperative action of small groups of motors and test the previous results. Some examples could be membrane tube extraction experiments[4], long-range transport of vesicles along microtubule networks[5] or gliding assay experiments[6].

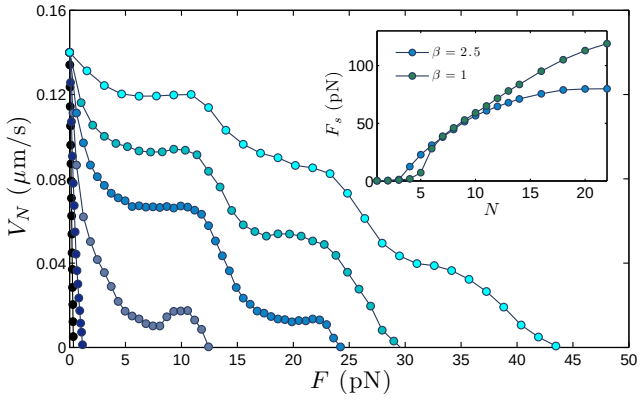


FIG. 1. Velocity-force curves for $N = 2, 3, 4, 5, 6$ and 8 motors (from left to right). We notice the remarkable enhancement of the stall force of the system when the number of motors is increased. Inset: stall force evolution versus the number of motors for two different ratios between the de-excitation rate ($\omega$) and the hydrolysis rate ($\omega^\star$) of motors ($\beta = \omega/\omega^\star$).

* oriola@ecm.ub.es

[1] Y. Okada, H. Higuchi and N. Hirokawa, Nature **424**,574 (2003).
[2] J. Brugués and J. Casademunt, Pys. Rev. Lett., **102**, 118104 (2009)
[3] J. G. Orlandi, C. Blanch-Mercader, J. Brugués and J. Casademunt, Phys. Rev. E, **82**, 061903 (2010).
[4] C. Leduc, O. Campàs, J-F. Joanny, J. Prost, and P. Bassereau, Biochem. et Biophys. A, **1798**, 1418-1426 (2010)
[5] C. Herold, C. Leduc, R. Stock, S. Diez, P. Schwille, Chemphyschem **13**, 1001-1006 (2012)
[6] T. Korten, A. Månson, S. Diez, Curr. Opinion. Biotechnol., **21**, 477-488, (2010)

# Spatio-temporal dynamics of cellular decision making

David Palau-Ortin*, Pau Formosa-Jordan, José María Sancho, Marta Ibañes
*Departament d'Estructura i Constituents de la Matèria.*
*Facultat de Física*
*Universitat de Barcelona*
*08028 Barcelona*

In biology, cells change of state according to biochemical signals. This process is known as cellular decision making and can be highly stochastic[1,2]. For instance, when the same signal acts in a group of equivalent cells, not all cells respond in the same manner. Some cells do not respond, while others change of state (e.g. differentiate). The choice of which new state is reached is often stochastic too. From a theoretical point of view, cellular decision making involves multistable nonlinear stochastic dynamics[3].

Cellular decision making occurs recurrently during the development of multicellular organisms. As a result of it, spatiotemporal patterns of different cell types arise. In some cases cell differentiation takes place cell-autonomously, without cell-to-cell communication. This process can be controlled by signals which can set the final population distribution of different cell states. In contrast, some other cellular decisions occur with cell-to-cell communication, creating an ordered spatiotemporal pattern of different cell types. Once one faces this type of process theoretically, many questions can be raised: How does this decision depend on the characteristics of the signal? When is the decision made? How does it depend on stochastic gene expression? Can a pattern be selected dynamically and how? In this poster we will address all these issues[4,5].

---

* palau@ecm.ub.es

[1] Perkins TJ, Swain PS., *Mol Syst Biol* **5**, pp. 326 (2009)
[2] Balazsi G, Van Oudenaarden A, Collins JJ, *Cell* **144**, pp. 910-25 (2011)
[3] R. Guantes and J. F. Poyatos, *PLOS Comp Bio* **4**, 11, pp. 1-13 (2008)
[4] D. Palau-Ortin, M. Ibañes, *Reversibility and memory in cellular decision making*, Preprint (2012)
[5] D. Palau-Ortin, P Formosa-Jordan, JM. Sancho, M. Ibañes, *Dynamical selecction of patterns*, Preprint (2012)

# Effects of a defect and drift on dissipative solitons

P. Parra, D. Gomila, M.A. Matías, P. Colet
*IFISC, Instituto de Física Interdisciplinar y Sistemas Complejos*
*CSIC-Universidad de las Islas Baleares 07122-Palma (Mallorca)*

In this work we show that a re-entry mechanism leading to excitability can be implemented by adding a defect and drift in a finite system. In this case, when a superthreshold perturbation creates an localized structures (LS) (or dissipative solitons (DS)) on the defect, the drift pulls it out and drives it to the limits of the system, where the LS disappears and the system goes back to the original state. This makes excitability commonplace in systems displaying DS when a defect and drift are introduced. Excitability appears through a number of different mechanism depending on the size of the defect and the intensity of the drift.

We analyze this scenario in the general Swift-Hohenberg equation close to the degenerate Hamiltonian-Hopf bifurcation where DS appear[1]:

$$\frac{\partial u}{\partial t} = -\left(\frac{\partial^2}{\partial x^2} + k_0^2\right)^2 u + c\frac{\partial u}{\partial x} + r(x)u + au^2 - gu^3 + b(x)$$

where $u$ is a real field, $b(x) = hexp\left(-(x-x_0)^2/\sigma^2\right)$ is a defect modeled by a Gaussian function, and $c$ the strength of the drift. $r(x) = r_0 - 1 + exp\left(-(x-x_0)^{18}/\epsilon^{18}\right)$ is a supergaussian profile to model a finite system where the spatial structures advected away by the drift will die at the boundary.

The competition between the defect that produce a pinning of the localized state and the advection term that try to drift the solution away leads to different pinning-unpinning transitions. Fig.1 shows the bifurcation diagram of the localized solutions as a function of the size of the defect $h$ for $c = -0.2$.

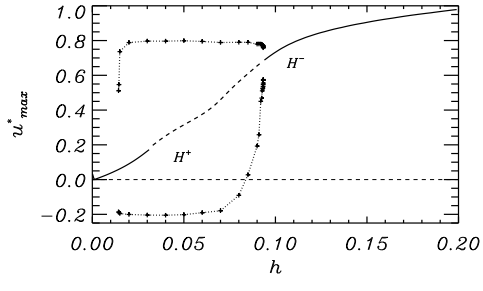


FIG. 1.

For that drift we can see that DS are unpinned from the defect through two Hopf bifurcations. The first one ($H^+$) is subcritical and leads to a limit cycle where DS grow out of the (low amplitude) fundamental solutions and then are drifted away to die at the boundary of the system, creating a train of soliton or soliton tap[2]. Since the bifurcation is subcritical, the system exhibits Type II excitability. If the system is set below $H^+$, a perturbation the (low amplitude) fundamental solution grows to generate a DS that is advected away to die at the boundary, and the system comes back to the resting state. An excitable excursion in this case is shown in Fig.2 for $c = -0.7$ and $h = 0.06$.

For larger values of $h$, large amplitude DS are again pinned to the defect. In this case, decreasing $h$ the drift is eventually able to detach the DS and a new one is formed creating again a cycle in a Hopf bifurcation $H^-$. In this case the bifurcation is supercritical, showing small oscillations close to threshold, but decreasing $h$ very little this small oscillations become already very large in a sort of canard, creating a source of DS. This is again a mechanism leading to Type II excitability.

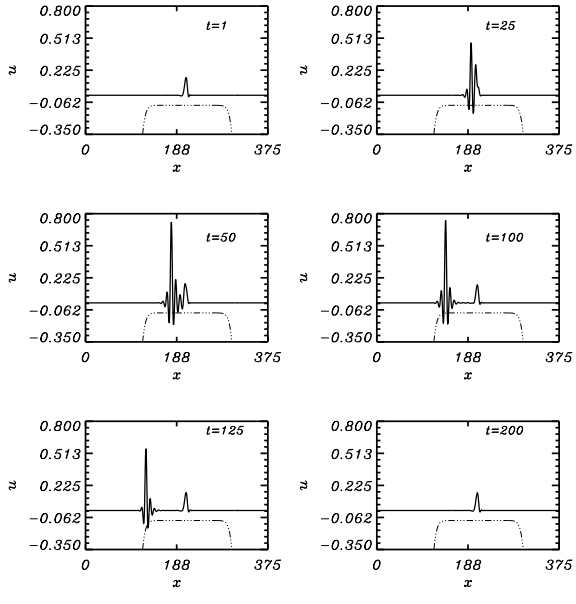


FIG. 2. Excitable excursion close to the $H^+$ point

This scenario has a third mechanism leading to excitability, namely the SNIC. In this case a (high amplitude) DS is also unpinned leading to the excitable excursion, similar to the case of the supercritical Hopf $H^-$, but in a Type I fashion.

[1] P. Woods and A. Champneys, Physica D **129**, 147 (1999).
[2] E. Caboche, *et al.*, Phys. Rev. Lett. **102** 163901 (2009).
* parrariv@ifisc.uib-csic.es

# Modelling the Self-Assembly of a Model Cationic Surfactant by Lattice Monte Carlo Simulations

Javier Burgos, Conxita Solans, Alessandro Patti*
*Institute of Advanced Chemistry of Catalonia (IQAC-CSIC) and*
*CIBER de Bioingeniería, Biomateriales y Nanomedicina (CIBER-BBN)*
*Jordi Girona 18-26, 08034 Barcelona, Spain*

Above the critical micellar concentration (*cmc*), surfactants with the right solvophobic/solvophilic ratio, are able to self-assemble and form aggregates. At the *cmc*, the concentration of free surfactants in solution stops increasing, whereas that of aggregates starts to increase. Depending on several conditions, such as temperature, solvent, electrolytes, cosurfactants, and on the surfactant architecture as well, the *cmc* can vary rather significantly as well as the shape and size of micelles at equilibrium.[1] Due to their large applications in formulation chemistry and in nanotechnology as templates for the synthesis of advanced materials, the principles controlling self-assembly and micellization of surfactants are of fundamental relevance. In the last decades, computer simulations have played a key role in determining the phase and aggregation behavior of many different amphiphilic systems,[2] via the implementation of both rigorous atomistic[3,4] and coarse-grained (CG)[5–7] models.

In this work, by performing lattice Monte Carlo (MC) simulations, we investigate the self-assembly of a cationic surfactant (ricinoleamidopropyltrimonium methasulfate) which finds large applications in formulation chemistry and, more specifically, in cosmetics. We apply an efficient CG model[7] where the surfactant molecules are represented as linear chains of connected beads in a three-dimensional lattice network. The headgroups, carrying the charge, are neutralized by a number of monovalent counterions. The charged groups interact via a Coulombic potential and a hard core repulsion, whereas neutral tail-tail interactions are only established between close neighbors, defined by the lattice coordination number. All the lattice sites are occupied by the surfactant or by the solvent. By tuning the mutual interaction between the solvophilic and solvophobic groups, and that between them and the solvent, we are able to observe aggregation and formation of micelles. We compute the *cmc*, the density distribution profiles in the micelles and their aggregation number, and estimate the dependence of these parameters on temperature.

---

* alpnqb@iqac.csic.es

[1] J. N. Israelachvili, *Intermolecular and Surface Forces*, Academic Press, $2^{nd}$ Ed., 1998.
[2] J. C. Shelley and M. Y. Shelley, Curr. Opin. Colloid Interface Sci. **5**, 101 (2000)
[3] M. Jorge, J. Mol. Struct.: THEOCHEM, **946**, 88 (2010).
[4] S. Pal *et al.*, J. Phys. Chem. **109**, 12879 (2005).
[5] A. Patti *et al.*, Langmuir **23**, 6771 (2007).
[6] A. Patti *et al.*, J. Phys. Chem. B **116**, 2687 (2012).
[7] D. W. Cheong and A. Z. Panagiotopoulos, Langmuir **22**, 4076 (2006).

# Self-pulsations, excitability and polarized rogue waves induced by orthogonal optical injection in Vertical-Cavity Surface-Emitting Lasers

P. Pérez[1,2*], L. Pesquera[1], A. Valle[1]
[1] *Instituto de Física de Cantabria (CSIC-UC) 39005-Santander*
[2] *Departamento de Física Moderna (Universidad de Cantabria)*

Optical injection in vertical-cavity surface-emitting lasers (VCSELs) is a technique that is employed to improve the performance of these lasers without modifying their design. Optical injection can also induce rich nonlinear dynamics in the light emitted by the VCSEL. In contrast with edge emitters VCSELs have an extra degree of freedom associated to the polarization of light. An example of nonlinear polarization dynamics has been recently observed in 1550nm wavelength VCSELs subject to orthogonal optical injection[1,2]. In those experiments linearly polarized light from a tunable laser source is injected orthogonally to the linear polarization of a free-running VCSEL (parallel polarization). The control parameters are the master power $P_m$ and the detuning $\Delta\nu$, defined as the frequency difference between the master laser and the orthogonal polarization of the slave laser. When $P_m$ is increased polarization switching of the VCSEL to the polarization of the external injection and injection locking are obtained. Bistability, periodic, period doubling and irregular dynamics for both linear polarizations were observed before injection locking is achieved. Pulses observed in the irregular regime are similar to those resulting from excitability in optically injected quantum well and quantum dot edge-emitting semiconductor lasers[3]. Rare extreme pulses (rogue waves) have been also observed in optically injected 980nm wavelength VCSELs subject to parallel optical injection[4].

In this work we perform a theoretical study of the polarization-resolved nonlinear dynamics of a long wavelength single-mode linearly polarized VCSEL when subject to orthogonal optical injection. We use a rate equation model[1] based on the spin-flip model. We show that self-pulsations appear in the total power and in both linear polarizations at negative detuning when $P_m$ is smaller but close to the injection power required to achieve stable injection locking, $P_{IL}$. These self-pulsations correspond to those observed in 1550nm wavelength VCSELs subject to orthogonal optical injection[1,2]. When $P_m$ is slightly increased above $P_{IL}$, excitable pulses can be triggered by perturbing laser variables above a certain threshold level. Single, double, triple and multi-pulse behaviors are obtained at a detuning of -2, -2.5, -2.4 and -2.7GHz, respectively. These excitable pulses are identical to the self-pulsations obtained when $P_m < P_{IL}$. This behavior is observed in the deterministic case and when spontaneous emission noise is taken into account. Multi-pulse excitability can be due to $n$-homoclinic bifurcation tongues[5]. A periodic behavior is obtained at a detuning of -2, -2.5 and -2.4GHz in the deterministic case when $P_m < P_{IL}$. However, irregular multi-pulse behavior is obtained without spontaneous emission noise for -2.7GHz and $P_m < P_{IL}$ (see Fig. 1). In this case the parallel polarization is excited at the end of every pulse train. Train pulses are sporadic and the histogram show a long tail (see inset in Fig. 1 for the total power). We obtain pulses with a height higher than the mean value plus 8 standard deviations. This is one of the criteria used to define rogue waves[4]. Similar long-tailed histograms are obtained for the power of both polarizations. Then, polarized rogue waves are obtained in VCSELs subject to orthogonal optical injection.

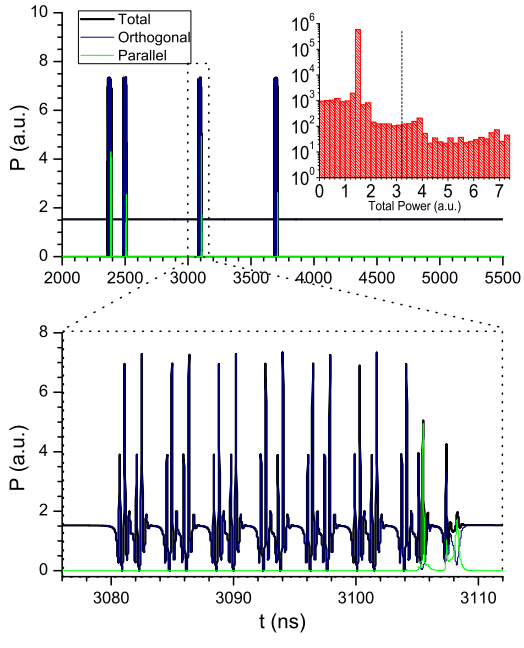


FIG. 1. Time traces of the total and both linear polarizations power at a detuning of -2.7GHz without noise. Inset: Histogram of the total power. The vertical dashed line denotes the mean value plus 8 standard deviations

* perezg@ifca.unican.es

[1] A. Quirce, P. Pérez, A. Valle, and L. Pesquera, JOSA B **28**, 2765 (2011).
[2] J. P. Toomey *et al.*, Opt. Express **20**, 10256 (2012).
[3] B. Kelleher, C. Bonatto, G. Huyet, and S. P. Hegarty, Phys. Rev. E **83**, 026207 (2011).
[4] C. Bonatto *et al.*, Phys. Rev. Lett. **107**, 053901 (2011)
[5] S. Wieczorek, B. Krauskopf, and D. Lenstra, Phys. Rev. Lett. **88**, 063901 (2002).

# Dopant segregation in semiconductor crystal growth due to stochastic g-jitter in microgravity

X. Ruiz,[a] P. Bitlloch,[b] L. Ramírez-Piscina,[c] J. Casademunt[b]
*IEEC Institut d'Estudis Espacials de Catalunya, Barcelona, Spain*

In microgravity environments there exist residual accelerations (g-jitters) that typicaly contain a broad spectrum of frequencies. These accelerations can be modelled as stochastic processes, and can have a relevant influence in fluid systems. In this work[1] we have quantitatively addressed the effects of a generic stochastic g-jitter into the quality of semiconductor crystals grown in realistic directional solidification setups. In particular we evaluate, by means of direct numerical simulations and by a simplified model, the dopant segregation effects due to thermosolutal convection as a function of the parameters characterizing the statistics of the stochastic force.

Simulations are specified for material parameters of two doped semiconductors (Ge : Ga and GaAs : Se) in realistic conditions of actual microgravity environments. The numerical simulation of the growth process involves the resolution of the time dependent transport equations in the melt ahead of the solidification front with the appropriate boundary conditions at the moving interface. We have considered a Boussinesq, incompressible fluid, and we have neglected deformations of the interface. For the stochastic gravity we have used narrow-band noise, which is a stochastic process characterized by its amplitude $G$, a temporal correlation $\tau$, and a dominant frequency $\Omega$, given by the main peak of its power spectrum

$$P(\omega) = \frac{G^2\tau}{2\pi}\left(\frac{1}{1+\tau^2(\Omega+\omega)^2} + \frac{1}{1+\tau^2(\Omega-\omega)^2}\right). \quad (1)$$

Additionaly we have considered deterministic oscillations of the same frequency.

We have explored the response of the system for the two semiconductors considered for different thermal profiles of the setup and different amplitudes of the stochastic signal. As a general result of the direct simulations, the response of the system is very weak, and essentialy linear in the amplitude of the g-jitter.

In addition, we have developed a simplified model of the problem based on linear response theory that projects the dynamics into very few effective modes. The model involves two effective time scales, one from viscous dissipation and one from solutal diffusion. Those can be fitted from the simulation of a single convenient case, and on the basis of linear response theory, the model can be extended to arbitrary signals.

Careful analysis of the model predicts that the response of the system is strongly dominated by the low-frequency part of the g-jitter spectrum. This was confirmed by the numerical results of the complete model. We have also shown that the model captures remarkably well the segregation effects for an arbitrary time-dependent acceleration of small amplitude, while it implies an enormous reduction of computer demands. This model could be helpful to analyze results from real accelerometric signals and also as a predictive tool for experimental design.

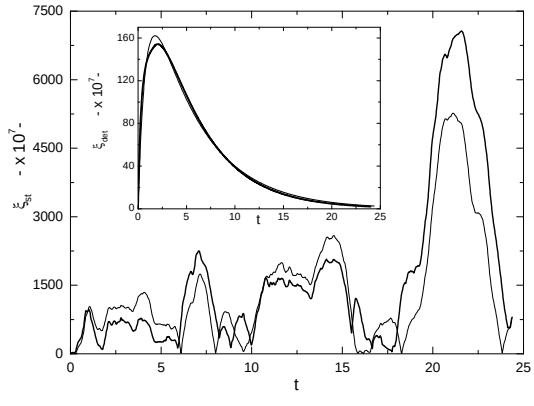


FIG. 1. Transversal segregation parameter as a function of time, for GaAs : Se, obtained from both the complete simulation (thick line) and the integration of the simple model (thin line) by employing the same noisy signal. Inset: nonlinear fitting of the model to the simulation of the complete system for the deterministic case, which is used to obtain the value of the three parameters needed in the noisy case.

[a] Dept. Química Física i Inorgànica, Universitat Rovira i Virgili. Tarragona, Spain.
[b] Dept. Estructura i constituents de la Matèria, Universitat de Barcelona. Barcelona, Spain.
[c] Dept. Física Aplicada, Universitat Politècnica de Catalunya. Barcelona, Spain.

[1] X. Ruiz, P. Bitlloch, L. Ramírez-Piscina and J. Casademunt, *Impact of stochastic accelerations on dopant segregation in microgravity semiconductor crystal growth*, submitted to Journal of Crystal Growth.

# Resolución de problemas de coherencia mediante redes de consenso

M. Rebollo*
*Universitat Politècnica de València*
*Camino de Vera s/n 46021 Valencia*

El problema del cálculo de la coherencia[5] de una red consiste en, dado un conjunto de elementos y de relaciones positivas (coherentes) y negativas (incoherentes) entre ellos, determinar la división de sus nodos en dos conjuntos de tal forma que se maximice la consistencia de la red. Es un problema que aparece en diferentes actividades humanas relacionadas con las decisiones, opiniones, elecciones, recomendaciones, gestión de la confianza, justificación ética o legal, etc.

El problema se representa mediante un grafo no dirigido y ponderado donde los pesos $a_{ij} \in [-1, 1]$. Se trata de encontrar una partición de los elementos de la red en dos conjuntos $N^+$ y $N^-$ de forma que dos elementos $i, j$ pertenecen a $N^+$ si y solo si $a_{ij} > 0$ y uno de ellos pertenece a $N^+$ y otro a $N^-$ cuando $a_{ij} < 0$. La coherencia de la partición se define como

$$W = \frac{\sum_{i,j \in N^+} a_{ij} - \sum_{i \in N^+, j \in N^-} a_{ij}}{|N|} \qquad (1)$$

La solución óptima es la que maximiza el valor de $W$ (ver Fig. 1). Es un problema intratable: no existe una solución en tiempo polinómico que garantice el óptimo. Habitualmente resuelve como un problema de satisfacción de restricciones[4] y se emplean métodos que proporcionan una solución aproximada a travÃ©s de técnicas de optimización no lineal o redes neuronales (como redes de Hopfield[1]).

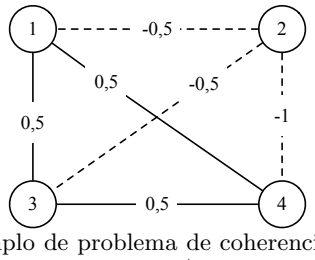


FIG. 1. Ejemplo de problema de coherencia. La partición que maximiza la coherencia es $N^+ = \{1, 3, 4\}, N^- = \{2\}$, con $W = \frac{0,5+0,5+0,5+0,5+0,5+1}{6} = 0,583333$

En el presente trabajo se propone emplear redes de consenso[3] para determinar la partición óptima. Cada nodo $i$ de la red actualiza su valor $x_i$ como la media ponderada de los valores recibidos de sus vecinos. La dinámica de las redes de consenso queda definida a través de la laplaciana de la matriz de adyacencia $L = D - A$, donde $D$ es una matriz diagonal que contiene el grado de los nodos y $A$ es la matriz de adyacencia de la red. Se garantiza que la red converge a la media ponderada global si $L$ es definida positiva. Pero esto no se cumple en el caso de los problemas de coherencia debido a la presencia de los pesos negativos en la red. Por ello, debe modificarse en cálculo de $L$ para el caso de *signed graphs*[2]. Llamaremos a esa matriz $\bar{L}$.

En el caso discreto, la dinámica de la red queda definida por $x(t+1) = \bar{P}x(t)$, siendo $\bar{P} =$ una matriz estocástica obtenida a partir de $\bar{L}$. Inicializando cada nodo de la red con un valor $x_i$ aleatorio, se observa que cuando la red se estabiliza, los nodos quedan separados en dos grupos por el signo del valor final de $x_i$.

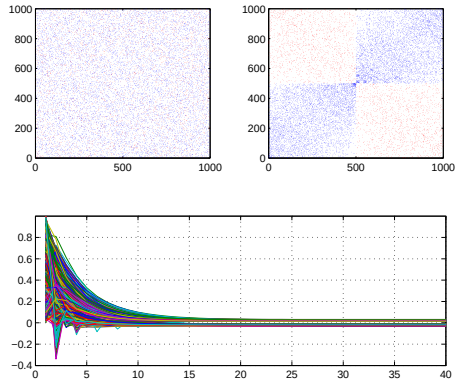

FIG. 2. Coherencia en una red de 1000 nodos. [Arriba] Red inicial y grupos detectados tras la estabilizacion (los puntos rojos representan pesos negativos y los azules positivos) [Abajo] Evolucion de los valores de los nodos. A partir de la iteracion 15 aparecen 2 grupos

La ventaja de este método es que se puede implementar de forma completamente descentralizada, de manera que no sea necesario conocer la estructura de la red completa. Cada nodo intercambia información con sus vecinos y, cuando se estabiliza, los nodos quedan divididos en 2 grupos de manera que cada nodo puede saber si un vecino dado pertenece o no a su grupo.

* mrebollo@dsic.upv.es

[1] J. J. Hopfield, *PNAS*, **79**(8), 2554–2558, (1982).
[2] Jerome K. et al., in *Proc. of the 10th SIAM International Conference on Data Mining*, pp. 559–559, (2010).
[3] R. Olfati-Saber and R.M. Murray, IEEE T-AC **49**(9), 1520 – 1533, (2004).
[4] P. Thagard and K. Verburgt, in *Cognitive Science*, **22**(1), 1–24, (1998).
[5] P. Thagard, in *Coherence in Tought and Action* (MIT Press, 2000).

# Single molecule derivation of base pair free energies in DNA and RNA

Josep M. Huguet[1], C.V. Bizarro[1], M. Ribezzi-Crivellari[1] and F. Ritort[1,2]
*(1) Departament de Fisica Fonamental, Universitat de Barcelona*
*Martí i Franques 1, 08028 Barcelona.*
*email: marco.ribezzi@gmail.com, URL: http://www.ffn.ub.es/ritort/*
*(2) Ciber de Bioingeniería, Biomateriales y Nanomedicina,*
*Instituto de Sanidad Carlos III, Madrid*

Recent developments in micro and nano-technologies allow for the controlled manipulation of individual molecules by exerting and detecting forces in the piconewton range[1]. Molecular unzipping is a force-induced reaction that makes possible to disrupt the bonds that hold molecular structures in nucleic acids and proteins. In this way, for example, a double stranded DNA molecule can be converted into two individual single strands by pulling apart the two strands (molecular unzipping)[2]. The capability of single molecule techniques of detecting weak forces together with the ability of measuring extensions with nanometer resolution allow scientists to monitor molecular reactions in real time (e.g. molecular folding). In this comunication we will show some of the most recent applications of molecular unzipping in our lab that make possible to derive base-pair free energies in DNA and RNA with unprecedented accuracy and extract folding free energies of proteins with 1kcal/mol resolution[3,4].

[1] F. Ritort, Single molecule experiments in biological physics: methods and applications, Journal of Physics C (Condensed Matter),18 (2006) R531-R583
[2] N. Forns, S. De Lorenzo, M. Manosas, K. Hayashi, J. M. Huguet and F. Ritort, Improving Signal/Noise Resolution in Single-Molecule Experiments Using Molecular Constructs with Short Handles , Biophysical Journal, 100 (2011) 1765-1774
[3] J. M. Huguet, C. V. Bizarro, N. Forns, S. B. Smith, C. Bustamante and F. Ritort, Single-molecule derivation of salt dependent base-pair free energies in DNA, Proceedings of the National Academy of Sciences, 107 (2010) 15431-15436
[4] C. V. Bizarro, A. Alemany, F. Ritort. Non-specific binding of Na+ and Mg2+ to RNA determined by force spectroscopy methods, Nucleic Acids Res., 2012

# Fluctuation Relations and Entropy production in a Dual Trap Optical Tweezers Setup

Marco Ribezzi-Crivellari[1], Felix Ritort[1,2]
*(1) Departament de Fisica Fonamental, Universitat de Barcelona*
*Martí i Franques 1, 08028 Barcelona.*
*email: marco.ribezzi@gmail.com, URL: http://www.ffn.ub.es/ritort/*
*(2) Ciber de Bioingeniería, Biomateriales y Nanomedicina,*
*Instituto de Sanidad Carlos III, Madrid*

Recent theoretical developments in nonequilibrium statistical physics have shown how it is possible to recover free energy differences (FED) and free energy landscapes (FEL) from irreversible work measurements in thermodynamic transformations of small systems.

These developments go under the name of Fluctuation Relation (FR) and have found several applications in the field of single molecule manipulation [1],[2],[3]. A crucial concern in using FRs is the identification of the right observables which satisfy the relation: the use of the wrong observable can lead to a large error in the estimated FED or FEL [4]. In this communication we will discuss the applicability of FRs to non-equilibrium measurements obtained in Dual Trap Optical Tweezers setups (DTOTs), the standard high resolution tool in single molecule biophysics. We will show that in general three different observables satisfy a FR. In particular our study proves that the differential work measurement, based on the differential coordinate [5] (which provides the highest resolution in DTOTs) satisfies a FR and can be used in FED or FEL estimates, independently of how the pulling is carried on. The theoretical results will be confronted with experimental results obtained on several DNA tethers in a novel counter-propagating DTOT setup which directly measures forces by linear momentum conservation.

[1] J. Liphardt, B. Onoa, SB. Smith, I. Tinoco, Jr. and C. Bustamante, Equilibrium Information from Nonequilibrium Measurements in an Experimental Test of Jarzynski's Equality, Science **296**, 1832-1835 (2002)

[2] D. Collin, F. Ritort, C. Jarzynski, S. B. Smith, I. Tinoco Jr and C. Bustamante, Verification of the Crooks fluctuation theorem and recovery of RNA folding free energies, Nature, **437** (2005) 231-234

[3] A.N. Gupta, A. Vincent, K. Neupane, H. Yu, F. Wang and M.T. Woodside, Experimental validation of free-energy-landscape reconstruction from non-equilibrium single-molecule force spectroscopy measurements. Nat. Phys. **7**, 631-634 (2011)

[4] A. Mossa, S. De Lorenzo, J.M. Huguet, F. Ritort, Measurement of work in single molecule experiments. J. Chem. Phys. **130**, 234116 (2009)

[5] J.R. Moffitt, Y.R. Chemla, D. Izhaky and C. Bustamante, Differential detection of dual traps improves the spatial resolution of optical tweezers Proc. Natl. Acad. Sci, **103**, 9006-9011 (2006)

# Estudio del efecto de la temperatura, presión y tipo de catión sobre la estructura flexible de la zeolita RHO mediante técnicas de simulación molecular

S. Rodríguez–Gómez,* J. J. Gutiérrez–Sevillano y S. Calero
*Departamento de Física, Química y Sistemas Naturales*
*Universidad Pablo de Olavide, Sevilla*

Las zeolitas son aluminosilicatos con poros y huecos de dimensiones moleculares. Estas estructuras no muestran grandes deformaciones y son conocidas por su rigidez. A pesar de ello, existen ciertas zeolitas que son particularmente flexibles como las estructuras BIK, SOD y RHO.[1] La zeolita RHO muestra deformaciones estructurales únicas y se han corroborado experimentalente mediante deshidratación,[2] por las posiciones de los cationes, el tipo de catión y mediante cambios en la condiciones de presión—temperatura.[3] Estas deformaciones pueden verse en la FIG. 1.

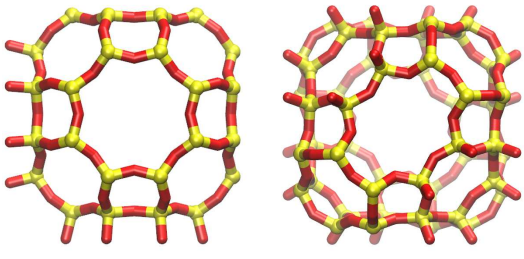

FIG. 1. Transición de fase estructural de la zeolita RHO.

Un estudio reciente muestra una selectividad altísima en la separación de dióxido de carbono y metano; inducida presumiblemente por las deformaciones estructurales durante la adsorción.[4]

Hemos usado avanzadas técnicas de simulación para reproducir el fenómeno completo: (1) el colectivo osmótico —mediante un método híbrido Monte Carlo/Dinámica Molecular— para la predicción de la adsorción de dióxido de carbono en la estructura flexible,[5,9] y (2) los efectos de la temperatura, presión, tipo de catión sobre estructura flexible son estudiados mediante Dinámica Molecular en el colectivo isotermo—isobaro.

Todo esto ha sido posible mediante el desarrollo de un nuevo campo de fuerzas basado en una combinación de trabajos anteriormente validados: estructuras flexibles,[6–8] e interacciones en la adsorción de dióxido de carbono en zeolitas.[10] Este nuevo campo de fuerzas es capaz de reproducir el fenómeno completo.

---

* salrodgom@gmail.com

[1] V. Kapko *et al.*, Phys. Chem. Phys., 2010, 12, 8531-8541
[2] J. B. Parise *et al.*, J. Chem. Phys., 1984, 88, 1635-1640
[3] D. R. Corbin *et al.*, J. Am. Chem. Soc. 1990, 112, 4821-4830
[4] M. Palomino *et al.*, Chem. Commun., 2012, 48, 215-217
[5] Ji Zang *et al.*, J. Chem. Phys., 2011, 134, 184103
[6] J. B. Nicholas *et al.*, J. Am. Chem. Soc., 1991, 113, 4792-4800
[7] J. R. Hill & J. Sauer, J. Phys. Chem, 1994, 98, 1238-1244
[8] J. R. Hill & J. Sauer, J. Phys. Chem, 1995, 99, 9536-9550
[9] Coudert *et al.*, J. Am. Chem. Soc., 2008, 130, 14294-14302
[10] A. García-Sánchez *et al.*, J. Phys. Chem. C, 2009, 113, 8814-8820

# Effects of topology on the one-dimensional Kardar-Parisi-Zhang universality class

Javier Rodriguez-Laguna[†,§,♯*], Silvia N. Santalla[†,‡], Rodolfo Cuerno[†,♯]
[†] *Grupo Interdisciplinar de Sistemas Complejos (GISC), Universidad Carlos III de Madrid*

The mathematical problem of modeling the evolution of a non-equilibrium rough interface arises for a huge variety of physical processes, such as thin film growth, fluid dynamics, flame-front propagation or undifferentiated biological growth.[1] In many relevant situations, the dynamics is characterized by the so-called Kardar-Parisi-Zhang (KPZ) universality class.

For the case of one-dimensional (1D) interfaces, this KPZ class is receiving an increasing attention lately. The reason is that not only the critical exponents are universal, but also the probability distribution for the fluctuations.[2] Such functions turn out to depend strongly on the topology of the interface in the embedding 2D space. In the so-called band-geometry, the interface is a closed curve wrapping around a cylinder. In this case, the height fluctuations follow the Tracy-Widom distribution associated with the Gaussian orthogonal ensemble (GOE) from random matrix theory.[4] The circular growth geometry takes place when the embedding space is just the Euclidean plane, the interface being a simple closed curve. In this case, the probability distribution for the interface radius corresponds to the Gaussian unitary ensemble (GUE), see [ 3] and references therein.

Recent experimental results[3] provide support for these results, which arise from exact solutions of the KPZ equation or from numerical simulations of discrete models. Unfortunately, different theoretical models or *ad-hoc* initial conditions are used for the analysis of the band-geometry and the circular geometry cases.

We propose a single stochastic partial differential equation defined on a 2D embedding space using only intrinsic geometry, i.e.: all terms in the equation are covariant. Thus, no distinction between the growth and the tangent directions to the interface are made *a priori*. The only difference between the band-geometry and the circular growth modes corresponds to the boundary conditions, namely, to the topology of the relation between the interface and the underlying space.[5] The equation reads

$$v_n(\vec{r}) = A_0 + A_1 K(\vec{r}) + A_2 \nabla^2 K(\vec{r}) + A_n \eta(\vec{r}), \qquad (1)$$

where $v_n$ is the velocity along the local normal direction at any point of the interface, $\vec{r}$, $K$ is the local curvature, $\nabla^2$ is the Laplace-Beltrami operator, and $\eta$ is a zero average, Gaussian white noise, uncorrelated both in space and time. Thus, the constants $A_0$, $A_1$, $A_2$, and $A_n$ are free parameters.

Solving this single equation in the band and circular settings, we obtain profiles like those in Fig. for the former, and those in Fig. for the latter. We will show how the statistics of these profiles provide insight about the effects of topological constraints on the 1D KPZ universality class, that can thus be studied within a single framework.

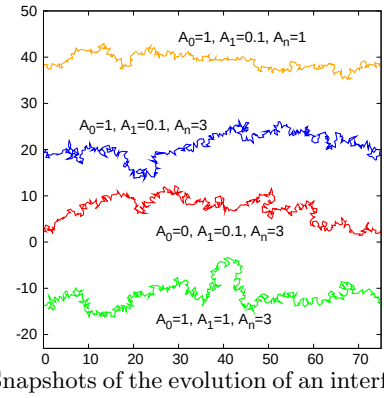


FIG. 1. Snapshots of the evolution of an interface described by Eq. (1) in the band-geometry setting.

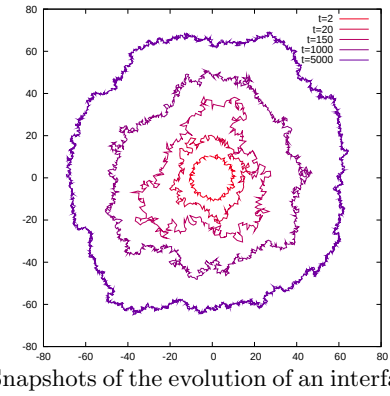


FIG. 2. Snapshots of the evolution of an interface described by Eq. (1) in the circular-geometry setting.

* javier.rodriguez@icfo.es
§ ICFO–Institute of Photonic Sciences, Castelldefels, Barcelona
♯ Departamento de Matemáticas, Universidad Carlos III de Madrid
‡ Departamento de Física, Universidad Carlos III de Madrid

[1] A.-L. Barabási and H. E. Stanley, *Fractal concepts in surface growth* (Cambridge University Press, Cambridge, 1995).
[2] T. Kriecherbauer and J. Krug, J. Phys. A: Math. Theor. **43**, 403001 (2010).
[3] K. A. Takeuchi, M. Sano, T. Sasamoto and H. Spohn, Sci. Rep. **1**, 34 (2011).
[4] P. Calabrese and P. Le Doussal, Phys. Rev. Lett. **106**, 250603 (2011).
[5] J. Rodriguez-Laguna, S.N. Santalla, R. Cuerno, J. Stat. Mech. P05032 (2011).

# Viscoelastic properties of vesicles

Guillermo R. Lázaro[a], Aurora Hernández-Machado[a] and Ignacio Pagonabarraga[b]
[a] *Dept. d'Estructura i Constituents de la Materia Facultat de Fisica, Universitat de Barcelona*
[b] *Dept. de Fisica Fonamental, Facultat de Fisica, Universitat de Barcelona*

Blood is a complex fluid whose viscoelastic properties are basically dominated by the elasticity and interactions of the cells that it contains. Blood is composed of a newtonian fluid, the blood plasma, representing some 55% of the total blood volume, while the remaining volume is occupied by blood cells. Among the wide variety of corpuscles usually found in blood, around 99% are red blood cells (RBCs), an anucleated cell whose shape and mechanical properties are entirely determined by its membrane. Consequently, the study of the viscoelastic behaviour of RBCs immersed in water could be relevant to improve our understanding of the macroscopic behaviour of blood[1].

The blood resistance to flow through thin capillaries is governed by the deformability of the RBCs, which in turn depends on the rigidity of its membrane. Experimental evidence shows that at high shear rates RBCs adopt an asymmetric shape, usually known as slipper, which seems to minimize blood resistance favouring fluid circulation. How this and other intriguing phenomena affect to the viscoelasticity of blood remains under debate[3].

The RBC membrane is a complex structure formed by a lipid bilayer with a spectrin cytoskeleton anchored to its inner leaflet, which prevents from pinching and vesiculization. The cytoskeleton is relaxed when the cell is close to its equilibrium shape, the so-called discocyte, and its stress energy is then negligible. Accordingly, the unique contribution to the elastic energy of the membrane is due to the presence of the bilayer, and usually represented by the Helfrich free energy[2]:

$$\mathrm{F_{mem}} = \frac{\kappa_\mathrm{b}}{2}\int(\mathrm{H}-\mathrm{c_o})^2\mathrm{dA}, \qquad (1)$$

where $\kappa_b$ is the bending rigidity, $H$ is the mean curvature of the cell shape and $c_o$ reflects any asymmetry in the membrane. We use this energy to simulate the elastic behaviour of the cell membrane via a phase-field model, coupled to the Navier-Stokes equation which describes the hydrodynamics of the surrounding fluid. The model has proven to capture the essential physics of the system.

Linear viscoelasticity is a useful way to characterize and understand the complex behaviour of the fluid, since it relates the macroscopic response of the fluid with the microscopic mechanical properties of the cells that introduce the elasticity. In our simulations, vesicles immersed in water are externally forced by a oscillatory forcement, similar to the mechanism used in a rheometer. The dynamic and stress modulii can be easily computed and hence the fluid could be characterized by a macroscopic model such as the one-relaxational time Maxwell model.

* lazaro@ecm.ub.es

[1] J. McWhirter, H. Nogushi and G. Gompper. Flow-induced clustering and alignement of vesicles and red blood cells in microcapillaries. *PNAS* 106(15), 6039 (2009).
[2] O.Y. Zhong-can, and W. Helfrich. Instability and deformation of a spherical vesicle by pressure. *Phys. Rev. Lett.* 59, 2486 (1987).
[3] B. Kaoui, G. Biros and C. Misbah. Why do red blood cells have asymmetric shapes even in a symmetric flow? *Phys. Rev. Lett.* 103(18), 188101 (2009).

# Entropía negativa entre esferas metáticas debida al efecto Casimir.

Pablo Rodriguez-Lopez*
*GISC y Departamento de Matemáticas, Universidad Carlos III de Madrid, 28911 Leganés (Madrid).*

Debido a las fluctuaciones de vacío, entre dos placas metálicas descargadas aparece una fuerza atractiva[1]. Estas fuerzas de Casimir son ubicuas en la Naturaleza, y han sido estudiadas en muy diferentes contextos[2].

El cálculo general de las fuerzas de Casimir entre cuerpos de geometría arbitraria ha sido inabordable hasta hace bien poco, cuando Emig et. al.[3,4] propusieron un método de multiscattering y calcularon por primera vez la fuerza de Casimir entre dos esferas metálicas en 2007.

Desde entonces, se han podido estudiar nuevas geomerías y diferentes propiedades de la interacción de Casimir, como es la no monotonicidad de la interacción entre dos cuerpos en presencia de un tercero, la "levitación cuántica" (efecto Casimir repulsivo) o la aparición de entropías negativas en diferentes configuraciones muy naturales y experimentalmente relevantes.

En este trabajo[5] estudiamos la aparición de entropías negativas en sistemas de dos cuerpos que interaccionan mediante el efecto Casimir. En particular, por simplicidad, nuestro estudio se centra en el caso de dos esferas perfectamente metálicas de radio $R$ que interaccionan a través de la fuerza de Casimir. Los casos de esferas con modelos más realistas de metales (Drude y Plasma) también han sido estudiados.

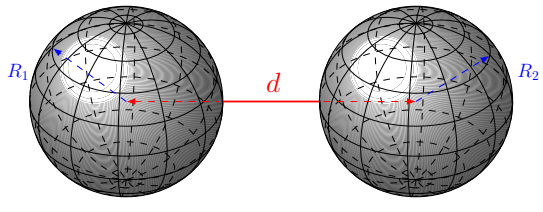


FIG. 1. Representación del sistema en estudio. Dos esferas perfectamente metálicas de mismo radio $R$, cuyos centros se hayan separados una distancia $d$, sometidas a una temperatura $T$.

Incluso en este sistema tan sencillo, encontramos que a cualquier temperatura no nula, existe un intervalo de distancias entre las esferas en el cual la entropía es negativa. Además, demostramos que la entropía es siempre positiva tanto a cortas como a largas distancias.

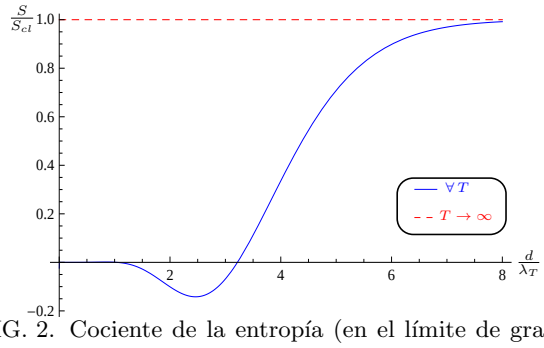


FIG. 2. Cociente de la entropía (en el límite de gran distancia entre las esferas) entre dos esferas metálicas y su límite de alta temperatura como una función de la variable adimensional $z = \frac{d}{\lambda_T} = 2\pi \frac{k_B T d}{\hbar c}$, donde $d$ es la distancia entre los centros de las esferas y $T$ la temperatura del sistema en estudio.

Obtenemos que el origen de las entropías negativas en este sistema es el acoplo de los modos TE y TM de los cuerpos en interacción, lo que implica que este efecto es característico del efecto Casimir electromagnético, sin análogo escalar.

Por último, haciendo un estudio termodinámico del sistema, demostramos que este verifica la segunda y tercera ley de la Termodinámica y que la única consecuencia de la aparición de entropías negativas en el sistema en estudio es una no monotonicidad de la fuerza de Casimir con la temperatura.

Concluyendo, en este trabajo explicamos el origen de entropías negativas en un tipo de sistemas sujetos a efecto Casimir y las consecuencias que se derivan de dicho fenómeno.

---

* pabrodri@math.uc3m.es.

[1] H. B. G. Casimir, Proc. K. Ned. Akad. Wet. **51**, 793 (1948).
[2] M. Kardar and R. Golestanian, Rev. Mod. Phys. **71**, 1233 (1999).
[3] T. Emig, N. Graham, R.L. Jaffe, and M. Kardar, Phys. Rev. Lett. **99**, 170403 (2007).
[4] S.J. Rahi, T. Emig, N. Graham, R.L. Jaffe, and M. Kardar, Phys. Rev. D **80**, 085021 (2009).
[5] P. Rodriguez-Lopez, Phys. Rev. B **84**, 075431 (2011)

# Amplitude death in globally coupled chaotic systems with delay

V. M. Rodríguez* and M.G. Cosenza**
*IFISC (CSIC-UIB), Instituto de Física Interdisciplinar y Sistemas Complejos*
*Campus Universidad de las Islas Baleares*
*E-07122-Palma de Mallorca*
*Centro de Física Fundamental, Facultad de Ciencias, Universidad de Los Andes*
*Merida, Venezuela*

The phenomenon of amplitude death refers to a situation where individual oscillators cease oscillating and become synchronized in a fixed point state when they are coupled. In this work we investigate the emergence of amplitude death in systems of chaotic oscillators, such as Rössler and Lorenz, subject to a global interaction with a time delay. The appearance of synchronization in general, as well as the phenomenon of amplitude death are studied on the space of parameters of the system, given by the strength of the coupling and the amount of time delay. The regions of parameters where amplitude death emerges on this space exhibit a complex structure, such as islands of chaotic synchronization and islands of death. We have uncovered two distinct scenarios for the occurrence of amplitude death: (i) synchronization and amplitude death occur simultaneously, and (ii) synchronization precedes amplitude death. We identify the conditions for the occurrence of both scenarios and propose a simple geometric interpretation for them.

* vrodriguez@ifisc.uib-csic.es
** mcosenza@ula.ve

[1] K. Bar-Eli, *Physica* D14, **242** (1985).
[2] A. Prasad, *PRE* **72**, 056204 (2005).
[3] V. M. Rodríguez, M. Sc. Thesis, Universidad de Los Andes, Merida (2011).

# La corriente promedio en los "rocking ratchets"

N. R. Quintero, R. A. Nodarse y J. Cuesta[?]
*Universidad de Sevilla y Universidad Carlos III de Madrid*

El efecto ratchet, identificado con el movimiento de partículas o solitones, en una dirección preferencial como consecuencia de perturbaciones periódicas o aleatorias de promedio nulo, puede ser observado en diversos sistemas físicos. En los modelos matemáticos (y también en los experimentos) que describen la evolución de partículas o solitones forzados con una fuerza temporal periódica, $f(t)$, de media nula, y que son invariantes frente al desplazamiento temporal en medio período aparece una corriente ratchet cuando $f(t)$ rompe dichas simetrías. Un ejemplo sería la fuerza biarmónica $f(t) = \epsilon_1 \cos(q\omega t + \phi_1) + \epsilon_2 \cos(p\omega t + \phi_2)$ que es capaz de inducir el efecto ratchet si $p$ y $q$ son dos enteros coprimos de forma que $p + q$ sea impar para casi cualesquiera fases $\phi_1$ y $\phi_2$.

En esta presentación demostraremos que la corriente ratchet inducida por esta fuerza, cuando las amplitudes son pequeñas, está determinada por $v \propto \epsilon_1^p \epsilon_2^q \cos(p\phi_1 - q\phi_2 + \theta_0)$ donde $\theta_0$ depende de la disipación y de la frequencia, $\omega$, ($\theta_0 = \pi/2$ para el caso no amortiguado y $\theta_0 = 0$ si el sistema es sobreamortiguado)[1]. *Mostraremos cómo esta ley física es independiente del sistema y puede ser obtenida a partir de simples análisis de simetrías y con la ayuda de técnicas del análisis funcional.* Discutiremos brevemente resultados significativos como la optimización de la corriente ratchet aumentando la disipación[2] y la dependencia de la fase $\theta_0$ de $\epsilon_1$ y $\epsilon_2$ cuando las amplitudes no son tan pequeñas (ver resultados experimentales en redes ópticas[3]). Finalmente, comentaremos cómo podría generalizarse nuestra teoría a otros sistemas ratchets.

---

[1] Niurka R. Quintero, José Cuesta and Renato Alvarez-Nodarse. Phys. Rev. E, **81**, 030102(R) (2010).
[2] Niurka R. Quintero, Renato Alvarez-Nodarse and José Cuesta. J. Phys. A: Math. and Theoretical **44**, 425205 (2011).
[3] D. Cubero, V. Lebedev, and F. Renzoni. Phys. Rev. E **82**, 041116 (2010).

# Estudio de simulación por ordenador de líquidos iónicos en las cercanías de la transición vítrea

Álvaro Rodríguez-Rivas[†], José Manuel Romero-Enrique[‡] y Luis F. Rull
*Universidad de Sevilla, Dept. de Física Atómica, Molecualr y Nuclear, Avenida Reina Mercedes s/n, 41012, Sevilla, Spain*

Presentamos un trabajo de simulación por ordenador de Dinámica Molecular en el colectivo NPT sobre un modelo simple de líquidos iónicos superenfriados cercanos a la transición vítrea. El líquido iónico se ha modelado de la siguiente forma: los aniones son considerados como esferas blandas cargadas, y los cationes como cadenas completamente flexibles de esferas blandas tangentes, con una carga positiva situada en el centro de uno de los monómeros finales. En este estudio hemos considerado cadenas de hasta 5 monómeros. La transición vítrea se ha caracterizado mediante diferentes propiedades de transporte, tales como los coeficientes de autodifusión y viscosidad[1,2], así como las diferentes funciones de correlación temporal asociadas. Asimismo, hemos considerado otras funciones relacionadas con la presencia de dinámica heterogénea[3], como son la susceptibilidad dinámica[4] y el parámetro no-gaussiano[5]. Hemos observado una alta asociación entre monómeros cargados, y cierto grado de segregación entre monómeros cargados y neutros. A cierta presión y temperatura, los tiempos de relajación decrecen cuando se incrementa la longitud de la cadena, indicando una reducción de la temperatura de transicion vítrea a una presión fija. Los resultados del coeficiente de viscosidad sugiere que los líquidos iónicos son generadores de vídrios frágiles.

[†] arodriguezrivas@us.es
[‡] enrome@us.es

[1] M.H. Kowsari, S. Alavi, M Ashrafizaadeh, y B. Najafi, J. Chem. Phys **130**, 014703 (2009).
[2] C.E. Resende, y L.C. Gomide, J. Mol. Struct.: TheoChem **847**, 93 (2007).
[3] L. Berthier, G. Biroli, J.-P. Bouchaud, y R. L. Jack en *Dynamical Heterogeneities in Glasses, Colloids and Granular Media*. International Series of Monographs on Physics **150** (Oxford University Press, Oxford, 2011); arXiv: 0901.0493, (2010).
[4] L. Berthier, G. Biroli, J.-P. Bouchaud, L. Cipelletti, D. El Masri, D.L'Hôte, F. Ladieu, y M. Pierno, Science **310**, 1797 (2005).
[5] S.S. Sarangi, W. Zhao, F. Müller-Plathe, y S. Balasubramanian, Chem. Phys. Chem. **11**, 2001 (2010).

# Modeling dynamics of pluripotency in ES cells

Pau Rué, Jordi Garcia-Ojalvo*
*Departament de Física i Enginyeria Nuclear, Universitat Politècnica de Catalunya, Edifici GAIA, Rambla de Sant Nebridi s/n, Terrassa 08222, Barcelona, Spain*

Silvia Muñoz-Descalzo, Fernando Faunes, Alfonso Martinez-Arias
*Department of Genetics, University of Cambridge, Cambridge, United Kingdom.*

Embryonic Stem (ES) cells are cells derived from the epiblast tissue in inner cell mass of the mammalian blastocyst[1]. ES cells are characterized by two distinctive aspects: their potential to differentiate to any adult cell type in response to proper external signals, and their ability to self-renew indefinitely in culture. Both properties are what make ES cells very appealing from both the biomedicine and developmental biology points of view. Although pluripotency is, in fact, a short transient state of cells *in vivo*, clonal populations of these cells are kept in the pluripotent state *in vitro* thanks to a network of transcription factors involving Sox2/Oct4, Nanog[2] and Tcf3. Thus, understanding the mechanisms underlying the network of proteins is a must in controlling pluripotency.

Based on comprehensive quantitative data of the key regulatory components at the single-cell level, we have developed a detailed mathematical model of the network interactions. The model, expressed in terms of stochastic molecular reactions, includes both interactions at the transcriptional and post-translational levels (see Fig. 1A). Despite the fact that previous mathematical models exist that account for the regulated fluctuations of the key factor Nanog[3], the model presented here is, to our knowledge, the first based on precise quantitative data for more than one factor. The model, mainly fed with parameters estimated from the quantitative measurements (as opposed to fitted to data) is able to reproduce the experimental distributions of mRNA and protein concentrations of the involved factors (Nanog, Oct4, Tcf3, and $\beta$-catenin. See panel B from Fig. 1).

Another novel feature of this model is the inclusion of post-translational interactions and protein complex formation, an aspect that has shown crucial in understanding the high correlations observed among the protein concentrations (see Fig. 1C).

All in all, the pluripotency model presented here, founded on solid experimental data, brings new insight to the dynamics of the underlying network of molecular regulation.

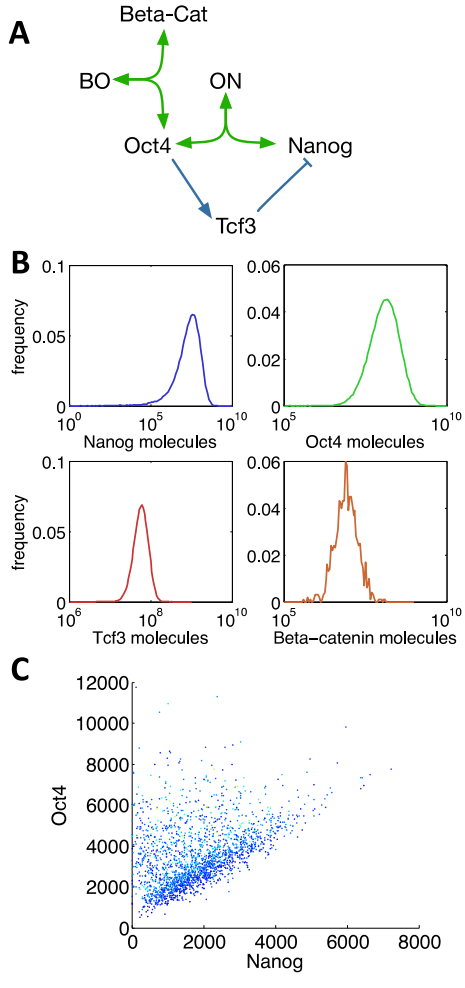


FIG. 1. Mathematical model of pluripotency dynamics. (A) Schematic representation of the network of molecular interactions. The key components of the model are the pluripotency factors Nanog and Oct4, together with Tcf3 and $\beta$-catenin. These factors interact both at the transcriptional and the post-translational levels. (B) Observed distributions of protein concentrations are reproduced by the stochastic model. Furthermore, the correlations among the species observed in the experimental single-cell data are also predicted by the model.

* jordi.g.ojalvo@upc.edu

[1] A. Smith, Annu. Rev. Cell Dev. Biol. **17**,435-462 (2001).
[2] L. A. Boyer, D. Mathur, R. Jaenisch Curr. Opin. Genet. Dev. **16**,455-462 (2006)
[3] T. Kalmar, *et al.* PLoS Biol. **7** (2009) e1000149.
[4] S. Muñoz Descalzo, P. Rué, J. Garcia-Ojalvo, and A. Martinez Arias *In preparation (2012).*

# Accelerometric nonlinearities in the International Space Station, ISS

N. Saez, X. Ruiz,[a] Jna. Gavalda
*Dept. Química Física i Inorgànica, Universitat Rovira i Virgili. Tarragona, Spain.*

The aim of this work is to detect and study nonlinearities in accelerometric records from the International Space Station, ISS. These records have been obtained downloading and reading the corresponding public binary files from the NASA web[1] or using files from past experiments[2].Nonlinearities, which are the potential sources of Gaussian deviations, are detected from the digital signals themselves using higher order statistical analysis techniques[3,4].

The first nonlinearity studied is the so-called quadratic phase coupling phenomenon. In this case phase coupling between two frequency components results in a contribution at a frequency equal to their sum (difference). These additional harmonics, called distortion harmonics, are also phase coupled to the original ones. Because such coupling affects the third order cumulant, equivalently its Fourier transform, the bispectrum is the only tool to detect and characterize such kind of nonlinear effects. The detection and quantification of the quadratic phase coupling is also supported by the bicoherence index. Remember that bicoherence is a squared normalized version of the bispectrum, that is to say, computed from a single signal, the bicoherence measures the proportion of the signal energy at some bifrequency that is quadratically phase coupled.

The second kind of nonlinearity investigated here is the so-called cubic phase coupling. It appears when the frequency and the phase of a component is the sum of the frequencies and phases of the three other components of the signal. Because the bispectrum is blind to the cubically-coupling components (in the same way, the trispectrum cannot resolve quadratically-coupled components), to detect this second nonlinearity the trispectrum is mandatory.

The comparison of the results between the different signals in different positions and days enabled us to present a complete enough vibrational picture of the Station. In addition, isolation in the payload racks that can be accommodated in the European Columbus module and/or in the American Destiny Lab, more near the center of mass of the Station, will also be discussed.

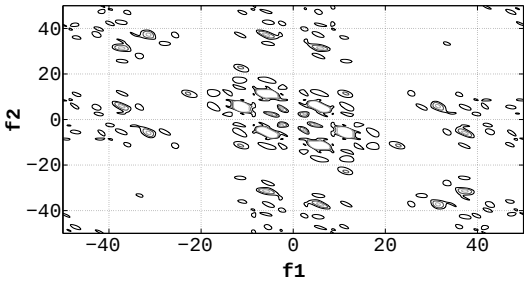


FIG. 1. Bicoherence of a real accelerometric run (number 29, start time : 08/12/09 10:40 ; end time :09/12/09 05:12) of the experiment called Influence of VIbrations on DIffusion, IVIDIL. This experiment was installed inside the Microgravity Science Glovebox, MSG, on September 23, 2009 by Frank de Winne (Expedition 21, ESA) and Robert Thirsk (Expedition 21, CSA). The experiment began October 5, 2009 and carried out more than 50 experimental runs until January 20, 2010. Finally, on January 28, 2010 IVIDIL was uninstalled by Soichi Noguchi (Expedition 22, JAXA).

---

[a] IEEC Institut d'Estudis Espacials de Catalunya, Barcelona, Spain.

[1] http://pims.grc.nasa.gov/html/ISSAccelerationArchive.html

[2] V. Shevtsova, *IVIDIL experiment onboard the ISS*. Advances in Space Research (2010) 46, 672-679.

[3] J. M. Mendel, *Tutorial on Higher-Order Statistics (Spectra) in Signal Processing and System Theory: Theoretical Results ans Some Applications*. Proceedings of the IEEE (1991)79, 278-305.

[4] A. Swami, *HOSA, Higher Order Spectral Analysis Toolbox*, 2003, MATLAB-Toolbox.

# Synchronization of moving integrate and fire oscillators with a minimal interaction rule

Luce Prignano, Oleguer Sagarra, Albert Diaz-Guilera
*PHYSCOMP2 group, Facultat de Física*
*Universitat de Barcelona 08028-Barcelona (Barcelona)*

In the framework of the study of synchronization on populations of moving agents[1][2], we present a model of moving integrate and fire oscillators[3] that interact using a first-neighbor rule in a box with periodic boundary conditions. The time spent in synchronization ($T_{sync}$) is shown to be strongly dependent on the velocity in a non-uniform way.

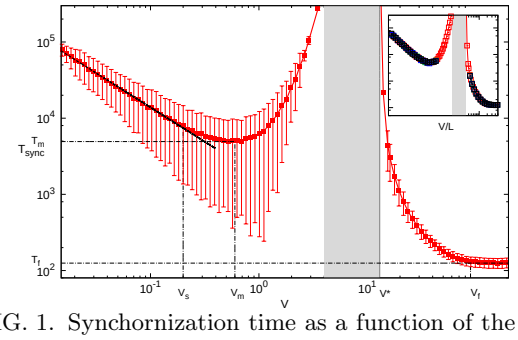


FIG. 1. Synchornization time as a function of the velocity of the agents. The shaded zone corresponds to the no-sync regime.

In doing so, we have detected the emergence of two distinct regimes that are separated by a peaked zone in which an interplay between movement and internal phases time scales inhibits the synchronization.

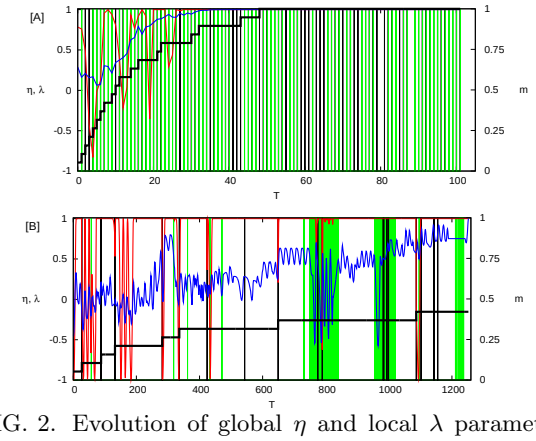


FIG. 2. Evolution of global $\eta$ and local $\lambda$ parameters as well as mixing $m$ for a single run on the system as a function of reference time $T$. We observe sharp differences between fast (top) and slow (bottom) regime.

In order to investigate such zone we have introduced novel parameters (cumulative individual and total interaction network and mixing) providing empirical insights on the mechanisms that allow the system to reach the coherent state.

We have furthermore studied the dependence of our system with respect to the number of agents involved $N$, the coupling constant $\epsilon$ and the velocity $v$, detecting two distinct regimes[4]. A complete characterization of both the fast regime (where synchronization emerges gradually and globally on the system) and the slow one (where sync is attained through competition between local phases) is presented and scaling expression for the behaviour of the relevant magnitudes of the model are derived.

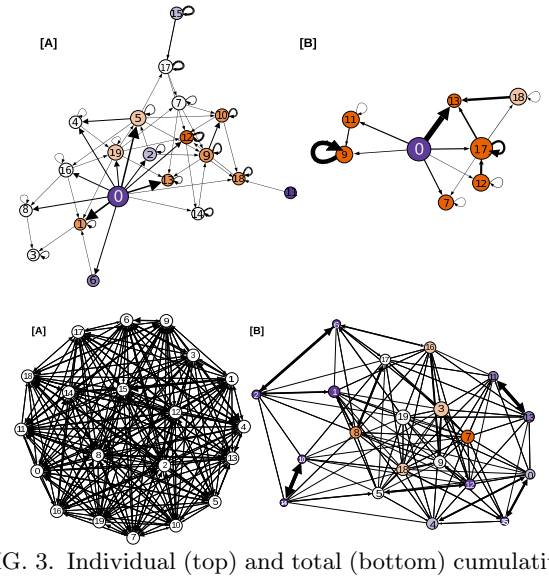


FIG. 3. Individual (top) and total (bottom) cumulative interaction networks of the system for fast (left) and slow (right) regimes that show the interaction among agents of the system using different sync mechanisms.

[1] Frasca, M. et altr. *Synchronization of moving chaotic agents* PRL 100, 044102.
[2] Fujiwara, N. et altr. Synchronization in networks of mobile oscillators PRE 83, 025101
[3] Mirollo, R. E. & Strogatz, S. H. [1990] *Synchronization of Pulse-Coupled biological oscillators* SIAM J. Appl. Math. 50, 1645 1662.
[4] Prignano, L. et altr. *Synchronization of moving integrate and fire oscillators* IJBC D 11 00476 [in press].

# A new Percus–Yevick equation of state for hard spheres, as derived from the chemical-potential route

Andrés Santos*
*Departamento de Física, Universidad de Extremadura, E-06071 Badajoz, Spain*

As is well known, the hard-sphere (HS) model is of great importance in liquid state theory from both academic and practical points of view. The model is also attractive because it provides a nice example of the existence of non-trivial exact solutions of an integral-equation theory, namely the Percus–Yevick (PY) theory.

As generally expected from an approximate theory, the radial distribution function (RDF) provided by the PY integral equation suffers from thermodynamic inconsistencies, i.e., the thermodynamic quantities derived from the same RDF via different routes are not necessarily mutually consistent. In particular, the PY solution for HSs of diameter $\sigma$ yields the following expression for the compressibility factor $Z \equiv p/\rho k_B T$ (where $p$ is the pressure, $\rho$ is the number density, $k_B$ is Boltzmann's constant, and $T$ is the temperature) through the virial (or pressure) route:

$$Z_v(\eta) = \frac{1+2\eta+3\eta^2}{(1-\eta)^2}. \tag{1}$$

Here, $\eta = \frac{\pi}{6}\rho\sigma^3$ is the packing fraction and the subscript $v$ is used to emphasize that the result corresponds to the virial route. In contrast, the compressibility route yields

$$Z_c(\eta) = \frac{1+\eta+\eta^2}{(1-\eta)^3}. \tag{2}$$

Equation (2) is also obtained from the scaled-particle theory (SPT). The celebrated and accurate Carnahan–Starling (CS) equation of state (EOS) is obtained as the simple interpolation

$$Z_{\rm CS}(\eta) = \frac{1}{3}Z_v(\eta) + \frac{2}{3}Z_c(\eta) = \frac{1+\eta+\eta^2-\eta^3}{(1-\eta)^3}. \tag{3}$$

Except perhaps in the context of the SPT, little attention has been paid to the chemical-potential route to the EOS of HSs. In particular, the possibility of obtaining the EOS via this route by exploiting the exact solution of the PY equation for HS mixtures seems to have been overlooked. The aim of this work is to fill this gap and derive the result[1]

$$Z_\mu(\eta) = -9\frac{\ln(1-\eta)}{\eta} - 8\frac{1-\frac{31}{16}\eta}{(1-\eta)^2}, \tag{4}$$

where the subscript $\mu$ in Eq. (4) denotes that the compressibility factor is here obtained via the chemical-potential route. Equation (4) differs from Eqs. (1) and (2) in that it includes a logarithmic term and thus it is not purely algebraic. Nevertheless, $Z_\mu(\eta)$ is analytic at $\eta = 0$ and provides well-defined values for the (reduced) virial coefficients $b_n$ defined by $Z(\eta) = 1 + \sum_{n=2}^{\infty} b_n \eta^{n-1}$. Comparison of the first ten virial coefficients obtained from Eqs. (1), (2), and (4) with the exact analytical ($n = 2$–$4$) and Monte Carlo values shows that those given by the chemical-potential route are more accurate than those from the virial route, although less than the ones from the compressibility route. This suggests the possibility of exploring a CS-like interpolation of the form $Z_{\mu c}(\eta) = \alpha Z_\mu(\eta) + (1-\alpha)Z_c(\eta)$ with $\alpha > \frac{1}{3}$. A simple and convenient choice is $\alpha = \frac{2}{5}$. Thus,

$$\begin{aligned} Z_{\mu c}(\eta) &= \frac{2}{5}Z_\mu(\eta) + \frac{3}{5}Z_c(\eta) \\ &= -\frac{18}{5}\frac{\ln(1-\eta)}{\eta} - \frac{13-50\eta+28\eta^2}{5(1-\eta)^3}. \end{aligned} \tag{5}$$

The superiority of $Z_{\mu c}$ over $Z_{\rm CS}$ is confirmed by Fig. 1, where the differences $Z_{\mu c} - Z_{\rm CS}$ and $Z_{\rm MD} - Z_{\rm CS}$ (where $Z_{\rm MD}$ denotes molecular dynamics simulation values[2]) are compared. As can be seen, $Z_{\mu c}$ is closer than $Z_{\rm CS}$ to $Z_{\rm MD}$ up to $\eta \simeq 0.46$.

Equation (4) can be further extended to additive mixtures with the result

$$\begin{aligned} Z_\mu = &\frac{1}{1-\eta} + 3\frac{M_1 M_2}{M_3}\frac{\eta}{(1-\eta)^2} \\ &-9\frac{M_2^3}{M_3^2}\left[\frac{\ln(1-\eta)}{\eta} + \frac{1-\frac{3}{2}\eta}{(1-\eta)^2}\right], \end{aligned} \tag{6}$$

where $M_n \equiv \sum_i x_i \sigma_i^n$.

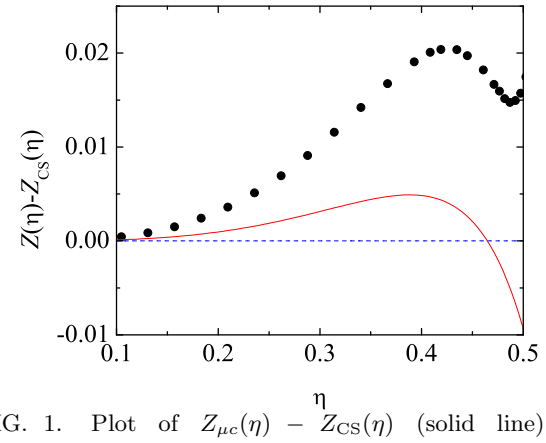


FIG. 1. Plot of $Z_{\mu c}(\eta) - Z_{\rm CS}(\eta)$ (solid line) and $Z_{\rm MD}(\eta) - Z_{\rm CS}(\eta)$ (circles).

* andres@unex.es
http://www.unex.es/eweb/fisteor/andres

[1] A. Santos, unpublished (2012).

[2] S. Labík, J. Kolafa, and A. Malijevský, Phy. Rev. E **71**, 021105 (2005).

# Impact of roughness on the entropy of a granular gas in the homogeneous cooling state

Andrés Santos* and Gilberto M. Kremer†,‡
*Departamento de Física, Universidad de Extremadura, E-06071 Badajoz, Spain*

The dynamics of a dilute granular gas, modeled as a system of hard spheres colliding inelastically with constant coefficients of normal ($\alpha$) and tangential ($\beta$) restitution, can be described at a mesoscopic level by the (inelastic) Boltzmann equation for the one-body velocity distribution function $f(\mathbf{r},\mathbf{v},\boldsymbol{\omega},t)$[1]. A granular gas is intrinsically out of equilibrium and thus, in contrast to the case of energy conservation (elastic collisions), the evolution of $f$ does not obey an H theorem, even if the system is isolated. On the other hand, it is worthwhile introducing the Boltzmann entropy density[2]

$$s(\mathbf{r},t) = -\int d\mathbf{v} \int d\boldsymbol{\omega}\, f(\mathbf{r},\mathbf{v},\boldsymbol{\omega},t) \ln f(\mathbf{r},\mathbf{v},\boldsymbol{\omega},t).$$

Although $s(\mathbf{r},t)$ does not qualify as a Lyapunov function in the inelastic case, its introduction is justified by information-theory arguments and also to make contact with the Boltzmann entropy density of a conventional gas. The local *relative* entropy per particle is

$$s^*(\mathbf{r},t) = \frac{s(\mathbf{r},t) - s_0(\mathbf{r},t)}{n(\mathbf{r},t)} = -\langle \ln R(\mathbf{r},\mathbf{v},\boldsymbol{\omega},t)\rangle, \quad (1)$$

where $s_0(\mathbf{r},t)$ is the local equilibrium entropy density, $R(\mathbf{r},\mathbf{v},\boldsymbol{\omega},t) \equiv f(\mathbf{r},\mathbf{v},\boldsymbol{\omega},t)/f_0(\mathbf{r},\mathbf{v},\boldsymbol{\omega},t)$, $f_0$ being the (two-temperature) local equilibrium distribution, and $\langle\cdots\rangle \equiv n^{-1}\int d\mathbf{v}\int d\boldsymbol{\omega}\cdots f$. Obviously, $s_0 \geq s$ and thus $s^* \leq 0$.

In general, the ratio $R$ can be expanded in a complete set of orthonormal polynomials $\{\Psi_{\mathsf{k}}\}$ as $R(\mathbf{r},\mathbf{v},\boldsymbol{\omega},t) = 1 + \sum_{\mathsf{k}} A_{\mathsf{k}}(\mathbf{r},t)\Psi_{\mathsf{k}}(\mathbf{r},\mathbf{v},\boldsymbol{\omega},t)$, where $\mathsf{k}$ denotes the appropriate set of indices and $A_{\mathsf{k}}(\mathbf{r},t) = \langle \Psi_{\mathsf{k}}(\mathbf{r},\mathbf{v},\boldsymbol{\omega},t)\rangle$. In the *linear* approximation $\ln R \approx R - 1$, Eq. (1) becomes

$$s^*(\mathbf{r},t) \approx -\sum_{\mathsf{k}} A_{\mathsf{k}}^2(\mathbf{r},t).$$

Now we particularize to a homogeneous and isotropic system. In that case, neglecting coefficients $A_{\mathsf{k}}$ associated with polynomials of degree higher than four, we have

$$s^*(t) \approx -\frac{15}{8}a_{20}^2(t) - \frac{15}{8}a_{02}^2(t) - \frac{9}{4}a_{11}^2(t) - \frac{9}{4}b^2(t),$$

where the cumulants $a_{20}$, $a_{02}$, $a_{11}$, and $b$ are defined by

$$a_{20} = \frac{3}{5}\frac{\langle v^4\rangle}{\langle v^2\rangle^2} - 1, \quad a_{02} = \frac{3}{5}\frac{\langle \omega^4\rangle}{\langle \omega^2\rangle^2} - 1,$$

$$a_{11} = \frac{\langle v^2\omega^2\rangle}{\langle v^2\rangle\langle\omega^2\rangle} - 1, \quad b = \frac{9}{5}\frac{\langle(\mathbf{v}\cdot\boldsymbol{\omega})^2\rangle - \frac{1}{3}\langle v^2\omega^2\rangle}{\langle v^2\rangle\langle\omega^2\rangle}.$$

In this work we make use of a recent Sonine approximation for the collisional rates of change of $a_{ij}(t)$ and $b(t)$[3,4] to study the temporal evolution of $s^*(t)$ in the homogeneous cooling state. The asymptotic stationary value $s^*(\infty)$ is also analyzed as a function of both $\alpha$ and $\beta$.

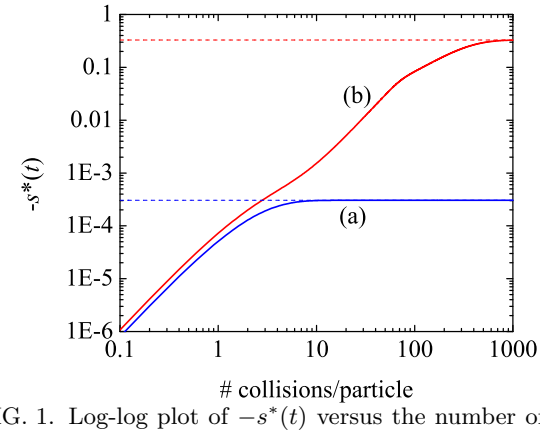


FIG. 1. Log-log plot of $-s^*(t)$ versus the number of collisions per particle for (a) $\alpha = 0.8$ and $\beta = -1$ and (b) $\alpha = 0.8$ and $\beta = -0.9$.

As an example, Fig. 1 shows the temporal evolution of the relative entropy $s^*(t)$ for (a) smooth particles ($\beta = -1$) and (b) slightly rough particles ($\beta = -0.9$), in both cases with $\alpha = 0.8$. We can observe the dramatic influence of roughness: both the relaxation time (measured by the number of collisions) and the stationary value $|s^*(\infty)|$ have increased by three orders of magnitude in the rough case (b) with respect to the smooth case (a).

* andres@unex.es
http://www.unex.es/eweb/fisteor/andres
† Departamento de Física, Universidade Federal do Paraná, Curitiba, Brazil
‡ kremer@fisica.ufpr.br

[1] A. Santos, G. M. Kremer, and V. Garzó, *Prog. Theor. Phys. Suppl.* **184**, 31 (2010).
[2] G. M. Kremer, *Physica A* **389**, 4018 (2010).
[3] A. Santos, G. M. Kremer, and M. dos Santos, *Phys. Fluids* **23**, 030604 (2011).
[4] A. Santos, F. Vega Reyes, and G. M. Kremer, unpublished (2012).

# Self-organized beat of cilia through the non-equilibrium dynamics of ratchets

Pablo Sartori[1], V. Geyer[2], J. Howard[2] & F. Juelicher[1]
*Max Planck Institute for the Physics of Complex Systems, Dresden, Germany*
*Max Planck Institute of Molecular and Cell Biology, Dresden, Germany*

## I. INTRODUCTION

Cilia are elongated cillyndrical structures present in many eukariotic cells, such as mammalian Sperm cells, human lung cells, or the unicellular algae Chlamydomonas (Fig. 1, left). Their fundamental role is motility, achieved by a periodic beat pattern. The internal structure of a cillia is composed of 9 microtubule dublets (MT's), which can bend; Dynein motors connecting the MT's, which consume ATP to shear them; and nexin connecting adjacent MT's, which constrain the shearing forces producing bending (Fig. 1, right).

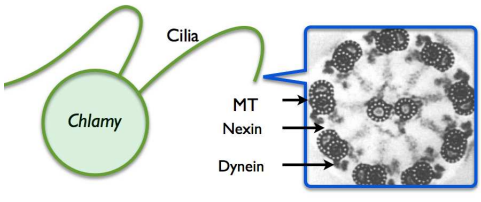


FIG. 1. **Left.** Schematic view of Chlamydomonas with two cilia. **Right.** Cross section of cilia with its main components.

The two main open questions which we address are: Can a minimal model based on these ingredients explain the beat pattern and swimming behaviour of cilia? And what is the mecano-chemical feedback to the motors which gives raise to the periodic beat? Ultimately, we would like to infer properties of the motors by comparing our theory to different experimental conditions.

## II. MECHANICS AND HYDRODYNAMICS

Our cilia model is characterized by the free energy $G$, which accounts for elastic and active forces; and a simple fluid model, resistive force theory:

$$G = \int_0^L [\frac{\kappa_b}{2} C^2 + f\Delta + \Lambda \mathbf{t}^2]\mathrm{ds} \;\Rightarrow\; [\mathbf{nn}\xi_\mathrm{n} + \mathbf{tt}\xi_\mathrm{t}]\cdot\partial_\mathrm{t}\mathbf{r} = \frac{\delta \mathrm{G}}{\delta \mathbf{r}}$$

In the free energy there is an elastic term characterized by $\kappa_b$ and the curvature $C$, a tensile term with the Lagrange multiplier $\Lambda$, and a term with work performed by an internal force $f$ in creating shear $\Delta$ (Fig. 2, left). This force itself has three components $f = f_m - \kappa_s\Delta - \xi_s\partial_t\Delta$. The first is the motor force, the second is the shearing elasticity $\kappa_s$, and the third the shear friction $\xi_s$ (Fig. 2, right). These elastic forces are balanced by fluid friction forces proportional to the velocity $\partial_t\mathbf{r}$ through two friction coefficients: $\xi_n$ in the normal direction $\mathbf{n}$, and $\xi_t$ in the tangential direction $\mathbf{t}$.

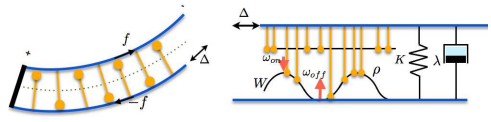


FIG. 2. .
**Left.** Schematic representation of a cilia, with opposing motors creatin a pair force $f$ which generates a shear $\Delta$.
**Right.** Ratchet model of the molecular motors.

This model is compared with experiments performed by our group with Chlamydomonas. We describe the motor force as a plane wave, of which we take all parameters from experiments besides the amplitude, which we fit. With this description we are able to obtain the right swimming of the cilia: translational and rotational velocity, as well as path curvature.

## III. SELF ORGANIZED CILIARY BEAT

In the previous model the oscillating motor force was provided ad-hoc, however it should emerge as a collective property of the interaction between motors and cilia. Several motor models are possible: motors could respond to normal forces, to stretching of their arms, to curvature, or to shear displacements. Here we use a ratchet model (Fig. 2, right), in which the localized detachment and attachment of motors in certain points of the cilia drives motor oscillations. The probability of bound motors evolves as:

$$\partial_t P(x) = -\partial_t\Delta\partial_x P + \omega_{on}(x)(1 - P(x)) - \omega_{off}(x)P(x)$$

As mentioned above, detailed balance violation $\omega_{off}(x) \neq \omega_{on}(x)e^{\Delta W(x)}$ (and thus ATP consumption) is necessary to drive the motors into an oscillatory regime. The elastic coupling of the motors through the ciliary structure coordinates the local motor oscillations, finally giving raise to a beat pattern.

Changing the parameters of the motors affects the beat pattern. Future work involves decoding properties of the dynein arms in cilia by comparing the beat patterns of several mutants to the beat patterns of the theoretical model when altering motor properties.

---

[1] Max Planck Institute for the Physics of Complex Systems.
[2] Max Planck Institute of Molecular and Cell Biology.

# Inhibitory Synaptic Conductances Mediate Transition From Delayed Synchronization to Anticipated Synchronization Between Neuronal Populations

Fernanda S. Matias*+, Leonardo L. Gollo, Pedro V. Carelli+, Mauro Copelli+, Claudio R. Mirasso
*IFISC, Instituto de Física Interdisciplinar y Sistemas Complejos CSIC-Universidad de las Islas Baleares*
*07122-Palma de Mallorca, Spain*

Two identical autonomous dynamical systems coupled in a master-slave configuration can exhibit anticipated synchronization (AS) if the slave is subjected to a delayed negative self-feedback[1]. One of the prototypical examples of AS is described by the equations[1]

$$\begin{aligned} \dot{x} &= f(x(t)), \\ \dot{y} &= f(y(t)) + K[x(t) - y(t - t_d)]. \end{aligned} \tag{1}$$

$f(x)$ is a function which defines the autonomous dynamical system. The solution $y(t) = x(t + t_d)$, which characterizes AS, has been shown to be stable in a variety of scenarios, including theoretical studies of autonomous chaotic systems[1], delayed-coupled maps[2] and non-autonomous dynamical system as FitzHugh-Nagumo models driven by white noise[3].

Recently, AS was shown to occur in systems of simplified neuron models, where the delayed inhibition is provided by an interneuron[4]. In this biologically plausible scenario, a smooth transition from delayed synchronization (DS) to AS typically occurs when the inhibitory synaptic conductance is increased.

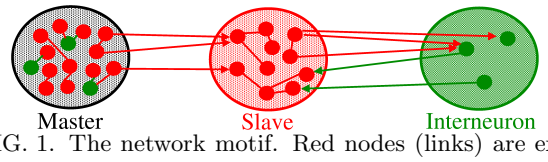


FIG. 1. The network motif. Red nodes (links) are excitatory neurons (synapses), green ones are inhibitory.

Here we investigate the synchronization of 3 large populations[5] of interconnected neurons. The master population contains both excitatory and inhibitory neurons. The slave population contains excitatory neurons and receives feedback from an interneuron population (see Fig. 1). Each neuron is modeled by the Izhikevich[6] model with parameters that reproduce firing patterns observed in the cortex. The links are unidirectional dynamical synapses mediated by $AMPA$ and $GABA_A$[7]. We find that this nework motif exhibits a transition from DS to AS. The mean time lag $\tau$ between the master population and the slave population is a function of the inhibitory synaptic conductance $g_{GABA_A}$ as shown in Fig. 2. By definition if $\tau < 0$ ($\tau > 0$) the system is in the DS (AS) regime. As occurs in the 3-neurons motif[4], here the anticipation time is not hard-wired in the dynamical equations, but rather emerges from the system's dynamics.

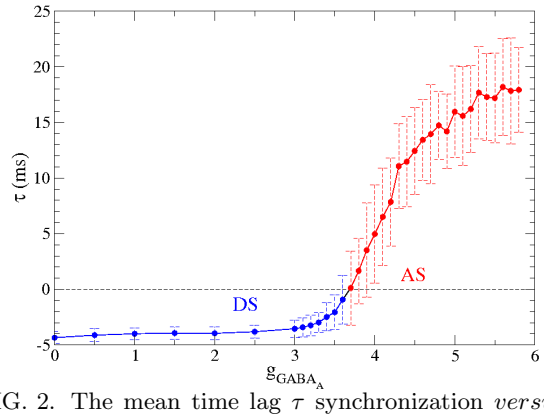


FIG. 2. The mean time lag $\tau$ synchronization *versus* inhibitory synaptic conductances. $\tau = 0$ is where the transition from DS (blue) to AS (red) regime occurs

* fernanda@ifisc.uib-csic.es
+ Departamento de Física, Universidade Federal de Pernambuco, Recife, Pernambuco 50670-901 Brazil

[1] H. U. Voss, *Phys. Rev. E*, vol.61, pp.5115, 2000 *Phys. Rev. E*, vol.64, pp.039904, 2001; H. U. Voss, *Phys. Rev. Lett*, vol.87, pp.014102, 2001
[2] C. Masoller and D.H. Zanette, *Physica A*, vol.300, pp.359-366, 2001
[3] M. Ciszak, O. Calvo, C. Masoller, C.R. Mirasso and R. Toral, *Phys. Rev. Lett.*, vol.90, pp.204102, 2003; M. Ciszak, F. Marino,R. Toral and S. Balle, *Phys. Rev. Lett.*, vol.93, pp.114102, 2004; R. Toral, C. Masoller, C.R. Mirasso, M. Ciszak and O. Calvo, *Physica A*, vol.325, pp.192, 2003.
[4] F.S. Matias, C.V. Carelli, C.R. Mirasso, M. Copelli *Phys. Rev. E*, vol.84, pp.021922, 2011.
[5] R. Vicente and L.L. Gollo and C.R. Mirasso and I. Fischer and G. Pipa *PNAS*, vol.105, pp.17157-17162, 2008.
[6] E.M. Izhikevich, J.A. Gally, G.M. Edelman *Cerebral Cortex*, vol.14, pp933-944, 2004.
[7] *Methods in Neuronal Modeling: From Ions to Networks*, 2nd ed., edited by C. Koch and I. Segev (MIT Press, Cambridge, MA, 1998).

# Modeling of the mechanical response of solid semicrystalline polymers

Maria Serral Serra*, Josep Bonet Avalos+
*Molecular Simulation Group: Polymers and Interfaces*
*DEQ-Departament d'Enginyeria Química - Universitat Rovira i Virgili*
*43007-Tarragona*

Mechanical properties of most of the solid materials are commonly determined experimentally. Predictions on what would be the material response under a certain load are hard because such a response also depends on the processing of the material. However, a model on the mechanical response would be helpful for the industry because it gives relevant information beforehand, needed to improve the design of new materials to be produced.

Within this framework, we will try to develop a mathematical model to predict the mechanical response of solid polymers. The mechanical behavior under dynamic loading depends on elastic as well as viscous properties, so we pretend to determine the linear viscoelastic features based on the theory developed by Ferry[1]. From viscoelasticity, we aim at elucidating a plausible morphology and molecular structure of the system through the macroscopic data, being that this property contain information on it[123].

To validate the model and find the model parameters we have available data corresponding to dynamic mechanical analysis experiments of polyethylene bars in the linear regime.

Nevertheless, the problem will not have a trivial solution because the polymer studied is not amorphous. A straight fitting to the literature available models for the amorphous polymers is not possible[4] and no time-temperature superposition with a single shift can be found[3]. It has to be taken into account that the polymer has a semicrystalline structure and their mechanical relaxation is complex[5].

Hence, we pretend that the microscopic mechanism leading to complex response can be depicted using a Generalized Maxwell model,as it has already been done by Klompen[6], with a small modification, which is represented by a combination of springs and dashpots and can be mathematically expressed by a real and an imaginary part:

$$G^* = G' + iG'' \tag{1}$$

$$G'(\omega) = k + \int_0^\infty \mathrm{d}\tau \frac{(\omega\tau)^2 \tilde{\mathrm{E}}(\tau)}{1+(\omega\tau)^2} \tag{2}$$

$$G''(\omega) = \eta\omega + \int_0^\infty \mathrm{d}\tau \frac{(\omega\tau) \tilde{\mathrm{E}}(\tau)}{1+(\omega\tau)^2} \tag{3}$$

where $G^*$ is the shear complex modulus, $G'$ and $G''$ are the storage and loss modulus, $\omega$ is the frequency, $\tau$ is the relaxation time, $\tilde{E}$ is the contribution of the modulus at each relaxation time, $k$ is the elasticity constant and $\eta$ is the pure viscous term.

The determination of the model parameters has been achieved by performing a parameter estimation as a global optimization problem using a simulated annealing algorithm to solve it. The probabilistic metaheuristic for global optimization brings the system from an arbitrary initial state to a state with the minimum possible "free energy".

Once the minimization is done it can be said that the Generalized Maxwell model is capable to satisfactorily fit the experimental data, available for the dynamic response, with the model proposed for both, the storage and the loss modulus.

A discrete relaxation spectrum is obtained for each experiment at a given temperature. The region where we have the data is where a lower deviation is obtained and as we move away from this window, some points with higher error appear. At different temperatures the spectrum keeps the same pattern but with some changes in position and height.

The elasticity constant $k$ added in parallel to the generalized Maxwell model decreases substantially as the temperature approaches the melting point, as expected. The pure viscous term $\eta$ also added in parallel, presents a maximum on the glass-transition temperature.

We consider that the results obtained are meaningful and the description of the microscopic structure could be done from them as next step. Further interpretation on the internal structure of the polymers might be done with that information obtained.

---

* maria.serral@urv.cat
+ josep.bonet@urv.cat

[1] Ferry, JD. (1980): Viscoelastic Properties of Polymers, 3rd. ed., John Wiley and Sons, New York.
[2] Rodriguez. F (1996): Principles of Polymer Systems, 4th. ed., Taylor and Francis, Washington.
[3] Ward IM., Hadley DW. (1993): An Introduction to the Mechanical Properties of Solid Polymers, John Wiley and Sons, New York.
[4] Tobolsky, AV. 1956 J. Appl. Phys. 27, 673-685
[5] Boyd, RH. 1985 Polymer 26, 1123-1133
[6] Klompen, Edwin T.J (2005): Mechanical properties of solid polymers: constitutive modeling of long and short term behavior, Techische Universiteit Eindhoven, Eindhoven.

# Defibrillation mechanisms on a one-dimensional ring of cardiac tissue

J. Bragard, A. Šimić*, E. M. Cherry†, F. Fenton‡, N. Otani‡
*Dept. of Physics and Applied Mathematics, Faculty of Sciences, University of Navarra, Pamplona, Spain*

Defibrillation is a medical treatment used to terminate ventricular fibrillation or pulseless ventricular tachycardia. An electrical device via a pair of electrodes delivers controlled amount of electrical energy to the heart in order to reestablish the normal heart rhythm. First generation of defibrillators applied monophasic shock, in which electrodes did not change polarity during the application of the shock. Later it was found that changing the polarity of the electrodes during the shock leads to better result with less energy applied. Optimal monophasic and biphasic shock release approximately 200 J and 150 J, respectively. It is desirable to use as less energetic shock as possible in order to reduce the damage done to the tissue by the strong electric current. However, to this day, there is no full understanding why biphasic shocks are better than monophasic shocks. To assess this question, we have used a bidomain model for cardiac tissue with modified Beeler-Reuter model[1] for transmembrane currents. Modifications account for anode break phenomena and electroporation effect known to happen during defibrillation. We have studied three different types of protocols for shock application (i.e. monophasic; symmetric biphasic; and asymmetric biphasic shock) in a one dimensional ring of cardiac tissue. The size of the ring was chosen to exhibit a discordant-alternans dynamics. Results of the numerical simulations reveal that monophasic shocks defibrillate with higher rate of success than the two biphasic shock protocols at lower energies. On the contrary for higher shock energies, the biphasic shock are significantly more effecient than monophasic shocks. This latter result confirms the medical common wisdom about defibrillators. Moreover, in this study, we were able to identify and classify the different defibrillation mechanisms that happen in this system. One identifies four different types: direct block, delayed block, annihilation and direct activation. Which defibrillation mechanism prevails depends on the energy level, the current dynamic state of the system and the shock protocol. This study has permitted to uncover and confirm the experimental fact stating that biphasic shocks are more efficient (at high energy) than monophasic shock to defibrillate cardiac tissue.

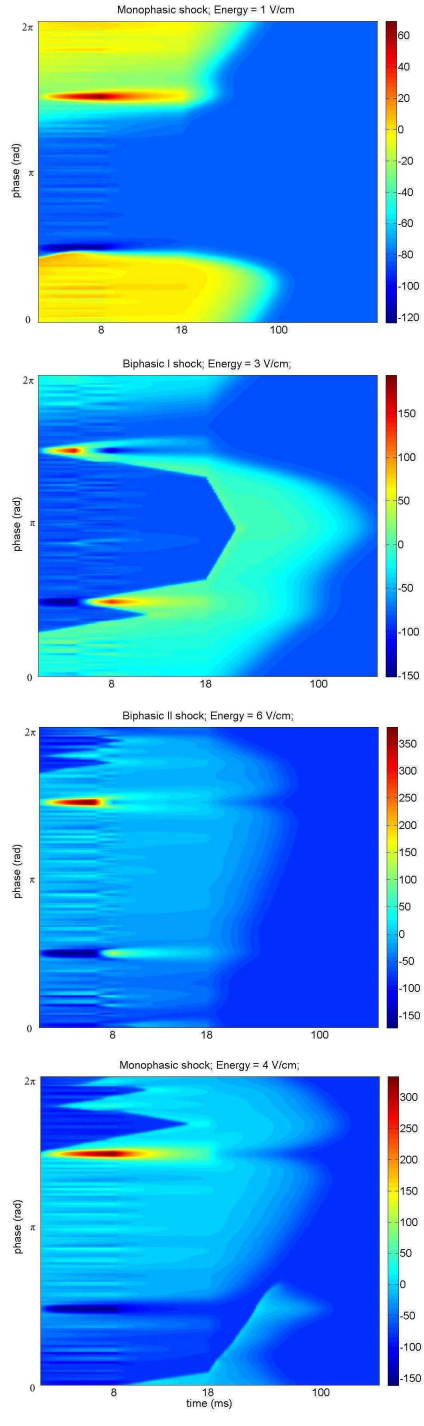


FIG. 1. Defibrillation mechanisms. Defibrillation by : direct block, annihilation of the fronts, direct activation and delayed block (from top to bottom).

* asimic@alumni.unav.es
† School of Mathematical Sciences, Rochester Insititute of Technology, Rochester, USA
‡ Dept.of Biomedical Sciences, Cornell University, Ithaca, USA

[1] G. W. Beeler, H. Reuter, J. Physiol. **268**, 177-210 (1992).

# Random walks on temporal networks

Michele Starnini, Andrea Baronchelli*, Alain Barrat** and Romualdo Pastor-Satorras
*Departament de Física i Enginyeria Nuclear, Universitat Politècnica de Catalunya, Campus Nord B4, 08034 Barcelona, Spain*

Many natural and artificial networks evolve in time[1]. Nodes and connections appear and disappear at various timescales, and their dynamics has profound consequences for any processes in which they are involved. Until recently however, a large majority of studies about complex networks have focused on a static or aggregated representation, in which all the links that appeared at least once coexist. In recent years, the interest towards the temporal dimension of the network description has blossomed, and at the same time, researchers have started to study how the temporal evolution of the network substrate impacts the behavior of dynamical processes.

Here, we study how random walks, as paradigm of dynamical processes, unfold on temporally evolving networks[2]. To this aim, we use empirical dynamical networks of contacts between individuals in various social contexts, as recorded by the SocioPatterns project[3]. These dynamical networks exhibit heterogeneous and bursty behavior, indicated by the long tailed distributions for the lengths and strength of conversations, as well as for the gaps separating successive interactions. We underline the importance of considering not only the existence of time preserving paths between pairs of nodes, but also their temporal duration: shortest paths can take much longer than fastest paths, while fastest paths can correspond to many more hops than shortest paths. Interestingly, the appropriate rescaling of these quantities identifies universal behaviors shared across the datasets considered.

Given the finite life-time of each network, we consider as substrate for the random walk process the replicated sequences in which the same time series of contact patterns is indefinitely repeated. At the same time, we propose two different randomization procedures to investigate the effects of correlations in the real dataset. The "sequence randomization" destroys any temporal correlation by randomizing the time ordering of the sequence. This allows to write down exact mean-field equations for the random walker exploring these networks, which turn out to be substantially equivalent to the ones describing the exploration of the weighted projected network. The "statistically extended sequence", on the other hand, selects random conversations from the original sequence, thus preserving the statistical properties of the original time series, with the exception of the distribution of time gaps between consecutive conversations.

We perform numerical analysis both for the coverage and the mean first passage time properties of the random walker. In both cases we have found that the empirical sequences deviate systematically from the mean field prediction, inducing a slowing down of the network exploration and of the mean first passage time. Remarkably, the analysis of the randomized sequences has allowed us to point out that this is due *uniquely* to the temporal correlations between consecutive conversations present in the data, and *not* to the heterogeneity of their lengths.

Finally, we address the role of the finite size of the empirical networks, which turns out to prevent a full exploration of the random walker, though differences exist across the different cases. In this context, we have also shown that different starting nodes provide on average different coverages of the networks, at odds to what happens in static graphs. In the same way, the probability that the node $i$ is reached by the random walker at any time in the contact sequence exhibits a common behavior across the different time series, but it is not described by the mean-field predictions for the aggregated network, which predict a faster process. Considering the fundamental prototypical role of the random walk process, we believe that these results could help to shed light on the behavior of more complex dynamics on temporally evolving networks.

---

* Department of Physics, College of Computer and Information Sciences, Bouvé College of Health Sciences, Northeastern University, Boston MA02120, USA
** Centre de Physique Théorique, Aix-Marseille Univ, CNRS UMR 7332, Univ Sud Toulon Var, 13288 Marseille cedex 9, France

[1] P. Holme and J. Saramaki, "Temporal networks", (2011), eprint arxiv:1108.1780v1.
[2] M. Starnini, A. Baronchelli, A. Barrat and R. Pastor Satorras, "Random walks on temporal networks", (2012), eprint arxiv:1203.2477v2.
[3] `http://www.sociopatterns.org` .

# Transporte y difusión anómalos de partículas Brownianas en superfícies desordenadas

Marc Suñé Simon*,†, J. M. Sancho**,† and A. M. Lacasta***,‡
†*Departament d'Estructura i Constituents de la Matèria,*
*Facultat de Física, Universitat de Barcelona,*
*Martí i Franquès, 1. E-08028 Barcelona, Spain*

El transporte (velocidad) y la difusión (dispersión aleatoria) de las partículas Brownianas se estudian a partir del primer momento y la varianza de la distribución de las posiciones de dichas partículas. Cuando el sistema en estudio incluye potenciales no lineales, los momentos anteriores dejan de ser funciones lineales del tiempo, con lo que aparecen fenómenos anómalos en el transporte y la difusión.

Consideramos el caso particular del movimiento *overdamped* de partículas Brownianas idénticas que no interactuan entre ellas, bajo la acción de una fuerza constante en cada punto $\vec{F}$, y en un potencial desordenado $V(\vec{r})$, que es gaussiano, isótropo y de media nula, el cual se puede generar a partir de su correlación espacial, $< V(\vec{r})V(\vec{r'}) >= V_0^2 g(\frac{|\vec{r}-\vec{r'}|}{\lambda})$. La ecuación que decribe el sistema es la ecuación de Langevin en dos dimensiones, cuya versión adimensional es, en cada una de las direcciones perpendiculares del plano,

$$\frac{dq_x}{d\tau} = -\frac{\partial U(\vec{q})}{\partial q_x} + \mathcal{F}\cos\theta + \xi_x(\tau),$$

$$\frac{dq_y}{d\tau} = -\frac{\partial U(\vec{q})}{\partial q_y} + \mathcal{F}\sin\theta + \xi_y(\tau).$$

Para llegar a las expresiones anteriores hemos aplicado las transformaciones de escala espaciales y temporales, $\vec{q} = \frac{\vec{r}}{\lambda}$ y $\tau = \frac{tV_0}{\eta\lambda^2}$, por lo que hemos introducido los parámetros adimensionales $\vec{\mathcal{F}} = \frac{\lambda\vec{F}}{V_0}$ y $\mathcal{T} = \frac{k_B T}{V_0}$. El término del ruido cumple la relación de fluctuación disipación,

$$< \xi_i(\tau)\xi_j(\tau') >= 2\mathcal{T}\delta_{ij}\delta(\tau-\tau'),$$

dónde $i, j$ pueden ser cualquiera de las dos direcciones perpendiculares en el espacio cartesiano $q_x, q_y$. La fuerza externa constante es $\vec{\mathcal{F}} = \mathcal{F}\cos\theta\ \hat{i} + \mathcal{F}\sin\theta\ \hat{j}$.

Los resultados de la simulación de la ecuación de Langevin por el método de Heun permiten obtener la velocidad y el tensor de difusión usando las siguientes prescripciones,

$$< \vec{v}(\tau) >= \lim_{\tau\to\infty} \frac{<\vec{q}(\tau)>}{\tau},$$

$$D_{ij}(\tau) = \frac{1}{2}\lim_{\tau\to\infty} \frac{<(q_i - < q_i >)(q_j - < q_j >)>}{\tau}.$$

A partir del tensor de difusión se pueden calcular los coeficientes de difusión paralela y perpendicular a la dirección de la fuerza formando un escalar con un vector unitario $\hat{e}$,

$$\hat{e}\cdot D\cdot\hat{e} = \sum_{i,j=1}^{2} e_i D_{ij} e_j.$$

Cuando $\vec{e}_\parallel = (\cos\theta, \sin\theta)$ es paralelo a la fuerza externa $\vec{\mathcal{F}}$ se obtiene el coeficiente de difusión paralela, $D_\parallel$, y cuando es perpendicular, $\vec{e}_\perp = (-\sin\theta, \cos\theta)$, el coeficiente de difusión perpendicular, $D_\perp$.

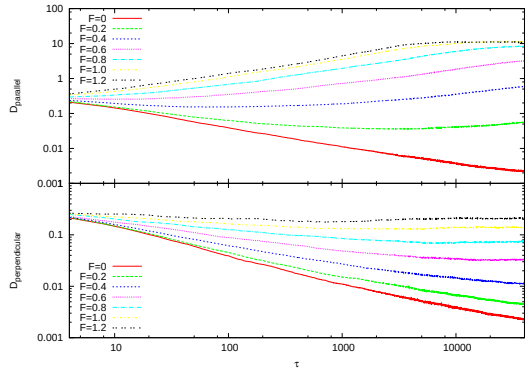


FIG. 1. Difusiones paralela y perpendicular a la dirección de la fuerza $\vec{\mathcal{F}}$. Los parámetreos de la simulación son N=1024 puntos de discretización en cada dirección, un espaciado $\Delta$=0.1 entre puntos, $\mathcal{T}$ = 0.2, $\lambda$=1, 100 partículas, 50 potenciales y $\tan\theta = 100/(20\cdot L\cdot\Delta)$.

La siguiente expresión $\alpha \approx \log\frac{<(\Delta q(10\tau))^2_\nu>}{<(\Delta q(\tau))^2_\nu>}$, dónde $\nu = \parallel, \perp$; nos permite determinar el exponente que caracteriza las anomalías $< (\Delta q(\tau))^2_\nu > \propto t^\alpha$ en la difusión. Los resultados obtenidos para los casos representados en la figura anterior han sido: $\alpha$=0.585 ($\mathcal{F}$ = 0), 1.196 ($\mathcal{F}$ = 0.2), 1.348 ($\mathcal{F}$ = 0.4), 1.405 ($\mathcal{F}$ = 0.6), 1.288 ($\mathcal{F}$ = 0.8), 1.117 ($\mathcal{F}$ = 1.0), 1.031 ($\mathcal{F}$ = 1.2) para la difusión paralela; y 0.592 ($\mathcal{F}$ = 0), 0.673 ($\mathcal{F}$ = 0.2), 0.792 ($\mathcal{F}$ = 0.4), 0.939 ($\mathcal{F}$ = 0.6), 1.012 ($\mathcal{F}$ = 0.8), 1.027 ($\mathcal{F}$ = 1.0), 1.014 ($\mathcal{F}$ = 1.2) para la difusión perpendicular. Podemos apreciar que cuando $\alpha \approx$1 hay difusión normal, mientras que si $\alpha$ <1 ó $\alpha$ >1 existe subdifusión o superdifusión respectivamente. También se presentarán resultados para el transporte anómalo.

‡ Departament de Física Aplicada, Universitat Politècnica de Catalunya, Avinguda Doctor Marañón, 44. E-08028 Barcelona, Spain
* sune@ecm.ub.es
** jmsancho@ecm.ub.es
*** anna@fa.upc.edu

# Experiments on Clustered Neuronal Networks

Sara Teller*, Jordi Soriano
*Departament d'Estructura i Constituents de la Matèria, Universitat de Barcelona, Barcelona, Spain*

Neuronal cultures are excellent systems to study the interplay between dynamics and connectivity in neuronal networks. Cultures not only bring a wealth of knowledge on the dynamics in living neuronal networks, but also provide fruitful insight on general principles governing brain processes. Neuronal cultures are highly versatile and can be prepared to fit diverse experimental requirements[1]. Cultures show a rich repertoire of spontaneous activity already few days after preparation, and although this activity is ultimately dictated by the underlying connectivity, the mechanisms that relate a particular network architecture with a specific dynamic behavior are still not well understood[2].

In order to investigate the dependence of neuronal network dynamics on architecture, we study spontaneous activity in a particular configuration of neuronal cultures known as clustered neuronal networks[3]. As shown in Fig. 1, these networks are formed by interconnected islands of highly packed neurons (clusters). By using different patterning techniques we can control the size and location of the clusters, therefore tailoring different network architectures.

In the experiments we monitor the spontaneous activity of the clustered network using high-speed calcium fluorescence imaging. Network's firing is characterized by bursts of activity, in which the clusters fire sequentially in a short time window, remaining silent until the next bursting episode (Fig.2a). With sufficient spatial and temporal resolution we are able to resolve, for a given burst, the activation sequence of the clusters (Fig.2b). The extension of this analysis for all the bursts of the recording finally provides the family of activation sequences.

The analysis of the experiments revealed interesting features. For instance, we observed that some activation sequences appeared more frequently than others, suggesting that a particular network architecture favors a specific dynamic motif. We also observed that the disruption of connectivity in the network by chemical or physical means preserved some dynamic motifs, hinting at the existence of dynamic robustness, even under strong perturbation of the nodes or links of the network.

Our experiments provide an interesting approach to study self-organization mechanisms in living neuronal networks and their interplay with neuronal architecture and dynamics. The analysis of the experiments in the context of network theory is providing new insights on the repertoire of activity in networks, as well as its origin, robustness and adaptability.

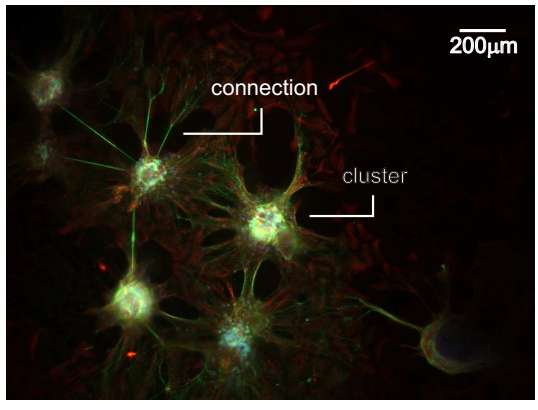


FIG. 1. Example of a clustered network. Colors corresponds to the fluorescence immunostaining of the different cell types: neurons and connections in green, glia in red and cells' soma in blue.

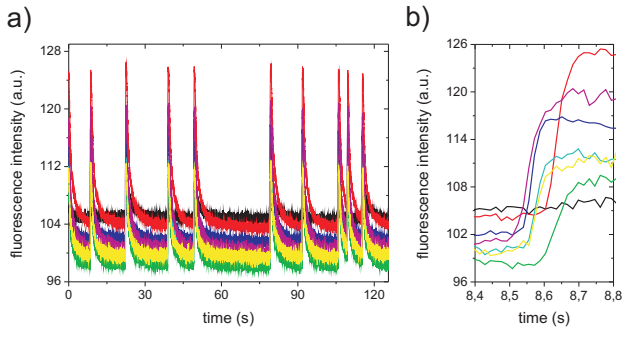


FIG. 2. **(a)** Temporal evolution of clusters bursting activity through fluorescence calcium imaging (fluorescence intensity in arbitrary units). Each color corresponds to a different cluster of the network. **(b)** Detail of a bursting episode showing that clusters fire at different times. The order of firing provides the clusters' activation sequence within the burst.

* teller.sara@gmail.com

[1] J. P. Eckmann , O. Feinerman, L. Gruendlinger, E. Moses, J. Soriano and T. Tlusty, Phys. Rep., **449**, 54 (2007).
[2] S.Feldt, P.Bonifazi, R.Cossart, Rev.Cell Press, **34 (5)**, 225-236 (2011).
[3] R.Segev, M.Benveniste, Y.Shapira, E.Ben-Jacob, Phys.Rev.Lett, **90 (16)**, 168101 (2003).

# Assessing Neuronal Connectivity in Cortical Cultures from Calcium Imaging Signals

Elisenda Tibau* and Jordi Soriano.
*Departament d'Estructura i Constituents de la Matèria, Universitat de Barcelona, Barcelona, Spain*

Large networks generate complex behavior, as is apparent in diverse systems such as computers, society and biology. Particularly attractive systems are neuronal tissues, with the brain the most prominent example.

Neuronal tissues show a wiring architecture and dynamics that are still far from being completely understood. Surprisingly, when natural neuronal tissues are dissociated and left to grow on a glass cover slip, their neurons self-organize to form a new network characterized by rich spontaneous dynamics and a non-trivial connectivity. The exquisite balance between the relative simplicity of these neuronal cultures and their rich behavior have made them one of the most attractive model systems in Physics [1].

Spontaneous activity in cultures is characterized by episodes of neuronal bursting in which the network fires collectively in a short time window, combined with silent intervals of relatively low activity (Fig.1a). In our experiments we monitor the spontaneous activity of 2000-4000 neurons in rat cortical cultures using high-speed fluorescence calcium imaging, and in combination with diverse perturbations of the neuronal network.

Connectivity is modified by targeting the excitatory and inhibitory synapses. We consider for instance the blockade of inhibitory synapses with bicuculline, a $GABA_A$ antagonist, to study the influence of inhibition on dynamics. We also consider the gradual disintegration of the excitatory connectivity with CNQX, an AMPA-receptor antagonist, as described in Refs.[2,3]. As shown in Fig.1a, the fluorescence amplitude of the bursts decreases with [CNQX], while the inter-burst interval increases, indicating a reduced excitability of the neurons in the network. The normalized amplitude $(F - F_0)/F_0$, with $F_0$ the baseline fluorescence, rapidly decreases with [CNQX] (Fig.1b).

The detailed analysis of the changes in the fluorescence amplitude of all neurons in the network provides information on the excitability of the system, and allows the identification of special traits such as strongly connected regions. Finally, we also note that fluorescence amplitude can be related with the number of actions potentials of a neuron [4]. This fact, in combination with graph-theoretical concepts and Transfer Entropy algorithms, may provide information of additional connectivity features of the network. Those features may be crucial for a better understanding of the interplay between activity and connectivity.

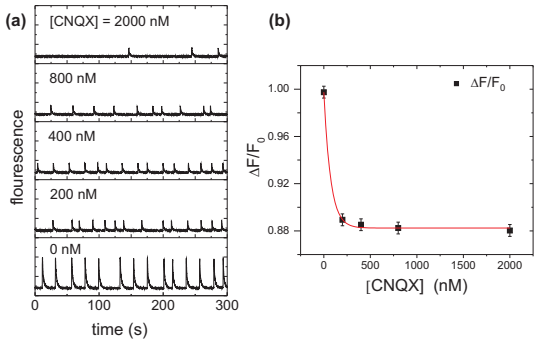


FIG. 1. **(a)** Fluorescence signal $F$ of the spontaneous activity in a neuronal culture, averaged over 2000 neurons, for different concentrations of CNQX. **(b)** Average values of $\Delta F/F_0$ (squares) as a function of the CNQX concentration. $\Delta F = F - F_0$ and $F_0$ is the fluorescence baseline. The red line is a guide to the eye.

* elisenda@ecm.ub.es

[1] J. P. Eckmann, O. Feinerman, L. Gruendlinger, E. Moses, J. Soriano and T. Tlusty, Phys. Rep., **449**, 54 (2007).
[2] I. Breskin, J. Soriano, T. Tlusty, and E. Moses. Phys. Rev. Lett **97**, 188102 (2006).
[3] J. Soriano, M. Rodríguez, T. Tlusty, and E. Moses. PNAS **105**, 13758 (2008).
[4] H. Takano, M. Mc Cartney, P.I. Ortinski, C. Yue, M. E. Putt, and D. A. Coulter. J. Neurosci. **32**, 4743 (2012).

# Role of delay in the stochastic birth and death process.

L. F. Lafuerza, R. Toral*
*IFISC, Instituto de Física Interdisciplinar y Sistemas Complejos*
*CSIC-Universidad de las Islas Baleares 07122-Palma (Mallorca)*

Fluctuations play an important role in many areas of science, and their study has become a well defined discipline. Delay in the interactions is also a common phenomenon in natural and artificial systems, and it is well known that it can alter qualitatively the dynamical behavior, for example inducing oscillations or even chaos.

The combined effect of stochasticity and delay is not completely understood. Stochastic processes that include delay are analytically difficult due to their non-Markovian character. Most theoretical studies consider a Langevin approach (stochastic differential equations) or systems in discrete time (where delay can be accounted for by increasing the number of variables). Stochastic models with continuous time but discrete variables are the natural description of many systems such as chemical reactions, population dynamics, epidemics, etc. In some cases, the discreteness can be a major source of fluctuations.

In this work we develop a rigorous derivation of the stochastic description of birth and death processes that include delay. The processes are schematically described by:

$$\emptyset \xrightarrow{C(n)} X, \qquad X \xrightarrow{\gamma} \emptyset, \tag{1}$$

with $n$ the number of species $X$. Here either the creation or the degradation reactions (that are initiated at a rate $C(n)$ and $\gamma$ respectively) take a time $\tau$ to be completed.

For the case of delay in the degradation[1], we solve the process exactly and find that the exact solution for the probabilities leads to equations for the mean values that do not comply with simple intuitive arguments and that oscillatory behavior does not exist (while it is usually believed to be present in this type of system). This clarifies and warns about the derivation of dynamical equations describing the evolution of the concentrations in cases in which delay plays a role. The exact solution is specially valuable for small system sizes, where approximated schemes typically fail.

For the case of delay in the creation[2] and feedback we develop an approximated analytical treatment that allows us to study the effect of delay and show that the delay can alter qualitatively the character of the fluctuations, amplifying them in the negative feedback case and reducing them in the positive feedback case. We also consider the situation with distributed delay and show that the effect of the delay decreases as the delay distribution becomes wider.

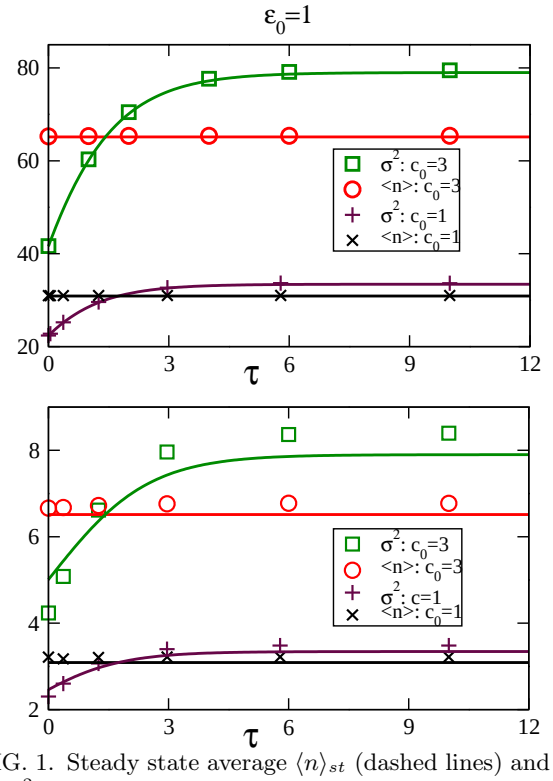


FIG. 1. Steady state average $\langle n \rangle_{st}$ (dashed lines) and variance $\sigma^2_{st}$ (solid lines), for the delay in the creation with negative feedback, as a function of the delay time $\tau$, for a creation rate $C(n) = \frac{c_0 \Omega}{1+\frac{\epsilon_0}{\Omega} n}$ with $c_0 = 3$ (upper part of each panel) and $c_0 = 1$ (lower part of each panel), and two system sizes ($\Omega$) (upper and lower panel) and $\epsilon_0 = 1$ in both cases. In each case, we plot with symbols the results coming from numerical simulations and by lines the theoretical expressions. Note that the fluctuations change from sub-Poissonian to super-Poissonian as the delay is increased.

* raul@ifisc.uib-csic.es

[1] L. F. Lafuerza and R. Toral, Phys. Rev. E 84, 051121 (2011).
[2] L. F. Lafuerza and R. Toral, Phys. Rev. E 84, 021128 (2011).

# Study of Fluid Interfaces in Microfluidics.

Claudia A. Trejo-Soto*, A. Ivón Rodríguez-Villareal and A. Hernandez-Machado
*Departament de ECM, Facultat de Física, Universitat de Barcelona.*
*Av. Diagonal #645, 08028, Barcelona, Spain.*

We study the interface fluid-air of water and some viscous fluids such as ethylenglicol an glycerol inside microchannels of different height and width. We have used two methods to observe this interface. The first method consists on injecting the fluid inside the microchannel at a constant flow rate of the order of microliters per minute using an injection pump. Once the fluid enters the microchannel we measure the velocity of the fluid front and we compare it with the injection rate. In the second method we observe the fluid interface using a constant pressure exerted by a liquid column submitted to atmospheric pressure. To accomplish this, we fix different heights and for each we measure the velocity at wich the font of fluid is moving. We repeat this treatment to different positions from the entrance of the fluid to the microchannel. Then our measurements of the velocity inside the microchannel are compared using the Darcy Law in order to obtain a relation with the fluids viscosities. With this method we have observed that for heights over the 2.5 cm between the column and the microchannel the velocity of the fluid behaves as constant. We have perfom measurements with blood plasma and blood at 5% and 10% of hematocrit and in this case we observed that the fluid properties generate effects at the channel walls wich are very diferent to those with water and ethylenglicol.

* claudiat@ecm.ub.es

# Grid computing for statistical and non-linear physics

Antònia Tugores*, Pere Colet
*IFISC, Instituto de Física Interdisciplinar y Sistemas Complejos*
*CSIC-UIB 07122-Palma (Mallorca)*

Grid computing is an arrangement of computer resources from multiple administrative domains to reach a common goal, complete tasks more efficiently. The grid can be thought of as a distributed system that involves a large number of files. What distinguishes grid computing from conventional high performance computing systems such as cluster computing is that grids tend to be more loosely coupled, heterogeneous, and geographically dispersed.

Since 2010, the pan-European Grid Infrastructure (EGI)[1] in collaboration with the National Grid Initiatives (NGIs) guarantees the long term availability of the generic e-infrastructures for all European research communities and their international collaborators. In this framework, the Spanish and the Portuguese National Grid Initiaves[2,3] are working hand by hand to create a large cooperative grid infrastructure, IBERGRID[4]. Nowadays Spanish researchers can access to more than 24000 cores and 20 PetaBytes of online storage just filling a form that can be found in the Spanish NGI web page[2]. IFISC[5] is member of the Grid-CSIC[6] project and shares its computational resources between all the european grid users, in particular with the IBERGRID ones.

Scientific grid has been proven to be a useful tool in some very computationally demanding fields as for example in analysis of particle physics or astrophysics data. While it has been extended to other fields such as plasma research it is still viewed as a tool associated to large projects. These large projects are the ones that can afford to have fine-tuned sophisticated interfaces for the researchers involved on these projects. Without these interfaces the access to grid using shell commands is quite cumbersome by nowadays point and click standards.

However, grid has the potential to be a key instrument for a wide variety of scientific topics which require to perform many calculations, for example to explore the dynamics as function of parameters as a typical case in nonlinear dynamics of complex systems and to perform statistics. While this high throughput computational needs are very much suitable for what grid was intended for, very few users take advantage of it because the access is cumbersome and requires a learning period that many researchers, mainly in small groups, can not afford.

To popularize grid in all scientific areas it is required to have user friendly interfaces where simple programs can be uploaded and executed in a simple way. Those interfaces should not compete with the sophisticated interfaces developed for specific applications rather they should cover the most basic aspects with suitable default options. The minimal capabilities would be submitting a job, recovering the results, monitoring the existing jobs and check the grid status (load, availability of free cores,...).

To make grid usage as common as computational clusters, user friendly interfaces are needed, and IFISC developed in the framework of Grid-CSIC project Web4Grid[7], a web interface to allow easy access to the grid infrastructure to those (until now) non-usual grid users.

By using this portal, researchers can submit applications, recover the results and monitor the status without any prior grid knowledge. After authenticating and configuring the account, job submission has been simplified: the user just uploads the application to be run and sets the parameters and the input files. All other information is the same for all the users by default but can be overwritten by each user within her own profile. When the job has benn submitted, a background script manages all the job workflow from proxy creation to results recovery and data cleaning.

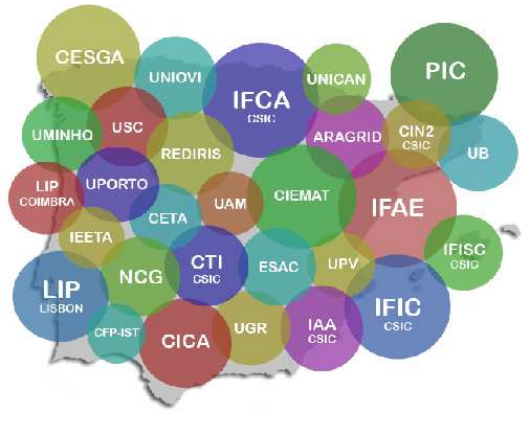


FIG. 1. IBERGRID resources map.

* antonia@ifisc.uib-csic.es

[1] European Grid Infrastructure. http://www.egi.eu
[2] es-NGI. http:www.e-ciencia.esngi
[3] INGRID. http://www.gridcomputing.pt/
[4] Ibergrid Initiative. http://ibergrid.eu
[5] IFISC. http://ifisc.uib-csic.es
[6] Grid-CSIC project. Ref: 200450E494. http://www.grid.csic.es
[7] Tugores, A.; Colet, P.: Web interface for generic grid jobs, Web4Grid. Computing and Informatics, Vol. 31, 2012, pp. 173–186

# Modeling information diffusion from empirical data

Paula Tuzón*, José J. Ramasco, Víctor M. Eguíluz and Maxi San Miguel
*IFISC, Instituto de Física Interdisciplinar y Sistemas Complejos*
*CSIC-Universidad de las Islas Baleares 07122-Palma (Mallorca)*

Models about social spreading processes, such as rumours, fashions or innovations, can be divided in two main classes: the ones that only consider one source to trigger contagion (contact), i.e. epidemic-like models (see e.g. the Bass model[1] as one of the first proposals in the context of social sciences), and the ones that consider more than one source; in these models "contact" is not enough to spread the infection and additional sources are needed[2,3].
Despite the amount of theoretical models in both directions, it is not clear yet which one is more appropriate to the empirical data on social diffusion[4]. For example, how does the probability for a consumer to buy a new product depend on the number of neighbours buying this product? Is this probability larger after meeting more neighbours in social spreading? In this work, we aim to advance in our understanding of the outcome of these two basic mechanisms. For that, we propose a model inspired by the empirical data and discuss the behaviour of the system depending on the form of the adoption probability function.

---

* paula@ifisc.uib-csic.es

[1] F. M. Bass, Management Science **15**, Theory Series 215-227 (1969).
[2] M. Granovetter, The American Journal of Sociology **83**, 6 1420-1443 (1978).
[3] D. Centola, V. M. Eguíluz and M. W. Macy, Physica A **374**, 449-456 (2009).
[4] J. Borge-Holthoefer, A. Rivero and Y. Moreno, arXiv:1111.4181.

# Thermodynamic properties and cavitation mechanism of water at negative pressure

C.Valeriani, M.A.Gonzales, J.L.Aragones and J.L.F.Abascal
*Departamento de Quimica Fisica I, Facultad de Ciencias Quimicas,*
*Avenida Complutense, Universidad Complutense de Madrid 28040 Madrid (Spain).*

Bubble nucleation is relevant in many different technological contexts, such as explosive boiling[1], cavitation erosion[2] and sonochemistry[3]. In spite of the practical relevance of these phenomena, the mechanism by which the vapor phase nucleates from a homogeneous, metastable liquid is still under debate. In order to be able to study bubble nucleation of water, one needs to have a potential model capable to predict the equation of state in the metastable region with high accuracy. In this work, we report numerical calculations of a number of thermodynamic properties of TIP4P/2005 water at negative pressures, such as the equation of state, the spinodal and the cavitation lines, the line of maximum densities (TMD) and the speed of sound. To be able to capture the kinetics of bubble formation, we perform Molecular Dynamics simulations of the TIP4P/2005 water model[4] with the GROMACS 4.5 package[5]. TIP4P/2005 is an interaction potential that represents water as a rigid and non-polarizable molecule. When available, we compare our results to recent experimental results from Professor Caupin's group in Lyon.

Even in the stable liquid phase, spontaneous density fluctuations occur in the bulk system. In a superheated liquid, some of these local density fluctuations may grow to nucleate a bubble of the stable vapor phase. Wang and coworkers have recently reported a Molecular Dynamics study of homogeneous bubble nucleation in a Lennard-Jones fluid[6], observing that cavitation started with compact bubbles rather than with ramified structures as suggested by Ref.[7] and that local temperature fluctuations were strongly correlated to the subsequent bubble formation. In the same year, Wedekind and coworkers studied the opposite phenomenon, vapor condensation, in the same monoatomic Lennard-Jones fluid and observed a crossover between a "nucleation-and-growth" and a "spinodal decomposition" regime, depending on the supersaturation. More recently, Pereza and Rubio[9] investigated condensation of the super-saturated vapor of TIP4P/2005 water, using Mean First Passage Time[10] to analyze the influence of charged species on nucleation dynamics. The authors found that the presence of charged species had a dramatic impact on the dynamics and that the TIP4P/2005 water model predicted anions inducing faster formation of water clusters than cations of the same charge. However, as far as we are aware, bubble nucleation from an over-stretched metastable liquid water has never been tackled so far.

In our work, we investigate the cavitation mechanism at negative pressures by means of Mean First Passage Time[10]: we compute the nucleation rate and study how the nucleation mechanism changes depending on the supersauration from the spinodal line of the metastable liquid. When studying cavitation, we also investigate the effect of the chosen order parameter by comparing the nucleation rate computed using a local order parameter (the volume of the largest vapor bubble in the system) to the one obtained using a global order parameter (the total volume of the vapor in the system). Moreover, to identify a vapor bubble in the metastable liquid, we define two independent local order parameters: one sensitive to the formation of large, connected void spaces (as in Ref.[6]) and another based on a Voronoi tesselation[11]. An example of a nucleating bubble at a state point not close to the spinodal line is given in Fig.1.

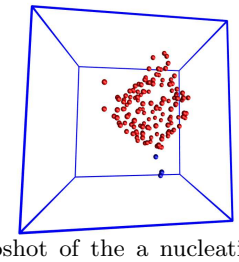

FIG. 1. Snapshot of the a nucleating bubble (in red) at T=280K and p=-2630bar.

* cvaleriani@quim.ucm.es

[1] M. Shusser, D. Weihs, *Int. J. Multiphase Flow*, **25**, 1561 (1999).
[2] C. Brennen, *Cavitation and Bubble Dynamics*, Oxford University Press: New York, (1995).
[3] K. .S. Suslick, *Science*, **247**, 1439 (1990).
[4] J. L. .F. Abascal and C. Vega, *J. Chem. Phys.*, **123**, 234505 (2005).
[5] B. Hess, C. Kutzner, D. van der Spoel, and E. Lindahl, *J. Chem. Theory Comput.*, **4**, 435 (2008).
[6] Z. Wang, C. Valeriani and D. Frenkel, *J.Phys.Chem.B* **113**, 3776 (2009).
[7] V. Shen and P. G. Debenedetti, *J. Chem. Phys.*, **111**, 3581 (1999).
[8] J. Wedekind, G. Chkonia, J. Wolk, R. Strey and D. Reguera, *J. Chem. Phys.* **131**, 114506 (2009).
[9] A. Pereza and A. Rubio, *J. Chem. Phys.* **135**, 244505 (2011).
[10] J. Wedekind, R. Strey and D. Reguera, *J. Chem. Phys.* **126**, 134103 (2007).
[11] J. L. .F. Abascal, C. Valeriani, M. Gonzalez and J. .L. Aragones, *in preparation* (2012).

# Computer simulation of a 2D liquid crystal confined in a circular cavity

D. de las Heras[1]* and E. Velasco[2]†
[1] *Theoretische Physik II, Physikalisches Institut, Universität Bayreuth, D-95440 Bayreuth, Germany*
[2] *Departamento de Física Teórica de la Materia Condensada, Universidad Autónoma de Madrid, 28049 Madrid*

Nematic fluids in confined geometries are a subject of much interest from both fundamental and technological points of view. In these systems there exists competition between orientational ordering, anchoring (favoured director alignment at surfaces) and elasticity. The equilibrium configuration depends sensitively on the imposed conditions. This interplay involves frustration and formation of defects. Here we consider two-dimensional (2D) nematics, which are easier to analyse and at the same time present some interesting peculiarities[1,2]. Recently vibrated quasimonolayers of macroscopic particles with anisotropic shape have been studied, using circular containers; patterns and behaviours similar to those found in thermal anisotropic fluids were observed, including nematic and smectic ordering[3]. Our recent, exploratory theoretical work on this problem considered the thermodynamics, phase behaviour and structure using a simple version of density-functional theory[4,5].

In the present work we use Monte Carlo (MC) simulation to study the ordering properties of a fluid of rectangles in a circular cavity. The rectangles have a length-to-width ratio of 40, with $L$ the length and $\sigma$ the width; this value was dictated by the recent experiments on vibrated quasimonolayers of Galanis et al.[6]. Our aim is to compare our simulation results with those obtained from the density-functional theory, on the one hand, and with those coming from the experiments on granular matter, on the other, in an effort to shed some light on the true properties of the equilibrium system, and also on the similarities between a thermal system and a granular system driven by dissipation.

In bulk conditions, our model fluid presents stable isotropic and nematic phases, with a continuous phase transition at some critical value of density. In the confined geometry, and due to the circular geometry, the fluid is subject to frustration since particles try to respect the orientation favoured at the surface (long axes of particles along the tangential direction), while at the same time elastic modes are excited due to the director distorsion. These factors imply the existence of defected regions in the fluid, where the nematic director is not defined.

In our MC experiments on small cavities ($R < 15L$), we obtain a collection of equilibrium configurations from the very dilute régime to high packing densities[7]. Particles are added one by one, and every time a particle is added we thermally equilibrate the fluid. Fig. 1 shows two structures for $R = 7.5L$: one at low density (top panels), where the fluid adopts an isotropic configuration; and another at high density (bottom panels), where the fluid is in a nematic state, but two line structures (domain walls) are created at opposite sides with respect to the cavity centre. The walls fluctuate in position quite rapidly. In this configuration director distortion is minimised, while at the same time surface energy is optimised. For such small cavity radii we do not observe the expected structure with tangential symmetry and a point defect at the centre[5]. Changes in the structure of the fluid for larger cavities and connection with density-functional theory are discussed.

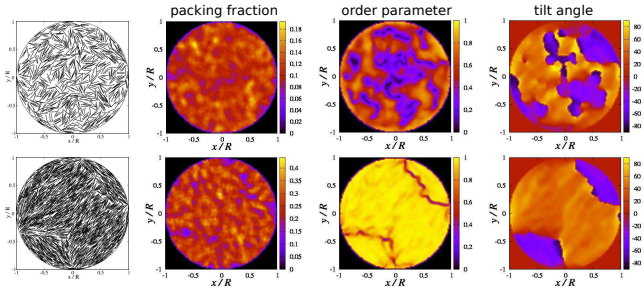


FIG. 1. Panels from left to right: particle configurations and packing fraction, uniaxial order parameter and director tilt angle local fields. Top panels correspond to a number of particles $N = 800$, while the bottom panels pertain to the case $N = 1970$. In all cases the cavity radius is $R = 7.5L$.

* daniel.delasheras@uam.es
† enrique.velasco@uam.es

[1] J. A. Cuesta and D. Frenkel, Phys. Rev. A **42**, 2126 (1990).
[2] M. A. Bates and D. Frenkel, J. Chem. Phys. **112**, 10034 (2000).
[3] V. Narayan, N. Menon and S. Ramaswamy, J. Stat. Mech. (2006) P01005.
[4] D. de las Heras, E. Velasco and L. Mederos, Phys. Rev. E **79**, 061703 (2009).
[5] D. de las Heras, L. Mederos and E. Velasco, Liq. Cryst. **37**, 45 (2010).
[6] J. Galanis, R. Nossal, W. Losert and D. Harries, Phys. Rev. Lett. **105**, 168001 (2010).
[7] D. de las Heras and E. Velasco (to be published).

# Uso de líquidos iónicos a temperatura ambiente en estructuras metalorgánicas cristalinas para almacenamiento y separación de dióxido de carbono

José M. Vicent-Luna*, J. J. Gutiérrez-Sevillano, J. A. Anta, y S. Calero
*Departamento de Física, Química y Sistemas Naturales.*
*Universidad Pablo de Olavide. Ctra. Utrera km. 1. 41013 (Sevilla)*

La separación de mezclas gaseosas en las que se vea envuelto el dióxido de carbono ($CO_2$), no tienen sólamente interés científico si no también tienen un gran interés social. Debido a la implicación de dicho gas en el calentamiento global[1], esto supone un reto desde el ámbito de la protección medioambiental. Por ello es interesante estudiar los mecanismos de captura y separación del dióxido de carbono mas efectivos que se puedan desarrollar.

Los líquidos iónicos a temperatura ambiente – room temperature ionic liquids (RTILs) – se han propuesto como disolventes potencialmente interesantes para capturar $CO_2$ debido a su alta selectividad para la adsorción de $CO_2$ en comparación con otros gases[2]. RTILs (FIG.1) son sales fundidas a temperatura ambiente compuestas por un catión orgánico y un anión orgánico o inorgánico. Debido a que hay muchos y muy conocidos cationes y aniones, el número potencial de RTILs es enorme. Sus propiedades únicas han suscitado un alto interés en los últimos años[3].

Por otra parte las estructuras metalorgánicas cristalinas – Metal-Organic Frameworks (MOFs) – son materiales relativamente novedosos bien conocidos por su gran área superficial, volumen de poro, y capacidad de almacenamiento entre otras características. Estas estructuras poseen gran cantidad de topologías y esto se puede usar para mejorar el almacenamiento o la separación de dióxido de carbono[4] de otros gases, como el metano o el nitrógeno.

En este estudio hemos investigado el efecto en la adsorción de $CO_2$ cuando se introduce un líquido iónico dentro de los poros de una estructura metalorgánica cristalina. Para este propósito hemos usado técnicas de simulación molecular Monte Carlo y dinámica molecular. El efecto de la adsorción de $CO_2$ se analiza a partir de dos aspectos (1) la modificación el tipo de anión del que está compuesto el RTIL y (2) la varición la cantidad de líquido iónico introducido en los poros del MOF.

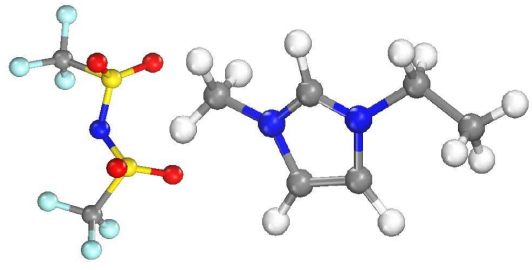

FIG. 1. Ejemplo de líquido iónico, $[emim]^+$ (derecha) y $[Tf2N]^-$ (izquierda).

* jmviclun@upo.es

[1] Peter M. Cox, Richard A. Betts, Chris D. Jones, Steven A. Spall and Ian J. Totterdell. *Nature vol. 408 (9)* **2000**, 184-187

[2] Ravichandar Babarao, Sheng Dai, and De-en Jiang. *J. Phys. Chem. B* **2011**, 115, 9789-9794

[3] Plechkova, N. V.; Seddon, K. R. Applications of ionic Liquids in the chemical industry. *Chem. Soc. Rev.* **2008**, 37, 123-150

[4] David Britt, Hiroyasu Furukawa, Bo Wang, T. Grant Glover, Omar M. Yaghi and Jack Halpern. *PNAS. Vol. 106(12)*, **2009**, 49, 20637-20640

# Influence of topology in neural networks dynamics

Paula Villa Martín*, Miguel A. Muñoz
*Departamento de Electromagnetismo y Física de la Materia e Instituto de Física Teórica y Computacional Carlos I Universidad de Granada 18071 - Granada.*

We study the influence of topology in simple dynamics with the idea of study a recent and interesting discovery in neural behaviours. This is the appearance of up and down states[1].

We study a modified contact process with a first order phase transition in a hierchical modular network. We obtain surprising preliminary results. The most important one is that the phase transition of the dynamics becomes slower and seems to be a second order phase transition.

* pvilla@ugr.es

[1] Compte A, Sanchez-Vives MV, McCormick DA, Wang XJ. J Neurophysiol 89: 2707-2725.

# On the irrationality of consensus in heterogeneous networks

Daniele Vilone*,[1], José J. Ramasco[1], Maxi San Miguel[1], Angel Sánchez[2,3]
[1] *Instituto de Física Interdisciplinar y Sistemas Complejos, CSIC-Universidad de las Islas Baleares, 07122-Palma (Mallorca)*
[2] *Grupo Interdisciplinar de Sistemas Complejos, Departamento de Matemáticas, Universidad Carlos III de Madrid, 28911-Leganés (Madrid)*
[3] *Instituto de Biocomputación y Física de Sistemas Complejos, Universidad de Zaragoza, Campus Río Ebro, 50018-Zaragoza*

The problem of reaching consensus in social systems is a very interesting issue[1]. Actually, the appearance of uniform behaviours, such as the convergence to the same opinion, can be observed in different situations. Understanding when and how this phenomenon occurs is one of the main goals of sociophysics. In this work we present a new model where agents chamge their opinion, which can assume one of two possible states, say $A$ and $B$, by means of a mixed dynamics. At each elementary time step, we pick up an individual at random. This individual evolves following the voter model (VM) dynamics[1] with probability $q$, and with probability $1-q$ according to the coordination game (CG) dynamics with imitate-the-best update rule[2]. In practice, the chosen agent imitates with probability $q$ a randomly chosen neighbour, and with probability $1-q$ the one which collects the largest total payoff in a round of the game (of course, if no neighbour performs better than the chosen agent, nothing happens). The CG has the simplest possible rule: an agent earns 1 for each neighbour with her same opinion, 0 otherwise. We can say, from a sociological point of view, that the VM dynamics is an irrational way to evolve, whilst the CG rule represents a rational behaviour.

The evolution and the final fate of such a system strongly depend on the value of the parameter $q$ and on the topology on which it runs. The common feature of all the results we collected in many numerical simulations is the following: if the system reaches the consensus in one limit ($q=0$ or $q=1$) remaining disordered in the other one, we observe a smooth cross-over between the two limits. This is the case in one- and two-dimensional lattices: the system ends up reaching total consensus for $q=1$ and in a frozen but disordered configuration for $q=0$, while in a complete graph (mean-field) in the thermodynamical limit it reaches the consensus for $q=0$ and remains disordered (in an active state) for $q=1$.

The most interesting phenomenology appears on random topologies. Let us consider for instance what happens on an Erdös-Rényi (ER) network. In this case, neither a pure VM dynamics nor a pure CG one drive the system to the complete ordering (in the thermodynamical limit). In particular, for $q=0$ it reaches a frozen disordered configuration, while for $q=1$ it ends in an active state, in both cases with individuals of opposite opinion still coexisting. Conversely, if $0<q<1$, after a transient (whose length depends on $q$) the system goes always to consensus. The time $\tau_q$ needed to reach the final ordered state is not a monotonic function of $q$, and there is an optimum value $q^*$ where it is minimum, as shown in Fig. 1, that also proves how these results are not consequence of finite size effects. It is quite noticeable that even a very small mixture of the two dynamics is enough to make the system reach consensus, as if each dynamics works as a noise with respect to the other, and as if the disordered state were an unstable configuration. Moreover, the ordering time diverges differently in the two limits:

$$\tau_{q\to 0^+} \sim K^{\frac{1}{\nu q}} \quad , \qquad \tau_{q\to 1^-} \sim \frac{1}{1-q}$$

where $K>1$ and $\nu$ are suitable constants. This peculiar behaviour is similar to what is observed in some glassy transitions[3].

Interestingly, this picture is qualitatively the same also with other kinds of complex networks, as for instance small-world and scale-free networks. We also provide a theoretical analysis and a sociological interpretation of the results: in this respect, our main conclusion is that global consensus on an issue requires some people making their decision in a non-strategic manner.

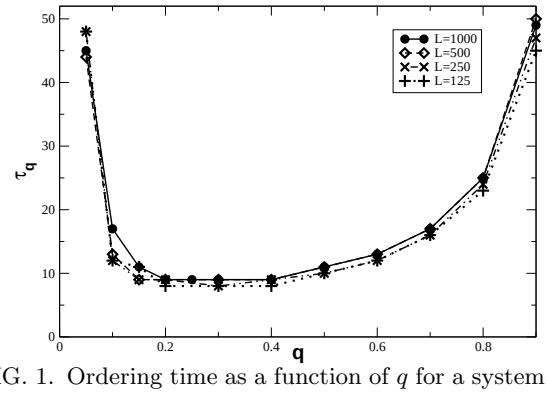


FIG. 1. Ordering time as a function of $q$ for a system in an ER network (average degree $\langle k\rangle = 14$) and different sizes $L$.

* daniele.vilone@gmail.com

[1] C. Castellano, S. Fortunato and V. Loreto *Rev. Mod. Phys,*, **81**, 591 (2009).
[2] C.P. Roca, J.A. Cuesta and A. Sánchez, *Phys. of Life Rev.*, **6**, 208 (2009).
[3] J.P. Bouchaud, L.F. Cugliandolo, J. Kurchan amd M. Mézard in "Spin-glasses and random fields", Ed. A.P. Young, World Scientific (1998).

# Strong anisotropy in surface kinetic roughening: theory and experiments

Edoardo Vivo*, Matteo Nicoli,† and Rodolfo Cuerno
*Departamento de Matemáticas and Grupo Interdisciplinar de Sistemas Complejos (GISC)*
*Universidad Carlos III de Madrid*
*Avenida de la Universidad 30, E-28911 Leganés (Madrid)*

It is well known that surfaces subject to growth or erosion processes, as in thin-film production, solid fracture, etc. display a self-affine behavior that can be studied through appropriate observables in real space (roughness and correlation functions) or in Fourier space (power spectral density, PSD). Such observables typically exhibit power-law behavior whose exponents characterize the long time and large length-scale behavior of the system under consideration.[1]

When the physical phenomena driving the growth or erosion process do not depend on the substrate direction, we are in the presence of isotropic scaling, the behavior of which is in general well described by the well known Family-Vicsek Ansatz.[1] However, there are many cases in which the growth of the surface depends on the direction considered along the substrate. Examples include the erosion of a tilted landscape by the action of wind and rain,[2] interfaces arising in simplified models of running sand-piles in the context of self-organized criticality,[3] or thin film growth[4,5] or erosion.[6,7] In these cases, the flux of material follows a preferred direction so that dynamics is not the same in the directions parallel and perpendicular to the external flux. Considering a two-dimensional surface, one has to define different sets of exponents associated with the different substrate directions.

In the specific context of thin film production in the presence of anisotropy, it is important to understand the relationship between the scalings of the two-dimensional PSD of the surface and the PSD of one-dimensional cuts along the directions parallel and perpendicular to the flux. This is due to the fact that many experimental setups are often designed to measure either the former (using e.g. X-ray diffraction), or the latter (using AFM or STM microscopies),[5] and therefore a quantitative comparison with theoretical models cannot be done unless this relationship is fully understood. On the other hand, from a theoretical point of view little is known about the conditions required for an interface equation that describes the evolution of a rough surface, to display anisotropic scaling in the asymptotic state (*strong anisotropy, SA*).

In this work, we formulate an anisotropic scaling Ansatz that clarifies the relationship among one and two-dimensional PSDs, and with correlation functions in real space. Our Ansatz is exact for *linear* equations with SA, and is useful to understand the long-time and large length-scale behavior of nonlinear equations, such as the one put forward by Hwa-Kardar (HK) in the context of running sand piles.[3] We moreover validate this hypothesis against experimental data from surface nanopatterning of silicon targets by ion-beam sputtering, both in the morphologically stable[7] and unstable situations.[6]

Additionally, using Dynamic Renormalization Group analysis and direct numerical simulations, we study from a theoretical point of view the appearance of *strong anisotropy* in nonlinear stochastic equations, both with conserved[3,8] and non conserved[4] dynamics. Our preliminary conclusions suggest that, in order to take place, asymptotic SA requires special (non-generic) conditions from the shape of the dynamical equation.

Partial support for this work has been provided by MICINN (Spain) Grant No. FIS2009-12964-C05-01. E.V. acknowledges support by Universidad Carlos III de Madrid.

---

* evivo@math.uc3m.es
† Physique de la Matière Condensée, École Polytechnique, CNRS, 91128 Palaiseau, France.

[1] A.-L. Barabási and H. E. Stanley, *Fractal Concepts in Surface Growth*, Cambridge University Press, Cambridge, England (1995).
[2] R. Pastor-Satorras and D. H. Rothman, J. Stat. Phys. **93**, 477 (1998).
[3] T. Hwa and M. Kardar, Phys. Rev. Lett. **62**, 1813 (1989).
[4] D. E. Wolf, Phys. Rev. Lett. **67**, 1783 (1991).
[5] Y. Zhao, G.-C. Wang, and T.-M. Lu, *Characterization of amorphous and crystalline rough surface: Principles and applications* (Academic Press, San Diego, 2001).
[6] J. A. Sánchez-García, R. Gago, R. Caillard, A. Redondo-Cubero, J. A. Martin-Gago, F. J. Palomares, M. Fernández, and L. Vázquez, J. Phys.: Condens. Matter **21**, 224009 (2009).
[7] S. Macko, F. Frost, M. Engler, D. Hirsch, T. Höche,J. Grenzer, and T. Michely, New J. Phys. **13**, 073017 (2011).
[8] E. Vivo, M. Nicoli, and R. Cuerno, *in preparation.*

# Noise Induced Phase Transitions and Coupled Brownian Motors: Non Standard Hysteretic Cycles

Horacio S. Wio
*Instituto de Física de Cantabria. Santander. Spain.*

Recent work[1–3] have shown the possibility, through a noise induced symmetry breaking leading to a nonequilibrium phase transition, of obtaining a set of coupled Brownian motors. It was also shown[4] that in some parameter region such a system could show negative mobility (that is motion opposed to the applied force) and anomalous hysteretic behavior (clockwise in opposition to the usual counter-clockwise). Using an explicit mean-field approximation and colored multiplicative noises, it was found a contraction of the ordered phase (and reentrance as a function of the coupling) on one hand, and a shift from anomalous to normal hysteretic behavior on the other[5]. This behavior was obtained in systems presenting a noise induced phase transition that originates from a short time instability. Here we discuss a similar system, but where the noise induced phase transition is originated in an entropic mechanism[6]. Some preliminary studies that exploits such a mechanism indicate the possibility of obtaining no standard hysteretic cycles: anti-clockwise but showing a staircase-like structure. Depending on the parameter region, the hysteresis diagram could have one or more blocks, that can be explored as a whole or step by step, opening the possibility of exploiting it as a noise-controlled multipurpose logic gate.

* wio@ifca.unican.es

[1] Sagués et al, Rev. Mod. Phys. **79**, 829 (2007).
[2] van den Broeck et al, Phys. Rev. E **55**, 4084 (1997).
[3] Mangioni et al, Phys. Rev. E **61**, 223 (2000).
[4] Reimann et al, Europhys.Lett. **45**, 545 (1999).
[5] Mangioni et al, Phys. Rev. E **66**, 051106 (2002).
[6] Carrillo et al, Phys. Rev. E **67**, 04611 (2003).

# Robustness of self-sustained oscillations in complex networks

A. Yáñez Santamaría*, A. von Kameke, A.P. Muñuzuri
*Group of Nonlinear Physics, Faculty of Physics, University of Santiago de Compostela, E-15782 Santiago de Compostela, Spain.*

Complex networks of excitable nodes represent a thriving field of research with many applications, among which we can find neural networks. Under certain conditions, i.e., small world connections, the network can exhibit a self-sustained network oscillatory behavior, without external stimulus. It is known[1] that in order for this oscillations to occur, the excitation must travel through a loop, whose length must be compatible with the refractory period of the excitable cells. We study a directed graph with nearest neighbor connections and a fraction $q$ of the edges being small world. The excitation mechanism of each cell consists of a cellular automaton with variable excitation time scales. In particular, we want to understand how a net with a stationary oscillating pattern reacts to the removal of nodes, and the robustness of these oscillations.

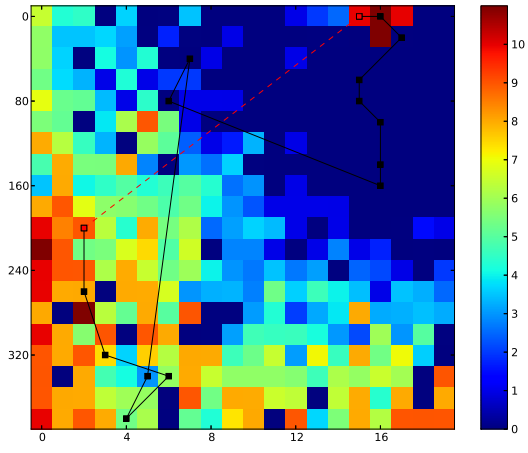


FIG. 1. Example of oscillation in a $20 \times 20$ network. States above 6 are excited, below are refractory and 0 is the resting state. The small squares joined by lines display the nodes of the loop that causes the oscillation. There is a long range connection (red dashed line) that sends the excitation back to the unexcited area in the top right corner, triggering thus a new target wave.

* antonio.yanez.santamaria@gmail.com

[1] Xuhong Liao, Qinzhi Xia, Yu Qian, Lisheng Zhang, Gang Hu, and Yuanyuan Mi *Pattern formation in oscillatory complex networks consisting of excitable nodes* Physical review E 83, 056204 (2011)

# Synchronization and quantum correlations in networks

Gonzalo Manzano,Fernando Galve, Gianluca Giorgi, Pere Colet, Emilio Hernández-Garcìa, Roberta Zambrini
*IFISC, Instituto de Física Interdisciplinar y Sistemas Complejos*
*CSIC-Universidad de las Islas Baleares 07122-Palma (Mallorca)*

Synchronization phenomena have been observed in a broad range of physical, chemical and biological systems but there are few attempts to describe them in the quantum regime. Most of the attention in this regime has been devoted to the problem of entrainment induced by an external driving[1] and not to spontaneous synchronization. We also mention recent research by different groups on synchronization of nano/microscopic systems. Even if these works[2–4] are concerned with classical (average) properties these devices are indeed susceptible of having quantum behaviour, being the subject of an intense experimental effort. In Ref.[5], for the first time, we established the connections between the phenomenon of synchronization and quantum correlations.

We initially considered a fundamental quantum system[6,5], two coupled and detuned quantum harmonic oscillators dissipating into the environment. Different dissipation mechanisms, corresponding to the situations in which (i) every oscillator dissipate in an independent bath (separate baths, SB), or (ii) the correlations length in the bath is larger than the oscillators systems (common bath, CB), are considered.

The dynamics of the system[6] for Gaussian states, is fully characterized by first and second order moments of positions and momenta of the oscillators. We identify the conditions leading to spontaneous synchronization showing that the ability of the system to oscillate at a common frequency is related to the existence of disparate decay rates of the normal modes[5]. We then analyzed different measures of correlations and their temporal decay due to decoherence. We showed that this phenomenon is accompanied by robust quantum discord[7] and mutual information between the oscillators, preventing the leak of information from the system.

Once identified the conditions for synchronization and its quantum aspects, we extended our analysis to the case of a quantum network[8]. At difference from the case of a couple of oscillators, we showed that even in presence of diversity between the nodes (in their frequencies and in the couplings with the rest of the network) it is possible to have asymptotic entanglement. We discuss several situations, like the possibility to synchronize the whole network by tuning one of the oscillators frequencies, or by inducing synchronization only in one part of the cluster, or the conditions to connect two oscillators to a network inducing asymptotic entanglement between them.

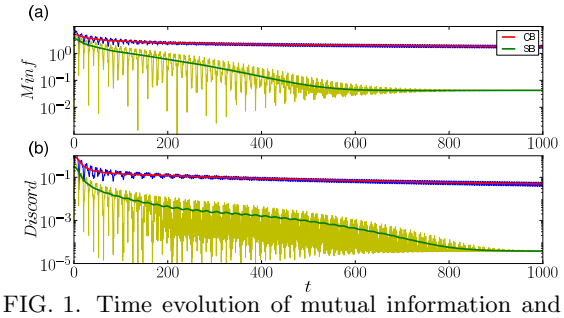


FIG. 1. Time evolution of mutual information and quantum correlations (discord) in the cases of a common bath (CB) and separate baths (SB). More details in Ref.[5].

[1] I. Goychuk, J. Casado-Pascual, M. Morillo, J. Lehmann, and P. Hänggi, Phys. Rev. Lett. **97**, 210601 (2006); O. V. Zhirov and D. L. Shepelyansky, *ibid.* **100**, 014101 (2008); S-B. Shim, M. Imboden and P. Mohanty, Science, **316**, 95 (2007).
[2] M.Zhang, G. Wiederhecker, S. Manipatruni, A. Barnard, P. L. McEuen and M. Lipson, arXiv:1112.3636v1.
[3] G. Heinrich, M. Ludwig, J. Qian, B. Kubala and F. Marquardt, Phys. Rev. Lett. **107** 043603 (2011).
[4] C. A. Holmes, C. P. Meaney, G. J. Milburn, arXiv:1105.2086.
[5] G-L. Giorgi, F. Galve, G. Manzano, P. Colet, and R. Zambrini, Phys. Rev. A 85, 052101 (2012)
[6] F. Galve, G-L. Giorgi, and R. Zambrini Phys. Rev. A 81, 062117 (2010)
[7] H. Ollivier and W. H. Zurek, Phys. Rev. Lett. **88**, 017901 (2001).
[8] G. Manzano, F. Galve, G-L. Giorgi, Emilio Hernández-Garcìa, Roberta Zambrini, in preparation

# Synchronization transitions in a growing complex network of Stuart-Landau oscillators

Jordi Zamora-Munt*, Manuel A. Matías, Pere Colet
*IFISC (CSIC-UIB) Palma de Mallorca - Spain.*

Complex Systems composed out of dynamical elements exhibit universal collective behaviors in fields like Physics, Biophysics, Neuroscience, Social Sciences, etc., and the interplay between local dynamics and topology of interaction can be often rationalized[1–3]. In the present work we are interested in transitions from an incoherent or quiescent state to a coherent state occuring as a function of the number of interacting oscillators (depending also on the local dynamics and coupling topology). Two different transitions of this type, that have been recently reported in the literature, are known as Crowd Synchrony (CS) and Dynamical Quorum Sensing (DQS) transitions. The first is characterized by a smooth transition first observed in London Millenium Bridge[4]. The second is a sharp transition introduced to describe the sudden increase of production of signaling molecules in bacteria colonies and that was also observed in yeast cells[5] and coupled chemical oscillators[6].

In Ref.[7] it was recently reported that a system of delay coupled lasers with a star network topology may exhibit both transitions when the number of coupled lasers exceeds a certain threshold number. This study showed that the type of transition that is found, CS or DQS, depends on the existence (or lack) of oscillations in the uncoupled lasers, depending on whether they are above (below) threshold, respectively. More recent investigations have revealed that the coupling strength and the number of lasers play an equivalent role in the transition, and demonstrated the existence of a second transition, past the DQS, to a more synchronized state[8].

However, it is not well understood which are the minimal characteristics of a system, both regarding local dynamics and coupling topology, that allow it to show one, the other or both types of transitions.

So, in the present work we introduce and study a minimum model that contains what we think are the essential ingredients to reproduce the DQS and CS transitions. The system is constituted of $N$ complex Stuart-Landau oscillators, $z_j$, coupled through a common damped linear oscillator, $F$:

$$\dot{z_j} = (\mu_j + i\theta_j)z_j - |z_j|^2 z_j + \kappa(F - z_j), \quad (1)$$

$$\dot{F} = (-\Omega + i\Delta)F + \kappa \sum_{j=1}^{N} z_j, \quad (2)$$

where $\mu$ is the gain factor, $\theta$ is the detuning frequency and $\kappa$ is the coupling strength. $\Omega$ is the filter bandwidth and $\Delta$ the central frequency.

As the DQS can appear when the oscillators are identical, when they exhibit a sudden transition to synchronization as a function of $N$, we have described the problem using the Master Stability Function (MSF) technique[9]. Instead, the CS transition appears to require heterogeneity in the interacting elements. So, we have considered the extension of the MSF formalism that allows for some heterogeneity among the oscillators[10]. In addition, we have used the Ott-Antonsen technique to analyze the CS synchronization transition[11]. In this case, the role of a passive filtering of a finite number of frequencies is discussed. Finally, the effect of time delay in the coupling channel is also considered and compared with the case of instantaneous coupling.

Our study suggests that CS and DQS could be observed in a large variety of natural systems and opens the door to the possibility of investigate these transitions in other coupling topologies.

* jordi@ifisc.uib-csic.es

[1] A. Arenas, A. Díaz-Guilera, J. Kurths, Y. Moreno, and C. Zhou, Phys. Rep. **469**, 93 (2008).
[2] S. N. Dorogovtsev, A. V. Goltsev, and J. F. F. Mendes, Rev. Mod. Phys. **80**, 1275 (2008).
[3] S. Boccaletti, V. Latora, Y. Moreno, M. Chavez, and D.-U. Hwang, Phys. Rep. **424**, 175 (2006).
[4] S. H. Strogatz, D. M. Abrams, A. McRobie, B. Eckhardt, and E. Ott, Nature **438**, 43 (2005).
[5] J. Aldridge and E. Kendall Pye, Nature (London) **259**, 670 (1976).
[6] A. F. Taylor, M. R. Tinsley, F. Wang, Z. Huang, and K. Showalter, Science **323**, 614 (2009).
[7] J. Zamora-Munt, C. Masoller, J. García-Ojalvo, and R. Roy, Phys. Rev. Lett. **105**, 264101 (2010).
[8] J. Zamora-Munt and E. Ott, Europhys. Lett., (to be published).
[9] L. M. Pecora and T. L. Carroll, Phys. Rev. Lett. **80**, 2109 (1998).
[10] J. Sun , E. M. Bollt, and T. Nishikawa, Europhys. Lett. **85**, 60011 (2009).
[11] E. Ott and T. M. Antonsen, CHAOS **18**, 037113 (2008).

# Parte IV
# Índice de autores

# Índice de autores


Abad, E., 59
Abascal, J. L. F., 112, 187
Ackemann, T., 85, 111
Alarcón, F., 60
Albericio, F., 77
Alemany, A., 37, 62, 63, 76
Alonso, D., 78
Álvarez, F. X., 92
Álvarez-Lacalle, E., 47
Álvarez-Nodarse, R., 64, 168
Anta, J. A., 189
Aparicio, J. M., 65
Aragones, J. L., 112, 187
Aragoneses, A., 66
Arenas, A., 41, 116, 145
Ares, S., 42, 67, 68, 148
Arts, D. G. A. L., 50
Astillero, A., 69
Baró, J., 70
Baronchelli, A., 179
Barrat, A., 179
Barreiro, M., 93
Benet, J., 71
Bergues, J., 99
Bergues-Pupo, A. E., 99
Bettencourt, J. B., 130
Bianchi, E., 114
Bitlloch, P., 159
Bizarro, C. V., 77, 161
Blanch-Mercader, C., 61, 72, 81
Boguñá, M., 87
Boguñá, M., 34
Bois, J. S., 150
Bonet, J., 177
Bores, C., 73
Bragard, J., 178
Brey, J. J., 107
Buceta, J., 38
Buldú, J. M., 137
Burgos, J., 157
Cabrales, A., 117
Calabrese, J. M., 136
Calero, C., 74
Calero, S., 163, 189
Calvo, A-M., 75
Camunas-Soler, J., 76, 77
Cantarero, A., 92
Capello, G., 95
Capitán, J. A., 78
Carbadillo-Landeira, J., 118
Carelli, P., 176
Carro, A., 79, 80
Casademunt, J., 47, 61, 72, 81, 154, 159
Casanellas, L., 39
Castro, M., 146
Cates, M. E., 55
Cerdà, J., 82
Cerdeiriña, C. A., 83
Chacón, E., 71
Chamorro, M. G., 106
Chembo, Y. K., 86
Cherry, E. M., 178
Chowdhury, D., 150
Clotet, X., 84
Colet, P., 85, 86, 88, 110, 111, 138, 156, 185, 195, 196
Colomer, P., 87
Copelli, M., 44, 176
Corte, H., 100
Cortés, J. M., 123
Cosenza, M. G., 167
Cozzo, E., 145
Crespo, P., 28
Creton, C., 151
Cuello, G., 121
Cuenda, S., 78
Cuerno, R., 149, 164, 192
Cuesta, J., 45
Cuesta, J. A., 64, 78, 117, 168
Cuetos, A., 89
d'Onofrio, A., 90
de Franciscis, S., 90
de la Rubia, J., 65, 101
de la Torre, J. A., 91
de las Heras, D., 188
de Lorenzo, S., 77
de Mendizábal, N., 59
de Tomas, C., 92

Dev, S. B., 77
Deza, J. I., 93, 94
Deza, R. R., 94
Díaz-Aguilera, A., 41, 172
Dimitriou, C. J., 39
Dinis, L., 95
Dodzyuk, H., 73
Domínguez, A., 96
Domínguez-García, V., 97
Doppelbauer, G., 114
Dubois, R., 49
Duque, D., 91
Durán-Olivencia, M. A., 40
Eguiluz, V. M., 25, 102, 134, 186
Eke, B., 117
Elizalde, E., 98
Elvira, V. H., 108
Eritja, R., 77
Erola, P., 41
Español, P., 91, 143
Evans, R., 26
Falo, F., 99
Faunes, F., 170
Fenton, F. H., 178
Fernández, A., 101
Fernández, E. M., 71
Fernández, M., 103
Fernández, M. A., 100
Fernández-Barvero, A., 27
Firth, W. J., 85
Fisher, M. E., 83
Fleurquin, P., 102
Formosa-Jordán, P., 42, 155
Frade, J. M., 42
Frutos, S., 77
Fuentes-Pérez, M. E., 77
Galeano, J., 103, 104, 105
Galli, V., 95
Galve, F., 195
García, M. I., 107, 141
García, N., 43
García-Algarra, J., 105
García-Ojalvo, J., 59, 170
Garcimartín, A., 120
Garcon, V., 122
Garriga, A., 109
Garzó, V., 106
Gavaldà, J., 171
Geyer, V., 175
Giorfi, G., 195
Giralt, E., 77
Goehring, N. W., 150
Gollo, L. L., 44, 134, 176
Gómez, S., 41, 116
Gomila, D., 120, 111, 156
González, M., 115
González, M. A., 112
Granell, C., 116
Grill, S. W., 150
Grujic, J., 117
Guàrdia, E., 74, 75, 121, 152
Güell, O., 120
Guiu-Souto, J., 118
Gutiérrez, J. J., 163, 189
Gutiérrez-Roig, M., 119
Henao, A., 121
Hernández-Carrasco, I., 122
Hernández-García, E., 122, 130, 195
Hernández-Machado, A., 165, 184
Hernando A., 28
Hidalgo, C., 103
Hidalgo, J., 123
Hita, J. L., 132
Howard, J., 175
Hudspeth, A. J., 46
Huguet, J. M., 109, 161
Huhn, F., 56, 124
Humbert, F., 95
Hurtado, P. I., 128
Hyman, A. A., 150
Ibañes, M., 42, 155
Iriondo, J. M., 105
Ivell, S., 50
Jacobo, A., 110
Jamie, E. A. G., 50
Jonhson, S., 97, 125
Jörg, D. J., 67
Jülicher, F., 67, 175
Junier, I., 62
Kahl, G., 114
Khuc, P., 150
Kinouchi, O., 44

Klein, M., 95
Korona, T., 73
Korutcheva, E., 100, 101
Kremer, G. M., 174
Krioukov, D., 34
Lacasa, L., 126, 133
Lacasta, A., 180
Lafuerza, L., 127, 183
Lara, R., 144
Larger, L., 86
Lasanta, A., 128
Lázaro, G. R., 165
Lenz, M., 95
Lim, J. S., 53, 129
Lira, S. A., 61
Lomba, E., 73
Lopeandia, A., 92
López, C., 122, 130, 135, 136
López, R., 53, 129
Lozano, C., 131
Lumay, G., 131
Luque, B., 126, 133, 153
Luque, J., 133
MacDowell, L. G., 71, 108
Maestre, M. A. G., 113
Manzano, G., 195
Manzi, J., 95
Maoiléidigh, D. O., 46
Maritan, A., 29
Marro, J., 125
Martí, J., 74
Martínez, I. A., 51
Martínez, J. H., 137
Martínez, L. A., 45
Martínez, R., 135, 136
Martínez-Arias, A., 170
Martínez-Llinàs, J., 138
Martínez-Ratón, Y., 115, 140
Masia, M., 75, 152
Masoller, C., 66, 93
Matías, F. S., 176
Matias, M. A., 110, 156, 196
Maynar, P., 107, 141
McIntyre, C., 85
McKinley, G. H., 39
Meléndez, M., 142, 143
Mirasso, C., 134, 176
Miritello, G., 144
Modeste, R., 86, 88
Morelli, L. G., 67, 68
Moreno, A., 146
Moreno, Y., 145
Moreno-Herrero, F., 77
Moretti, P., 147
Morlot, S., 95
Moro, E., 144, 149
Mossa, A., 62
Muñoz, M. A., 97, 123, 147, 190
Muñoz-Descalzo, S., 170
Muñoz-García, J., 148
Muñuzuri, A. P., 56, 118
Nesic, S., 149
Nicola, E. M., 46, 150
Nicoli, M., 151, 192
Nicolini, P., 152
Noblet, Y., 85
Noya, E. G., 114
Núñez, A. M., 153
Oates, A. C., 67, 68
Ober, T. J., 39
Oppo, G-L., 85
Oriola, D., 154
Orkoulas, G., 83
Orlandi, J. G., 47
Ortín, J., 39, 84
Ortiz, J. M., 132
Otálora, F., 40
Otani, N., 178
Pagonabarraga, I., 60, 165
Palanco, J. M. G., 108
Palau-Ortin, D., 155
Pardo, L. C., 121
Parra, P., 156
Parrondo, J. M. R., 51
Parry, A. O., 50
Pasamar, S. M., 59
Pastor, J. M., 104, 105, 137
Pastor, R., 179
Patricio, J., 153
Patti, A., 89, 157
Paulau, P. V., 85
Pazó, D., 30

Perelló, J., 119
Pérez, A., 194
Pérez, P., 158
Pérez-Carrasco, R., 48
Pérez-Muñuzuri, V., 56, 124
Pérez-Rodríguez, M., 139
Pesquera, L., 158
Petrov, D., 51
Pigolotti, S., 31
Piñeiro, M. M., 139
Pont, O., 49
Poon, W. C. K., 55
Pothoczki, S., 121
Prados, A., 128
Prignano, L., 172
Pusey, P. N., 55
Quintero, N. R., 64
Radwell, N., 85
Ramasco, J. J., 102, 105, 186, 191
Ramírez-Piscina, L., 159
Ramsch, R., 77
Rascón, C., 50
Rebollo, M., 160
Recio, F. J., 28
Ribezzi-Crivellari, M., 161, 162
Ritort, F., 37, 62, 63, 76, 77, 109, 161, 162
Rodríguez, A., 169
Rodríguez, I., 184
Rodríguez, N., 168
Rodríguez, S., 163
Rodríguez, V. M., 167
Rodríguez-Laguna, J., 164
Rodríguez-López, P., 166
Rojas-Gómez, O. A., 52
Roldán, E., 51
Romero-Enrique, J. M., 52, 169
Rossi, V., 122
Roux, A., 95
Rovira-Esteba, M., 121
Rubido, N., 66
Rué, P., 170
Ruiz, X., 159, 171
Rull, L. F., 169
Sáez, N., 171
Sagarra, O., 172
Sagués, F., 32, 120
Sala, J., 152
San Miguel, M., 79, 80, 102, 186, 191
Sánchez, A., 45, 117, 191
Sánchez, D., 53, 129
Sánchez, R., 33
Sancho, J. M., 48, 155, 180
Santalla, S. N., 164
Santos, A., 69, 113, 173, 174
Santos, M. J., 54
Santucci, S., 84
Sanz, E., 55
Sartori, P., 31, 175
Seoane, L. F., 123
Serral, M., 177
Serrano, M. A., 34, 120
Simic, A., 178
Sintes, T., 82
Solans, C., 77, 157
Soriano, J., 47, 181, 182
Soriano, M. C., 88
Sorrentino, T., 66
Startini, M., 179
Suñé, M., 180
Tanguy, F., 151
Tarazona, E., 71
Teller, S., 47, 181
Thorneywork, A., 50
Tibau, E., 182
Tinoco, I., 76
Toral, R., 79, 80, 127, 183
Torrent, M. C., 66
Torres, J. J., 125
Trejo, C., 184
Trizac, E., 141
Tugores, A., 185
Tuzón, P., 186
Uriu, K., 68
Valeriani, C., 55, 112, 187
Valle, A., 158
Vega, F., 106
Velasco, E., 115, 140, 188
Vicent, J. M., 189
Vilchez, S., 77
Villa, P., 190
Villoslada, P., 59
Vilone, D., 191

Vives, E., 70
Vivo, E., 192
von Kameke, A., 56, 124, 194
Walgraef, D., 111
Weber, M., 38
White, J. A., 54
Wio, H. S., 94, 193
Yahia, H., 49
Yáñez, A., 194
Zaccarelli, E., 55
Zambrini, R., 195
Zamora-Munt, J., 196
Zanin, M., 137
Zuriguel, I., 131

# Parte V
# Asistentes al congreso

# Asistentes al congreso

1. **Abad Adan, Elena**
   - Universitat Politècnica de Catalunya
   - abad.e.bcn@gmail.com

2. **Alarcón Oseguera, Francisco**
   - Facultat de Física, Universitat de Barcelona
   - falarcon@ffn.ub.es

3. **Albuquerque Lira, Sérgio Henrique**
   - Universitat de Barcelona
   - sergiobodoh@gmail.com

4. **Alemany Arias, Anna**
   - Universitat de Barcelona
   - aalemany@ffn.ub.es

5. **Alvarez Nodarse, Renato**
   - IMUS, Universidad de Sevilla
   - ran@us.es

6. **Aparicio Reinoso, José María**
   - Universidad Nacional de Educación a Distancia
   - jmaparicio@bec.uned.es

7. **Aragoneses Aguado, Andrés**
   - Universitat Politècnica de Catalunya
   - andres.aragoneses@upc.edu

8. **Arenas, Alex**
   - Universitat Rovira i Virgili
   - alexandre.arenas@urv.cat

9. **Ares García, Saúl**
   - Centro Nacional de Biotecnología - CSIC
   - saul.ares@csic.es

10. **Astillero Vivas, Antonio**
    - Universidad de Extremadura
    - aavivas@unex.es

11. **Barjau Rico, Ignasi**
    - Facultat de Ciències, Universitat de les Illes Balears
    - barjau_mas@hotmail.com

12. **Baró i Urbea, Jordi**
    - Facultat de Física, Universitat de Barcelona
    - jordibaro@ecm.ub.es

13. **Benet Villanueva, Jorge**
    - Universidad Complutense de Madrid
    - jorgebenet@hotmail.com

14. **Bergues Cabrales, Jesús Manuel**
    - Universidad San Jorge, Zaragoza
    - jmbergues@usj.es

15. **Blanch-Mercader, Carles**
    - Universitat de Barcelona
    - blanch@ecm.ub.es

16. **Bores Quijano, Cecilia**
    - Instituto de Química Física Rocasolano, CSIC
    - cbores@iqfr.csic.es

17. **Brey Abalo, José Javier**
    - Universidad de Sevilla
    - brey@us.es

18. **Brito, Ricardo**
    - Universidad Complutense de Madrid
    - brito@fis.ucm.es

19. **Buceta, Javier**
    - Parc Científic de Barcelona
    - jbuceta@gmail.com

20. **Burgos, Javier**
    - Institut de Química Avançada de Catalunya - CSIC
    - javier.burgos@iqac.csic.es

21. **Calero Borrallo, Carlos**
    - Universitat Politècnica de Catalunya
    - carles.calero@upc.edu

22. **Calvo Minguillón, Ausias-March**
    - Universitat Politècnica de Catalunya
    - ausias.march@upc.edu

23. **Camuñas Soler, Joan**
    - Universitat de Barcelona
    - joan.camunas@gmail.com

24. **Capitán Gómez, José Ángel**
    - Centro de Astrobiología, INTA-CSIC
    - joseangel.capitan@cab.inta-csic.es

25. **Carro, Adrián**
    - IFISC (CSIC-UIB)
    - adrian.carro@ifisc.uib-csic.es

26. **Casademunt Viader, Jaume**
    - Universitat de Barcelona
    - jaume.casademunt@ub.edu

27. **Casanellas Vilageliu, Laura**
    - Universitat de Barcelona
    - laurac@ecm.ub.es

28. **Cerdà Pino, Joan Josep**
    - IFISC (CSIC-UIB)
    - joan@ifisc.uib-csic.es

29. **Cerdeiriña Álvarez, Claudio**
    - Universidad de Vigo
    - calvarez@uvigo.es

30. **Chacón Fuertes, Enrique**
    - Instituto Ciencias de Materiales de Madrid - CSIC
    - echacon@icmm.csic.es

31. **Clotet i Fons, Xavier**
    - Facultat de Física, Universitat de Barcelona
    - x.clotetfons@gmail.com

32. **Colet, Pere**
    - IFISC (CSIC-UIB)
    - pere@ifisc.uib-csic.es

33. **Colomer de Simón, Pol**
    - Universitat de Barcelona
    - polcolomerdesimon@gmail.com

34. **Cornelles Soriano, Miguel**
    - IFISC (CSIC-UIB)
    - miguel@ifisc.uib-csic.es

**35. Corral, Álvaro**
- Centre de Recerca Matemàtica
- acorral@crm.cat

**36. Cuesta Ruiz, Jose A**
- Universidad Carlos III de Madrid
- cuesta@math.uc3m.es

**37. Cuetos Menéndez, Alejandro**
- Universidad Pablo Olavide
- acuemen@upo.es

**38. de Franciscis, Sebastiano**
- European Institute of Oncology (IEO)
- sebastiano.defranciscis@ifom-ieo-campus.it

**39. de la Torre Rodríguez, Jaime Arturo**
- Universidad Nacional de Educación a Distancia
- jatorre@bec.uned.es

**40. de Tomas, Carla**
- Universitat Autònoma de Barcelona
- Carla.Tomas@uab.cat

**41. Deza, Juan Ignacio**
- Universidad Politècnica de Catalunya
- juan.ignacio.deza@upc.edu

**42. Deza Bevilacqua, Roberto Raúl**
- Instituto de Investigaciones Físicas de Mar del Plata (CONICET - U. Nacional Mar del Plata)
- deza@mdp.edu.ar

**43. Diaz Guilera, Albert**
- Universitat de Barcelona
- albert.diaz@ub.edu

**44. Dinis Vizcaino, Luis**
- Universidad Complutense de Madrid
- ldinis@fis.ucm.es

**45. Domínguez Alvarez, Alvaro**
- Universidad de Sevilla
- dominguez@us.es

**46. Domínguez García, Virginia**
- Universidad de Granada
- virginia@onsager.ugr.es

**47. Durán-Olivencia, Miguel Ángel**
- Instituto Andaluz de Ciencias de la Tierra (CSIC - Universidad de Granada)
- maduran@lec.csic.es

**48. Eguiluz, Victor**
- IFISC (CSIC-UIB)
- victor@ifisc.uib-csic.es

**49. Elizalde, Emilio**
- Institut de Ciencies de l'Espai (CSIC - IEEC)
- elizalde@ieec.uab.es

**50. Erola, Pau**
- Universitat Rovira i Virgili
- pau.erola@urv.cat

**51. Español, Pep**
- Universidad Nacional de Educación a Distancia
- pep@fisfun.uned.es

**52. Evans, Robert**
- University of Bristol
- Bob.Evans@bristol.ac.uk

**53. Falo Forniés, Fernando**
- BIFI - Universidad de Zaragoza
- fff@unizar.es

**54. Fdez. Abascal, Jose Luis**
- Universidad Complutense de Madrid
- abascal@quim.ucm.es

**55. Fernandez Alvarez, Miguel Angel**
- Universidad Nacional de Educación a Distancia
- miguel_a_fernandez@hotmail.com

**56. Fernandez Barbero, Antonio**
- Universidad de Almería
- afernand@ual.es

**57. Fernández del Río, Ana**
- Universidad Nacional de Educación a Distancia
- ana.fernandez@invi.uned.es

**58. Fleurquin, Pablo**
- IFISC (CSIC-UIB)
- pfleurquin@ifisc.uib-csic.es

**59. Floría, Luis Mario**
- BIFI - Universidad de Zaragoza
- mario.floria@gmail.com

**60. Formosa Jordan, Pau**
- Universitat de Barcelona
- pformosa@ecm.ub.es

**61. Galeano Prieto, Javier**
- Universidad Politécnica de Madrid
- javier.galeano@upm.es

**62. García Almarza, Noé**
- Instituto de Química-Física Rocasolano - CSIC
- noe@iqfr.csic.es

**63. García Chamorro, Moisés**
- Universidad de Extremadura
- moises@unex.es

**64. Garcia de Soria Lucena, Maria Isabel**
- Universidad de Sevilla
- gsoria@us.es

**65. Garcia Ojalvo, Jordi**
- Universitat Politècnica de Catalunya
- jordi.g.ojalvo@upc.edu

**66. García Palanco, Jose M.**
- ETSI Aeronáutica y del Espacio, Universidad Politécnica de Madrid
- jose.gpalanco@upm.es

**67. Garriga, Adan**
- Centro Internacional de Métodos Numéricos en Ingeniería
- adan.garriga@gmail.com

**68. Giannini, Andrea**
- Universidad Carlos III de Madrid
- agiannin@math.uc3m.es

**69. Gómez, Sergio**
- Universitat Rovira i Virgili
- sergio.gomez@urv.cat

**70. Gomez Gardeñes, Jesus**
- BIFI - Universidad de Zaragoza
- gardenes@gmail.com

**71. Gomila Villalonga, Damia**
- IFISC (CSIC-UIB)
- damia@ifisc.uib-csic.es

**72. González González, Miguel Ángel**
- Universidad Complutense de Madrid
- miguelangel.gonz20@gmail.com

**73. González Maestre, Miguel Ángel**
- Universidad de Extremadura
- maestre@unex.es

**74. González Noya, Eva**
- Instituto de Química Física Rocasolano, CSIC
- eva.noya@iqfr.csic.es

**75. González Pinto, Miguel**
- Universidad Autónoma de Madrid
- miguel.gonzalezp@uam.es

**76. Granell, Clara**
- Universitat Rovira i Virgili
- clara.granell@urv.cat

**77. Grujic, Jelena**
- Universidad Carlos III de Madrid
- jgrujic@math.uc3m.es

**78. Guàrdia, Elvira**
- Universitat Politècnica de Catalunya
- elvira.guardia@upc.edu

**79. Guiu Souto, Jacobo**
- Universidad de Santiago de Compostela
- jacobo.guiu@usc.es

**80. Gutiérrez Roig, Mario**
- Universitat de Barcelona
- mariogutierrezroig@gmail.com

**81. Güell Riera, Oriol**
- Universitat de Barcelona
- oguell@ub.edu

**82. Henao Aristizábal, Andrés**
- Universitat Politècnica de Catalunya
- andres.henao@upc.edu

**83. Hernandez Machado, Aurora**
- Universitat de Barcelona
- a.hernandezmachado@gmail.com

**84. Hernandez-Carrasco, Ismael**
- IFISC (CSIC-UIB)
- ismael@ifisc.uib-csic.es

**85. Hernandez-Garcia, Emilio**
- IFISC (CSIC-UIB)
- emilio@ifisc.uib-csic.es

**86. Hernando, Antonio**
- Instituto de Magnetismo Aplicado, RENFE-Universidad Complutense de Madrid
- secretaria@externos.adif.es

**87. Hidalgo Aguilera, Jorge**
- Insitituto Carlos I de Física Teórica y Computacional, Universidad de Granada
- jhidalgo@onsager.ugr.es

**88. Horowitz, Jordan**
- Universidad Complutense de Madrid
- jordanmhorowitz@gmail.com

**89. Huhn, Florian**
- Universidade de Santiago de Compostela
- florian.huhn@usc.es

**90. Ibañes Miguez, Marta**
- Universitat de Barcelona
- mibanes@ub.edu

**91. Johnson, Samuel**
- Imperial College London
- samuel@onsager.ugr.es

**92. Lacasa , Lucas**
- Universidad Politécnica de Madrid
- lucas.lacasa@upm.es

**93. Lafuerza, Luis F.**
- IFISC (CSIC-UIB)
- luis@ifisc.uib-csic.es

**94. Lasanta Becerra, Antonio**
- Universidad de Sevilla
- alasanta@us.es

**95. Lim, Jong Soo**
- IFISC (CSIC-UIB)
- lim.jongsoo@gmail.com

**96. López , Cristóbal**
- IFISC (CSIC-UIB)
- clopez@ifisc.uib-csic.es

**97. Lopez Martin, Juan Manuel**
- Instituto de Física de Cantabria (CSIC - Universidad de Cantabria)
- lopez@ifca.unican.es

**98. Lozano Grijalba, Celia**
- Universidad de Navarra
- clozano@alumni.unav.es

**99. Luis Hita, Jorge**
- Universidad Complutense de Madrid
- jluishita@gmail.com

**100. Luque Serrano, Bartolo**
- ETSI Aeronáuticos, Universidad Politécnica de Madrid
- bartolome.luque@upm.es

**101. Luque Serrano, Jordi**
- Universidad Politécnica de Madrid
- jorge.luque@upc.edu

**102. Lyra Gollo, Leonardo**
- IFISC (CSIC-UIB)
- leonardo@ifisc.uib-csic.es

**103. Manrubia, Susanna C.**
- Centro de Astrobiología (INTA - CSIC)
- scmanrubia@cab.inta-csic.es

**104. Maritan, Amos**
- University of Padova
- amos.maritan@pd.infn.it

**105. Martinez Garcia, Ricardo**
- IFISC (CSIC-UIB)
- ricardo@ifisc.uib-csic.es

**106. Martínez Huartos, Johann Heinz**
- Universidad Politécnica de Madrid
- jh.martinez@alumnos.upm.es

**107. Martínez Llinàs, Jade**
- IFISC (CSIC-UIB)
- jade@ifisc.uib-csic.es

**108. Martínez Piñeiro, Manuel**
- Universidade de Vigo
- mmpineiro@uvigo.es

**109. Martínez Ratón, Yuri**
- Universidad Carlos III de Madrid
- yuri@math.uc3m.es

**110. Martínez Vaquero, Luis Alberto**
- Universidad Carlos III de Madrid
- luisalberto.martinez@uc3m.es

**111. Matias, Manuel**
- IFISC (CSIC-UIB)
- manuel@ifisc.uib-csic.es

**112. Maynar Blanco, Pablo**
- Universidad de Sevilla
- maynar@us.es

**113. Mayol Serra, Catalina**
- Universitat de les Illes Balears
- cmayols@yahoo.es

**114. Maza Ozcoidi, Diego**
- Universidad de Navarra
- dmaza@unav.es

**115. Mederos Martín, Luis**
- Instituto de Ciencia de Materiales de Madrid (CSIC)
- lmederos@icmm.csic.es

**116. Meléndez Schofield, Marc**
- Universidad Nacional de Educación a Distancia
- mmelendez@fisfun.uned.es

**117. Miritello, Giovanna**
- Universidad Carlos III Madrid & Telefonica Research
- giov0mir@gmail.com

**118. Moreno, Yamir**
- BIFI - Universidad de Zaragoza
- yamir.moreno@gmail.com

**119. Moreno Barrado, Ana**
- Universidad Pontificia de Comillas
- ana.moreno@iit.upcomillas.es

**120. Moretti, Paolo**
- Universidad de Granada
- moretti.paolo@gmail.com

**121. Muñoz García, Javier**
- Universidad Carlos III de Madrid
- javiermunozgarcia@gmail.com

**122. Nesic, Svetozar**
- Universidad Carlos III de Madrid
- snesic@math.uc3m.es

**123. Nicola, Ernesto M.**
- IFISC (CSIC-UIB)
- ernesto.nicola@ifisc.uib-csic.es

**124. Nicoli, Matteo**
- Ecole Polytechnique - CNRS
- matteo.nicoli@polytechnique.edu

**125. Nicolini, Paolo**
- Universitat Politècnica de Catalunya
- paolo.nicolini@upc.edu

**126. Núñez Núñez, Ángel M.**
- E.T.S.I. Aeronáuticos, Universidad Politécnica de Madrid
- angel.nunhez@gmail.com

**127. Nuño, Juan Carlos**
- Universidad Politécnica de Madrid
- juancarlos.nuno@upm.es

**128. Oriola Santandreu, David**
- Universitat de Barcelona
- davidoriola@gmail.com

**129. Orlandi, Javier G.**
- Universitat de Barcelona
- orlandi@ecm.ub.es

**130. Ortín Rull, Jordi**
- Universitat de Barcelona
- ortin@ecm.ub.es

**131. Ortiz de Zárate Leira, José María**
- Universidad Complutense de Madrid
- jmortizz@fis.ucm.es

**132. Pagonabarraga, Ignacio**
- Universitat de Barcelona
- ipagonabarraga@ub.edu

**133. Palau Ortin, David**
- Universitat de Barcelona
- palau@ecm.ub.es

**134. Parra Rivas, Pedro**
- IFISC (CSIC-UIB)
- parrariv@gmail.com

**135. Patti, Alessandro**
- Instituto de Química Avanzada de Cataluña - CSIC
- alpnqb@iqac.csic.es

**136. Pazó, Diego**
- Instituto de Física de Cantabria (CSIC - Universidad de Cantabria)
- pazo@ifca.unican.es

**137. Pérez García, Pablo**
- Instituto de Física de Cantabria (CSIC - Universidad de Cantabria).
- perezg@ifca.unican.es

**138. Pérez-Carrasco, Rubén**
- Universitat de Barcelona
- 2piruben@gmail.com

**139. Pigolotti, Simone**
- Universitat Politècnica de Catalunya
- simone.pigolotti@gmail.com

**140. Pont, Oriol**
- INRIA, Talence, Francia
- oriol.pont@inria.fr

**141. Ramírez de la Piscina, Laureano**
- Universitat Politècnica de Catalunya
- laure@fa.upc.edu

**142. Rascón Díaz, Carlos**
- GISC, Uniersidad Carlos III de Madrid
- carlos.rascon@uc3m.es

**143. Rebollo Pedruelo, Miguel**
- Universitat Politècnica de València
- mrebollo@dsic.upv.es

**144. Ribezzi-Crivellari, Marco**
- Universitat de Barcelona
- marco.ribezzi@gmail.com

**145. Ritort Farran, Felix**
- Universitat de Barcelona
- fritort@gmail.com

**146. Rodríguez Díaz, Miguel Angel**
- Instituto de Física de Cantabria (CSIC - Universidad de Cantabria)
- rodrigma@ifca.unican.es

**147. Rodríguez Gómez, Salvador**
- Universidad Pablo de Olavide
- salrodgom@upo.es

**148. Rodríguez Laguna, Javier**
- ICFO - Instituto de Ciencias Fotónicas
- jvrlag@gmail.com

**149. Rodríguez Lázaro, Guillermo**
- Universitat de Barcelona
- grolazaro@gmail.com

**150. Rodríguez López, Pablo**
- Universidad Carlos III de Madrid
- pablo.rodriguez.lopez@math.uc3m.es

**151. Rodriguez Mendez, Victor Manuel**
- IFISC (CSIC-UIB)
- vrodriguez@ifisc.uib-csic.es

**152. Rodríguez Parrondo, Juan Manuel**
- Universidad Complutense de Madrid
- parrondo@fis.ucm.es

**153. Rodriguez Quintero, Niurka**
- Universidad de Sevilla
- nrquintero@gmail.com

**154. Rodríguez Rivas, Álvaro**
- Universidad de Sevilla
- arodriguezrivas@us.es

**155. Roldan, Edgar**
- Universidad Complutense de Madrid
- callmeyaw@gmail.com

**156. Romero Enrique, José Manuel**
- Universidad de Sevilla
- enrome@us.es

**157. Rubi, Miguel**
- Universitat de Barcelona
- mrubi@ub.edu

**158. Rué, Pau**
- Universitat Politècnica de Catalunya
- pau.rue@upc.edu

**159. Ruiz Martí, Xavier**
- Universitat Rovira i Virgili
- josepxavier.ruiz@urv.cat

**160. Ruiz Montero, María José**
- Universidad de Sevilla
- majose@us.es

**161. Sagarra, Oleguer**
- Universidad de Barcelona
- oleguer.sagarra@gmail.com

**162. Sagues Mestre, Francesc**
- Universitat de Barcelona
- f.sagues@ub.edu

**163. San Miguel, Maxi**
- IFISC (CSIC-UIB)
- maxi@ifisc.uib-csic.es

**164. Sánchez, David**
- IFISC (CSIC-UIB)
- david.sanchez@uib.es

**165. Sánchez, Anxo**
- Universidad Carlos III de Madrid
- anxo@math.uc3m.es

**166. Sánchez Fernández, Luis Raúl**
- Universidad Carlos III de Madrid
- raul.sanchez@uc3m.es

**167. Sancho, José M.**
- Universitat de Barcelona
- josemsancho@gmail.com

**168. Santalla, Silvia**
- Universidad Carlos III de Madrid
- silvia.santalla@uc3m.es

**169. Santos Reyes, Andrés**
- Universidad de Extremadura
- andres@unex.es

**170. Santos Sánchez, María Jesús**
- Universidad de Salamanca
- smjesus@usal.es

**171. Sanz, Eduardo**
- Universidad Complutense de Madrid
- esa01@quim.ucm.es

**172. Sartori, Pablo**
- Max Planck Institute for the Physics of Complex Systems, Dresden, Alemania
- pablo.sartori@gmail.com

**173. Selingardi Matias, Fernanda**
- IFISC (CSIC-UIB)
- fernanda@ifisc.uib-csic.es

**174. Ser Giacomi, Enrico**
- IFISC (CSIC-UIB)
- erikgs@hotmail.it

**175. Serral Serra, Maria**
- Universitat Rovira i Virgili
- maria.serral@urv.cat

**176. Serrano Moral, M. Angeles**
- Universitat de Barcelona
- marian.serrano@ub.edu

**177. Simic, Ana**
- Universidad de Navarra
- asimic@alumni.unav.es

**178. Soriano Fradera, Jordi**
- Universitat de Barcelona
- jordi.soriano@ub.edu

**179. Starnini, Michele**
- Universitat Politècnica de Catalunya
- michele.starnini@upc.edu

**180. Suñé Simon, Marc**
- Universitat de Barcelona
- sune@ecm.ub.es

**181. Teller Amado, Sara**
- Universitat de Barcelona
- teller.sara@gmail.com

**182. Tibau i Martorell, Elisenda**
- Universitat de Barcelona
- elisenda.tibau@gmail.com

**183. Tirabassi, Giulio**
- Universitat Politècnica de Catalunya
- tirabassi.giulio@gmail.com

**184. Toral, Raúl**
- IFISC (CSIC-UIB)
- raul@ifisc.uib-csic.es

**185. Torrent Serra, Mª Carme**
- Universitat Politècnica de Catalunya
- carme.torrent@upc.edu

**186. Trejo Soto, Claudia**
- Universitat de Barcelona
- claudiat@ecm.ub.es

**187. Tugores, Antònia**
- IFISC (CSIC-UIB)
- antonia@ifisc.uib-csic.es

**188. Tuzon Marco, Paula**
- IFISC (CSIC-UIB)
- paula@ifisc.uib-csic.es

**189. Valeriani, Chantal**
- Universidad Complutense de Madrid
- cvaleriani@quim.ucm.es

**190. Velasco Caravaca, Enrique**
- Universidad Autónoma de Madrid
- enrique.velasco@uam.es

**191. Vicent Luna, José Manuel**
- Universidad Pablo de Olavide
- jmviclun@upo.es

**192. Villa Martín, Paula**
- Universidad de Granada
- pvilla@ugr.es

**193. Vilone, Daniele**
- IFISC (CSIC-UIB)
- daniele.vilone@gmail.com

**194. Vivo, Edoardo**
- Universidad Carlos III de Madrid
- doc.cap@gmail.com

**195. von Kameke, Alexandra**
- Universidad de Santiago de Compostela
- alexandra.vonkameke@usc.es

**196. White Sánchez, Juan Antonio**
- Universidad de Salamanca
- white@usal.es

**197. Wio Beitelmajer, Horacio**
- Instituto de Fisica de Cantabria (CSIC - Universidad de Cantabria)
- wio@ifca.unican.es

**198. Yanez Santamaria, Antonio**
- Universidade de Santiago de Compostela
- antonio.yanez.santamaria@gmail.com

**199. Zambrini, Roberta**
- IFISC (CSIC-UIB)
- roberta@ifisc.uib-csic.es

**200. Zamora Munt, Jordi**
- IFISC (CSIC-UIB)
- jordi.zm@gmail.com

# Organismos patrocinadores